# OUT-OF-PLANE SEISMIC PERFORMANCE OF UNREINFORCED CLAY BRICK MASONRY WALLS

by

CHRISTOPHER STEPHAN MEISL

B.A.Sc., University of British Columbia, 2002

A THESIS SUBMITTED IN PARTIAL FULFILMENT OF
THE REQUIREMENTS FOR THE DEGREE OF

MASTER OF APPLIED SCIENCE

in

THE FACULTY OF GRADUATE STUDIES

(Civil Engineering)

THE UNIVERSITY OF BRITISH COLUMBIA

April 2006

# ABSTRACT

Given sufficient anchorage to the diaphragms, out-of-plane walls in unreinforced masonry buildings have been shown to crack above mid-height and rock as two rigid bodies. This study investigates the sensitivity of the rocking response to the type of ground motion and the quality of the wall construction. A parametric study using a nonlinear-elastic single-degree-of-freedom model suggests that buildings located on firm ground sites are less likely to experience out-of-plane wall failures compared with buildings located on soft soil sites. Shake table tests were conducted on four full-scale multi-wythe walls with a height-to-thickness (h/t) ratio of 12, varying construction quality, and using three different ground motions. All walls experienced cracking at approximately peak ground acceleration (PGA) of the 2005 National Building Code of Canada (NBCC) level for Vancouver, but exhibited a stable rocking behaviour without collapse beyond a ground motion 1.5 times the 2005 NBCC level. Simple analytical methods were used to calculate the un-cracked wall stiffness, maximum force on an un-cracked wall, cracking strength, and the maximum total force acting on a cracked wall. These results compared well with those observed in the tests. Finally, a rigid body numerical model was developed using the commercially available software, Working Model. The results obtained using this model compared well to the full-scale tests, accurately predicting the maximum relative displacement at the crack location for the scaled ground motions used in the testing program.

# TABLE OF CONTENTS

# LIST OF TABLES

# LIST OF FIGURES

# ACKNOWLEDGEMENTS

I would first like to express my sincere thanks to my supervisor, Dr. Ken Elwood, for his encouragement and guidance through out my graduate studies. I value his insight and enthusiasm, and hope our paths cross again in the future. I would also like to thank Dr. Carlos Ventura, whose contributions to this project were most helpful.

This work was part of a larger program, UBC 100, and I would like to thank the other team members: Dr. Tim White and Dr. Graham Taylor, for their guidance and feedback during the course of the work. In particular, Dominic Mattman; with out his help this project would not have been a success. The technicians at UBC were most helpful during the construction of the testing apparatus. The efforts made by Max Nazar, Scott Jackson, and Doug Hudniuk are greatly appreciated.

Bill McEwan, and J.P. LeBerg from the Masonry Institute of British Columbia (MIBC) were instrumental in providing the materials, and technical support during the wall's construction and material testing. Also, thank you to the masons, who taught me how to put all the "mud n' bricks" together.

This research was conducted with the financial support of the British Columbia Ministry of Education, Western Economic Diversification Canada, and the MIBC. I would also like to acknowledge the technical support of the Association of Professional Engineers and Geoscientists BC's Seismic Task Force Peer Review Group, for their valuable professional insight and comments during the testing portion of this project.

I would like to thank my colleagues and friends at the University of British Columbia, particularly Andrew Seeton, Martin Turek, Kevin Riederer, and Anthony Peterson, for their help and motivational support.

To my loving family, my dad Werner, mom Corina, and the rest of the Meisl clan, Nick, Monica, Andrea, and my Omas, whom I owe so much. Finally, to Cynthia, whose patience, words of encouragement and inspiration will always be remembered. Thank you.

# 1 INTRODUCTION AND PREVIOUS RESEARCH

## 1.1 Introduction

Buildings with clay brick multi-wythe, unreinforced masonry walls as their primary structural system have suffered considerable damage in past earthquakes (e.g. Long Beach, 1933; Vancouver Island, 1946; Loma Prieta, 1989; Northridge, 1994). In the case of Loma Prieta, an increase in damage was observed for URM buildings located on soft soil sites [SEAOC, 1991]. Typical damage observed for unreinforced masonry (URM) buildings includes: collapse of parapets or gables, diagonal shear failure or sliding shear failure of in-plane walls, and out-of-plane wall failures. The potential collapse of parapets and gables poses a significant hazard to people next to the building at the time of the earthquake. Bracing is frequently provided during a seismic retrofit of a URM building to avoid this failure mode. In-plane wall failures result in a reduction in the lateral load capacity; however, without out-of-plane movement, such failure modes do not necessarily result in collapse of the wall due to continued support of gravity loads across the failure plane. In contrast, out-of-plane wall failures can result in collapse of the load bearing wall and partial or total collapse of the building. Examples of out-of-plane failures are shown in Figure 1.1 and Figure 1.2. In an effort to provide an improved assessment of the collapse potential of typical URM buildings during earthquakes, this study focuses on the out-of-plane response of multi-wythe URM walls.

Out-of-plane wall failures frequently occur due to inadequate anchorage of the wall to the floor diaphragms. In such cases, the wall behaves as a cantilever and collapses if the inertia forces on the wall push it beyond the point of instability or half of the wall width for the boundary condition shown in Figure 1.3a. Given sufficient anchorage to the diaphragms, out-of-plane walls will respond as vertical "beams" in bending as the inertia forces on the walls are distributed to the attached diaphragms. Due to limited tensile strength of the mortar, anchored URM walls will frequently crack just above mid-height. This results in rocking of the top and bottom wall segments in the out-of-plane direction. If the displacements induced by the ground motion are large enough (i.e. exceeding the wall width at the crack location, see Figure 1.3b), the wall can become unstable and collapse. Considering the improvement in behaviour for the

relatively modest cost of anchoring the walls to the diaphragms, it is assumed in this study that the walls are sufficiently anchored to the floor diaphragm to develop the beam bending mode of failure.

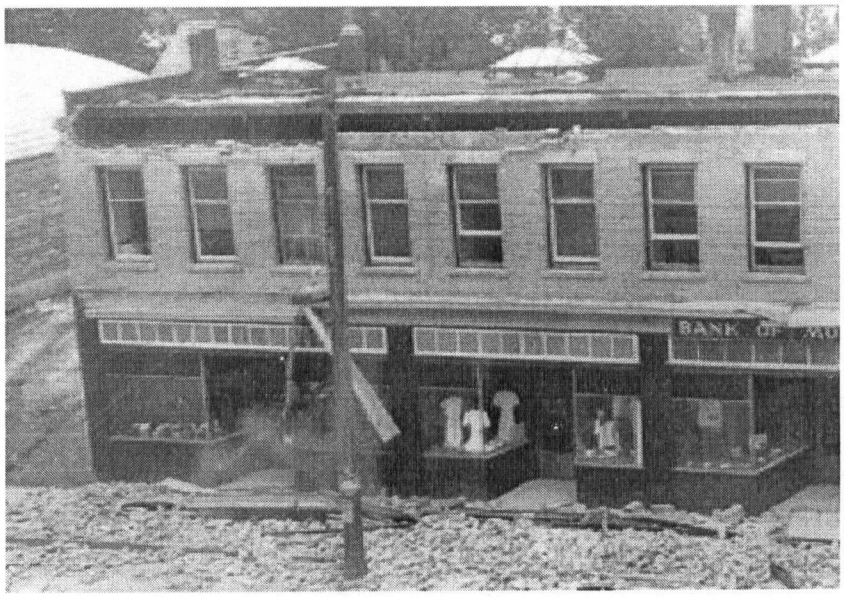

(a) Damage to the Bank of Montreal Building, Port Alberni B.C.

(b) Masonry Failure of Post Office, Courtenay B.C.

**Figure 1.1 URM Damage from the M7.3 Vancouver Island Earthquake of 1946**
[Natural Resources Canada, 2006]

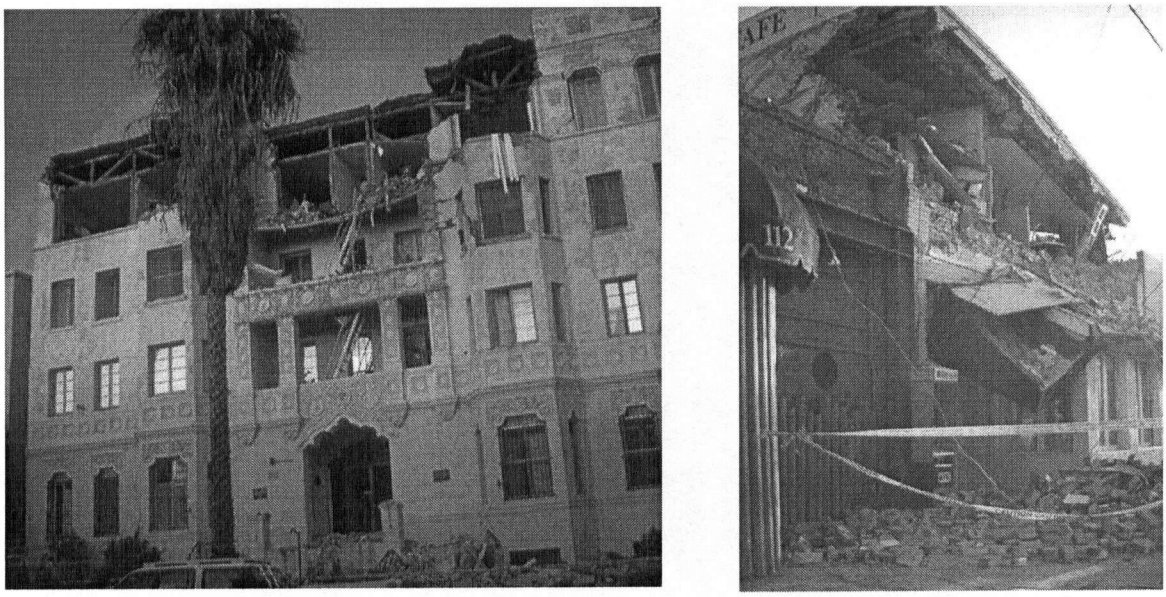

**Figure 1.2 Upper Storey Out-of-Plane URM Failure from the 1994 Northridge Earthquake**

[NISEE 2006a,b]

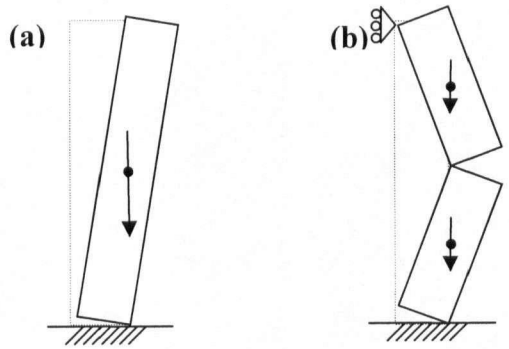


**Figure 1.3 Out-of-Plane Failure Modes**

**(a) Cantilever Mode and (b) Beam Bending Mode**

## 1.2 Previous Research

### 1.2.1 Out-of-Plane Testing

Out-of-plane testing of URM walls began in earnest in the early 1970's, when researchers were interested in the effect of wind loading on walls. These tests were largely quasi-static in nature. Only in the 1980's, did researchers begin to investigate the effect of earthquakes on the out-of-plane response of URM walls through dynamic testing. The following section provides a brief

introduction to past quasi-static and dynamics test that were conducted, proposed analytical models, and some background information on rigid body rocking.

#### 1.2.1.1 Quasi-Static Tests

Yokel et al. [1971] performed tests on simply supported walls with varying vertical compressive load (overburden load) on a variety of brick/block combinations. Increasing lateral pressure was applied by inflating an airbag. The walls cracked near the mid-height, and it was observed that walls that had higher axial load had a greater out-of-plane capacity. Similar tests were conducted with various support conditions by Yokel et al. [1976], and West et al. [1973, 1977].

Anderson [1994] also performed quasi-static tests with laterally loaded walls and varying boundary conditions. It was observed that the walls cracked at 60% of the height of the wall from its base, and that eccentricity of the vertical load due to rotation of the wall about its base was found to induce a stabilizing moment.

#### 1.2.1.2 Dynamic Tests

Dynamic out-of-plane testing of URM walls began with the tests conducted by the ABK Joint Venture [1981]. During this pioneering study of out-of-plane seismic performance of URM walls, 22 wall specimens of varying height to thickness ($h/t$) ratios and overburden loads were subjected to dynamic loading at the top and bottom of the walls. The ground motion at the top of the wall was amplified to include the effect of a flexible diaphragm. It was observed that even though the input motions at the top and bottom of the wall may be out of phase, the most critical time was when the motions were in phase. During testing the walls cracked at approximately mid-height and at the wall base. The walls were observed to remain 'dynamically stable,' allowing the walls to have significant reserve capacity above that of the 'semi-rigid threshold' force (Figure 1.4). It was found that neither static nor quasi-static analysis procedures satisfactorily defined the highly non-linear dynamic behaviour of the walls.

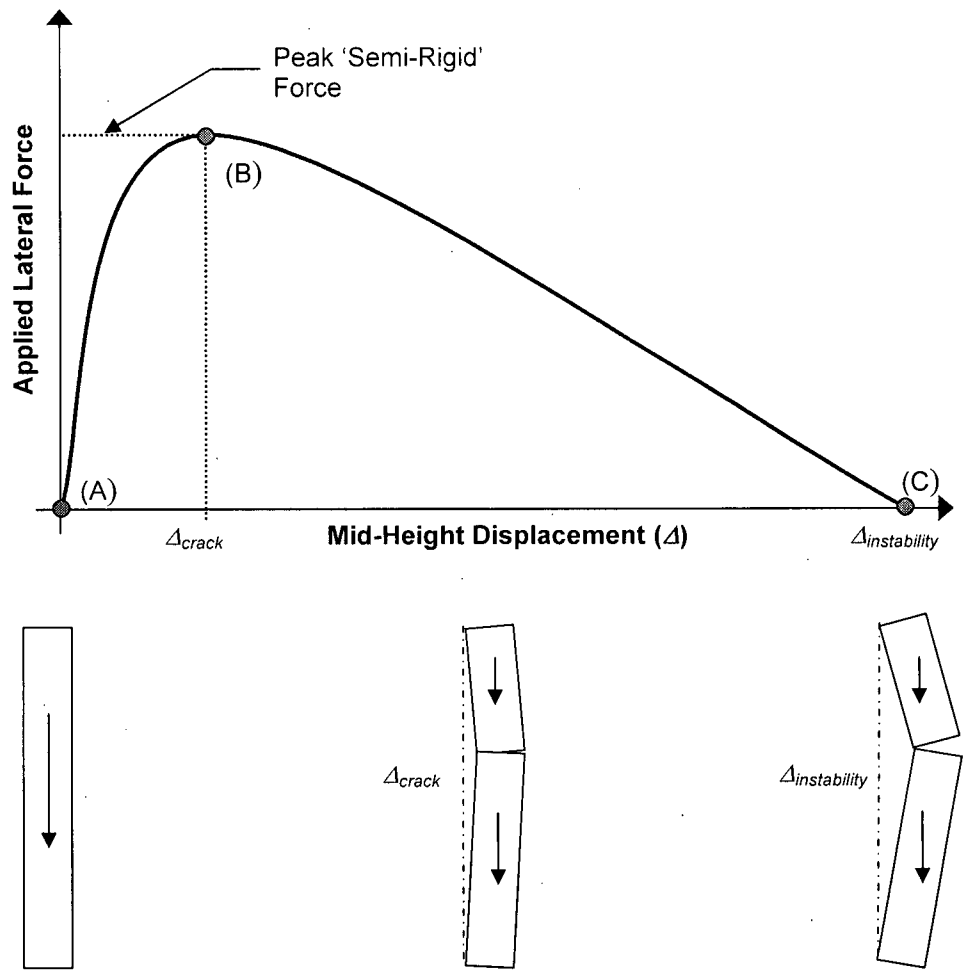


(A) Un-Cracked Wall (B) Crack Formed (C) Instability

**Figure 1.4 Semi-Rigid Force Displacement Relationship (No Overburden Force)**

From the ABK study, the key parameters affecting the dynamic stability of the walls were the height to thickness ratio (*h/t*), overburden load, and peak input velocities at the top and bottom of the wall. ABK proposed maximum allowable *h/t* ratios as a function of the overburden ratio (superimposed weight / wall weight) and peak input velocities at the top and bottom of the wall. These guidelines were then incorporated into the allowable limits defined in the Federal Emergency Management Agency (FEMA) 273 document entitled "NEHRP Guidelines for the Seismic Rehabilitation of Buildings" [FEMA, 1997]. However, for the out-of-plane assessment of URM walls, the limits were based on the spectral acceleration instead of velocity. The FEMA 273 guideline have since been replaced by FEMA 356 *Prestandard and Commentary for the*

*Seismic Rehabilitation of Buildings* [American Society of Civil Engineers (ASCE), 2000], and are discussed in further detail in Section 1.3.

Several shake table tests on single-wythe walls have demonstrated that, given sufficient anchorage to the diaphragms, out-of-plane URM walls can maintain stability when subjected to severe ground motions (Gulkan et al. 1990; Paquette et al. 2001; Griffith et al. 2004; Simsir et al. 2004). Gulkan et al. [1990] tested single-storey masonry houses and noted large displacements as the out-of-plane walls rocked at the mid-height crack without collapse. Gulkan et al. [1990] also noted no increase in the out-of-plane response when the walls were subjected to simultaneous in-plane and out-of-plane demands. Paquette et al. [2001] tested wall segments from an upper storey of a historic building to evaluate retro-fitting options. Three specimens were tested, of which two were retrofitted. Griffith et al. [2004] observed that the out-of-plane rocking response of the wall was sensitive to the displacement demand of the selected ground motion. Ground motions with low peak ground displacements (PGD) would not collapse the wall specimens, while ground motions with high PGD resulted in rocking beyond the stability limit. Simsir et al. [2004] included the effect of a flexible diaphragm and noted an increase in the out-of-plane wall displacements. Cracking at mid-height was not observed by Simsir et al. [2004] due to high overburden pressure applied to the wall. Despite the experimental evidence indicating that out-of-plane walls can remain stable given sufficient anchorage to the diaphragms, engineers have frequently chosen to not rely on the rocking response of the wall after cracking and have opted for expensive retrofit measures [ElGawady et al., 2004] such as attaching stiff vertical beams to support all out-of-plane walls.

### 1.2.2 Analysis Methods

The majority of the analyses methods in use by practicing engineers are simplified quasi-static analysis based methods. Only recently have researchers begun to develop tools to perform dynamic analyses of out-of-plane walls. Brief introductions to some of the methods developed are presented in the following section.

#### 1.2.2.1 Quasi-Static Analysis

For an un-cracked wall, with equal input motions at the top and base, one can use the peak acceleration to determine the inertial forces acting on the wall. This assumes very small relative

displacements, such that the induced inertial force can be assumed to be uniformly distributed over the height of the wall. As shown by previous researchers, (Yokel et al. [1971], Yokel et al. [1976], and West et al. [1973, 1977]), who conducted quasi-static tests, an un-cracked wall behaves essentially elastically. An estimate of the cracking force can, therefore, be obtained by calculating the moment capacity of the wall at a critical section, taking into account the flexural strength of the masonry and weight of the wall. The wall can be assumed to act as a simply supported beam and, since the deflections are small, the vertical reactions can be considered to act at the centre of the beam. One could also estimate the un-cracked wall stiffness/period allowing an estimate of the elastic spectral response acceleration to be determined from an elastic spectrum (response spectrum analysis).

Once the wall has cracked, one may also calculate the cracked natural frequency to get an estimate of the elastic spectral response. However, as shown by Housner [1963] and Doherty [2000], the natural frequency of the wall is not unique and is dependent on the relative displacement at the crack. Also, the applied inertial forces acting on the wall are no longer uniform over the height of the wall [Doherty, 2000]. As shown in previous tests, a cracked wall has considerable resistance to collapse. This resistance can be estimated using the rigid body equilibrium analysis method proposed by Priestly [1985] and Paulay [1992]. Martini [1997] developed a Block-Interface Model based on finite elements in an attempt to determine the real post cracking behaviour of the wall.

The quasi-static analysis methods discussed above are not time dependent, and only consider the wall at a critical point in time. As was shown in previous dynamic testing (ABK [1981], Doherty [2000], and Simsir [2004]), walls, when subjected to seismic ground motions, often remain stable beyond the predicted quasi-static limit.

#### 1.2.2.2 Dynamic Analysis

Doherty et al. [2002] proposed a simplified procedure to estimate the peak out-of-plane displacement demand of walls. The URM walls were modeled as an equivalent SDOF tri-linear system with suitable equivalent viscous damping. As was shown by Housner [1963], the frequency of the system is not constant, but rather changed with relative displacement of the centre of mass. This was dealt with by Doherty [2000] by using a variable secant stiffness and

Rayleigh damping. The damping term was calculated through an iterative procedure. Further details regarding this model can be found in Chapter 2.

Simsir [2004] developed three models to predict the dynamic out-of-plane behaviour of URM walls: SDOF, multi-degree-of freedom (MDOF), and 2-degree-of-freedom (2DOF) models. The SDOF system was intended to represent an un-cracked wall, and was modeled as a rigid bar that was free to rotate about its base and incorporated a spring at the top to represent a flexible diaphragm. A MDOF model was developed to compute the out-of-plane response of the wall that may crack at a bed joint. It accounted for diaphragm flexibility, wall stiffness, and the possibility for horizontal cracks to form under combined flexural moments and axial load. The bricks/blocks were modeled as lumped masses, and the mortar bed was represented as a multi-fiber element. The 2DOF model was proposed to be used for stability analyses conducted by practicing engineers. The model comprised of 2 rigid bars (representing a cracked wall), interconnected by hinges. The relative rotations of the bars were resisted by rotational springs located at the hinges. The stiffness of the rotational springs was determined through the post-cracked static moment-rotation relationship of the wall segments, as proposed by Doherty's [2000] semi-rigid relationship.

Other researchers, such as Azevedo et al. [2000] and Lemos et al. [1998], have modeled masonry structures using the discrete (or distinct) element method. This method was originally developed by Cundal [1971] to model rock mechanics. The element interaction laws are based on contact physics and the equations of motion are typically integrated explicitly in time. This method allows for large displacements and rotations between blocks, including; sliding of blocks, crack opening, the complete detachment of blocks, and automatically detects new contact surfaces. The discrete element method may become very computationally intensive if a large number of elements are used.

### 1.2.3 Rigid Body Dynamics

Research into how structures rock during an earthquake begun with investigations conducted by Housner [1963], in which the dynamic response of a rigid, slender block, freely supported at its base was studied. It was shown that the stability of the block is not dependent on its mass, but rather on the block thickness, height to the centre of mass, and gravity. This so called scale effect explains why the larger of two geometrically similar blocks is more stable than a smaller block.

Housner also concluded that the frequency of a freely rocking block increases with decreasing amplitude of the motion (i.e. frequency is not constant).

Priestley et al. [1978] validated some of Housner's theoretical results and developed a methodology to estimate the displacement of the centre of gravity due to rocking. This study was based on the assumption that 'it is possible to represent a rocking block as a SDOF oscillator with constant damping, whose period is dependent on the amplitude of rocking.' This was proven by Makris et al. [2003] to be an erroneous assumption. They showed that the typical SDOF oscillator, which behaves like a pendulum, is fundamentally different than a single rocking block, which behaves like an inverted pendulum (Figure 1.1). The restoring mechanism of an oscillator is governed by the elasticity of the structure ($k$), while that of a rocking rigid block is controlled by gravity ($g$). The frequency of an oscillator is related to the mass and stiffness of the system ($\omega$); while a rocking block does not have a distinct frequency, a frequency parameter ($p$) can be established based on gravity and the $h/t$ ratio. The damping in an oscillator can be accounted by viscous or Rayleigh damping ($\xi$); where as the coefficient of restitution, based on slenderness ($\alpha$), controls the damping of a rigid rocking block. [Makris, 2003]

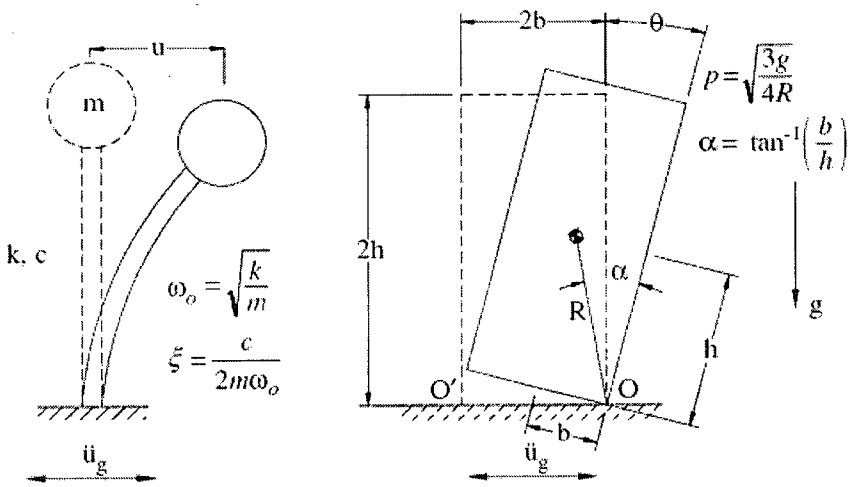


**Figure 1.5 Schematic of a Single-Degree-of-Freedom Oscillator (Left) and of a Free-Standing Block in Rocking Motion (Right)**

[after Makris 2003]

Makris et al. [2001] further showed that under free vibration a typical SDOF oscillator can be described by trigonometric functions, which have a period. The solution for a rigid body rocking block, however, is described by hyperbolic functions, which do not have a standard period, but

rather a complex/imaginary period. Also, in the oscillator, damping continuously dissipates energy from the system, while in a rocking body energy is absorbed nearly instantaneously at the moment of impact.

The findings presented by Makris [2001, 2003] seem to suggest that the oscillator/pendulum based analysis technique proposed by Doherty [2000] and Simsir [2004] may not be an appropriate representation of a rocking body/inverted pendulum system.

## 1.3 Current Out-of-Plane Assessment of URM Walls – FEMA Guidelines

The current standard of practice for practicing engineers is to assess the out-of-plane capacity of un-cracked URM walls using FEMA 356 *Pre-standard and Commentary for the Seismic Rehabilitation of Buildings* [ASCE, 2000]. This document will soon become 'standardized' as ASCE 41, *Seismic Rehabilitation Standard.* The acceptance criteria in FEMA 356 are based on the previously discussed tests conducted by ABK [1981].

For out-of-plane walls with sufficient anchorage to the diaphragms, the guideline specifies acceptance based on the required performance criteria of the building: Immediate Occupancy, or Life Safety and Collapse Prevention. For Immediate Occupancy, flexural cracking of the walls is not permitted, and is limited by the tensile strength of the masonry. For Life Safety, cracking of the wall is permitted, provided the wall remains stable based on the *h/t* criteria. Figure 1.6 provides the FEMA 356 *h/t* limits for walls at the top of a multi-storey building and the first storey of a one-storey building expressed as a function of the spectral acceleration at a structural period of 1.0 seconds ($S_a(1.0s)$). These are the most stringent *h/t* limits provided since the walls at the top storey are the most vulnerable to failure due to the low axial loads. A reduction of walls' effective thickness is required for walls with poor quality collar joints. If the walls do not meet this minimum criteria, stability must be verified using an analytical time-step integration model as per ABK [1981].

To asses URM walls that have pre-existing cracks or have been damaged in a past earthquake, FEMA 306 *Evaluation of Earthquake Damaged Concrete and Masonry Wall Buildings* [ATC, 1998] may be used. As shown in Table 1.1, this guideline specifies $\lambda_{h/t}$ factors, which, when multiplied to the *h/t* limits specified in FEMA 356, give permissible *h/t* ratios for damaged walls.

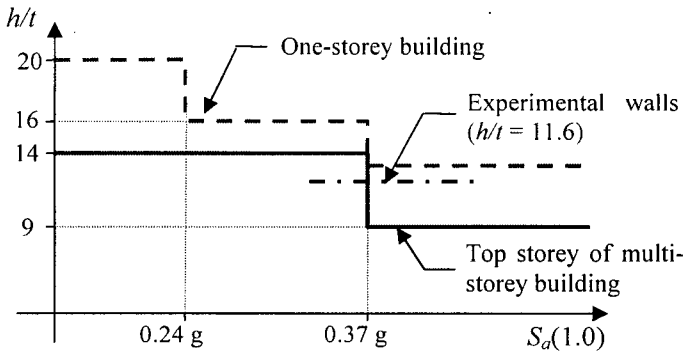


**Figure 1.6 Height to Thickness Life Safety Limits**

[ASCE, 2000]

**Table 1.1 Height to Thickness Factors for Damaged Walls**

[ATC 1998]

| Damage Level | Description of Damage Criteria | $\lambda_{h/t}$ | Typical Appearance |
|---|---|---|---|
| Insignificant | 1. Hairline cracks at floor/roof lines and mid-height of stories.<br>2. No out-of-plane offset or spalling of mortar along cracks. | 1.0 | 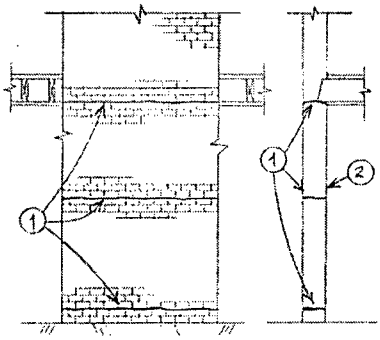 |
| Moderate | 1. Cracks at floor/roof lines and mid-height of stories may have mortar spalling up to full depth of joint.<br>2. Possible out-of-plane offsets along cracks of up to 1/8" (3.2mm). | 0.9 | |
| Heavy | 1. Cracks at floor/roof lines and mid-height of stories may have mortar spalling up to full depth of joint.<br>2. Spalling and rounding at edges of units along crack plane.<br>3. Out-of-plane offsets along cracks of up to 1/2" (12.7mm). | 0.6 | 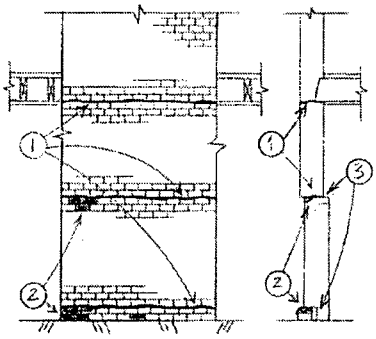 |

## 1.4 Research Objectives and Scope

This study focuses on the out-of-plane response of clay-brick multi-wythe URM walls typically used in turn-of-the-century school buildings in southwest British Columbia. These buildings are located on very dense or stiff soil sites (sites C and D based on NBCC 2005). Typically these multi-storey buildings have concrete diaphragms, therefore, limited amplitude increase of the ground motion to the upper stories can be assumed. The quality of construction, including the ability of the collar joints between the wythes to maintain composite action during out-of-plane response, is very difficult to assess for the existing structures. Given the limited number of tests on clay-brick multi-wythe walls discussed in the literature, it is not possible to determine the sensitivity of the out-of-plane response to soil conditions, local seismicity, and wall construction quality. This testing program will, therefore, include shake table tests designed to address these issues and assess the need for retrofit measures for walls adequately anchored to the diaphragms.

As FEMA 356 is the guideline used in current engineering practice, the observed results will be compared to the specified *h/t* criteria in order to determine if the guideline is over/under conservative. As the connection to the top of the URM wall is crucial in the out-of-plane stability of URM walls, simple analytical techniques are reviewed and developed, giving a practicing engineer tools to calculate dynamic reaction forces. As there are questions regarding the validity of the assumption of using a simple oscillator with damping to model the dynamic out-of-plane behaviour of a cracked wall, the tests results will be compared to those obtained using a previously developed SDOF numerical model and to a model based on rigid body dynamics.

# 2 GROUND MOTION SELECTION

## 2.1 Ground Motion Selection Methodology

A nonlinear-elastic SDOF model, developed at the University of Adelaide [Doherty, 2000], was used to estimate the post-cracking rocking behaviour of the unreinforced masonry walls, and to aid in the selection of suitable ground motions to be used in the full-scale dynamic tests. The program, ROWMANRY, performs non-linear dynamic analysis on a SDOF system with the relevant degree of freedom being the displacement at the mid-height of the wall. Thus the cracking of the wall is assumed to occur at that height. As the wall is subjected to a specified ground motion, the program calculates the displacement, velocity and acceleration time-histories at the mid-height of the wall. The stiffness utilized is based on the nonlinear-elastic force-displacement relationship shown in Figure 2.1, where $\Delta_1$ and $\Delta_2$ are selected based on the level of damage at the crack. The unreinforced clay brick masonry walls were modeled with no overburden, and the reaction at the top and bottom of the wall was assumed to be at the leeward face. The point of instability, $\Delta_{Instability}$, was taken as the width of the wall, as this is the point when the resultant of the weight of the upper portion of the wall is outside the wall width and the system becomes unstable (Figure 1.4).

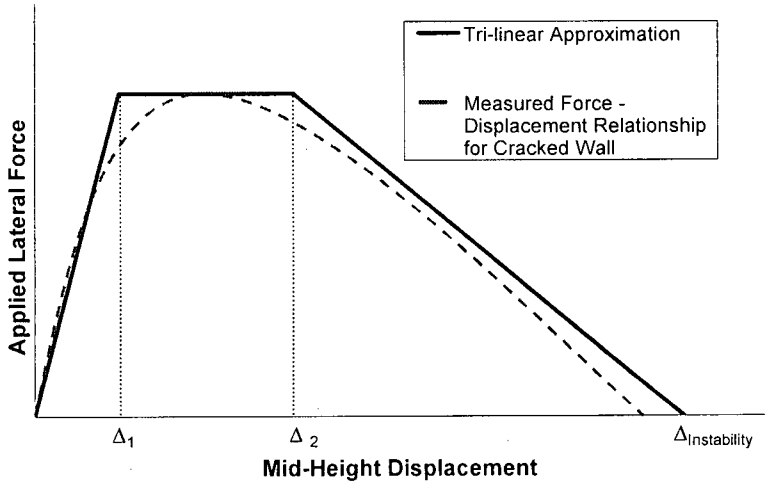


**Figure 2.1 Tri-linear Stiffness Model**

[adapted from Doherty, 2000]

Rayleigh damping was incorporated into the model with 5.9% of critical damping at a period 0.5s and 8.9% at 1.0s. The analysis was conducted assuming a moderate level of damage in the wall, which defines $\Delta_1/\Delta_{Instability}$ as 13% and $\Delta_2/\Delta_{Instability}$ as 40% [Doherty, 2000]. This model was calibrated based on the results of dynamic shake table tests on single-wythe walls. Further details on the equations of motion used and modeling procedure can be found in Griffith et al. [2003]. Results from the current study will enable verification of the model for three-wythe clay-brick walls.

A parametric study was undertaken for the purpose of evaluating the sensitivity of the out-of-plane response to the site conditions and for selecting the ground motions for the dynamic testing of the unreinforced clay-brick masonry walls. The suite of ground motions used in the study consisted of 80 records from various soil conditions; 20 ground motions from each of site class B (760 m/s < shear wave velocity ($V_s$) $\leq$ 1500 m/s), site class C (360 m/s < $V_s$ < 760 m/s), site class D (180 m/s < $V_s$ < 360 m/s) and site class E ($V_s$ < 180 m/s). A response spectrum was generated for each of the ground motions and compared to the appropriate Uniform Hazard Spectrum (UHS) for Vancouver from the proposed 2005 National Building Code of Canada [Adams and Atkinson, 2003]. The ground motion spectra were then scaled to match the UHS in the period range of 0.5 seconds to 1.0 seconds, as this was the anticipated period range of the cracked walls [Doherty, 2000] and the spectral acceleration at 1.0s is used to determine the allowable *h/t* ratio as per FEMA 256 [ASCE, 2000].

Analyses were conducted with the amplitude of each ground motion scaled from 0.10 to 2.50 of the NBCC level at 0.01 increments. The maximum mid-height displacement from each analysis was recorded. Figure 2.2 shows a plot of the maximum mid-height displacement vs. scaling factor for three ground motions from site classes C, D and E.

An instability factor was defined as the amount that the NBCC code scaled ground motion had to be multiplied by to achieve instability. The instability factor was determined for each of the 80 ground motions used in the study. After removing records which needed to be scaled by a factor greater than 7 to match the UHS, the distribution of scaling factors was plotted and can be seen in Figure 2.3. These values show that the soil conditions play a significant role in determining the stability of the wall. With the increased level of displacements seen in softer soil conditions, the average instability factor decreased from 2.09 for site class B to 0.98 for site class E.

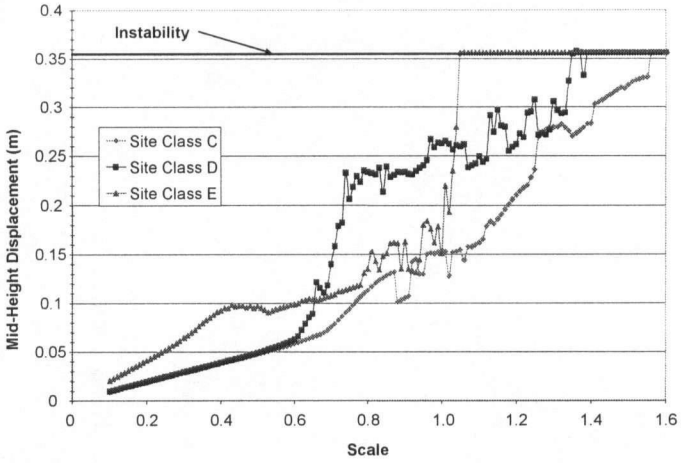


**Figure 2.2 Peak Mid-Height Displacement vs. Ground Motion Scaling**

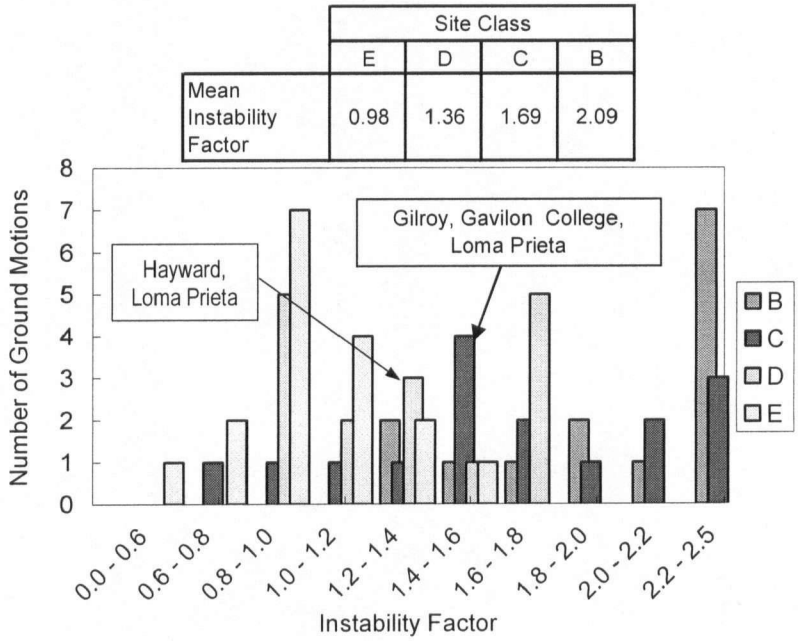


**Figure 2.3 Distribution of Instability Factors**

## 2.2 Ground Motions Used in Testing Program

Three ground motions were used for the shake table testing program. Two were crustal earthquake ground motions and one was a subduction earthquake. The first crustal strong motion was recorded on firm ground (site class C) in Gilroy, California during the 1989 Loma Prieta Earthquake and has an instability factor of 1.52. When scaled to the UHS, this record has a PGA of 0.93g (Figure 2.4) and a PGD of 6.60cm and $S_a(1.0)$ = 0.35g. The second crustal strong

motion was recorded on softer ground (site class D) in Hayward, California during the 1989 Loma Prieta Earthquake, and had an instability factor of 1.33. When scaled to the UHS, this record has a PGA of 0.79g (Figure 2.5) and a PGD of 5.35cm and $S_a(1.0)$ = 0.47g. As the British Columbian coast is susceptible to a mega thrust subduction event, a subduction earthquake recorded on a site class D soil from the September 26, 2003 Tokachi-oki, Japan (HKD 109) earthquake was also used. This record has a PGA of 0.63g (Figure 2.6) and a PGD of 11.2cm and $S_a(1.0)$ = 0.25g. The subduction record was not scaled to the UHS. Spectras of the ground motions can be found in Figure 2.7 through Figure 1.1. It should be noted that the motions shown below are the recorded table motions (observed in the tests), and are based on the selected ground motions.

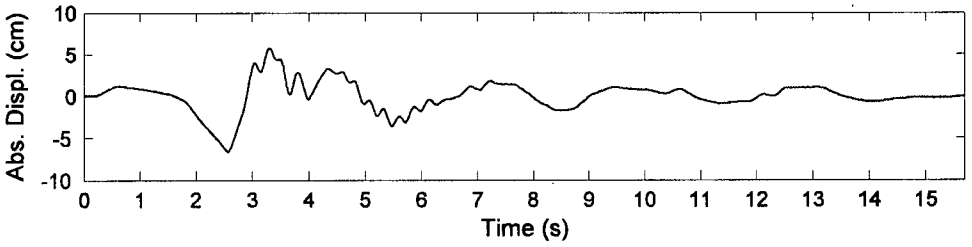


**Figure 2.4 Gilroy Ground Motion (Site Class C), Scaled to UHS**

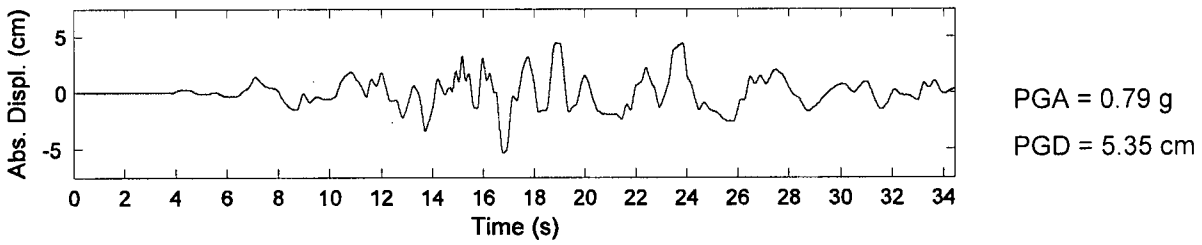


**Figure 2.5 Hayward Ground Motion (Site Class D), Scaled to UHS**

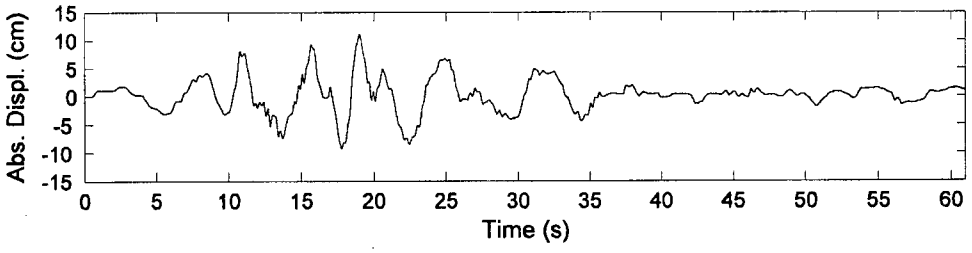


**Figure 2.6 Tokachi-oki, Japan (HKD 109) Ground Motion (Subduction Site Class D)**

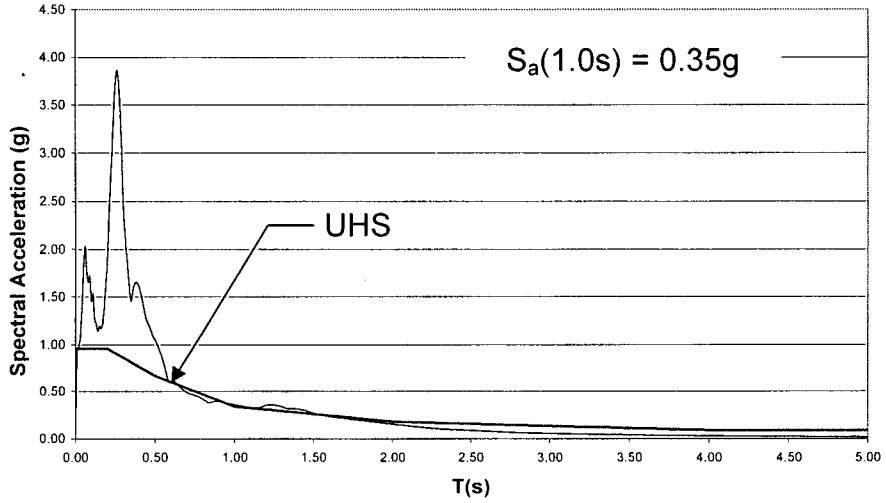


**Figure 2.7 Gilroy Spectra, Scaled to UHS Between 0.5-1.0s**

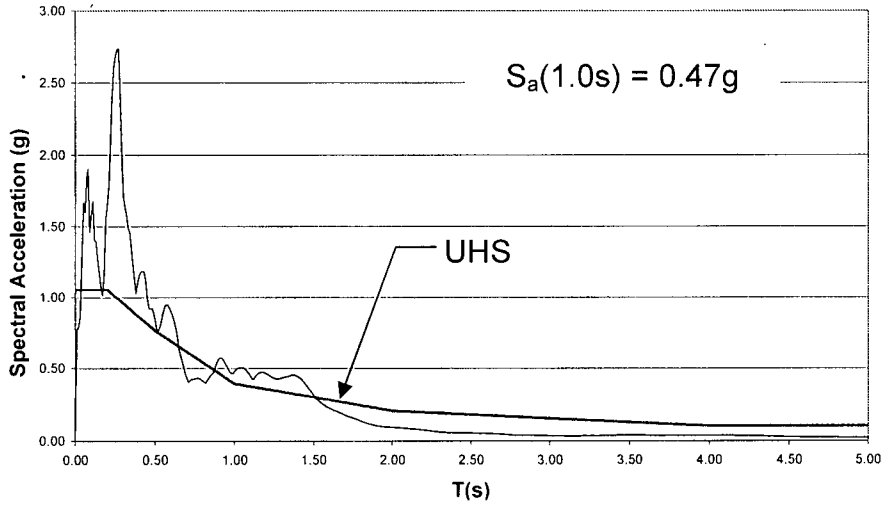


**Figure 2.8 Hayward Spectra, Scaled to UHS Between 0.5-1.0s**

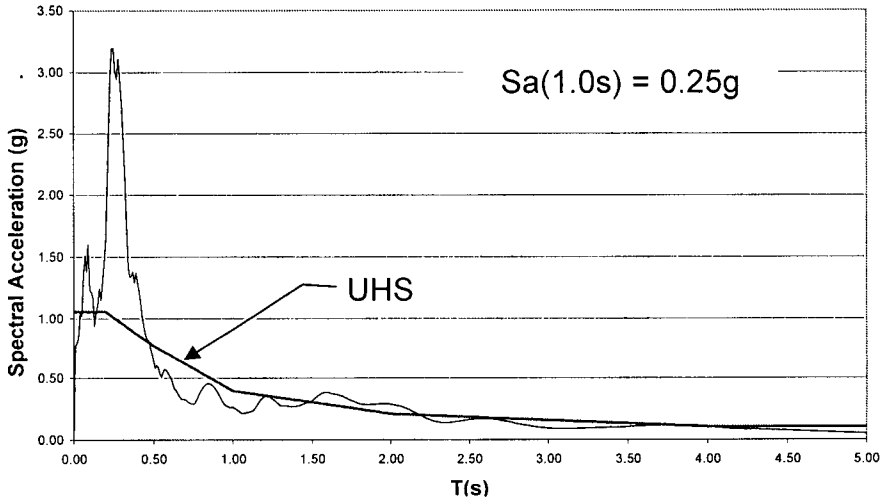


**Figure 2.9 Tokachi-oki, Japan (HKD 109) Spectra**

# 3 EXPERIMENTAL PROGRAM

## 3.1 Introduction

In order to observe the dynamic out-of-plane behaviour of simply supported URM walls with varying construction quality and soil properties, a series of shaking table tests were conducted on the earthquake simulator in the Earthquake Engineering Research Facility, at the University of British Columbia. This chapter provides an overview of experimental set-up, design and construction of the URM walls, instrumentation, and testing procedure. More details can be found in Appendices A through D.

### 3.1.1 URM Wall Specimen Design and Construction

Specimens were intended to represent a portion of the top storey of an early 1900's URM School building in British Columbia (Figure 3.1), including mortar quality and construction methods. The typical upper storey height of these buildings is 4.25m, with the load bearing URM wall being 3 wythes wide with common/American running bond and header at every sixth coarse. An example elevation can be seen in Figure 3.2.

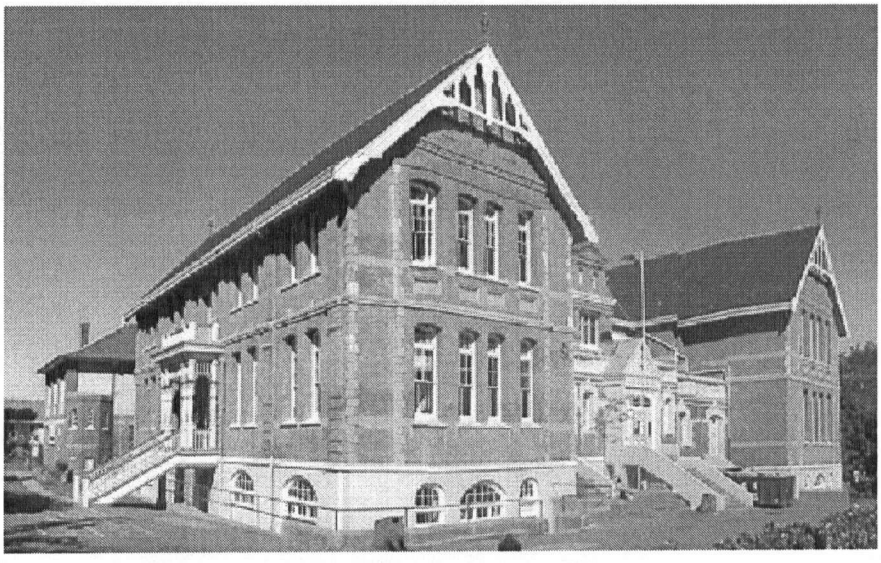

**Figure 3.1 Example of a URM School in British Columbia**

[Taylor, 2004]

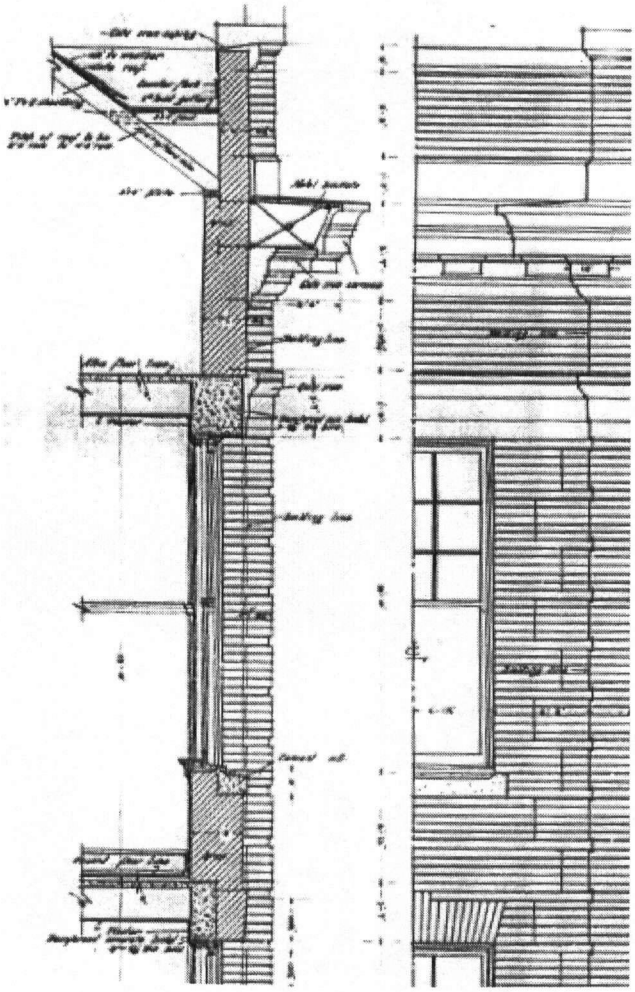

**Figure 3.2 Typical Elevation of the Upper Storey of a URM School Built in the Early 1900's**

Four three-wythe wall specimens were constructed. As there has been little research into how the quality of the collar joints (Figure 3.3) affects the wall behaviour, two of the walls were constructed with poor collar joints and two with good collar joints. The walls were 1.5m wide and 4.25 m high ($h/t$ = 12). American bond, with a header coarse at every sixth coarse, was used for all specimens (Figure 3.4).

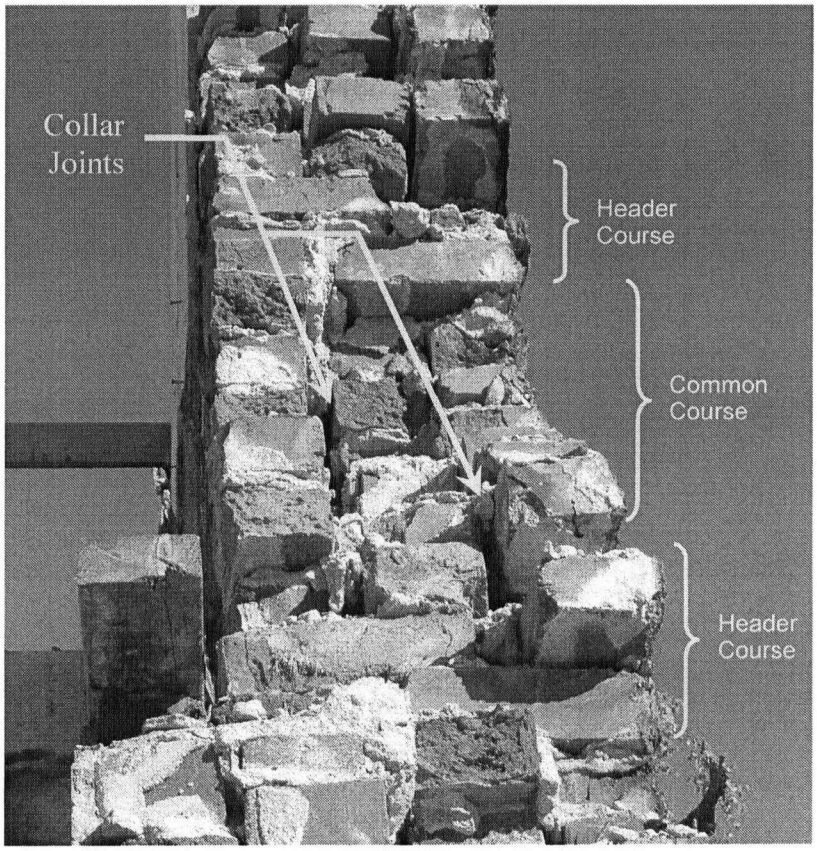


**Figure 3.3 Example of a Poor Quality URM Wall**

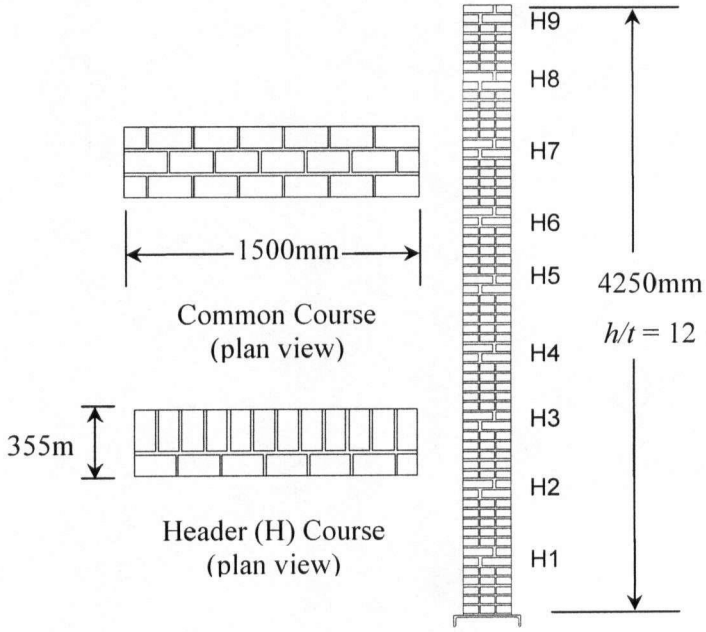


**Figure 3.4 Wall Dimensions**

URM school buildings built in the 1900's were typically built with better quality and care compared to other URM construction, such as industrial buildings, during that era [Zirpke, 2004]. Some of the weak mortars and poor brick laying observed in older construction are not as evident in older school construction. To match the existing mortar quality of existing URM buildings, Type O mortar was considered appropriate, due to its high lime content and relatively low compressive strength. The mortar was batched mixed off site at a Portland cement plant and delivered to the laboratory at UBC in mortar tubs with a cement retardant to slow down the setting of the mortar. To further represent the deterioration of mortar in existing buildings, the brick units were placed dry, thereby allowing the water to migrate quickly from the mortar to the brick unit causing the cement to not hydrate fully, resulting in reduced bond strength [Abrams, 2000]. Brick units used were solid, compressed, fired clay and measured 60x110x220 mm, slightly larger to those found in historic schools (60x114x220 mm).

As the expected rigid body rocking behaviour is dependent on the integrity of the URM wall, two types of collar joints were used to provide bounds on construction variability:

a) Poor quality collar joint

b) Good quality collar joint

The poor quality collar joints were made by using a light bed of furrowed mortar, laying the outer two wythes first, followed by the inner wythe. The collar joints were not slushed by the mason, but mortar was able to fall into the joint once the next course was laid. The good quality collar joints were made by placing a heavy bed of furrowed mortar, then laying the outer two wythes first, the inner wythe was pushed and slid into place to allow the mortar to rise-up and fill the collar joint. The collar joint was then slushed by the mason to fill the remaining void space. In both cases, the header bricks were buttered with mortar on 2/3 of the brick's face. The mortar bed joints for both walls were approximately 13mm thick. The construction sequence for the common and header course for both the poor and good quality collar joints are shown in Figure 3.5. Two professional masons were employed to construct the walls, each working on one type of wall, thereby making the walls consistent in construction quality.

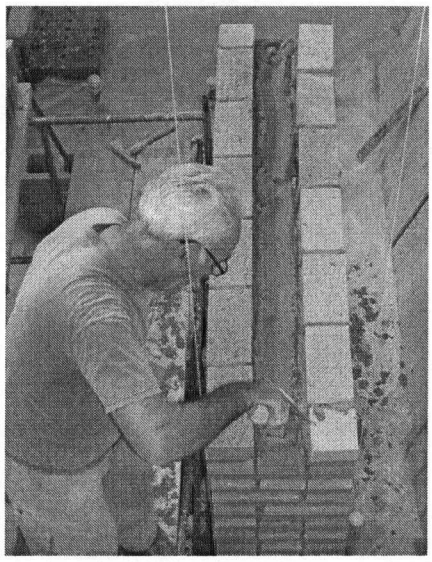

(a) Outer two wythes laid first (note mortar bed being furrowed).

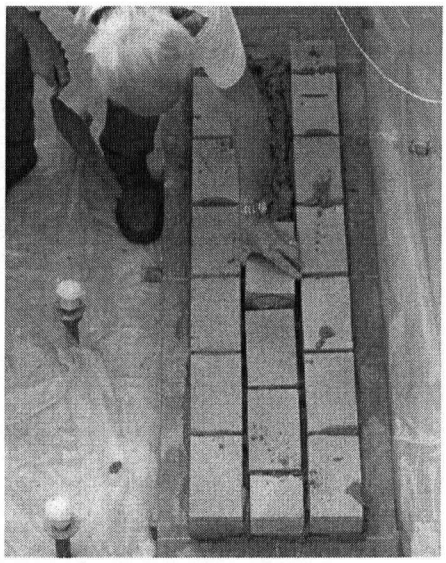

(b) Inner wythe bricks laid (note brick being pushed into place for good quality collar joint).

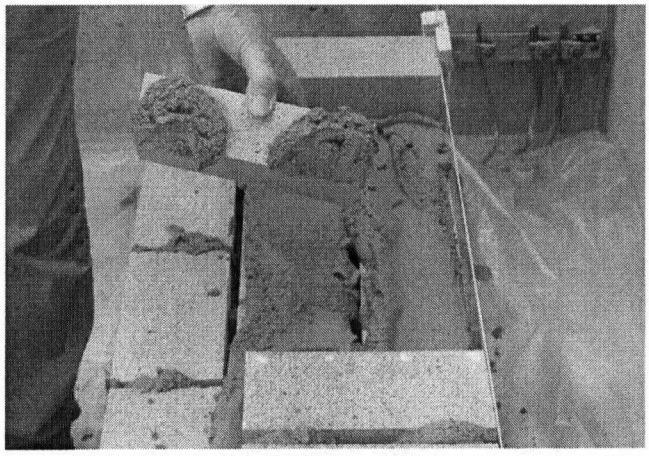

(c) Header course with brick being laid with mortar buttered onto 2/3 of the brick edge.

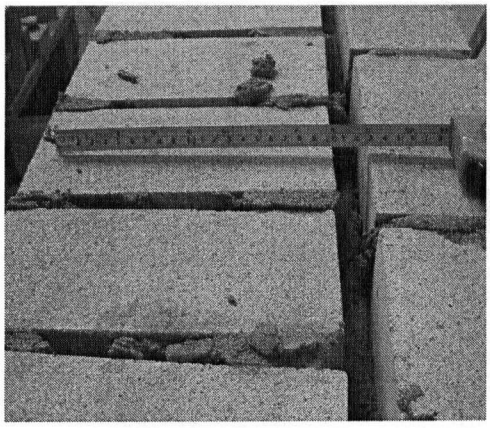

(d) Poor quality header (note collar joint is not slushed).

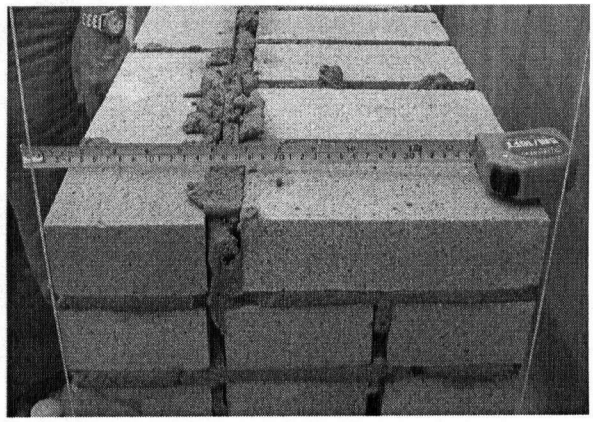

(e) Good quality header (note collar joint is slushed full).

**Figure 3.5 Construction Sequence of URM Walls**

The walls were constructed and cured under dry conditions in the laboratory (Figure 3.6). The average density of the walls was 1837 kg/m$^3$. This was measured by weighing the walls before testing, and weighing a representative sample of the broken wall after testing. In this way, mortar that partially filled the collar joints is taken into account. The mass, density, and geometry can be found in Appendix B. Before testing, the walls were painted white to help locate cracks.

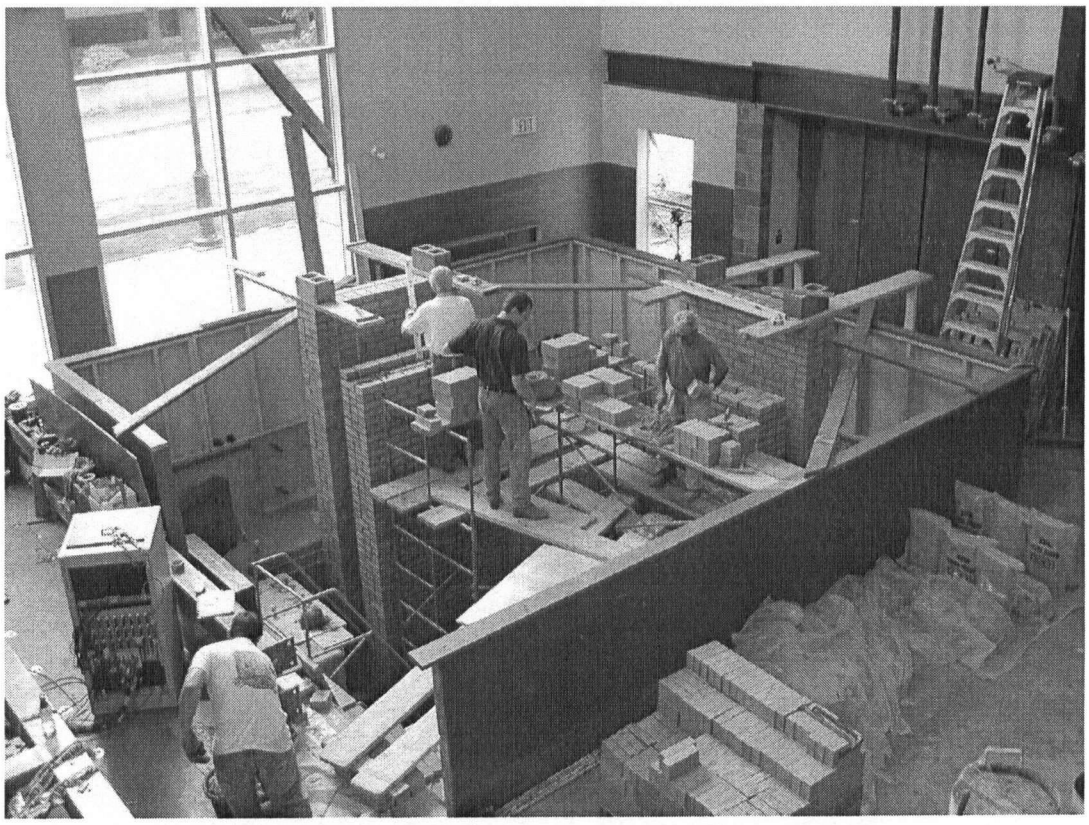

**Figure 3.6 URM Walls Under Construction**

In order to move the specimens onto the shake table, the walls were built on top of a steel channel section. A lifting beam was then lowered and placed on the top of the wall, and threaded rods were installed near the four corners of the wall. The rods were then tightened, placing a vertical compressive load onto the wall. The wall was then lifted using an overhead crane attached to the lifting beam, thereby lifting the wall from the base, and keeping the wall stable during transport (Figure 3.7). No cracking was observed in the walls due to transport.

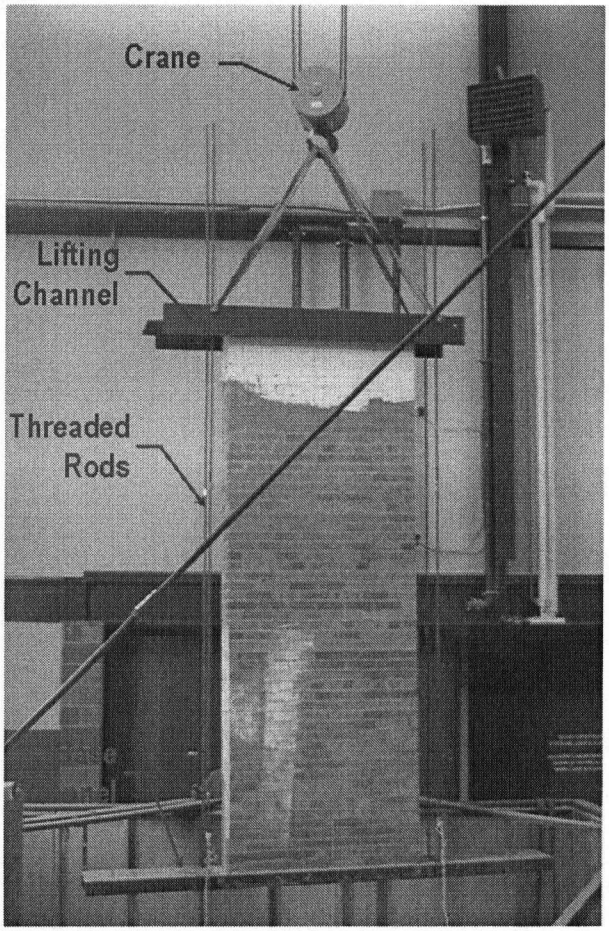


**Figure 3.7 Wall Lifting Apparatus**

## 3.2 Material Tests

During the construction of the walls, samples were made for material testing from each mortar batch by the masons. The samples were stored in the lab near the URM walls, but were covered with polyethylene plastic sheets while they were curing. On average, the material tests were performed approximately 12 months after the walls were constructed, 4.5 months after the walls were tested. As the URM walls were allowed to cure for a long duration, 7.5 months before testing, it is assumed that the material tests performed after the wall test will give a good indication of the wall properties, as the properties would not be expected to change significantly after two months of curing. These tests were performed to provide an indication of the quality of masonry tested and to obtain material properties, such as masonry flexural and compressive strength. Details of the material tests can be found in Appendix A.

### 3.2.1 Mortar Properties

As previously mentioned, Type O mortar was used. Mortar compression tests were performed as per the Canadian Standards Association (CSA) A179-04 [CSA, 2004], on 50 mm cubes. The mortar cubes had a mean compressive strength of 6.14 MPa, and stiffness of 26700 N/mm. Results are shown in Table 3.1, and the typical failure mechanism is shown in Figure 1.1. The compressive strength of the mortar is higher than the specified 28 day strength of 2.0 MPa. Further details can be found in Appendix A.1.

**Table 3.1 Mortar Properties**

| **Mortar Type:** | O | |
|---|---|---|
| **Mix Design:** | 1 Portland Cement : 2 Lime : 9 Sand | |
| **Compression Properties:** | $f_c$ (MPa) | $E_{elastic}$ (N/mm) |
| Mean | 6.14 | 26700 |
| Standard Deviation | 0.39 | 7480 |
| Sample Covariance | 0.06 | 0.28 |

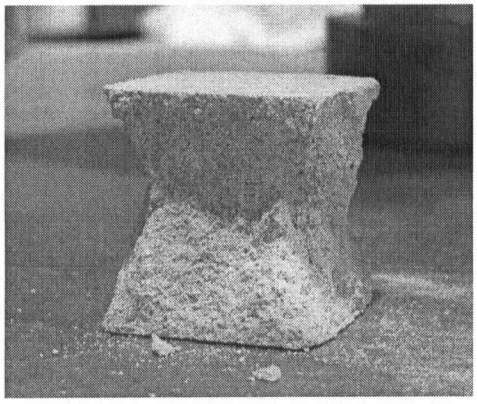

**Figure 3.8 Typical Mortar Cube Failure**

### 3.2.2 Brick Unit Properties

Both absorption and compression tests were performed as per CAN3-A82.2-M78 (R2003) [Canadian Standards Association (CSA), 2003] on the solid brick units, (length ($l$) = 220, width ($w$) = 110, thickness ($t$) = 60mm), in order to get an indication of quality control. During the compression tests, the brick specimens were initially tested flat, (i.e. $Area = l \times w$), but failure did not occur as the specimen height was not high enough to form a failure plane. Therefore, the bricks were tested on their edge, (i.e. $Area = l \times t$). This can be considered equivalent as the

bricks are solid and homogeneous. They had a mean compressive strength of 15.38 MPa, and elastic stiffness of 242000 N/mm. The brick units had a mean 24 hour submersion absorption of 9.81%, and 5 hour boiling absorption of 10.76%. Results are shown in Table 3.2, and the typical compressive failure mechanism is shown in Figure 3.9. Further details can be found in Appendix A.2-3.

**Table 3.2. Brick Unit Properties**

| **Brick Type:** | Solid compressed fired clay | |
|---|---|---|
| **Dimensions:** | 220x110x60mm (solid) | |
| **Absorption Properties:** | 24 hr. Submersion (%) | 5 hr. Boiling (%) |
| Mean | 9.81 | 10.76 |
| Standard Deviation | 0.65 | 0.56 |
| Sample Covariance | 0.07 | 0.05 |
| **Compression Properties:** | $f_b$ (MPa) | $E_{elastic}$ (N/mm) |
| Mean | 15.4 | 242000 |
| Standard Deviation | 3.85 | 75000 |
| Sample Covariance | 0.25 | 0.31 |

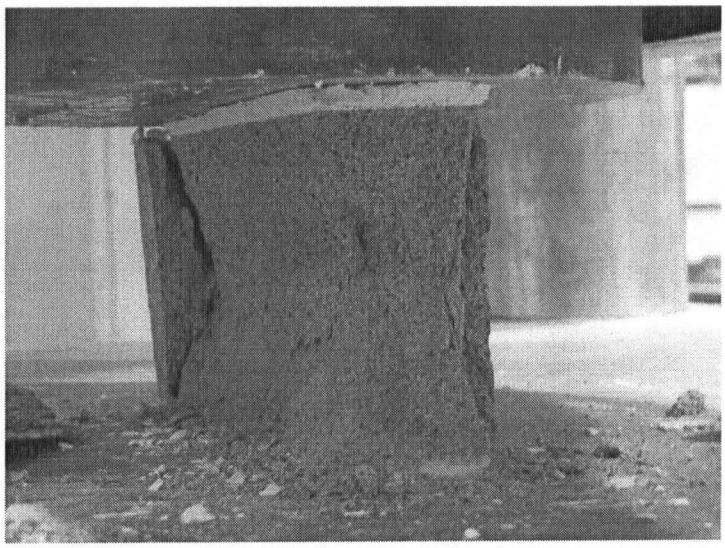

**Figure 3.9 Typical Brick Unit Compression Failure**

### 3.2.3 Masonry Unit Properties

In order to determine the compressive strength of the masonry, masonry prisms constructed from each mortar batch were tested as specified in CAN/CSA-A369.1-M90 (R2001) [CSA, 2001]. Peak compressive strengths were corrected to take into account the prisms' *h/t* ratios. The

samples had a mean compressive strength of 13.0 MPa. Results are shown in Table 3.3, and the typical failure mechanism is shown in Figure 3.10.

To estimate the flexural strength of the masonry, the bond wrench method was used as per ASTM C1072-00a [American Society for Testing and Materials (ASTM), 2000]. Samples were constructed from each of the mortar batches, and had a mean flexural strength of 0.424 MPa. Results are shown in Table 3.3, and the typical failure mechanism is shown in Figure 3.11. Note that all failures occurred at the brick-mortar interface.

**Table 3.3. Masonry Unit Properties**

| **Masonry Prism Compressive Strength:** | $f_m$ (MPa) | $E_{elastic}$ (N/mm) | $E_{modulus}$ ($N/mm^2$) |
|---|---|---|---|
| Mean | 13.0 | 234000 | 2110 |
| Standard Deviation | 2.46 | 75900 | 626 |
| Sample Covariance | 0.19 | 0.32 | 0.30 |
| **Bond Wrench Flexural Strength:** | $f_f$ (MPa) | | |
| Mean | 0.424 | | |
| Standard Deviation | 0.146 | | |
| Sample Covariance | 0.345 | | |

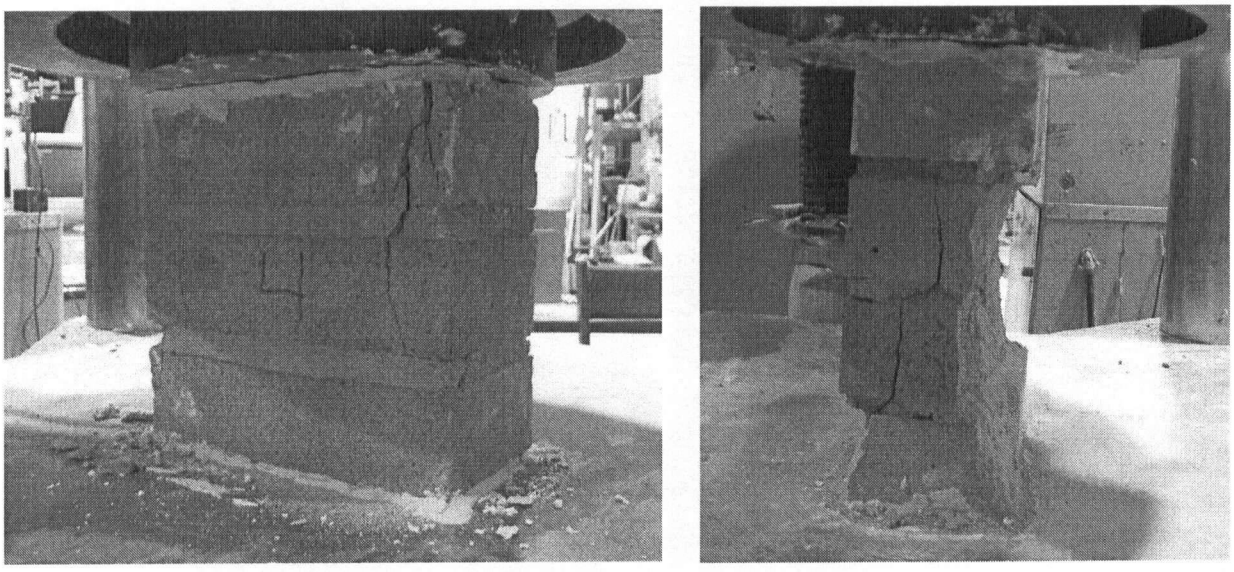

**Figure 3.10 Typical Masonry Unit Compression Failures**

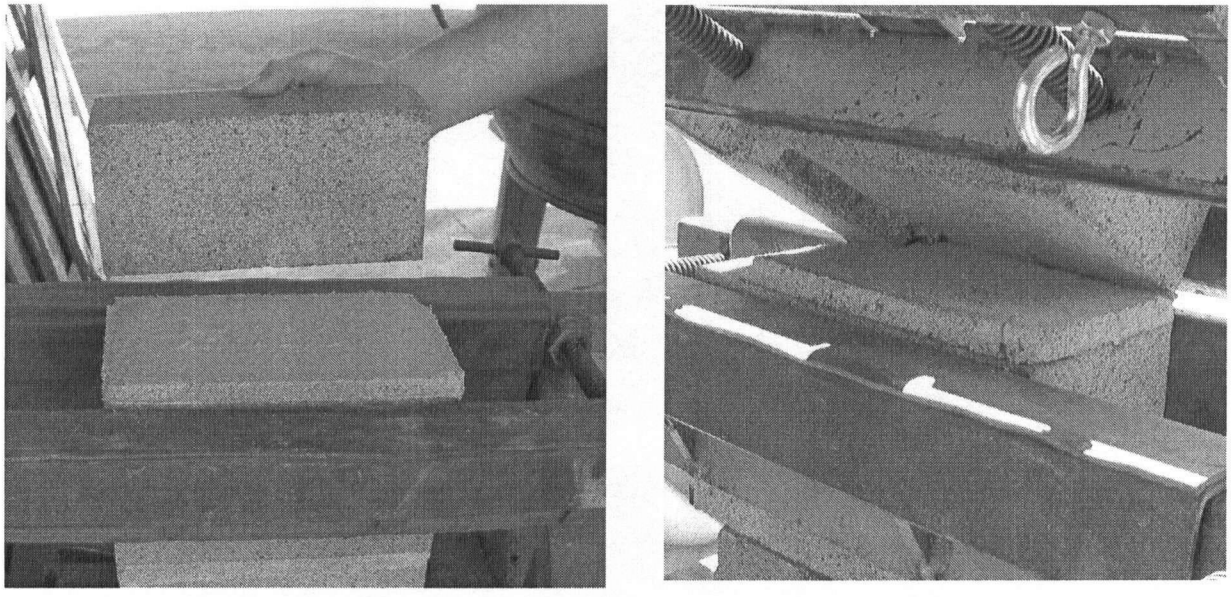

**Figure 3.11 Typical Masonry Bond Wrench Flexural Failure**

FEMA 356 gives default property values for masonry construction based on the observed masonry condition (Table 3.4). For a good quality wall, the compressive strength is specified as 6.21 MPa, and a flexural tensile strength of 0.14 MPa. The mean measured compressive and flexural tensile strengths are significantly greater than the FEMA 356 recommendations, which is not surprising as they are conservative lower-bound estimates that are to be used if no material tests are performed on a portion of the structure. However, the FEMA 356 values for good quality masonry compare well to the test's 5$^{th}$ percentile values; compressive strength of 8.08 MPa, elastic modulus of 858 MPa, and flexural tensile strength of 0.132 MPa.

**Table 3.4 Default Lower-Bound Masonry Properties**

[ASCE, 2000]

| | Masonry Condition | | |
|---|---|---|---|
| **Property (MPa)** | **Good** | **Fair** | **Poor** |
| Compressive Strength ($f'_m$) | 6.21 | 4.14 | 2.07 |
| Elastic Modulus in Compression ($550f'_m$) | 3416 | 2277 | 1139 |
| Flexural Tensile Strength | 0.14 | 0.07 | 0 |

## 3.3 Experimental Set-up

### 3.3.1 Shake Table

The testing of the URM walls took place on the single degree of freedom shake table at the UBC Earthquake Engineering Research Facility. This shake table was custom designed for a full-scale two-storey house test [Kharrazi, 2001], and was modified for the URM wall tests. The table consists of a 7.5 x 6.0m frame made of hollow steel sections mounted on low friction rollers. The table is controlled by a single hydraulic actuator located at the centre of the frame.

The shake table is powered by a 0.35 $m^3$/min pump that can supply 19.9 MPa of hydraulic pressure. Accumulators are attached to the hydraulic lines near the actuator to absorb some of the shock loading that occurs during dynamic testing. The actuator has a maximum displacement of ± 457 mm, and a static capacity of 298 kN. The table is displacement controlled. Hydraulic pressure, which controls the displacement position of the table, is electronically controlled by a positive feedback Proportional Integral Derivative (PID) MTS servo-controller. A command signal is sent to the servo-controller, which then sends a signal to a MOOG hydraulic proportional servo valve, thereby regulating the hydraulic pressure. The table position is feedback to the servo-controller by an MTS Temposonic displacement transducer. The command signal is generated using a PC, which is then amplified and sent to the servo-controller. The PC uses the DasyLab program to generate earthquake output signals. The displacements from a given signal are normalized as voltages. [Turek, 2002]

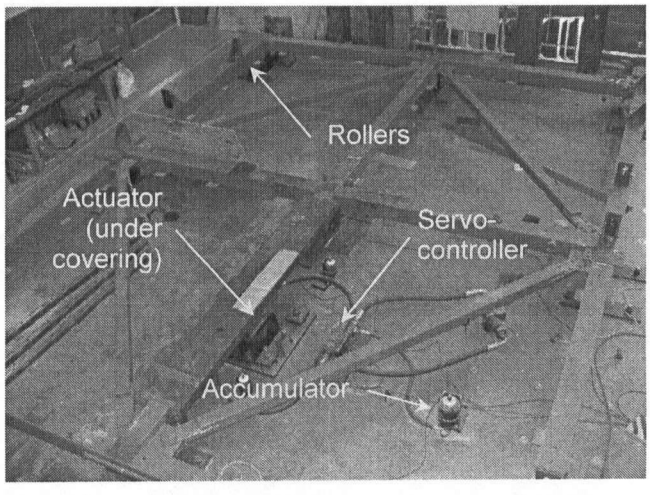


**Figure 3.12 Shake Table**

### 3.3.2 Support Frame

To provide representative boundary conditions of a simply supported URM wall, a braced steel frame was attached to the table (Figure 3.13, Appendix C). The stiffness of the braced frame was designed to represent, as closely as possible, a building system with URM shear walls and stiff concrete diaphragms. It was assumed that a URM building with this type of structural system provide equal and in phase input motions at the base and top of the wall. This is not the case, however, where the floor diaphragms are flexible (e.g. timber floor systems). In this situation, there may be different input motions at the base and top of the wall [Simsir, 2004], and is beyond the scope of this study. Equal and approximate in-phase input motions at the base and top of the wall were confirmed by comparing the absolute displacements of the table and top of the braced frame for each dynamic test, and showed close agreement (Figure 3.14).

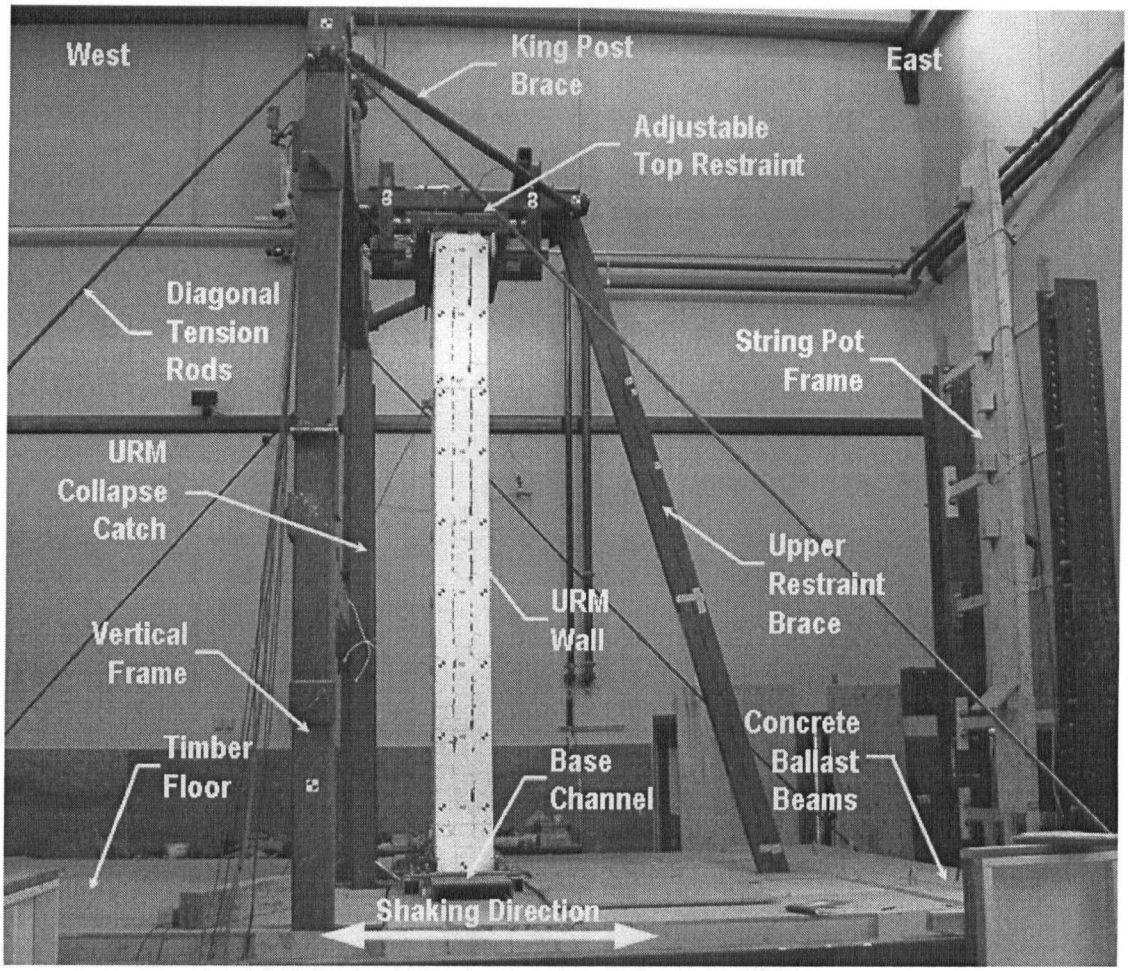


**Figure 3.13 Experimental Set-Up**

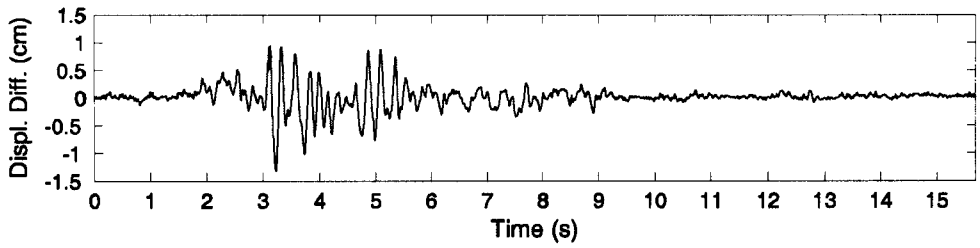


**Figure 3.14 Typical Example of the Error in Input Motion at the Top and Base of the Wall**

To achieve the required stiffness, it was necessary that the frame be adequately braced (Figure 3.13). To counteract potential uplifting of the shake table from the applied forces of the braced frame, concrete ballast beams were attached at the ends and centre of the table. These concrete ballast beams also helped to stiffen the shake table in the direction of motion. Diagonal, high strength threaded rods were attached to the upper portion of the vertical frame and far corners of the shake table. These rods were then pre-tensioned to ensure that inertial forces from the wall and top restraint would be transferred to the shake table with no slack in the upper portion of the frame (i.e. in-phase with the table). The diagonal rods had to be pre-tensioned enough to remove any sag due to their self-weight, but not be over pre-tension as to cause too much vertical reaction at the table ends, which could lead to table uplift during the test. The pair of rods on both the east and west side had to have the same pre-tension, otherwise, there could be the possibility of an undesirable torsion load being applied during the test. In order to obtain the correct pre-tension in all the rods, an accelerometer was attached to the rods and their natural frequencies were determined. The rods were then tensioned (i.e. 'tuned') until there natural frequencies matched. The frequency of the rods is proportional to the square root of the tension in the rods, and an estimate of the natural frequency can be expressed as:

$$f = \frac{1}{3L\sqrt{\mu}}\sqrt{T} \tag{3.1}$$

Where, $f$ = Fundamental frequency,

$L$ = Length of the rod,

$\mu$ = Linear density,

$T$ = Tension in the rod

To stiffen the top restraint, a king post brace and upper restraint brace were used (Figure 3.13). The stiffness of the frame was determined by attaching a load cell and come-along pulley in series to the top restraint and stiff columns connected to the lab's strong floor. The pulley was tightened and displacements at the top restraint were measured, resulting in a stiffness of 2960 N/cm (Appendix C.5).

To satisfy varying wall *h/t* ratios and inconsistencies in specimen dimensions, both the top and bottom connections were adjustable. The URM wall was attached to the shake table by 'keying' the channel in between two HSS sections rigidly connected to the table. An adjustable base connection was then installed that prevented horizontal movement, but allowed for rotation and vertical displacement at the wall base via a stiff rubber spacer (Figure 3.15). The base connection was installed snuggly to the wall; however, to ensure minimal bearing friction the connections were not over tightened. Before testing, the connection was tack welded to ensure that it did not slip during the tests.

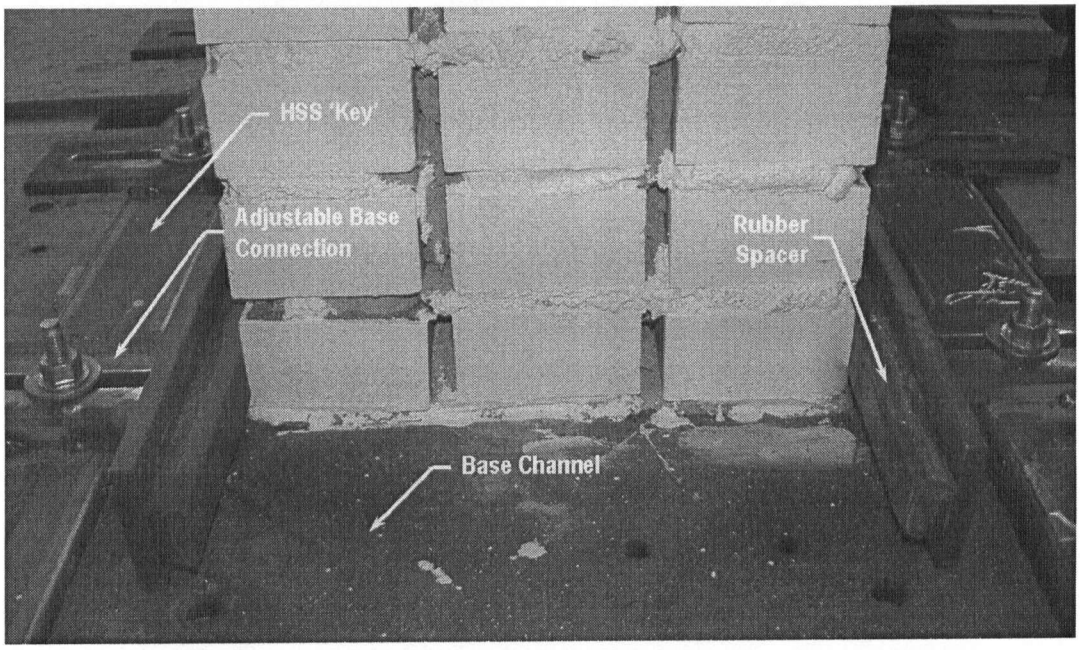


**Figure 3.15. Base Connection**

The top restraint was designed to be adjustable in both the horizontal and vertical directions to allow for varying wall geometry (Figure 3.16). The top restraint was designed to restrain movement in the out-of-plane direction, but allow for rotation and vertical movement of the top of the wall (Figure 3.17). The wall was restrained in the direction of the ground motion by a

steel angle. A stiff rubber spacer and an Ultra High Molecular Weight Polyethylene (UHMW) strip were attached to the wall; the angle on the restraint also had a UHMW strip. The UHMW strips are a wear resistant plastic with a low coefficient of friction and high impact strength, allowing for low friction during vertical movement of the wall. The stiff rubber spacer allows for the wall to rotate. The UHWM strips were not used for the first wall tested. During the first shake table test, it was noted that the top and upper edges of the wall bared against the top connection arm and angle (Figure 3.17) at large rotations during rigid body rocking. To prevent this contact, the upper edges of the wall were beveled, and bricks underneath the connection arm were removed (Figure 3.18). The top restraint was also designed to allow for varying floor diaphragm stiffness by the insertion of coiled springs. As previously mentioned, these series of tests considered only a rigid diaphragm so the coiled springs were replaced with steel tubing (Figure 3.17). Details of the top connection can be found in Appendix C.4.

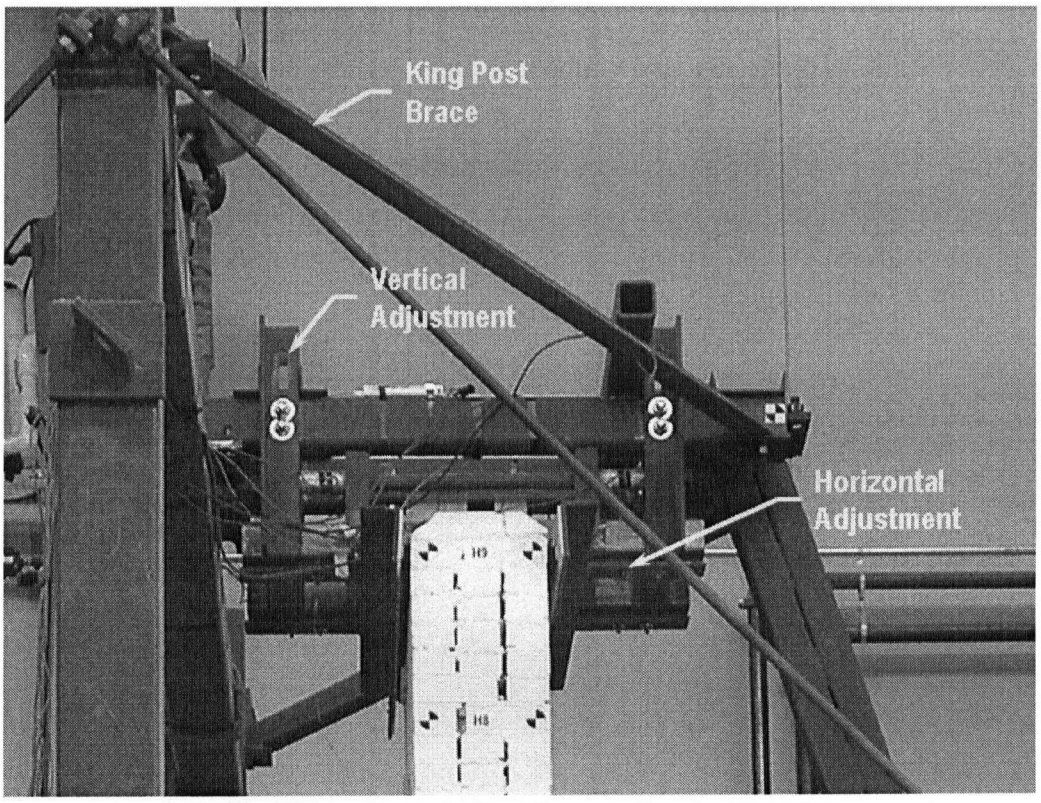


**Figure 3.16 Elevation View of Top Connection**

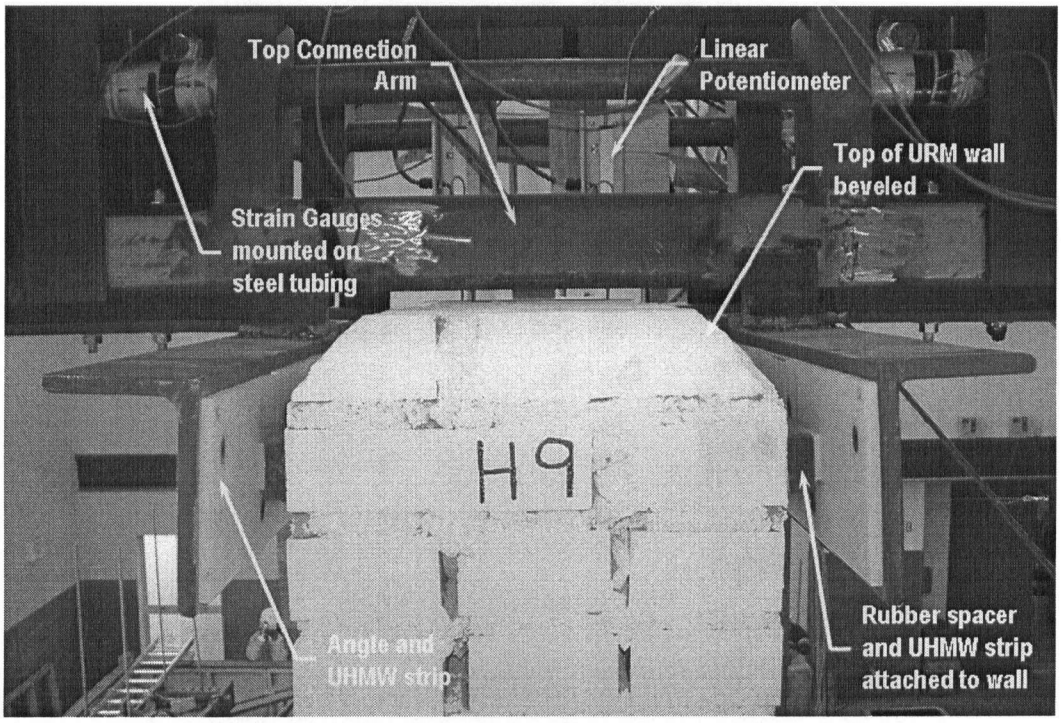


**Figure 3.17 Close-Up Elevation View of Top Connection**

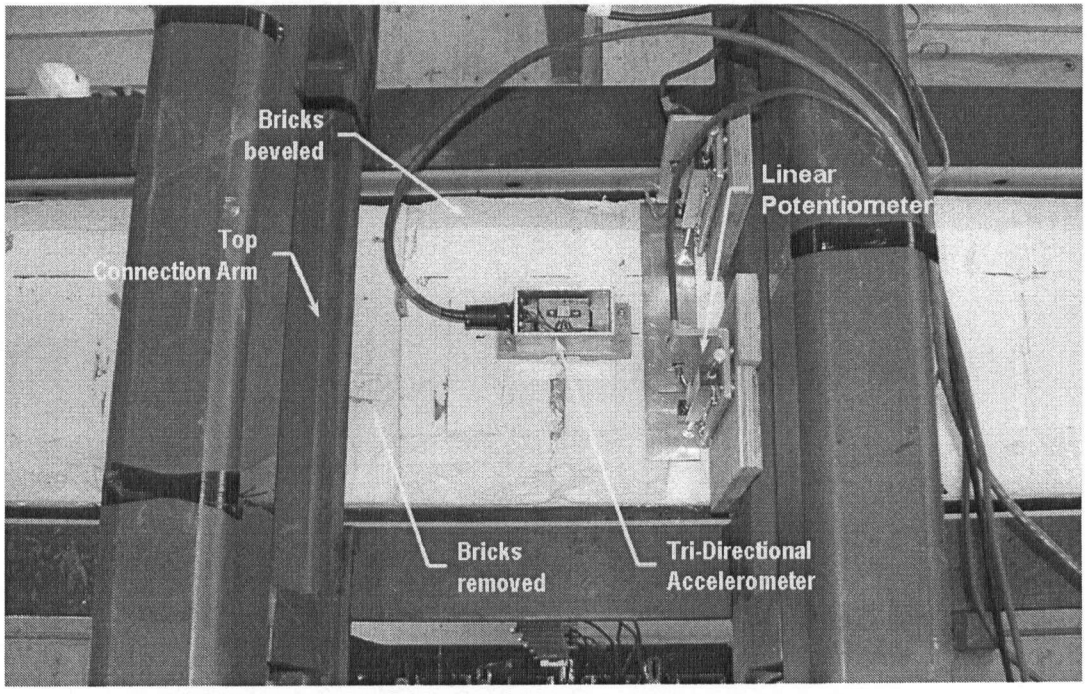


**Figure 3.18 Plan View of Top Connection**

## 3.4 Instrumentation and Data Collection

Data were recorded from 56 channels in order to observe the wall, shake table and support frame behaviour during the dynamic tests. The instrumentation consisted of force and displacement transducers, accelerometers, and strain gauges. This section summarizes the instrumentation setup. More details can be found in Appendix D.

### 3.4.1 URM Wall Instrumentation

In order to monitor the behaviour of the URM wall, accelerometers and displacement transducers were installed at each of the header courses (Figure 3.19). ICS 3022 piezo-resistive type accelerometers were used with an output range of +/-10g. The accelerometers were housed inside a steel case in order to protect them from impact of falling debris. Tri-directional accelerometers were also installed at the wall base and on the top of the wall (Figure 3.18). These tri-directional accelerometers consisted of three ICS 3026 piezo-resistive accelerometers with an output range of +/-5g mounted on an aluminum block, and are also housed in a steel case. To measure the amount that the wall lifts up during rocking, linear voltage potentiometers were installed at the top (Figure 3.18) and bottom corners of the wall. Cable-extension position transducers ('string pots') were used to measure the out-of-plane displacement of the wall (Figure 3.19). During the dynamic testing program some of the instrumentation was removed in order to prevent damage if the wall were to collapse. Locations of the instrumentation and channel listings can be found in Appendix C.

### 3.4.2 Shake Table and Support Frame Instrumentation

In order to capture the input displacements and accelerations to the URM wall, both the shake table and supporting frame were instrumented with accelerometers and displacement transducers. The shake table had an MTS Temposinic displacement transducer to measure the displacement and provide feedback of the actuator to the table control system. String pots and PCB 393A03 ICP type accelerometers with an output range of +/-5g were located at the base to measure the base input acceleration and displacement. Linear voltage potentiometers were located at the corners of the shake table and under the table at the URM wall to measure any potential rocking or uplift of the table.

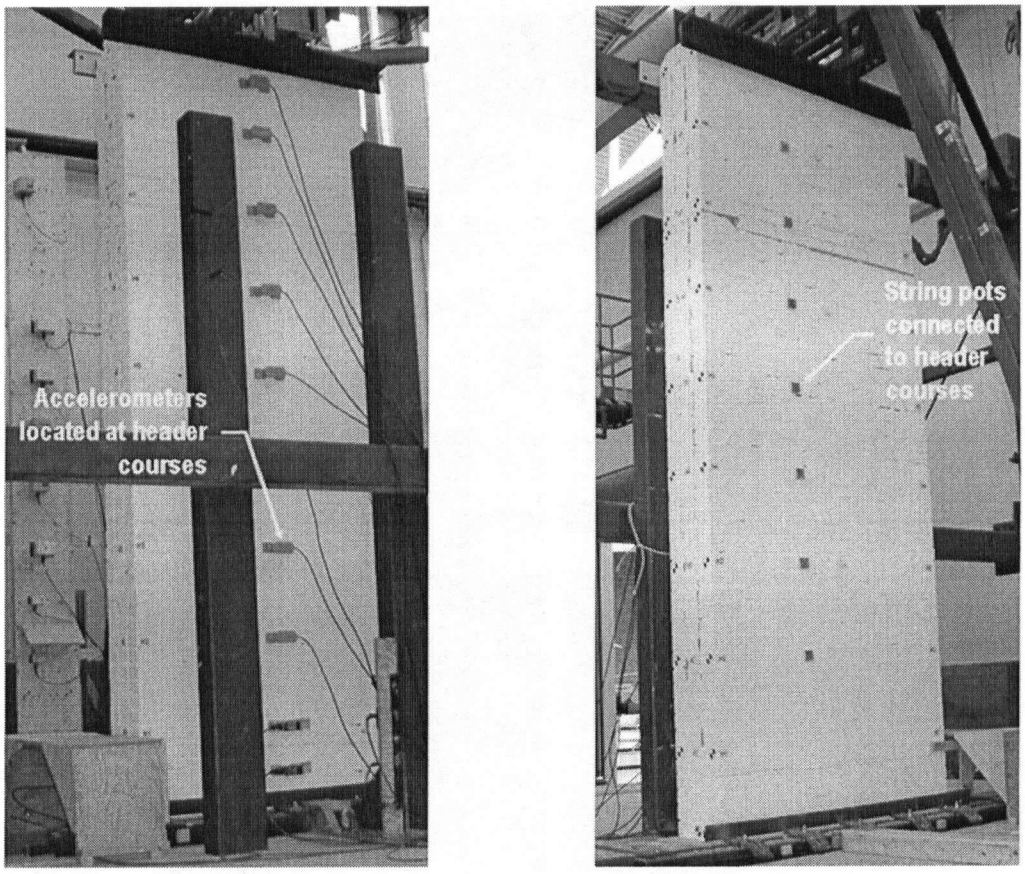


**Figure 3.19 Accelerometer and Displacement Transducer Locations on the URM Wall**

A PCB 393A03 ICP accelerometer was placed on the top and base connection to measure the input acceleration. Displacement transducers were also installed at the top of the support frame and wall base to measure the input displacement at the top and base of the wall.

### 3.4.3 Data Collection

A computer based data acquisition system using a National Instrument 16bit PCI 6052E multi-function board and a SCXI signal conditioning chassis with SCXI 1520 and 1100 modules was used. The SCXI 1520 module has a programmable filter set as a 100 Hz low pass, fourth order Butterworth filter, and was used for the accelerometers, linear voltage potentiometers, and strain gauges. The SCXI 1100 module has a 10 kHz RC filter used for the remaining instrumentation. The program DasyLab was used to acquire, control and store the data. Data were sampled at 500Hz (0.002 s).

### 3.4.4 Data Post Processing

All of the data collected during the shake table tests were post processed using MatLab scripts. In order to remove high frequency noise all channels were filtered using a low pass trapezoid filtering window. The window had a lower corner of 24 Hz and cut-off frequency of 25 Hz.

### 3.4.5 High Speed Digital Video

High speed digital video data can be used to measure displacements, velocity, and accelerations during shake table tests. It has the ability to give insight into the behaviour of a sample/system that can not be obtained through regular video and measurement techniques (e.g. linear potentiometers, string pots, and accelerometers). The use of high speed digital video data is particularly useful in destructive testing which would otherwise cause potential damage to expensive instrumentation. A Phantom v4.2 monochrome digital camera system was used during the dynamic tests. Details regarding the high speed digital video analysis can be found in Appendix I.

## 3.5 Dynamic Tests

To investigate the dynamic out-of-plane behaviour of the URM walls both, impact hammer and shake table tests were conducted. This section briefly describes the dynamic testing procedure.

### 3.5.1 Impact Hammer Tests

Before and after each shake table test, impact hammer tests were conducted on each wall in order to record the dynamic properties (natural frequencies and damping) of the wall. These tests also helped to understand how much damage has occurred in the wall after each test. Hammer tests were conducted at various locations on the wall (Headers 3, 6 and 8) in order to excite higher modes in the wall. At each header course, the hammer was swung at least 3 times (Figure 3.20), allowing sufficient time between each impact for the accelerations in the wall to dampen out. During the hammer tests, accelerations along the wall and the input force of the hammer were recorded.

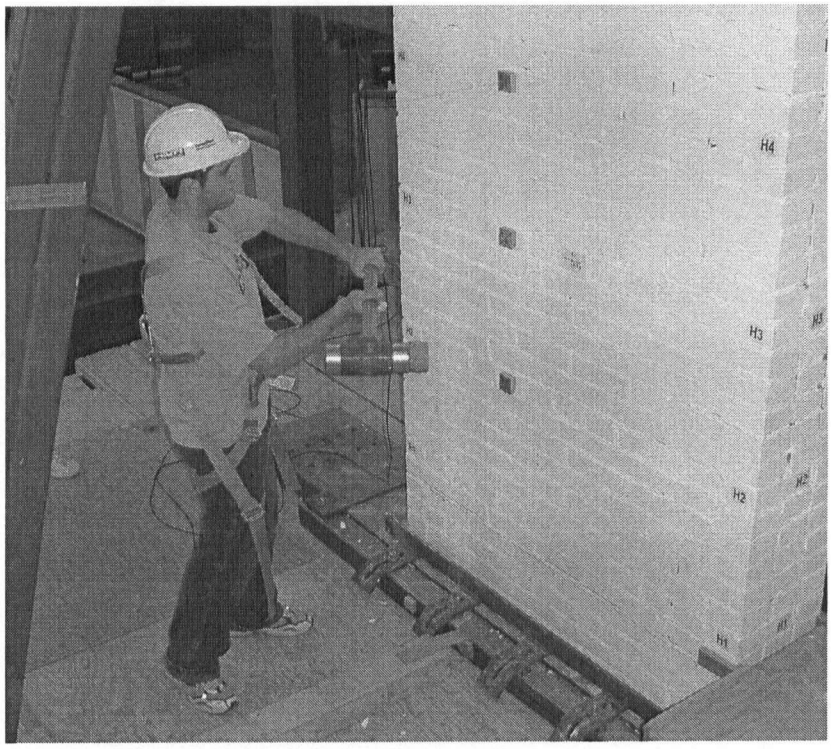


**Figure 3.20 Impact Hammer Test**

### 3.5.2 Shake Table Tests

Walls were grouped in pairs, each pair consisting of a wall with good collar joints and the other with poor collar joints. One pair was subjected to the site class C ground motion and the other to the site class D and subduction ground motion. Further information regarding the ground motions are discussed in Chapter 2. Table 1.1 shows the testing matrix. The ground motions were applied with increasing amplitude until collapse of the wall. The testing sequence for all the walls are summarized in Tables 3.6 through 3.9.

**Table 3.5 Testing Matrix**

| | | Ground Motion | Collar Joint Quality | |
|---|---|---|---|---|
| | | | Good | Poor |
| Soil Site Class | C | Gilroy | GC | PC |
| | | Hayward | GD | PD |
| | D | HKD 109 | GD(Sub1) | GD(Sub1) |
| | | HKD 085 | GD(Sub2) | PD(Sub2) |

**Table 3.6 Good Quality Collar Joint Wall – Site Class C Testing Sequence (GC)**

| Test Sequence | Test Number | Ground Motion | Scaling Factor to UHS | Scaled To | PGA (g) | PGD (cm) |
|---|---|---|---|---|---|---|
| 1 | GC1-0.71* | Gilroy | 0.71 | PGA | 0.34 | 1.91 |
| 2 | GC2-1.32* | Gilroy | 1.32 | PGA | 0.63 | 3.90 |
| 3 | GC3-0.64 | Gilroy | 0.64 | 0.5-1.0s | 0.71 | 4.96 |
| 4 | GC4-1.21 | Gilroy | 1.21 | 0.5-1.0s | 1.18 | 9.42 |
| 5 | GC5-1.49 | Gilroy | 1.49 | 0.5-1.0s | 1.15 | 11.6 |
| 6 | GC6-1.57 | Gilroy | 1.57 | 0.5-1.0s | 1.13 | 14.3 |
| 7 | GC7-1.71 | Gilroy | 1.61 | 0.5-1.0s | 1.21 | 14.3 |

**Table 3.7 Poor Quality Collar Joint Wall – Site Class C Testing Sequence (PC)**

| Test Sequence | Test Number | Ground Motion | Scaling Factor to UHS | Scaled To | PGA (g) | PGD (cm) |
|---|---|---|---|---|---|---|
| 1 | PC1-0.73* | Gilroy | 0.73 | PGA | 0.35 | 1.89 |
| 2 | PC2-1.10* | Gilroy | 0.59 | PGA | 0.53 | 3.84 |
| 3 | PC3-0.75 | Gilroy | 0.75 | 0.5-1.0s | 0.75 | 4.87 |
| 4 | PC4-1.40 | Gilroy | 1.40 | 0.5-1.0s | 1.3 | 9.35 |
| 5 | PC5-1.55 | Gilroy | 1.55 | 0.5-1.0s | 1.4 | 11.44 |
| 6 | PC6-1.57 | Gilroy | 1.57 | 0.5-1.0s | 1.8 | 14.08 |
| 7 | PC7-1.75 | Gilroy | 1.75 | 0.5-1.0s | 1.5 | 16.03 |

**Table 3.8 Good Quality Collar Joint Wall – Site Class D Testing Sequence (GD)**

| Test Sequence | Test Number | Ground Motion | Scaling Factor to UHS | Scaled To | PGA (g) | PGD (cm) |
|---|---|---|---|---|---|---|
| 1 | GD1-0.75 | Hayward | 0.75 | PGA | 0.40 | 3.09 |
| 2 | GD2-0.81 | Hayward | 0.81 | 0.5-1.0s | 0.52 | 3.83 |
| 3 | GD3-1.00 | Hayward | 1.00 | 0.5-1.0s | 0.76 | 5.40 |
| 4 | GD4-1.24 | Hayward | 1.24 | 0.5-1.0s | 1.0 | 6.50 |
| 5 | GD(Sub1)1-1.01 | HKD 109 | 1.01* | - | 0.76 | 11.34 |
| 6 | GD(Sub1)2-1.26 | HKD 109 | 1.26* | - | 0.78 | 14.11 |
| 7 | GD5-1.65 | Hayward | 1.65 | 0.5-1.0s | 1.51 | 9.16 |
| 8 | GD6-1.19 | Hayward | 1.19 | 0.5-1.0s | 1.16 | 6.62 |
| 9 | GD7-1.83 | Hayward | 1.83 | 0.5-1.0s | 1.40 | 11.20 |

*Subduction records scaled to PGD of original ground motion.

**Table 3.9 Poor Quality Collar Joint Wall – Site Class D Testing Sequence (PD)**

| Test Sequence | Test Number | Ground Motion | Scaling Factor to UHS | Scaled To | PGA (g) | PGD (cm) |
|---|---|---|---|---|---|---|
| 1 | PD1-0.79 | Hayward | 0.79 | PGA | 0.42 | 3.25 |
| 2 | PD2-0.78 | Hayward | 0.78 | 0.5-1.0s | 0.49 | 3.94 |
| 3 | PD3-0.97 | Hayward | 0.97 | 0.5-1.0s | 0.77 | 5.19 |
| 4 | PD4-1.20 | Hayward | 1.20 | 0.5-1.0s | 1.10 | 6.25 |
| 5 | PD(Sub1)1-1.02 | HKD 109 | 1.02* | PGD | 0.64 | 11.4 |
| 6 | PD(Sub1)2-1.11 | HKD 109 | 1.11* | PGD | 0.80 | 12.4 |
| 7 | PD(Sub1)3-1.25 | HKD 109 | 1.25* | PGD | 0.86 | 14.0 |
| 8 | PD5-1.66 | Hayward | 1.66 | 0.5-1.0s | 1.25 | 9.11 |
| 9 | PD(Sub2)1-1.10 | HKD 085 | 1.10* | PGD | 0.76 | 15.4 |
| 10 | PD6-2.22 | Hayward | 2.22 | 0.5-1.0s | 1.55 | 13.0 |

*Subduction records scaled to PGD of original ground motion.

# 4 DYNAMIC TEST RESULTS

## 4.1 Introduction

This chapter presents the results from the out-of-plane URM wall impact hammer and ground motion tests. Visual observations and the overall wall performance are first presented, followed by wall periods derived from the impact hammer tests. Finally, the measured results (acceleration, relative wall displacement, etc.) are discussed in detail. Further details from each wall test can be found in Appendices E through G.

## 4.2 Overall Wall Performance and Visual Observations

As was previously discussed, the walls were grouped in pairs, each pair consisting of a wall with good collar joints and the other with poor collar joints. One pair was subjected to the site class C ground motion and the other to the site class D and subduction ground motion as discussed in Chapter 2. The ground motions were applied with increasing amplitude until collapse. This section will describe the visual observations from the tests and the overall wall performance (e.g. peak relative wall displacement). Observations from each ground motion are discussed comparing the poor and good quality collar joint walls. Photos of progressive damage for each wall can be found in Appendix E.

### 4.2.1 Test Results – Site Class C Ground Motion

A summary of the results obtained from the site class C crustal earthquake can be found in Table 4.1. Photos showing typical damage can be found in the Appendix E.

Before wall cracking was observed, the walls experienced an approximately constant acceleration profile along the height, with very limited relative displacements. During Tests GC2-1.32 and PC2-1.10, both walls experienced cracking at the base and at header 6 (i.e. at approximately 55% and 65% of the wall height from the base of the wall). Rigid body rocking, where the wall acted as two rigid blocks pivoting about the top restraint, header 6, and the base was observed for the remainder of the tests.

**Table 4.1 Site Class C Observations**

| Test # | Test Name | | Scaling Factor to UHS | | PGA | | Observations | |
|---|---|---|---|---|---|---|---|---|
| | Good | Poor | Good | Poor | Good | Poor | Good | Poor |
| 1 | GC1-0.71* | PC1-0.73* | 0.71* | 0.73* | 0.34 | 0.35 | No Observed Damage | No Observed Damage |
| 2 | GC2-1.32* | PC2-1.10* | 1.32* | 1.10* | 0.63 | 0.53 | Crack Formed at Wall Base and Header 6 | Crack Formed at Wall Base and Header 6 |
| 3 | GC3-0.64 | PC3-0.75 | 0.64 | 0.75 | 0.71 | 0.75 | Rigid Body Rocking | Rigid Body Rocking |
| 4 | GC4-1.21 | PC4-1.40 | 1.21 | 1.40 | 1.18 | 1.3 | Rocking, Loss of Bricks at Header 6 | Rocking |
| 5 | GC5-1.49 | PC5-1.55 | 1.49 | 1.55 | 1.15 | 1.4 | Rocking, Interference at Top Restraint | Rocking, Crack Formed at Header 1 |
| 6 | GC6-1.57 | PC6-1.57 | 1.57 | 1.57 | 1.13 | 1.8 | Rocking, Interference at Top Restraint | Rocking |
| 7 | GC7-1.61 | PC7-1.75 | 1.61 | 1.75 | 1.21 | 1.5 | Rocking, Interference at Top Restraint | Rocking, Loss of one wythe of bricks at Header 1 |

Note: *Test scaled to PGA (all other tests scaled to 0.5-1.0s range)

For the good quality wall, during Test GC4-1.21 bricks at the edges of header 6 were dislodged, and crushing of the outside bricks was evident. Observed damage can be seen in Figure 4.1. For the good quality wall, at scaling levels of 1.49 and greater (Tests GC5-GC7) slight bearing between the wall and the top restraint was noted. As discussed below, this interference may have resulted in limiting mid-height displacements for these tests.

For the poor quality wall, cracks began to form at header 1 after Test PC5-1.55. Further damage also occurred at header 6 with crushing of the outside brick corners, and daylight was seen through the crack. During Test PC7-1.75, the outer wythe of two courses at header 1 were lost (Figure 4.2), thereby changing the wall's rocking behaviour and apparently decreasing the mid-height displacements. Due to this significant damage, the wall was considered to be unstable and all instruments were removed. These results suggest that the instability factor for the site C crustal ground motion is near 1.61.

Figure 4.3 shows the maximum displacements versus scale factor for the two walls. Both the good and poor quality walls had similar peak displacements for a given scale factor, indicating that the collar joint quality did not have a significant effect on the walls' responses. In wall PC,

there is a spike in the peak relative crack displacement (at PC6-1.57), indicating that collapse of the wall happened suddenly. The maximum displacement droped during Test PC7-1.75, due to the significant damage formed at header 1. Wall GC behaves similarly to PC up to Test GC4-1.21. Applied table motions above this level resulted in a moment being applied to the top of the wall due to interference with the top restraint. As shown by the dashed line in Figure 4.3, this interference appears to decrease the expected peak displacement by introducing a stabilizing arching action in the wall. This was also observed in quasi-static tests conducted by Anderson [1994]. Further investigation of this applied moment and its effect on wall stability is required.

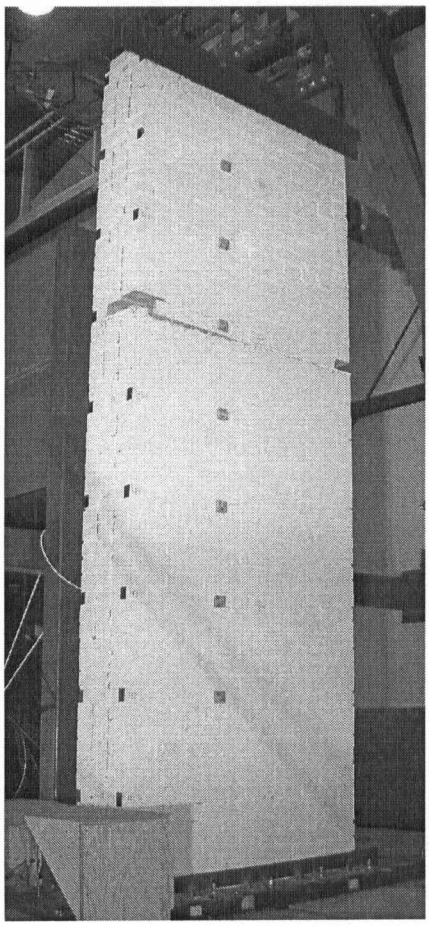

**Figure 4.1 Crack at Header 6 and Dislodged Bricks (GC4-1.21)**

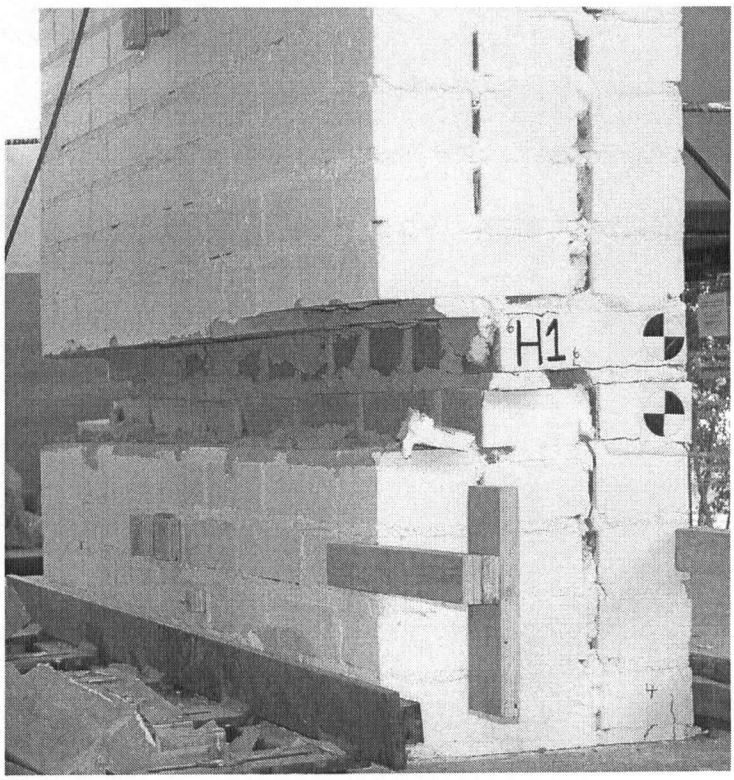


**Figure 4.2 Loss of Bricks at Header 1 (PC7-1.75)**

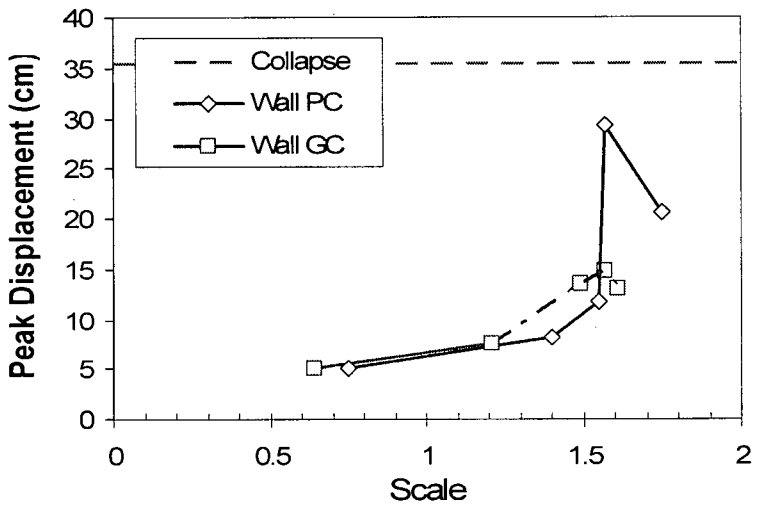


**Figure 4.3 Peak Mid-Height Displacement vs. Ground Motion Scaling (Site Class C)**

### 4.2.2 Test Results – Site Class D Ground Motion

A summary of the results obtained from the site class D crustal earthquake can be found in Table 4.2. Photos showing typical damage can be found in the Appendix E.

**Table 4.2 Site Class D Observations**

| Test # | Test Name | | Scaling Factor to UHS | | PGA | | Observations | |
|---|---|---|---|---|---|---|---|---|
| | Good | Poor | Good | Poor | Good | Poor | Good | Poor |
| 1 | GD1-0.75* | PD1-0.79* | 0.75* | 0.79* | 0.40 | 0.42 | Crack Formed at Header 7 | Crack Formed at Wall Base and Header 7 |
| 2 | GD2-0.81 | PD2-0.78 | 0.81 | 0.78 | 0.52 | 0.49 | Rocking, Crack Formed at Wall Base | Rocking, Crack Formed at Header 1 |
| 3 | GD3-1.00 | PD3-0.97 | 1.00 | 0.97 | 0.76 | 0.77 | Rigid Body Rocking | Rocking |
| 4 | GD4-1.24 | PD4-1.20 | 1.24 | 1.20 | 1.0 | 1.10 | Rocking | Rocking |
| 5 | GD5-1.65 | PD5-1.66 | 1.65 | 1.66 | 1.51 | 1.25 | Rocking, Loss of Brick at Header 7, Crack Formed at Header 2 and 3 | Rocking, Crack Formed at Header 9 |
| 6 | GD6-1.19 | PD6-2.22 | 1.19 | 2.22 | 1.16 | 1.55 | Rocking | Wall Collapse |
| 7 | GD7-1.83 | - | 1.83 | - | 1.40 | - | Wall Collapse | - |

Note: *Test scaled to PGA (all other tests scaled to 0.5-1.0s range)

During the first test, both walls experienced cracking at header 7 (i.e. at approximately 77% of the wall height from the base of the wall), approximately 17% higher than for both the site class C walls. The poor quality wall also formed a crack at the wall base. Rigid body rocking, where the wall acted as two rigid blocks pivoting about the top restraint, header 7, and the base, was observed for the remainder of the tests. During Test 2, the good quality wall had a crack form at the wall base, and the poor quality wall had a thin crack form at header 1.

At the Test 4, (GD4-1.24 and PD4-1.20), both walls exhibited crushing of the outer wythe bricks at the crack. For the poor quality wall, at scaling levels of 1.66 and greater (Tests 5 and 6), a crack formed at the top of the wall (header 9), with a row of bricks becoming dislodged, as shown in Figure 4.4. It is believed that this damage to the wall did not have a significant effect on the overall performance of the wall, as the dislodged bricks still tightly remained between the undamaged portion of the wall and the top restraint. For the good quality wall, for scaling levels of 1.65 and greater, a brick was lost at header 7 and a new thin crack formed at headers 2 and 3. Examples of the level of damage observed at the crack towards the later testing stages are shown in Figure 4.5.

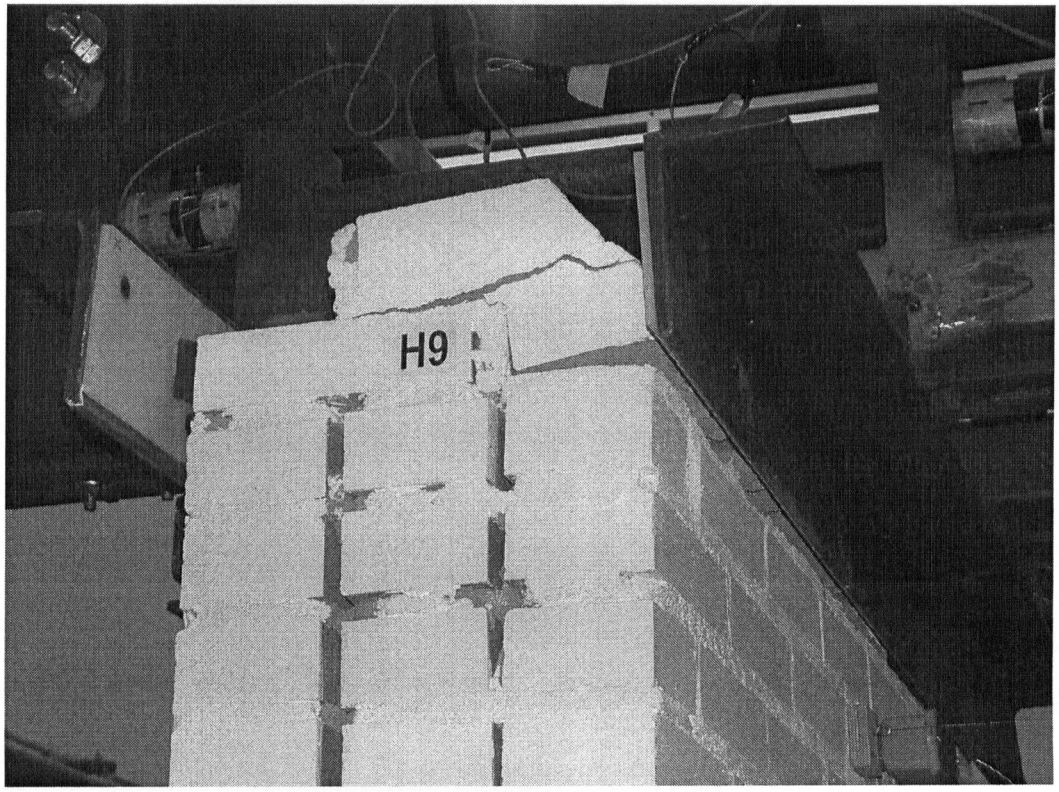


**Figure 4.4 Dislodged Bricks at Header 9 Formed During Test PD5-1.66**

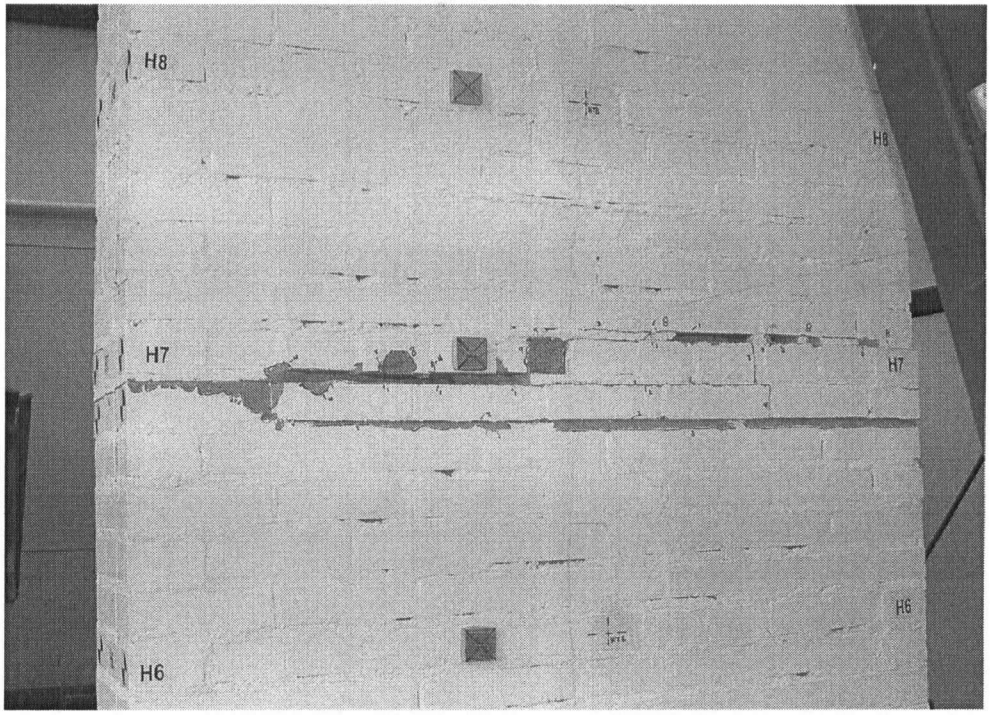


(a) Brick Crushing, and Mortar Spalling at Header 7, after Test PD5-1.66

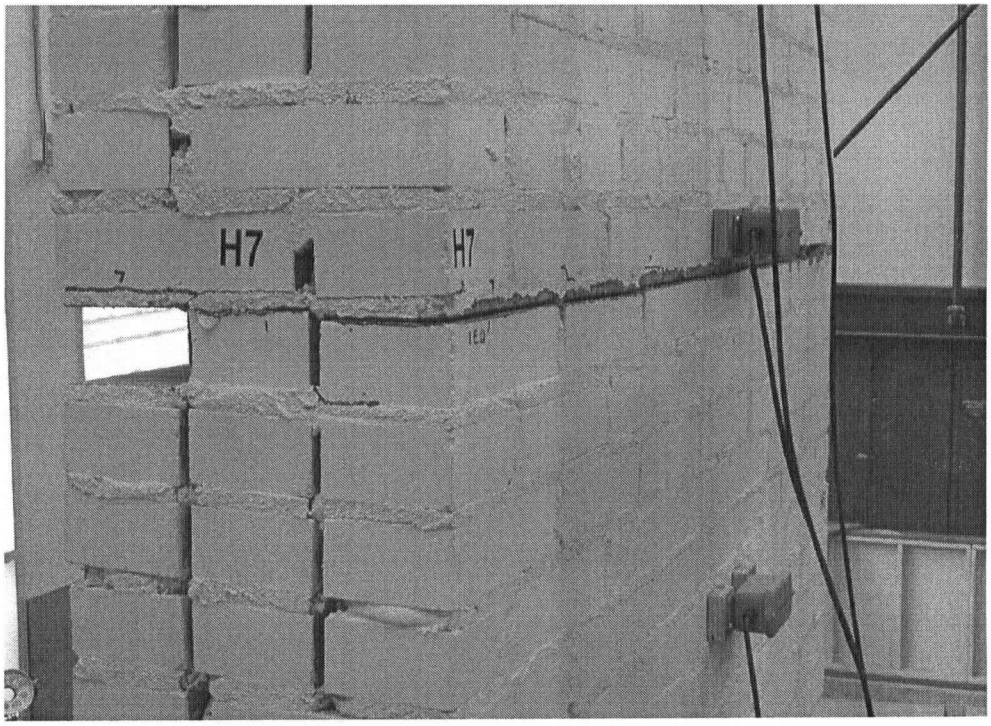


(b) Dislodged Brick and Mortar Crushing at Header 7 after Test GD5-1.65

**Figure 4.5 Examples of Crack Damage During Later Stages of Testing**

The poor quality wall collapsed at a scaling level of 2.22. In order to get a better estimate of the scaling factor resulting in instability of the wall for the site D crustal ground motion, a lower scaling factor of 1.83 was selected for Test 7 for the good quality wall. This test resulted in collapse of the wall. These results suggest that the instability factor for the site D crustal ground motion is between 2.22 and 1.83.

Figure 4.6 shows the maximum displacements versus scale factor for the two walls. Both the poor and good quality wall had very similar peak displacements indicating that the overall performance was not significantly affected by the quality of construction. For tests up to a scaling level of 1.65, there is a gradual increase in peak relative displacement at the crack. For tests slightly above 1.65, the walls become unstable, indicating that collapse of the wall happens suddenly.

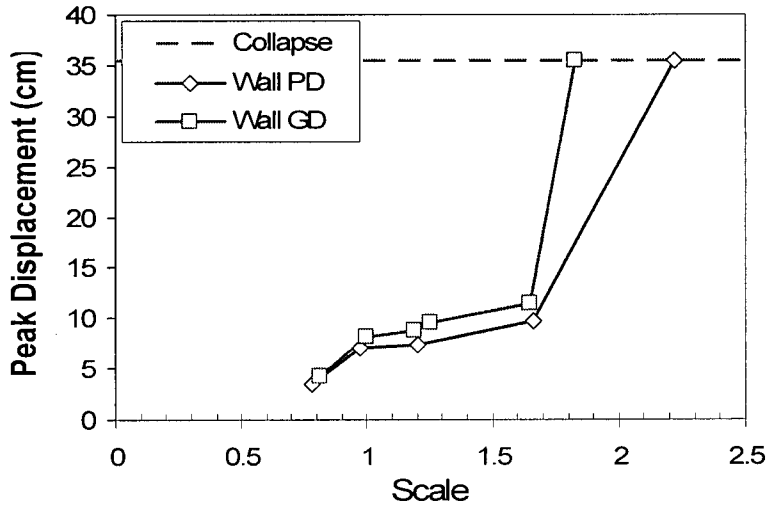


**Figure 4.6 Peak Mid-Height Displacement vs. Ground Motion Scaling (Site Class D)**

### 4.2.3 Test Results – Site Class D Subduction Ground Motion

As Vancouver and the South Western Coast of BC are susceptible to a mega-thrust subduction event, the walls were subjected to a subduction record. As these events are longer in duration compared to a crustal event, it was of particular interest to observe how the walls responded to more cycles. A summary of the results obtained from the site class D subduction earthquake ground motion can be found in Table 4.3. Photos showing typical damage can be found in Appendix E.

The tests using the subduction ground motion were conducted after Test 4 of the site class D crustal motion; hence the walls were already cracked and damaged. No new damage was observed and stable rigid-body rocking took place during each test. The maximum displacements vs. scale factor for the two walls are shown in Figure 4.7. Again, the poor and good quality wall had very similar peak displacements indicating little or no influence from the quality of construction.

**Table 4.3 Site Class D Subduction (HKD 109) Observations**

| Test # | Test Name | | Scaling Factor to UHS* | | PGA | | Observations | |
|---|---|---|---|---|---|---|---|---|
| | Good | Poor | Good | Poor | Good | Poor | Good | Poor |
| 1 | GD(Sub1)1 -1.01 | PD(Sub1)1 -1.02 | 1.01 | 1.02 | 0.76 | 0.64 | Wall Cracked From Previous Tests Rigid Body Rocking | Wall Cracked From Previous Tests Rigid Body Rocking |
| 2 | GD(Sub1)2 -1.26 | PD(Sub1)2 -1.11 | 1.26 | 1.11 | 0.78 | 0.80 | Rocking | Rocking |
| 3 | - | PD(Sub1)3 -1.25 | | 1.25 | | 0.86 | | Rocking |

Note: *Test scaled to PGD of original record

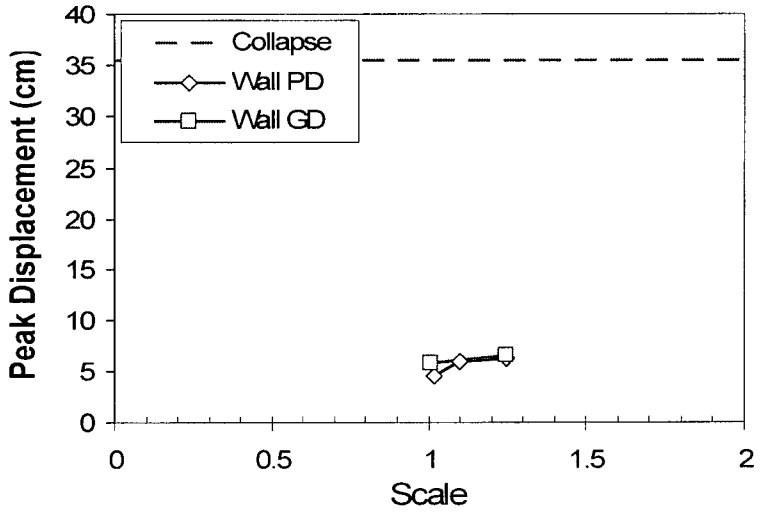


**Figure 4.7 Peak Mid-Height Displacement vs. Ground Motion Scaling (Subduction)**

## 4.3 Fundamental Period of Walls

As was previously discussed in Chapter 1, quantifying the system as a linear viscously damped oscillator using the walls' fundamental period and damping may not be the most appropriate

method; whereas interpreting the system as rocking rigid blocks using a frequency parameter and slenderness ratio may produce more realistic results. However, in order to compare the quality between the poor and good quality walls, and to quantify the degradation of the walls through multiple tests, their natural frequencies were compared.

Doherty [2000] showed that the frequency of a cracked wall decays logarithmically with increasing mid-height crack displacement. In order to determine the natural frequencies of the walls, hammer tests were conducted such that the crack displacement was negligible. Accelerations were recorded at various locations along the wall, and the hammer was impacted at headers 3, 6 and 8 in order to excite several modes of vibration. The impact at various locations all yielded similar results. The natural frequency of the wall was determined through standard experimental modal analysis techniques. The signals from the impact hammer and wall accelerometers were first transformed from the time domain into the frequency domain. The frequency response from each individual accelerometer (located at a header course) was then divided by the frequency response of the hammer resulting in a Frequency Response Function (FRF) for the impact at each header course. The computed FRF is a summation of resonance curves, (i.e. the overall response of a structure at any frequency is a summation of responses due to each of its modes). From the FRF, it is evident that there are fundamental frequencies that dominate the frequency response of the walls.

A sample FRF generated from a hammer test on an un-cracked wall is shown in Figure 4.8, with a fundamental frequency of 9.3 Hz (period of 0.11s) and second mode frequency of 17.6 Hz (period of 0.057s). An example of a cracked wall FRF is shown in Figure 4.9, with a fundamental frequency of 6.5 Hz (period of 0.15s) and second mode frequency of 12 Hz (period of 0.083s). Further details of the hammer test analysis can be found in Appendix F.

The behaviour of an un-cracked wall is highly non-linear and, as such, it does not have a finite fundamental frequency. Strictly speaking, a cracked wall behaves as two separate structures, each with their own natural frequency. However, at very small displacements the wall can be considered to be 'quasi-linear,' and the two portions of the wall act as a single structure. This assumption can be justified, as at very low crack displacements the two portions of the wall sit directly on top of each other (i.e. flush) and act as if they are attached to each other due to the large self-weight and friction along the crack surface. It should also be noted that these

fundamental frequencies are for the entire system including the wall and restraints, but still provide valuable information regarding the degradation of the walls through subsequent tests.

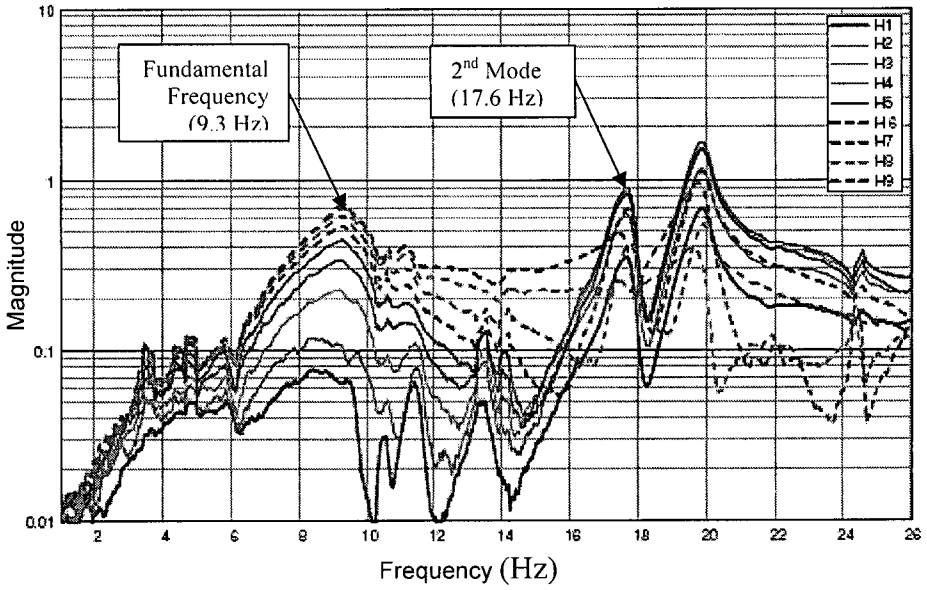


**Figure 4.8 FRF for the Un-Cracked Wall PC**

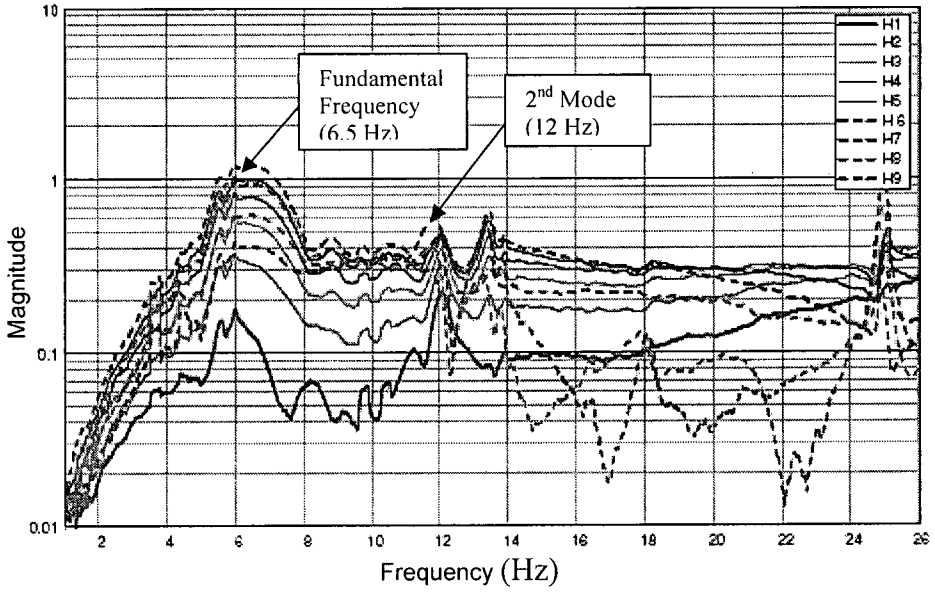


**Figure 4.9 FRF for the Cracked Wall PC4-1.40**

Natural frequencies from the impact hammer tests are shown in Figure 4.10 and Figure 4.11 for the walls at different stages in the testing sequence. As expected, these results show a significant decrease in the system's natural frequency when significant damage occurs (i.e. cracks forming

at headers). There is also a slight decrease in the natural frequency through subsequent tests even if no new major cracks appear. This may be due to damage at the crack plane caused by increased crack widths, loss of mortar and bricks, and crushing of mortar and bricks. In general, the good and poor quality collar joint walls have similar un-cracked and cracked natural frequencies, indicating that the collar joint quality had little effect on the walls natural frequency characteristics. For Wall GC, the wall appears to have undergone damage after the first test (test sequence 1), as indicated in the significant drop in natural frequency (Figure 4.10). However, this damage was not noted by any visual observations such as cracking. Also note that the frequencies of Wall GC are lower than those of Wall PC once the wall has cracked. This difference may be due to the location of the crack; as the crack in Wall PC formed at 65% of the wall height from the base, whereas in Wall GC the crack formed at 55% of the wall height. On average the un-cracked walls had a natural frequency of 9.0 Hz (period 0.11s), for a single crack at header 6 or 7 their natural frequency dropped to 5.9Hz (0.16s), and with further cracking (headers 1, 2, and 3) to 4.7Hz (0.21s).

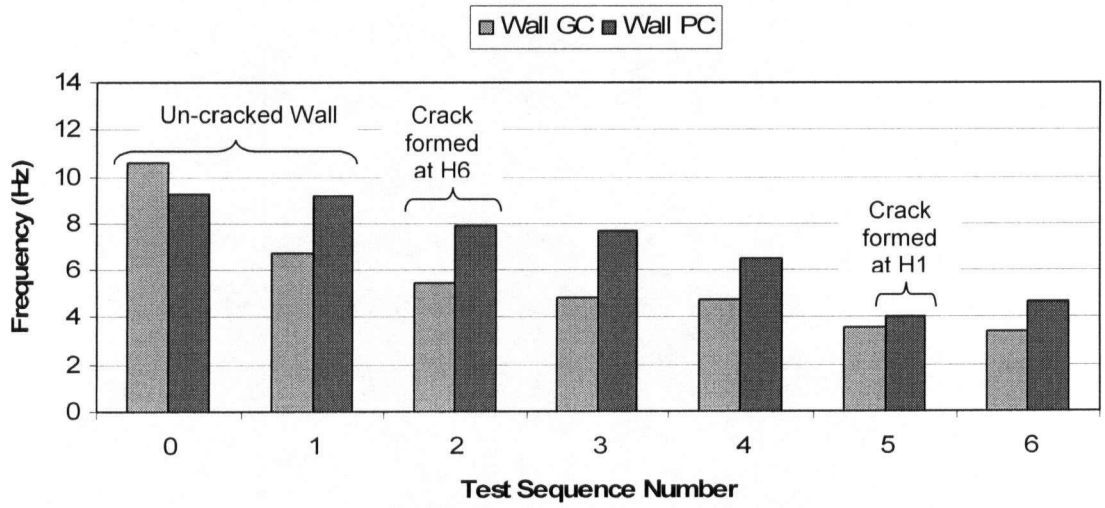


**Figure 4.10 Hammer Natural Frequencies for Site Class C Ground Motions**

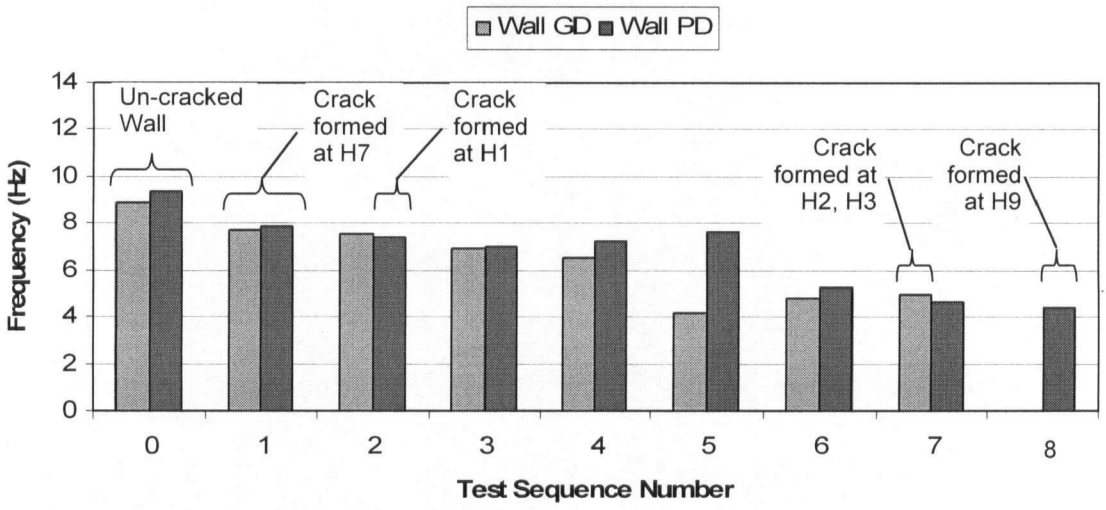


**Figure 4.11 Hammer Test Natural Frequencies for Site Class D Ground Motions**

In order to verify the results obtained from the FRF analysis and to provide more insight into the mode shapes of the wall system, the ARTeMIS Extractor software was used [Structural Vibration Solutions, 2005]. This robust program uses Frequency Domain Decomposition (FDD) and Stochastic Subspace Identification (SSI) time domain methods to provide modal characteristics (frequency, damping ratio, and mode shapes) of a structural system.

The frequencies obtained from ARTeMIS, for the first two modes, compare very well with those obtained using the FRF method. The un-cracked wall had a 1$^{st}$ mode frequency of 9.13 Hz, compared to 9.3 Hz from the FRF method; and a 2$^{nd}$ mode frequency of 17.52 Hz, compared to 17.6 Hz from the FRF method. The cracked wall had a 1$^{st}$ mode frequency of 6.35 Hz, compared to 6.5 Hz; and a 2$^{nd}$ mode frequency of 13.37 Hz, compared to 12.0 Hz. ARTeMIS also produces an estimate of the damping ratio. For the 1$^{st}$ mode, the un-cracked wall had a damping ratio of 7.01%, and the cracked wall had 11.62%. The 2$^{nd}$ modes of the un-cracked and cracked walls displayed significantly lower damping ratios of 0.78% and 2.62% respectively.

Mode shapes were also estimated using ARTeMIS, (Figure 4.12 and Figure 4.13). For the un-cracked wall, the mode shapes are smooth and continuous; indicating that the wall is indeed un-cracked. The flexibility of the rubber spacers can be seen at the top of the wall in the 1$^{st}$ mode shape. In Figure 4.13, the presence of a crack at header 6 is clearly evident in the mode shape and bending of the wall segments above and below the crack is very limited compared with the rigid body rotation of the segments.


**Figure 4.12 Mode Shapes of the Un-Cracked Wall PC**


**Figure 4.13 Mode Shapes of the Cracked Wall PC4-1.40**

## 4.4 Recorded Results

### 4.4.1 Relative Displacement Time History

The relative displacement is the key parameter in measuring wall stability. As was previously mentioned, under static conditions the wall is theoretically stable until the relative displacement at the crack is equal to the wall width (i.e. 355mm for these test walls). For the initial low level tests, the ground motion does not produce enough inertia to crack the wall. Figure 4.14 (a) shows the relative displacement profile of the un-cracked wall at the maximum relative displacement of the wall. The small linear relative displacement shown in Figure 4.14 (a) is due to flexibility in

the testing frame and the rubber spacers at the top of the wall. At the top of the wall, the maximum relative displacement is approximately 5mm.

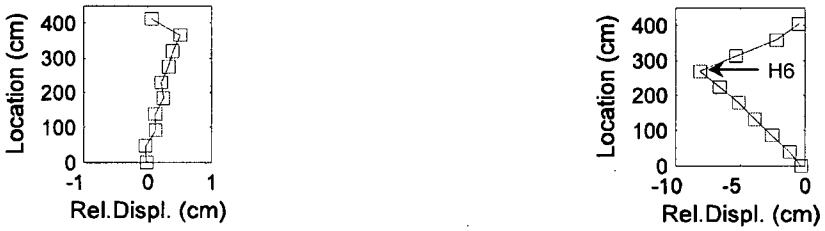


(a) Un-Cracked Wall, Test GC1-0.71* (b) Cracked Wall, Test GC2-1.32*

**Figure 4.14 Relative Displacement Profile for Wall GC**

Once the wall has cracked it behaves as two rigid rocking blocks. The cracked wall exhibits a triangular relative displacement profile, Figure 4.14 (b), with the peak maximum relative displacement occurring at the crack location, above the mid-height of the wall. For the two walls subjected to the site class C ground motion the peak relative displacement occurred at header 6 (H6); for the two walls subjected to the site class D ground motion, the peak relative displacement occurred at header 7 (H7).

The maximum relative displacement occurs as the table moves in the opposite direction of the middle portion of the wall. Typical examples of the absolute and relative wall displacement time histories are shown in Figure 4.15 and Figure 4.16, respectively. As was previously mentioned, an increase in the relative displacements was observed with increasing amplitude of input ground motion, (Figure 4.3, Figure 4.6, and Figure 4.7).

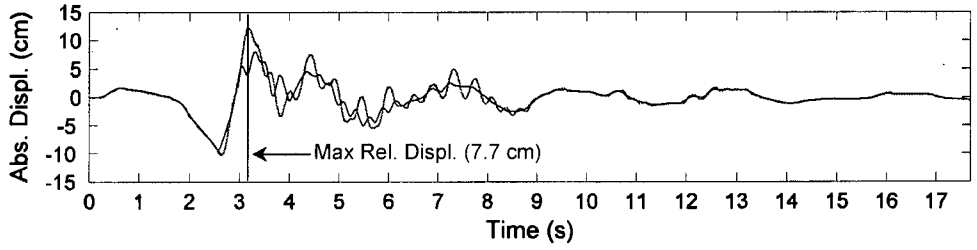


( —— H6, — Table Motion)

**Figure 4.15 Absolute Wall Displacement Time History, Test GC4-1.21**

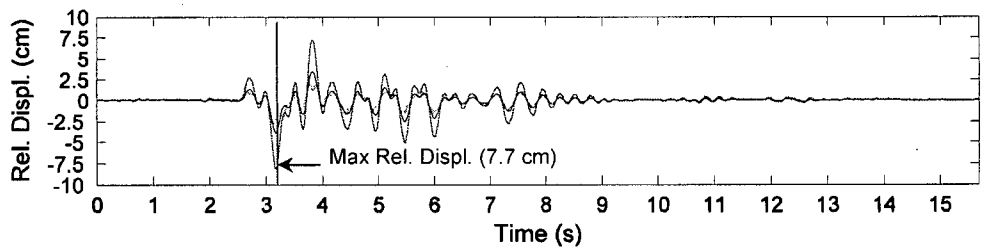


(—— H8, —— H6, —— H3)

**Figure 4.16 Relative Wall Displacement Time History, Test GC4-1.21**

### 4.4.2 Acceleration Time History

During dynamic excitation, an un-cracked wall undergoes a uniform or linearly varying acceleration profile. If the input motion at the top and bottom of the wall are of the same magnitude and in-phase (i.e. rigid diaphragms), the wall exhibit a uniform acceleration profile applied to it. If the diaphragms are flexible, the acceleration profile will be linearly varying. This can be seen in Figure 4.17 (a) in which the un-cracked wall exhibits a linearly varying acceleration profile. The trapezoidal acceleration profile, with increased acceleration at the top of the wall, is due to flexibility in the testing frame and the rubber spacers at the top of the wall.


(a) Un-Cracked Wall – Test GC1-0.71* (b) Cracked Wall – Test GC2-1.32*

**Figure 4.17 Example Acceleration Profiles for Wall GC**

Once the wall has cracked it behaves as rigid rocking blocks. The cracked wall exhibits a linear acceleration profile between cracks, Figure 4.17 (b), with the maximum accelerations occurring at the top of the wall and the crack location. For the two walls subjected to the site class C ground motion the walls behaved as two rigid blocks, rocking about the crack formed at header 6. For the two walls subjected to the site class D ground motion, they rocked as two rigid blocks during lower amplitude motions, about the crack formed at header 7. At higher amplitude records further cracks formed in the walls; at header 1 in the poor quality wall during

Test PD2-0.78, and header 2 and 3 during Test GD5-1.65 of the good quality wall. This caused the walls to rock as three and four rigid bodies respectively. The multiple, rigid body rocking can be seen in the acceleration profiles of the walls in Figure 4.18. An example acceleration time history is shown in Figure 4.19. Figure 4.19 (b) shows a close-up view of the acceleration time history. Note that the acceleration at header 6 (the crack location) is out of phase with header 9 and the table. Further time histories can be found in Appendix G.

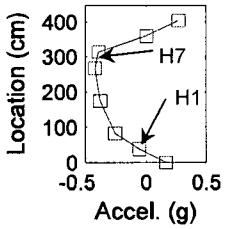


(a) Poor Quality Wall – Test PD5-1.65 (Crack at H1 and H7)

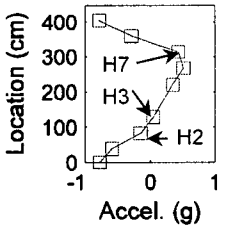


(b) Good Quality Wall – Test GD5-1.65 (Crack at H2, H3, and H7)

**Figure 4.18 Multiple Rigid Body Rocking Acceleration Profile**

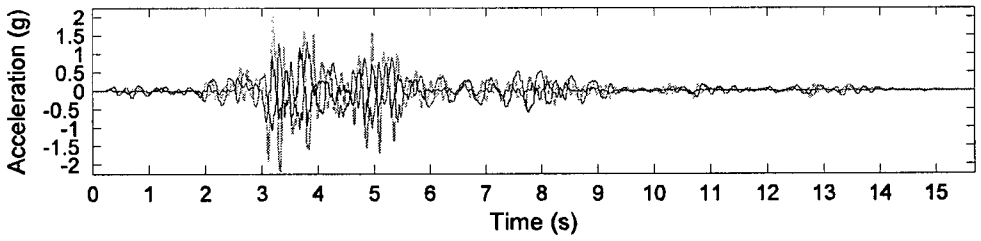


(a) Total Time History

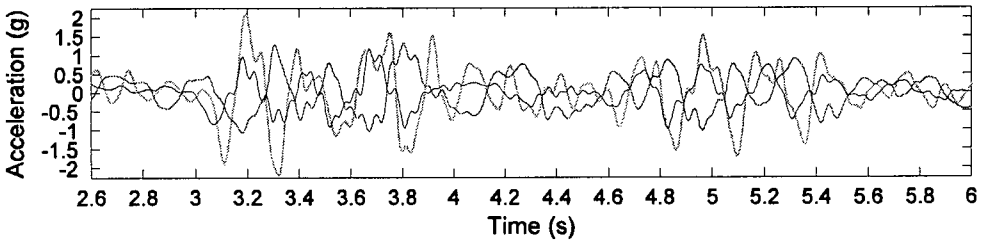


(b) Close-up of Time History showing H6 Out-of-Phase with Table Motion and Header 9 (— H9, — H6, — Table Motion)

**Figure 4.19 Acceleration Time History, Test GC4-1.21**

The acceleration profile exhibited by the wall consists of three components (Figure 4.20): the base motion, top connection flexibility (diaphragm stiffness), and the rigid body rocking motion due to the inertia of the rocking wall. The acceleration due to the top connection flexibility and rigid body motion may not necessarily be in phase with the base acceleration. Note that the total inertia force on the wall for the case shown below may approach zero even though the acceleration at the crack may be as high as 0.5g. If one were to consider the force displacement-relation in a typical lumped mass system, and the force were to approach 0, the system would be considered to be unstable. However, for this system it is still stable, due to varying acceleration profile. One must therefore not only look at the total force-displacement response, but also at the acceleration-displacement response. It is clear from the profile discussed here that each relation will give a different interpretation of when stability occurs.

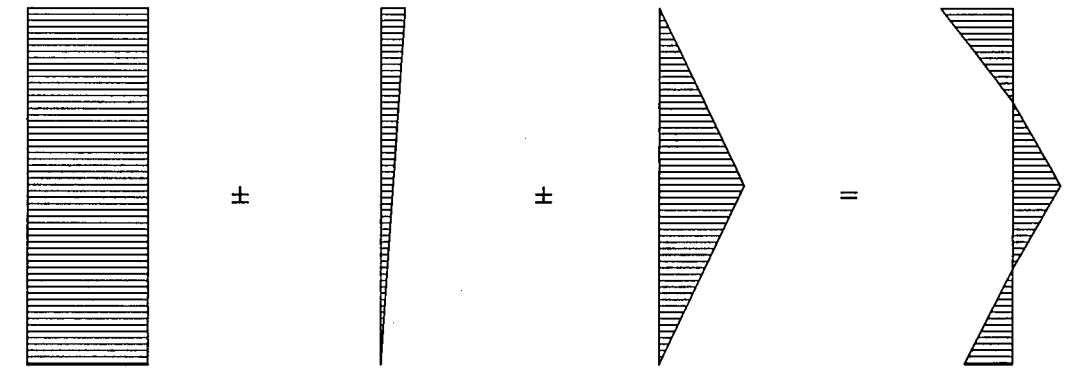


**Figure 4.20 Acceleration Profile Components**

### 4.4.3 Crack Acceleration - Displacement Hysteretic Behaviour

The nonlinear elastic rocking behaviour is evident in Figure 4.21 which shows the acceleration at the crack versus the relative crack displacement. In Figure 4.21, at point (A), the relative crack displacements are small (approximately less than 1cm), and the wall behaves essentially linearly. At greater displacements, point (B), the crack has opened sufficiently, allowing the wall to rock, resulting in the nonlinear behaviour.

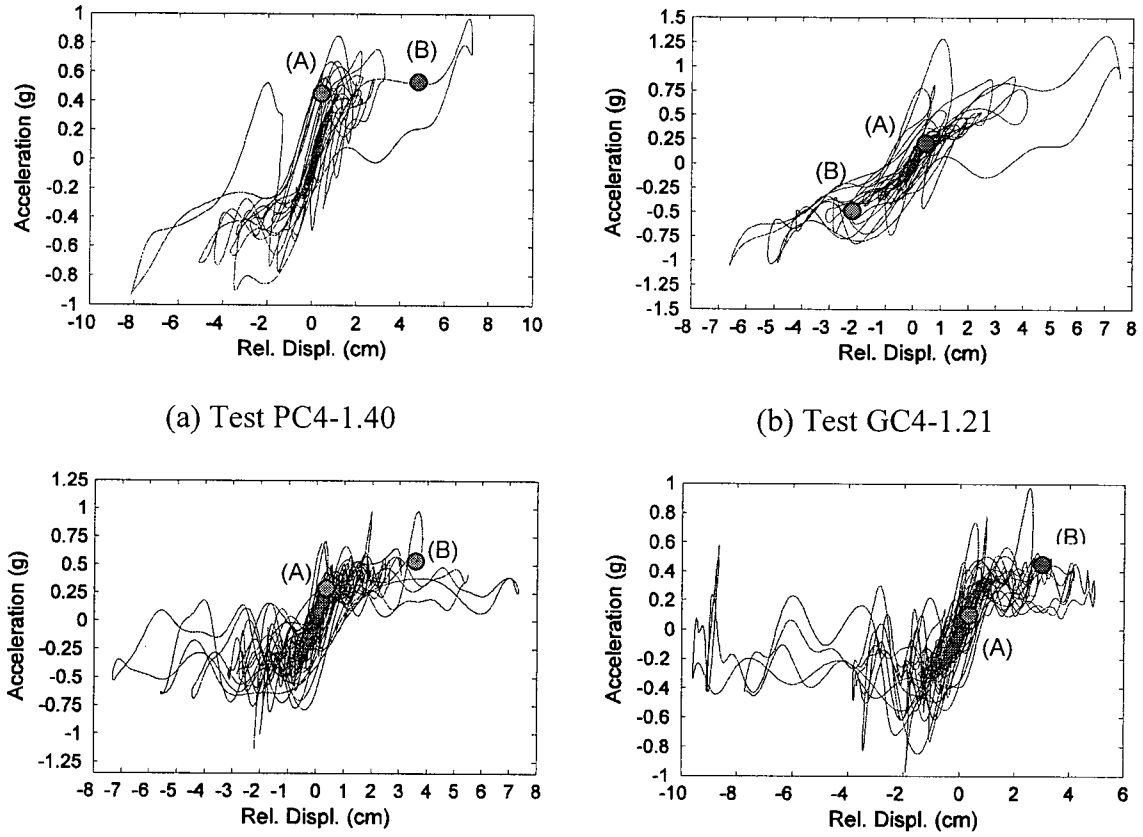


(a) Test PC4-1.40

(b) Test GC4-1.21

(c) Test PD4-1.20

(d) Test GD4-1.24

**Figure 4.21 Crack Acceleration vs. Relative Crack Displacement Hysteretic Response**

For the cracked walls, it was observed that the acceleration at the crack at which the walls began to rock was fairly consistent between tests. From the test results, the effective rocking acceleration ($a_{rocking}$) was visually estimated (Figure 4.22). Effective rocking accelerations from each wall are shown in Table 4.4. The relatively constant rocking acceleration would suggest that in order to initiate and maintain rocking, a 'threshold' acceleration at the crack is required. Once rocking begins, the acceleration at the top and base of the wall may change while the acceleration at the crack remains relatively constant. As the relative crack displacement decreases to less than approximately 1cm, the wall resumes its linear elastic behaviour. The walls began to rock on average at 0.57g. Note that walls with a higher crack location (walls PC, GD and PD) have lower effective rocking accelerations compared with a wall with a lower crack location (wall GC). The quality of the collar joints also appears to have little effect on the rocking acceleration.

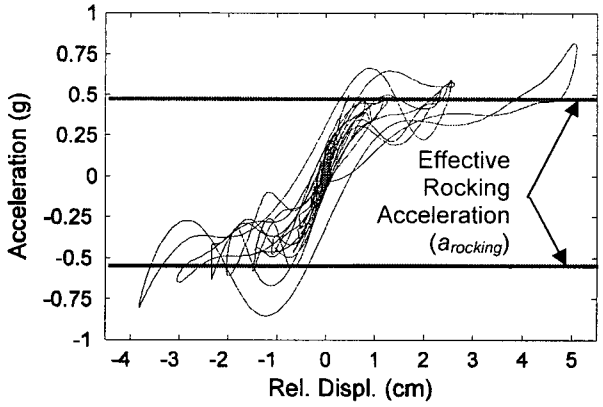


**Figure 4.22 Definition of Effective Rocking Acceleration at Crack**

**Table 4.4 Effective Rocking Acceleration at Crack**

| Wall | Effective Rocking Acceleration [g] |
|---|---|
| GC | 0.62 |
| PC | 0.56 |
| GD | 0.55 |
| PD | 0.56 |
| Average | 0.57 |

Figure 4.23 shows the acceleration versus crack relative displacement for a test that came near collapse. Note that at higher relative displacements (greater than approximately 10cm) the accelerations appear to oscillate. It appears that at some point during rocking, the wall becomes 'dynamically stable', and further rocking is able to occur about this new stability point. How this response affects the behaviour of the wall requires further study.

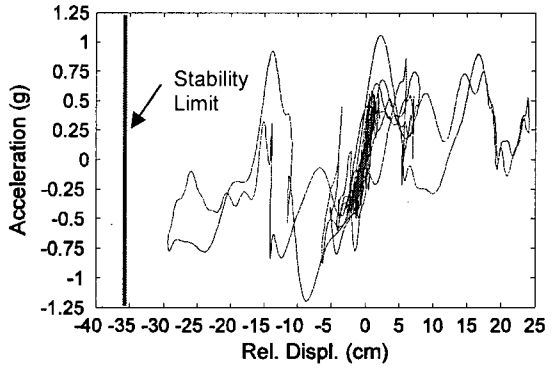


**Figure 4.23 Crack Acceleration vs. Crack Relative Displacement Near Collapse, Test PC6-1.57**

### 4.4.4 Force-Displacement Hysteretic Behaviour

The total inertia force acting on the wall was calculated by multiplying the acceleration at each header unit by the lumped wall mass at the header unit. As the table motions became more severe, instrumentation was removed and the acceleration profile was assumed to be piece-wise linear between the base, the crack location, and the top of the wall (header 9). This calculated force was then plotted against the relative displacement at the crack location.

The wall behaves essentially elastically until a crack is formed, Figure 4.24. Once the crack forms, there is an immediate drop in applied force on the wall, and the force-displacement relationship becomes non-linear. (The time when the crack was formed was confirmed by looking at the relative displacement time history). There was little difference in un-cracked stiffness between the good and poor quality collar joint walls, with the average un-cracked stiffness of all the walls being 42.6 kN/cm ( Table 4.5).

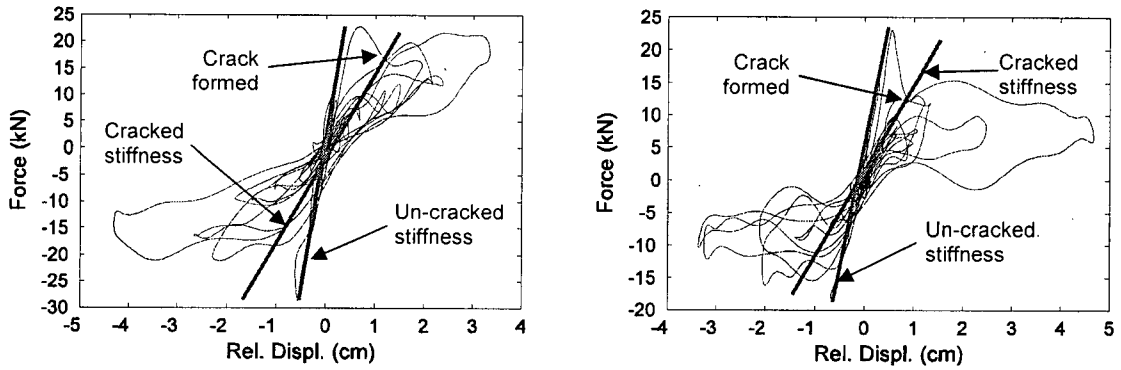


(a) Test GC2-1.32* (b) Test PC2-1.10*

**Figure 4.24 Cracking Wall Force-Displacement Behaviour**

**Table 4.5 Un-Cracked Wall Stiffness**

| Wall | Observed Un-Cracked Stiffness [kN/cm] |
|---|---|
| GC | 44.3 |
| PC | 43.9 |
| GD | 39.7 |
| PD | 42.4 |
| Average | 42.6 |

As was previously mentioned, once the walls crack they undergo a non-linear force-displacement response. For small relative crack displacements the wall response is approximately elastic; however, as shown in Figure 4.24, the stiffness is significantly reduced compared to that of an un-cracked wall. Cracked stiffness is shown in Figure 4.25 and Figure 4.26 for the walls at different stages in the testing sequence. As expected, these results show a significant decrease in the wall's initial stiffness when significant damage occurs (i.e. cracks forming at headers). There is also a slight decrease in the stiffness through subsequent tests even if no new major cracks appear. This may be due to increased crack widths, and crushing or loss of mortar and bricks. In general, the good and poor quality collar joint walls have similar un-cracked and cracked stiffness, indicating that quality of the collar joint did not appear to influence the elastic portion of force-displacement relationships. For a single crack forming at header 6 or 7, the initial stiffness of the walls dropped on average from 42.6 kN/cm to 12.6kN/cm.

Examples of typical non-linear force-displacement relations are shown in Figure 4.27, with key behavioural traits pointed out in Figure 4.28. As will be described in detail below, the negative stiffness evident in the force-displacement response is not comparable to strength degradation due to P-Delta effects or material degradation observed in typical lumped mass systems. Due to the rocking motion of the walls, the inertia force on the wall can drop to below zero with increasing crack displacement, and the walls still remain stable.

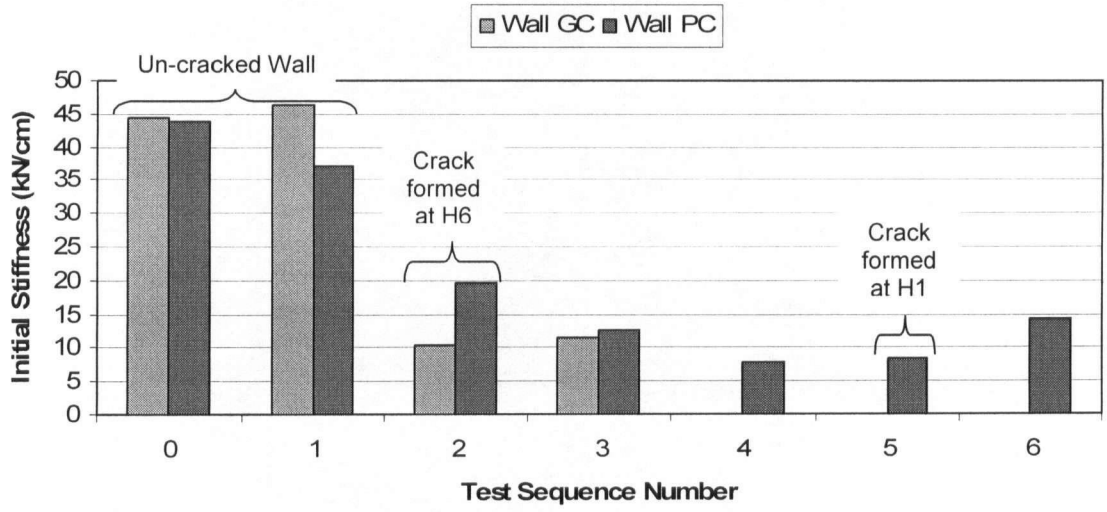


**Figure 4.25 Initial Wall Stiffness for Site Class C Ground Motions**

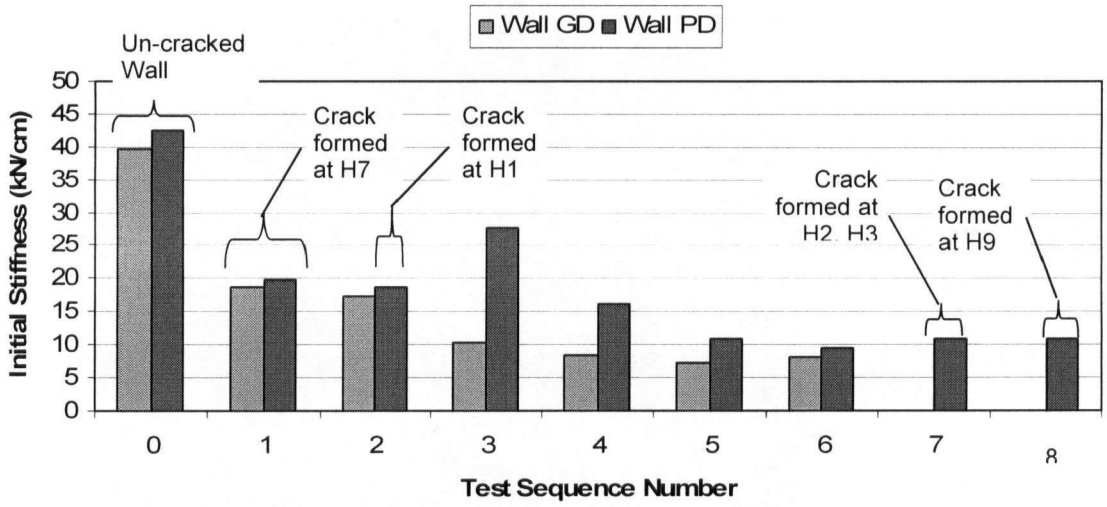


**Figure 4.26 Initial Wall Stiffness for Site Class D Ground Motions**

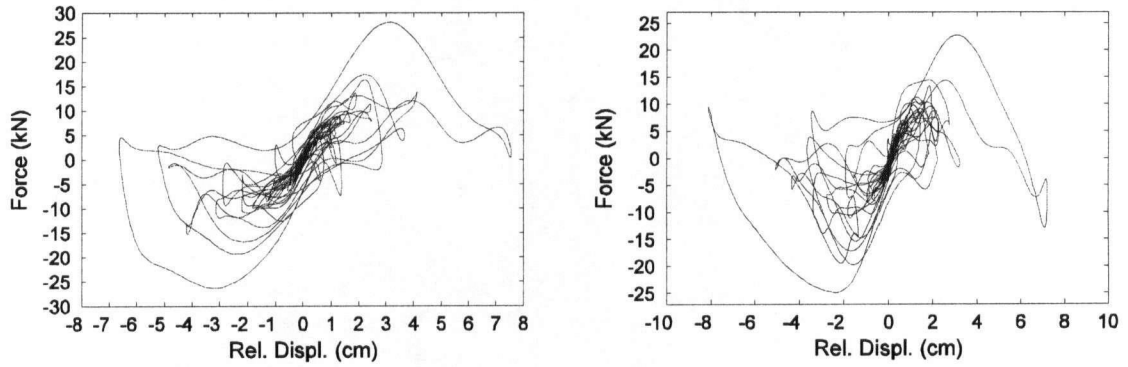


(a) Test GC4-1.21




(b) Test PC4-1.40

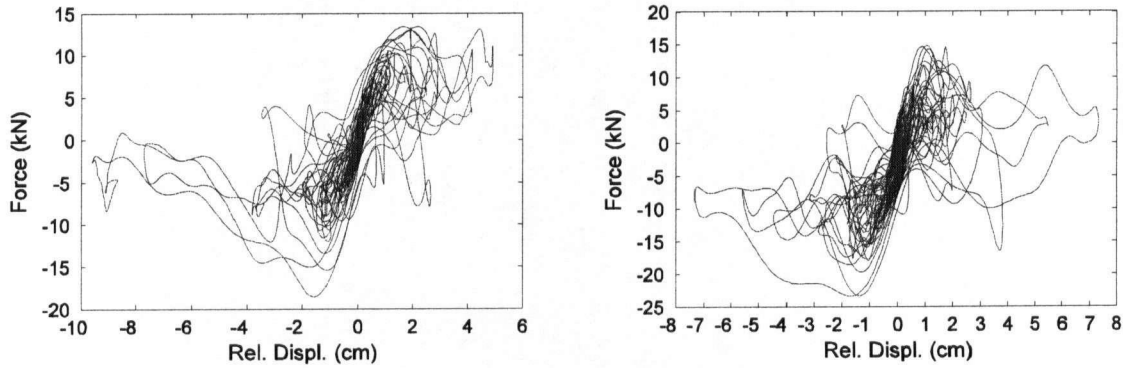


(c) Test GD4-1.24




(d) Test PD4-1.20

**Figure 4.27 Force vs. Crack Relative Displacement Hysteretic Response**

For these rocking walls, the negative stiffness occurs due to a drop in inertia force with increasing displacement. At point (A) in Figure 4.28, the wall experiences high applied forces with low relative crack displacements. This is due to the table acceleration and rocking wall inertial acceleration acting in the same direction, as the wall rocks in the positive direction (Figure 4.29). At point (B) the wall experiences a peak in the total force due to the combination of table and wall rocking motion. At point (C) the wall continues to displace in the positive direction, as does the rocking acceleration; however, the table acceleration has changed direction (Figure 4.29). This leads to a reduced acceleration profile for the wall (i.e. reduced total inertial force) with increasing relative crack displacement. At point (D) the table motion has again changed to the positive direction; however, due to the previous table motion cycle, the wall's rocking acceleration has switched to the negative direction, causing a reduction in the relative crack displacement and increase in total inertial force (Figure 4.29). There is a continued reduction in the relative crack displacement, point (E), such that the wall again behaves essentially elastically. Note that the acceleration profiles shown in Figure 4.29 are simplified, and for clarity do not include additional acceleration due to flexibility in the top restraint.

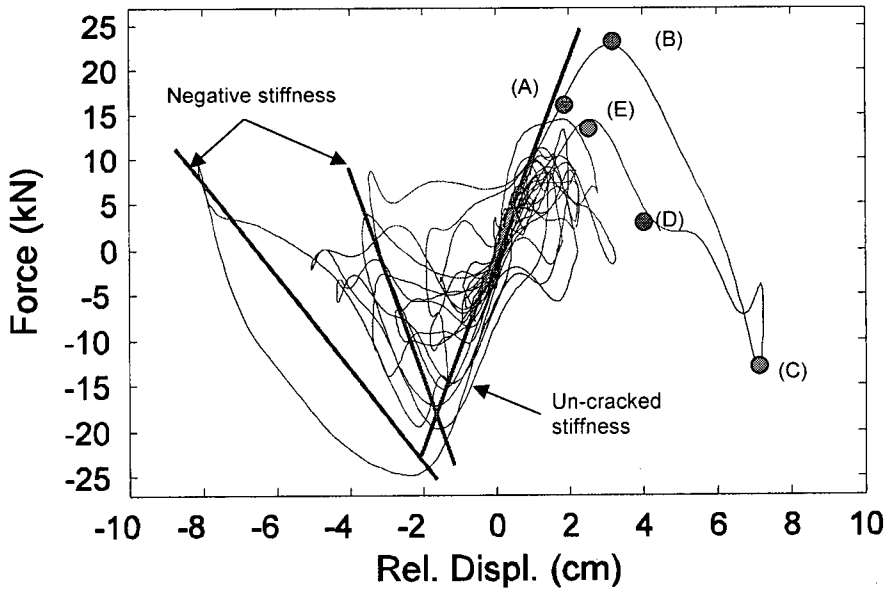


**Figure 4.28 Force vs. Relative Crack Displacement Behaviour**

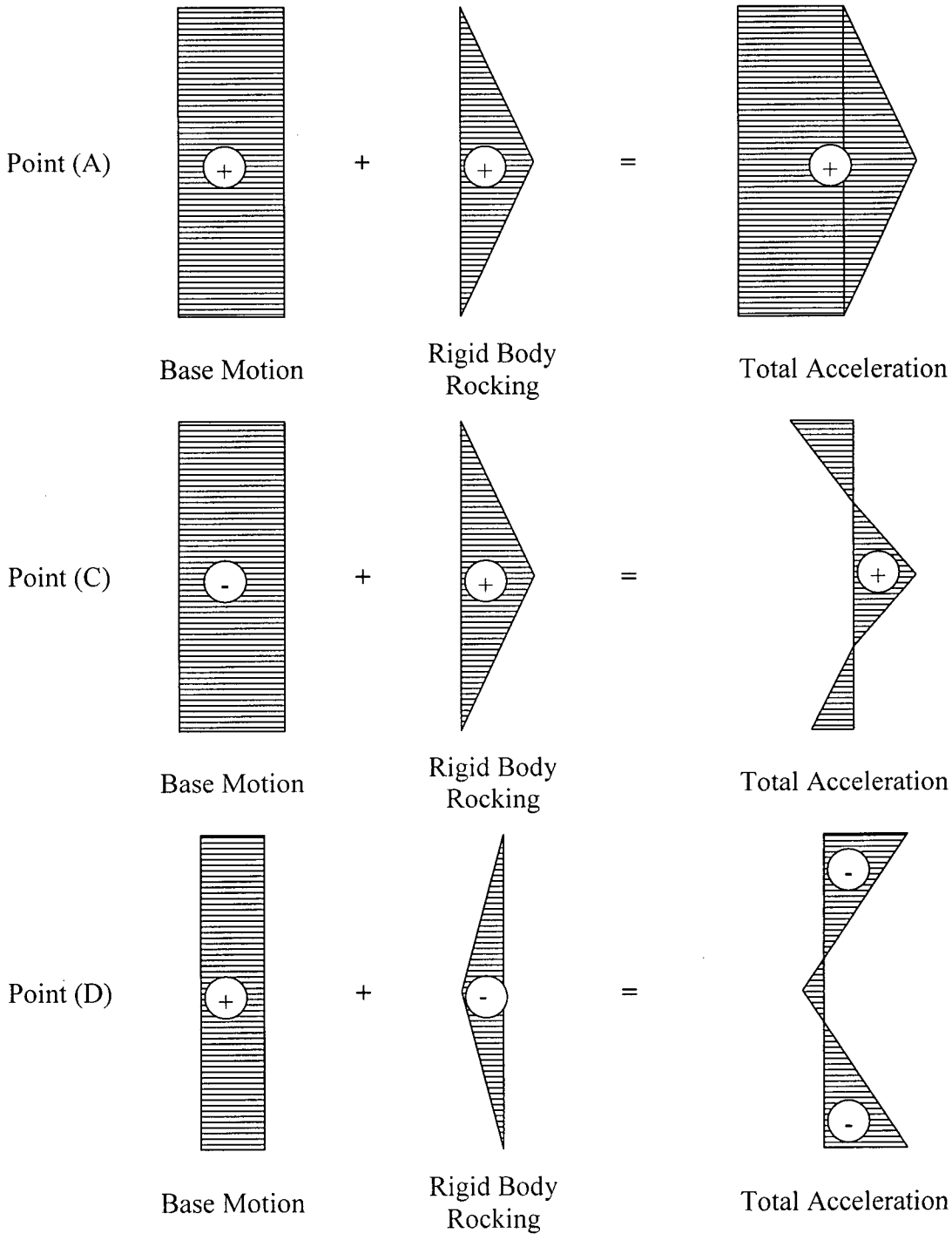


**Figure 4.29 Simplified Acceleration Profiles at Various Stages of Table Motion**

# 5 ANALYTICAL AND NUMERICAL MODELING

## 5.1 Introduction

In this chapter, simple mechanics based methods are presented that can be used by practicing engineers to estimate the key wall properties of un-cracked wall stiffness, maximum applied force on an un-cracked wall, and the cracking strength. These estimates are then compared to the results obtained from the full scale wall tests. An equation is also developed that relates the effective rocking acceleration at the crack location to the maximum total force on a wall, and is compared to the results seen in the tests. These simple analytical techniques can be used by engineers for estimating restraint forces. The test results are also compared to the predicted results obtained using a SDOF non-linear elastic model, and to the guidelines specified in the FEMA 356 and 306 in order to build confidence in the assessment criteria. Finally, a rigid body analysis method is proposed using commercially available software that can be used to model the out-of-plane response and stability of URM walls.

## 5.2 Un-Cracked Wall Stiffness

The un-cracked stiffness of the wall can be calculated through mechanics, assuming a simply supported prismatic beam of homogeneous material (i.e. constant elastic modulus and moment of inertia) with a uniformly distributed load (or acceleration) profile. The displacement, $\Delta$, at mid-height for a uniformly distributed load, $w$, is given by:

$$\Delta = \frac{5 \cdot w \cdot H^4}{384 \cdot E \cdot I} \tag{5.1}$$

Where $\Delta$ = Displacement at mid-height

$w$ = Uniformly distributed load

$E$ = Elastic Modulus (determined experimentally)

$I$ = Moment of Inertia

$H$ = Height of the Wall

And therefore the equivalent un-cracked stiffness, $k$, of the wall for an applied load of $wH$ can be defined as:

$$k = \frac{384 \cdot E \cdot I}{5 \cdot H^3} \tag{5.2}$$

The moment of inertia, $I$, was calculated assuming the wall consisted entirely of common courses. The equation for the moment of inertia can be defined as:

$$I = \frac{3 \cdot l_w \cdot w_b^{\,3}}{12} + 2 \cdot l_w \cdot w_b \left(\tfrac{1}{2} \cdot t_w - w_b\right)^2 \tag{5.3}$$

Where $l_w$ = Length/width wall

$w_b$ = Brick width

$t_w$ = Wall thickness

From mechanics the average calculated un-cracked stiffness was 46.2 kN/cm, slightly stiffer than that observed in the tests (42.6 kN/cm), but within one standard deviation (Table 1.1).

**Table 5.1 Un-Cracked Wall Stiffness**

| Wall | Un-Cracked Stiffness [kN/cm] | | |
|---|---|---|---|
| | **Observed** | **Calculated** | **Calculated Standard Deviation** |
| GC | 44.3 | 45.0 | 13.3 |
| PC | 43.9 | 45.4 | 13.4 |
| GD | 39.7 | 47.1 | 13.9 |
| PD | 42.4 | 47.2 | 14.0 |
| Average | 42.6 | 46.2 | 13.7 |

*Standard deviation based on the mortar elastic modulus standard deviation

## 5.3 Maximum Force on a Un-Cracked Wall

The estimated maximum force on an un-cracked wall was determined assuming a constant acceleration profile (i.e. acceleration at the base is equal to that at the top of the wall) equal to the PGA. The maximum force was calculated as:

$$F_{un-cracked} = M \cdot PGA \tag{5.4}$$

Where, $F_{un\text{-}cracked\ max}$ = Maximum applied force on an un-cracked wall

$M$ = Total wall mass

$PGA$ = Peak ground acceleration

The maximum force observed in the tests is compared to the calculated maximum un-cracked force in Table 5.2. The observed forces are at most 20% higher than the calculated values. This is due to the stiffness of the top restraint, which causes a trapezoidal acceleration profile with a higher acceleration at the top of the wall.

**Table 5.2 Maximum Force - Un-Cracked Wall**

| Wall/Test | Maximum Force [kN] | |
|---|---|---|
| | Observed | Calculated |
| GC1-0.71 | 18 | 15 |
| GC2-1.32 | 29 | 27 |
| PC1-0.73 | 15 | 13 |
| PC2-1.1 | 24 | 20 |
| GD1-0.75 | 14 | 15 |
| PD1-0.79 | 14 | 16 |

## 5.4 Cracking Strength

The cracking strength of the wall was estimated assuming the wall is simply supported, and having a constant acceleration profile as shown in Figure 5.1.

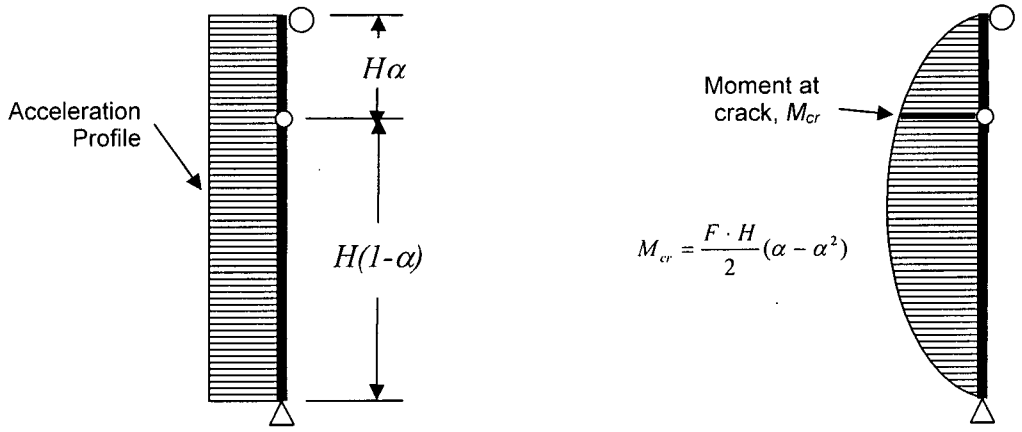


(a) Acceleration Profile (b) Moment Diagram

**Figure 5.1 Assumed Acceleration Profile and Bending Moment Diagram to Determine the Cracking Force**

The cracking force, ($F_{cr}$), considering both flexural resistance and axial load at the crack, can be defined as:

$$F_{cr} = \left[\sigma_{cr} + \frac{\alpha \cdot W}{A}\right] \frac{2 \cdot I}{H \cdot y \cdot (\alpha - \alpha^2)} \tag{5.5}$$

Where, $\sigma_{cr}$ = Cracking stress of masonry from bond wrench tests

$M$ = Applied moment at crack location

$y$ = Depth from extreme fiber to neutral axis, (i.e. ½ wall thickness)

$I$ = Moment of inertia (Equation 5.3)

$P$ = Axial load above crack

$W$ = Total wall weight

$A$ = Wall cross-sectional area

$H$ = Wall height

$\alpha$ = Crack location factor (defined in Figure 5.1)

The observed and calculated cracking force for each wall is shown in Table 5.3. The observed and calculated cracking strength matches very well for walls GD1-0.75 and PD1-0.79; within one standard deviation for wall PC2-1.1, and within two standard deviations for wall GC2-1.32. The standard deviation on the cracking strength based on the variability of the flexural stress of the mortar is also shown in Table 5.3.

**Table 5.3 Cracking Strength**

| Wall | Cracking Strength [kN] | | |
|---|---|---|---|
| | **Observed** | **Calculated** | **Calculated Standard Deviation*** |
| GC2-1.32 | 15 | 10 | 3.2 |
| PC2-1.1 | 13 | 11 | 3.5 |
| GD1-0.75 | 14 | 14 | 4.5 |
| PD1-0.79 | 13 | 14 | 4.5 |

*Standard deviation based on the mortar bending stress standard deviation

## 5.5 Maximum Total Force on Cracked Wall

The maximum total force on the wall is an important quantity as it can be used to determine forces acting on the restraints. An estimate of the maximum force can be found using the following equation:

$$F_{cracked\_max} = M \cdot a_{rocking} \tag{5.6}$$

Where, $F_{cracked\ max}$ = Maximum applied force on a cracked wall

$M$ = Total wall mass

$a_{rocking}$ = Effective rocking acceleration at crack

The estimated and observed maximum total force is shown in Figure 5.2, and the ratio of observed/calculated force is shown in Figure 5.3. On average, Equation 5.6 gives a good estimate of the maximum inertia force on the wall, with an average observed maximum total force of 22.8kN compared to the calculated estimate of 22.7kN (Table 5.4). As was previously discussed in Section 4.4.4, the observed maximum forces were calculated by multiplying the measured acceleration profile by the mass of the wall. From looking at wall acceleration profiles it is clear that this profile is not constant along the height of the wall at the time when the maximum force occurs. The results obtained from Equation 5.6, would seem to suggest that average acceleration along the height of the wall is approximately equal to the acceleration at the crack. At this time, the relationship between the effective rocking acceleration and maximum total force is being further investigated, and a method to calculate the effective rocking acceleration is being developed.

**Table 5.4 Average Maximum Total Force – Cracked Wall**

| Wall* | Maximum Total Force [kN] | |
|---|---|---|
| | Observed | Calculated |
| GC | 26.9 | 26.8 |
| PC | 24.1 | 22.0 |
| GD | 20.1 | 20.5 |
| PD | 20.2 | 21.34 |
| Average | 22.8 | 22.7 |

*Note: Only previously cracked walls considered.

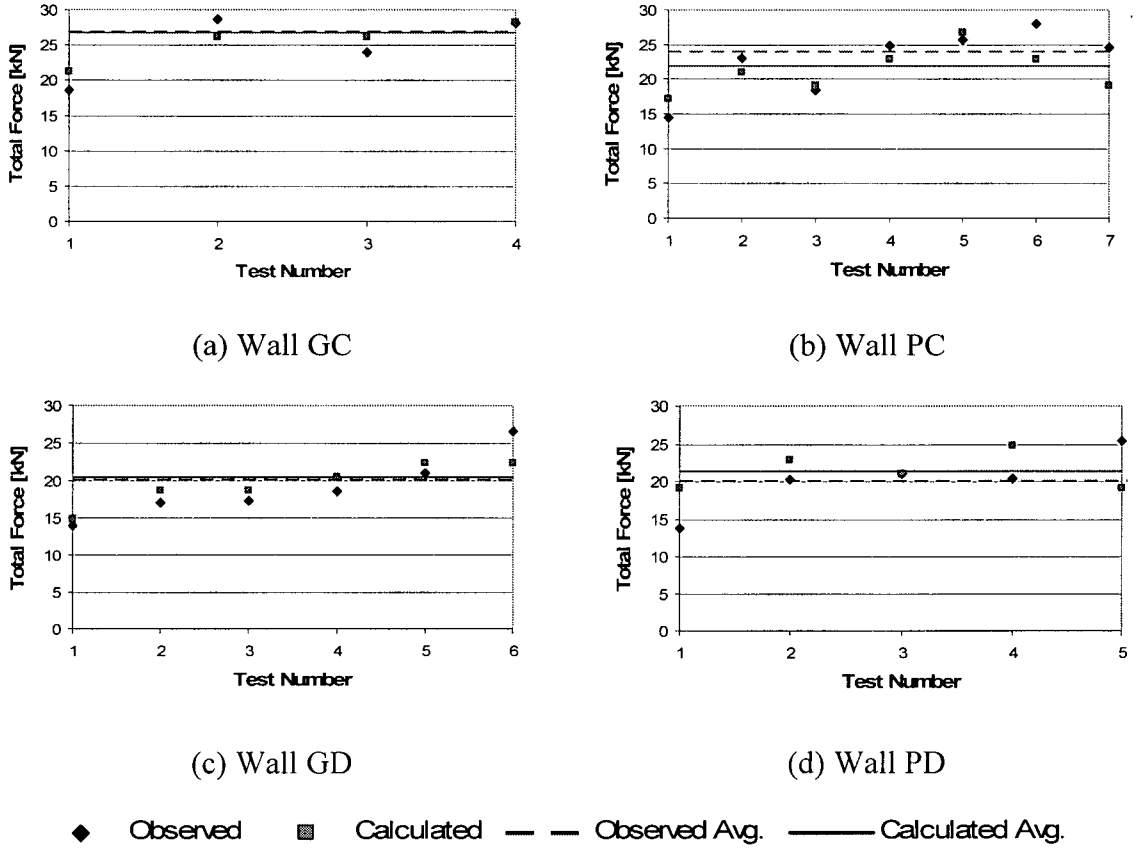


**Figure 5.2 Maximum Observed and Calculated Total Force**

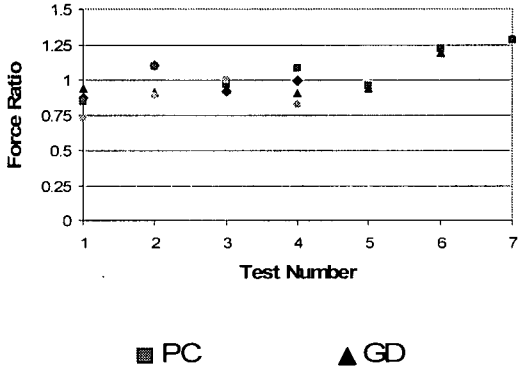


**Figure 5.3 Maximum Force Ratio (Observed/Calculated)**

By comparing the observed and calculated total forces applied either on an un-cracked wall, to cause cracking, or on a cracked wall (Tables 5.2, 5.3, and 5.4 respectively), it appears, that on average, the maximum force that a wall may experience occurs when it is cracked. Therefore, the

anchorage capacity must be designed for this level of force and deformation compatibility with the rocking wall.

## 5.6 FEMA Acceptance Criteria

As was previously discussed in Chapter 1, the FEMA 356 acceptance criteria for un-cracked walls is often used by practicing engineers to assess the out-of-plane vulnerability of URM walls. Acceptance is based on height to thickness ratio (*h/t*) limits expressed as a function of the spectral acceleration at a structural period of 1.0 seconds, $S_a(1.0s)$. Figure 5.4 and Figure 5.5 show the acceptance criteria for Vancouver and Victoria. For Vancouver, all un-cracked walls on a Site class C soil would be acceptable; however, for a wall on site class D, a top-storey wall of a multi-storey building would be unacceptable. For a building located in Victoria, on either a site class C or D soil, walls located on only a top-storey wall of a multi-storey building would be unacceptable.

FEMA 356 requires that the condition of the collar joints be considered when determining the effective wall thickness. Wythes separated by collar joints that are not bonded, or have an effective collar joint void ratio greater than 50%, are not to be considered as part of the effective wall thickness. In the experimental tests, the poor quality walls had an effective collar joint void ratio less than 50%, and therefore, would require a significantly lower effective wall thickness. In these tests all of the cracking and damage occurred at header courses and not at the common running bond courses. This would suggest that the quality of the collar joints at common courses is not as significant if the header courses are of adequate quality, and therefore no reduction in effective wall thickness would be required for poor collar joint quality.

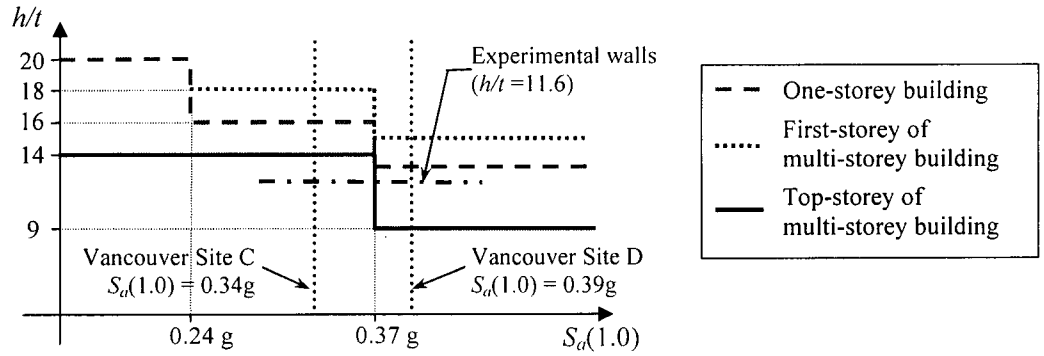


**Figure 5.4 FEMA 356 Acceptance Criteria for Vancouver**

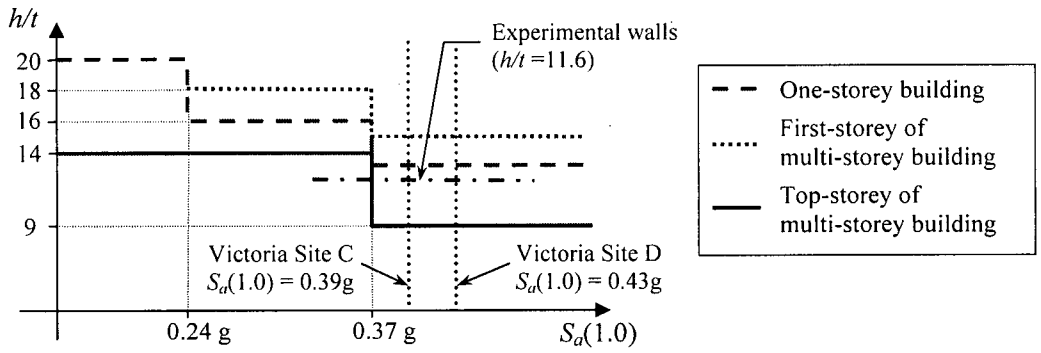


**Figure 5.5 FEMA 356 Acceptance Criteria for Victoria**

For walls that have undergone damage from a past earthquake, FEMA 306 can be used to assess URM out-of-plane susceptibility (Table 1.1). Depending on the level of damage to the wall, (i.e. crack widths, mortar spalling, out-of-plane offset), a *h/t* factor ($\lambda_{h/t}$) may be assigned thereby reducing the allowable *h/t* limit (Figure 5.4 and Figure 5.5). The damaged walls were classified after each test, as per the FEMA 306 guidelines, to obtain the *h/t* factor ($\lambda_{h/t}$). The $S_a(1.0s)$ were then obtained from the input table's motion response spectra, and allowable *h/t* limits according to FEMA 306 were then determined. Figure 5.6 shows the allowable *h/t* ratio for the damaged walls, Figure 5.7 shows each test's corresponding $S_a(1.0s)$. As expected, with each successive test the walls become further damaged, resulting in a lower $\lambda_{h/t}$ factor. As the walls were tested with increasing amplitude, the $S_a(1.0s)$ also increased, resulting in decreased allowable *h/t* limits. For the walls tested, the FEMA 306 criteria are conservative, particularly for a wall located on the top-storey of a multi-storey building. However, as the walls tested had a very stiff upper restraint (i.e. stiff diaphragm) the strict criteria may be justified in the top-storey of a multi-storey building as a flexible diaphragm may amplify the motion making the walls less stable.

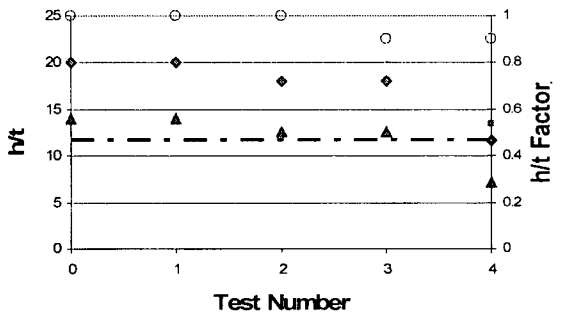


(a) Wall GC

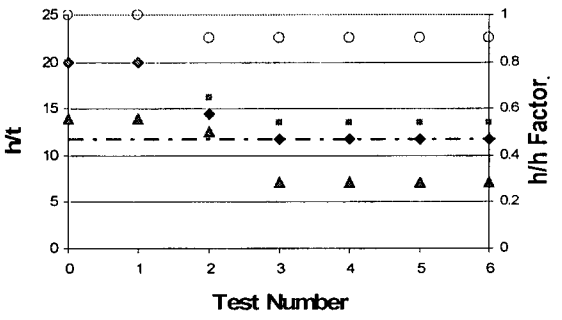


(b) Wall PC

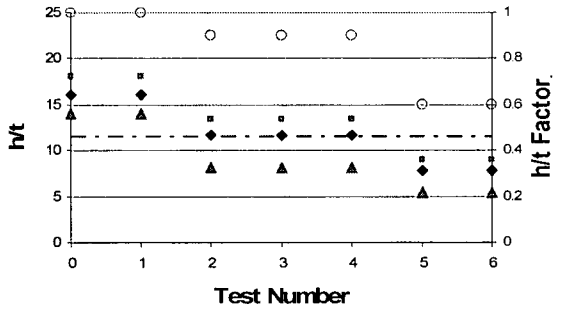


(c) Wall GD

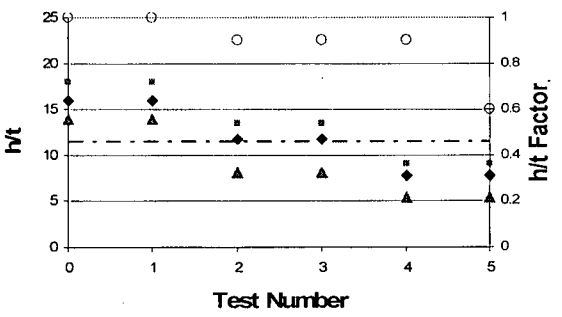


(d) Wall PD


**Figure 5.6 FEMA 306 Acceptance Criteria**

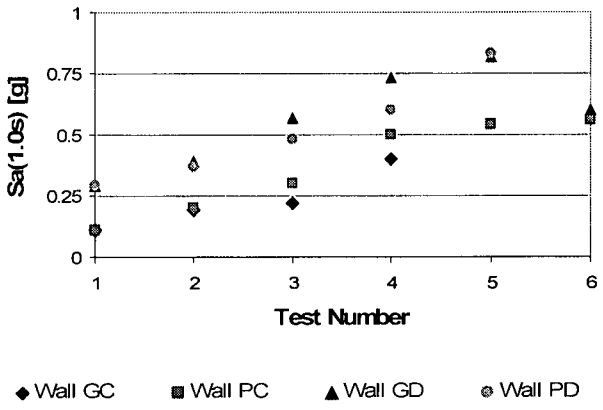


**Figure 5.7 Sa(1.0s) for Each Test**

## 5.7 Comparison to SDOF Non-Linear Elastic Model

As was previously discussed in Chapter 2, a SDOF non-linear elastic model [Doherty, 2000] can be used to estimate the out-of-plane response of the walls subjected to a specified ground motion. The measured maximum relative displacements at the crack location versus scale factor, compared against the analytical SDOF results, are shown in Figure 5.8. For all tests performed, the estimated peak relative crack displacement of the walls do not compare well to the analytical results, with the analytical model predicting higher displacements (i.e. more conservative). This may be due to the fact that the analytical model assumes a crack formed at the mid-height of the wall, while the experimental walls formed a crack at header courses above mid-height. Also multiple cracks formed in Walls GD and PD. Further study is required to investigate how the crack location and multiple cracks affect the rocking behaviour. As shown in the SDOF results in Figure 5.8 (a) and (b), both pairs of walls subjected to the crustal site C and D ground motions exhibited a sudden increase in peak relative crack displacement as the amplitude of the ground motion was increased. This suggests that the stability of the wall is very sensitive to the amplitude of the ground motion. Considering this sensitivity and the consequences of failure, it may be prudent to use a conservative assessment of the *h/t* limit.

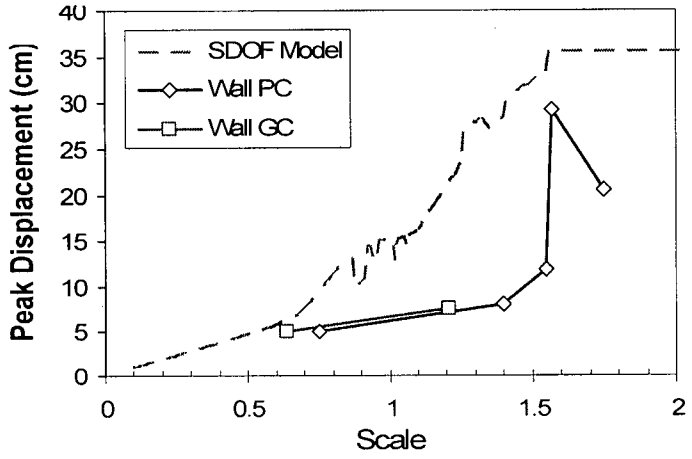


(a) Site Class C Ground Motion – Gilroy

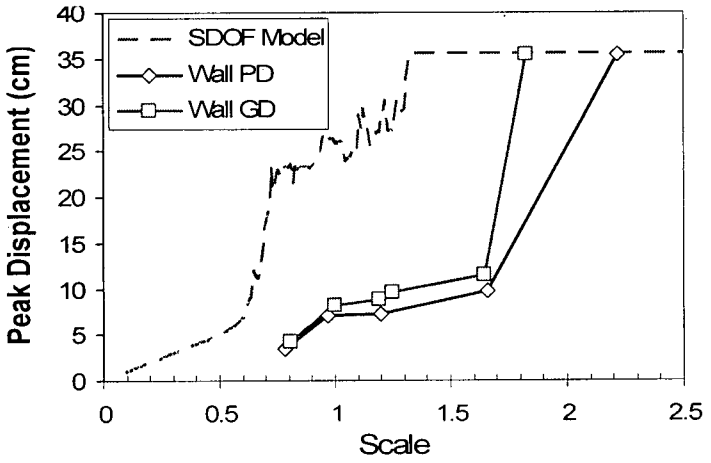


(b) Site Class D Ground Motion – Hayward

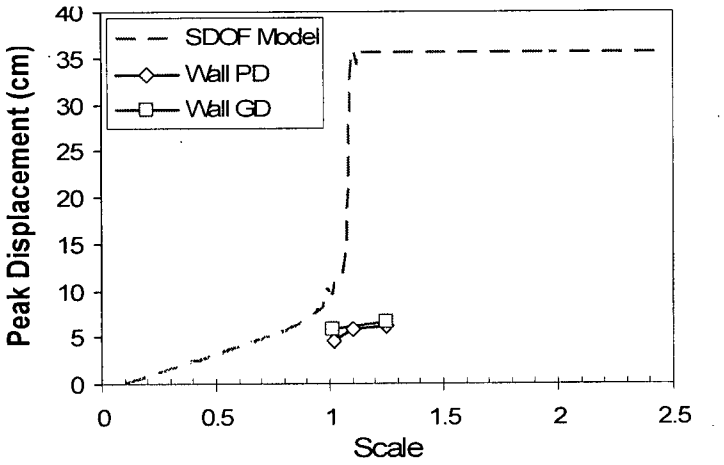


(c) Site Class D Subduction Ground Motion – HKD 109

**Figure 5.8 SDOF Non-Linear Elastic Model Comparisons**

## 5.8 Rigid Body Analysis Using Working Model 2D

As dynamic testing of full-scale walls is both expensive and resource intensive, it would be ideal to develop numerical models that could accurately predict the response of a cracked wall to out-of-plane dynamic excitations. As was previously discussed, models have been developed that model a URM wall as a non-linear elastic system assuming a tri-linear force displacement response and variable Ralyiegh damping [Doherty 2000]. However, it has been shown that this type of analysis may not be appropriate for a rocking body problem, and that a rigid-body rocking analysis may be more appropriate [Makris 2002].

Konstantinidis et al. [2005] performed a numerical investigation into the seismic response of multi-drum columns, similar to those found in ancient Greek temples. By performing a rigid body analysis using commercially available software, Working Model, they where able to validate the pure sliding and pure rocking response of a block, suggesting that the software could correctly model the seismic response of a rigid body. In order to verify the applicability of a rigid-body analysis to the out-of-plane response of the walls, Working Model 2D [Knowledge Revolution, 1996], was used.

Working Model (WM) allows a user to define a set of rigid bodies and constraints (e.g. actuators, springs, and joints), and performs a dynamic simulation using Newtonian mechanics and numerical methods. A problem is time-discretized such that the program can compute motions and forces, while making sure that the constraints are satisfied. One of the most challenging tasks in the dynamic analysis of the rigid bodies is the treatment of the contact surfaces. In the tangential direction, the interaction of the contact surfaces is governed by the static and dynamic Coulomb friction. During the course of the analysis two or more surfaces may overlap/collide. In WM, collisions are detected by finding the intersections between two bodies. This is done by tracking a 'master' node, such that the position and orientation of all the edges of the rigid body is known. When a collision is detected, WM employs an impulse based collision model, based on the coefficient of restitution, in order to calculate the impact forces. The solution of the body motion is governed by differential equations; for a two-dimensional problem, the following mechanical principles are considered: force, torque, instantaneous acceleration, instantaneous velocity, and instantaneous angular velocity. These differential relations are solved using either the Euler or Kutta-Merson (5th-order Runge-Kutta) numerical

methods. Integration error, model assembly and collision overlap tolerances can be set to achieve the desired precision. [Knowledge Revolution, 1996]

### 5.8.1 Modeling of Walls Using Working Model 2D

In order to study the rocking motion of a cracked wall, the following key parameters must be defined in the program:

1) *Body geometry:* the size of the rigid blocks, height/thickness ratio and crack location. The wall was modeled as two rigid blocks, consisting of an upper and lower portion, with the test wall geometry.

2) *Body density:* the mass of the test walls was used, assuming a uniform mass distribution.

3) *Mass moment of inertia*: the two portions of the wall were assumed to be uniform and have a uniform mass distribution.

4) *Elasticity:* corresponds to the coefficient of restitution, which is required in computing the collision/rocking response of the wall. The coefficient of restitution is equal to the ratio of the relative velocities of the collided objects immediately before and after collision. For example, if the coefficient of restitution was equal to 0, the bodies would stick together; if the coefficient was 1, the velocities after impact would be the same, but in the opposite direction. The coefficient of restitution is similar to a damping term, with a smaller value resulting in greater damping. Wall PC was modeled with a coefficient of restitution of 0.02, and 0.023 for wall PD (this is discussed further in the following section).

5) *Friction:* is taken into account by considering both static and kinetic coulomb friction. It is proportional to the normal force applied to the contact surface. From a survey of literature, typical values of friction coefficients for masonry range between 0.65 – 0.75 [Atkinson 1989]. The walls were modeled with a static coefficient of 0.75, and a dynamic coefficient of 0.70.

6) *Boundary conditions:* boundary conditions were chosen to mimic those in the full scale tests (Figure 5.9). Both the upper and lower portion of the walls where modeled to have a slotted connection allowing rotation and vertical translation. At the base of the wall a

frictionless plate was added to represent the base plate; this provides the vertical support for the weight of the wall.

7) *Input motion:* Table motions were introduced into the model by using displacement controlled actuators at the top and bottom of the wall (Figure 5.9). Displacement data recorded from the table and top restraint during the tests was used in the model.

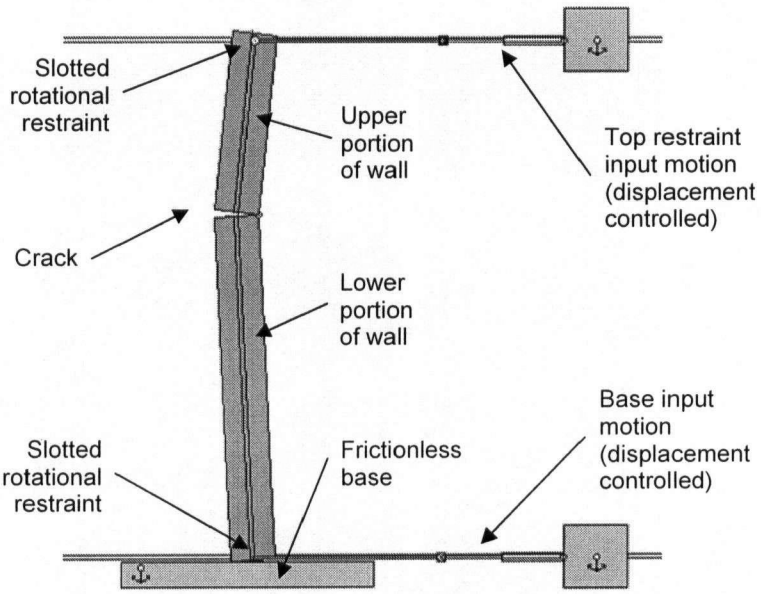


**Figure 5.9 Out-of-Plane Rocking, Modeled Using Working Model 2D**

### 5.8.2 Working Model (WM) Results

The model was adjusted to represent Walls PC and PD, considering the wall geometry (*h/t* and crack location), mass, and measured displacements at the top and base of the wall. Tests PC4-1.4 and PD3-0.97 were used to calibrate the model. These walls were chosen because they underwent rocking for a large portion of the record, and their relative displacements were not too large (approximately 30% of the instability limit). The coefficient of restitution was adjusted such that the relative displacements at the crack matched as closely as possible to those observed in the test. The coefficients were set to 0.020, and 0.023 for wall PC and PD respectively. The calibrated model was then used to evaluate the response to varying amplitudes of the table motions without the need for further calibrations.

Results from the WM analysis of walls PC4-1.4 and PD3-0.97 are compared to the results from the full scale tests in Figure 5.10 and Figure 5.11. The WM analysis does a good job of tracking

the general trend of the absolute displacements at the crack location. The model also adequately captures the peak relative displacement; however, there are times when it may slightly over estimate the relative displacement, causing the wall to over rock and miss-judge the actual response for a short period. The spikes in the WM computed crack acceleration appear to occur during impact between the upper and lower portion of the wall. These spikes are of very high frequency, and do not appear in the test results as the data had been post processed using a 25 Hz low pass filtering window. From the observed data it would be very difficult to distinguish the high frequency accelerations due to impact, and those due to noise. The total force obtained with WM is offset from those observed in the full-scale tests. This difference may be due to how the total force was calculated. In the tests the total force was calculated by multiplying the acceleration at each header by the lumped mass at the header. In the WM analysis, the total force was recorded from the displacement controlled actuators at the top and bottom of the wall. Further examples and comparisons from other tests can be found in Appendix H.

Figure 5.12 shows the peak relative crack displacements versus scaling factor for walls PC and PD. The input motions used were those recorded at the top restraint and wall base from the full scale tests. The peak relative displacements from the Working Model analyses for walls PC and PD are very close to those recorded from the shake table tests. It should be noted that for the high amplitude input motions, additional cracks formed during the full scale tests. Cracking occurred at header 1 during test PC5-1.55, at header 2 and 3 during test GD5-1.65, at header 1 during test PD2-0.78, and at header 9 during test PD5-1.66. These multiple cracks in the walls may decrease the peak relative displacements, thus making the wall more stable, but were not considered in the WM analysis. Work done by Konstantinidis et al. [2005], on free-standing columns, also showed that more rigid body segments will increase the assembly's stability.

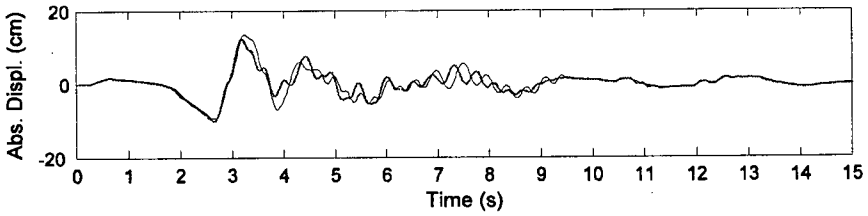


(a) Absolute Displacement Time History at Crack

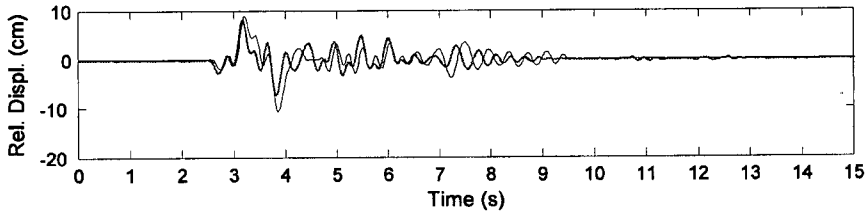


(b) Relative Displacement Time History at Crack

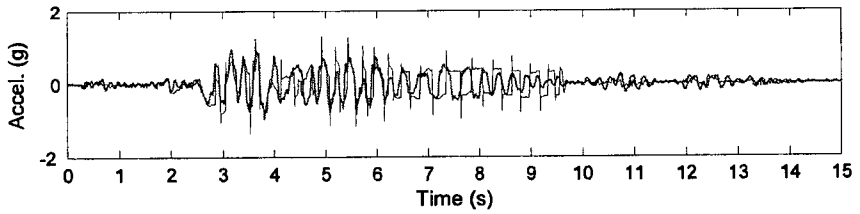


(c) Acceleration Time History at Crack

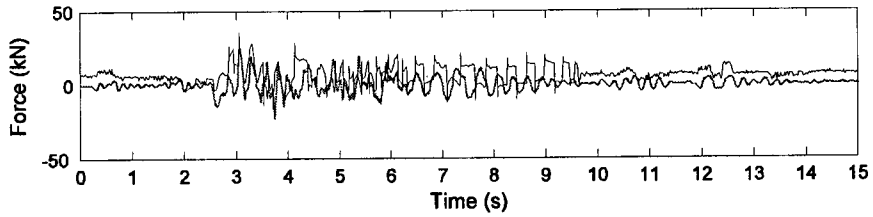


(d) Total Force Time History

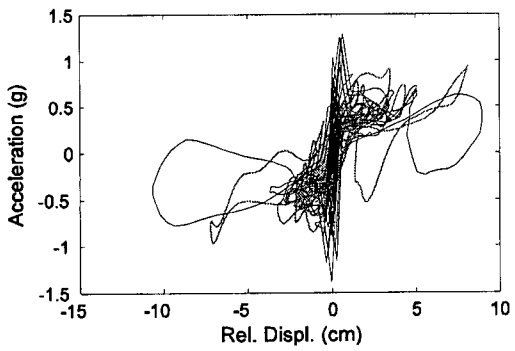


(e) Crack Acceleration vs. Relative Crack Displacement

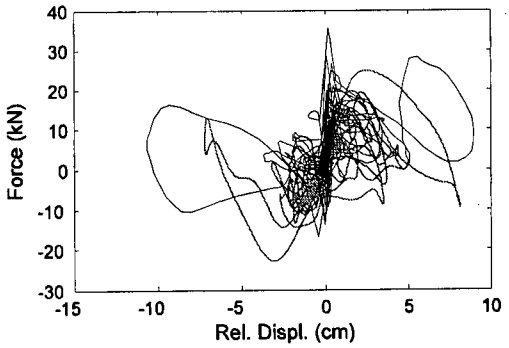


(f) Total Force vs. Relative Crack Displacement

( — Full Scale Test, — Working Model)

**Figure 5.10 Working Model and Full Scale Test Comparison, Wall PC4-1.4**

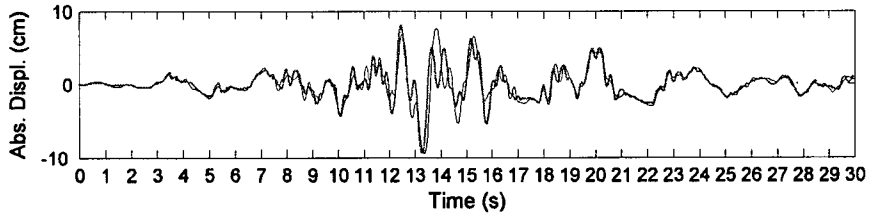


(a) Absolute Displacement Time History at Crack

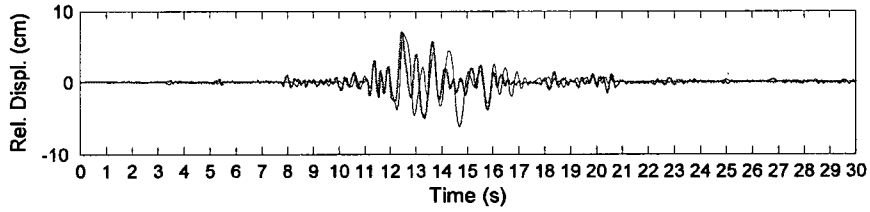


(b) Relative Displacement Time History at Crack

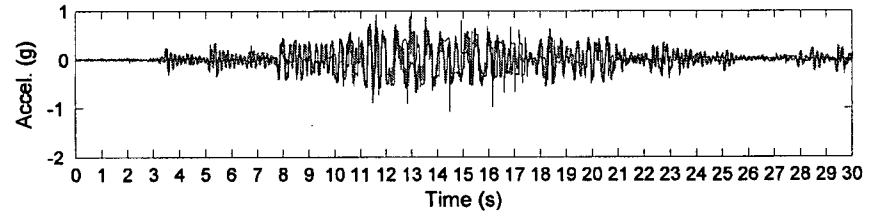


(c) Acceleration Time History at Crack

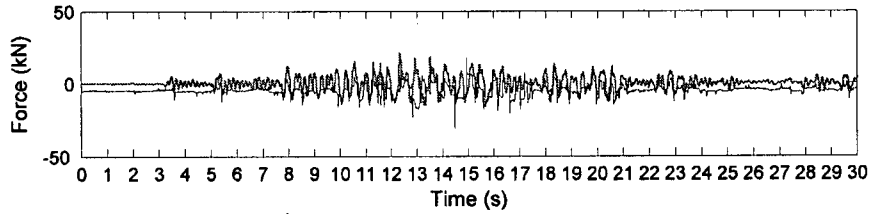


(d) Total Force Time History

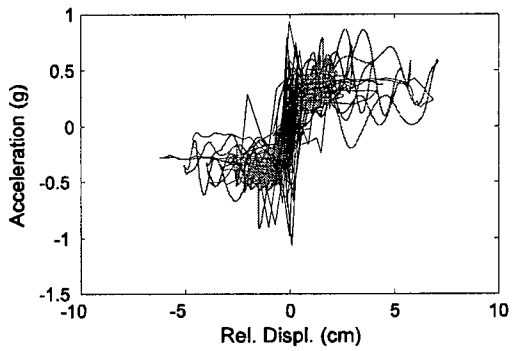


(e) Crack Acceleration vs. Relative Crack Displacement

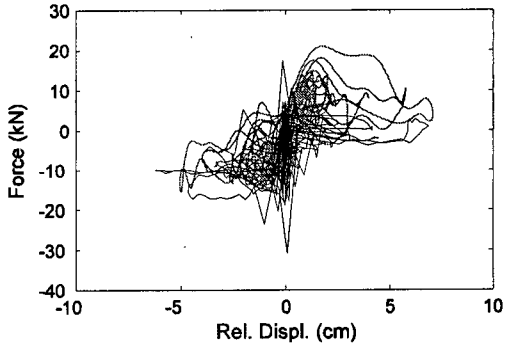


(f) Total Force vs. Relative Crack Displacement

( —— Full Scale Test, — Working Model)

**Figure 5.11 Working Model and Full Scale Test Comparison, Wall PD3-0.97**

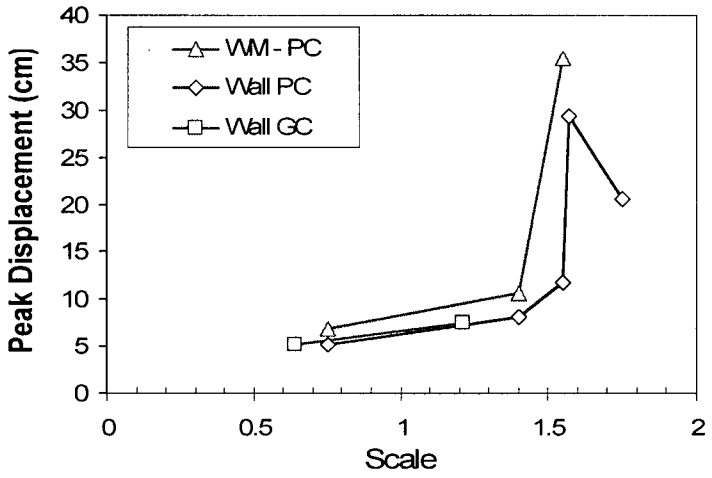


(a) Site Class C Ground Motion – Gilroy

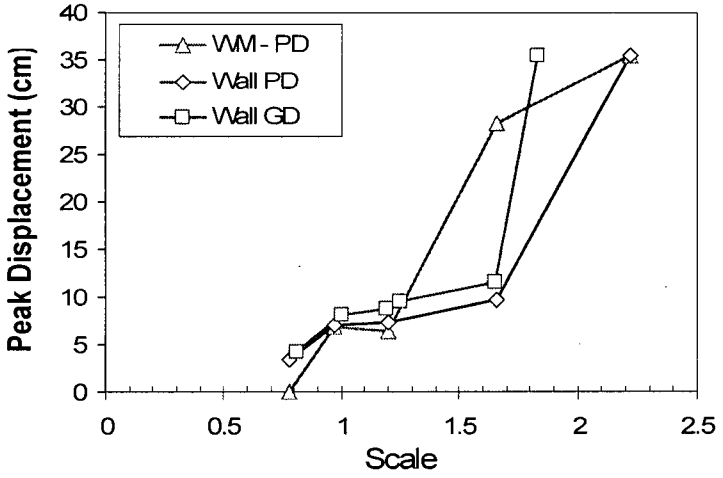


(b) Site Class D Ground Motion – Hayward

**Figure 5.12 Working Model Comparison**

An instability envelope, Figure 5.13, was developed for the site class C and D crustal ground motions using Working Model. The geometry of walls PC and PD were used, and 'code level' input motions were obtained by scaling the input motions used in the calibration models (Figure 5.10 and Figure 5.11) back to the code level (i.e. scale factor of 1.0). The analysis was then run by incrementally scaling the code level input motion, and peak relative displacements from the WM analysis were recorded for each run producing the instability envelope. The instability envelope produced for site class C represents the full scale tests very well. For the site class D ground motion, instability begins to occur at a scaling factor of approximately 1.1, earlier than a

scaling of 1.75 as observed in the tests. This difference may be due to the additional cracks which formed in the lower portion of the wall, (as mentioned above), for table motions with a scale factor above 0.78 for wall PD and 1.65 for wall GD, possibly reducing displacements and increasing stability. The peak relative displacements at scaling factors of 1.2 and 1.6 are higher compared to those obtained in the previous analysis (Figure 5.12). This is due to the input motions used; in the previous analysis the actual displacements recorded from the full-scale tests were used, while in the instability analysis, scaled 'code level' table motions were used. These motions may not be the exact same (i.e. different frequency content, amplitude, etc.), indicating that the response of the walls is sensitive to the input motions used.

As seen in the instability envelopes (Figure 5.13), there are instances were the wall can survive a ground motion that exceeds the previous motion which is capable of making the wall unstable (i.e. the response of the wall is multi-valued). This is due to the inherent nonlinearity of the problem, and has been shown by Makris and Zhang [1999] and Zhang and Makris [2001]. Also, it appears for the ground motions used, that the walls are more vulnerable on softer soil sites. Furthermore, the WM analysis shows a sudden increase in peak relative crack displacement as the amplitude of the table motion was increased. If engineers were to assess the stability of the walls using ground motions scaled to a particular code level, they should consider increasing the scaling of the ground motion to determine if they are near instability.

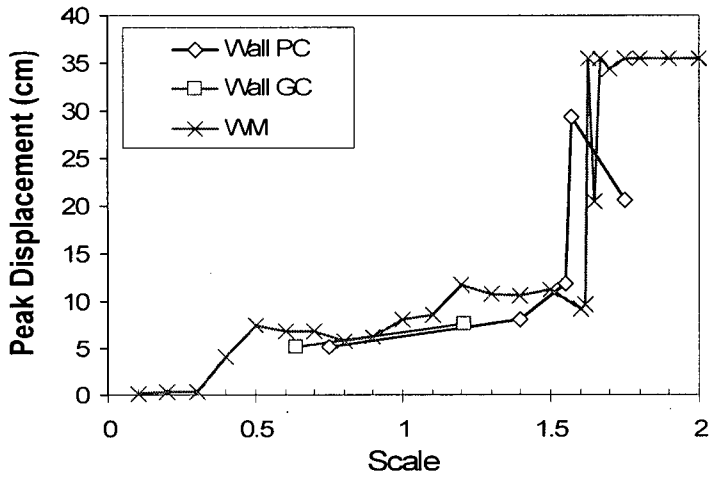


(a) Site Class C Ground Motion – Gilroy

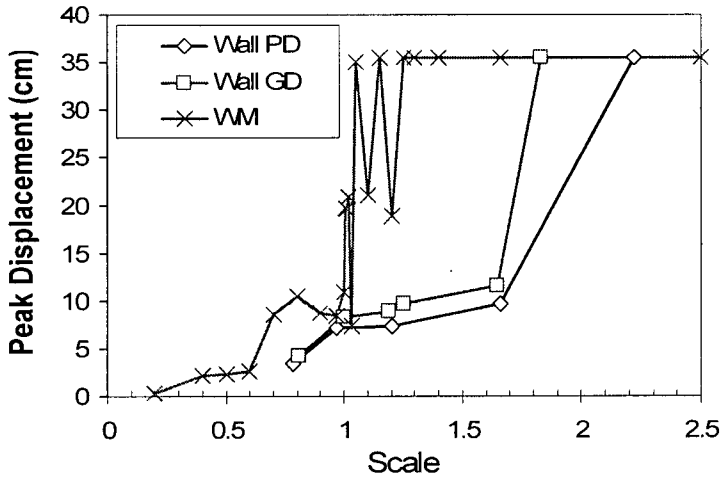


(b) Site Class D Ground Motion – Hayward

**Figure 5.13 Working Model Instability Envelopes**

### 5.8.3 Modeling Issues

While using Working Model, there were a few modeling challenges that arose. In order to get accurate results, especially higher frequency displacements, a small time step had to be used in Working Model, (0.01s). The overlap factor (i.e. accuracy of the rigid body contact surfaces) was required to be low (0.001m). Working Model also limits the number of data points used in the input motions to 2040. The raw data from the tests was sampled at 0.002s; for the site class C motion, the input motion was re-sampled at 0.01s, and the site class D was re-sampled at 0.03s. These low sampling rates, particularly for the site class D motion, have a significant effect on the

accuracy of the analysis. The most recent version, Working Model 2005, has removed this data limit. It should be noted that the analysis of a wall to a particular ground motion is very fast and efficient, taking approximately 10s for the above mentioned analysis.

### 5.8.4 Future Model Developments

The results that were previously presented were generated from a simple model. Further developments can be made to the model to investigate how the wall's behaviour may change and are presented below.

#### 5.8.4.1 Rigid Body Properties

During the course of the analysis it was observed that the results were sensitive to the coefficients used for coulomb friction and elasticity/coefficient of restitution. ElGawady et al. [2006] performed experiments on free rocking masonry and concrete blocks, showing that both the aspect ratio of the blocks and interface material had a significant influence on the rocking response. Further work needs to be done in order to determine bounds to these coefficients for modeling purposes.

#### 5.8.4.2 Crack Degradation

Degradation of the wall at the crack location was observed in the full scale tests, where mortar and brick crushing were evident (see Chapter 4). This crack deterioration, combined with the elasticity of the masonry, causes the contact between the upper and lower portion of the wall to act over a surface instead of a point (Figure 5.14 (a)). As the contact takes place over a surface, the resulting reactions shift towards the centre of the wall, decreasing the stability of the wall (due to a lower effective wall thickness). In the current Working Model analysis, the wall is modeled as two rigid blocks (Figure 5.14 (b)) causing the resulting reactions to be located at the outer most edge of the wall once rocking is initiated. In order to mimic the crack damage observed in the test walls, the contact surfaces could be modeled as a shallow ellipse (Figure 5.14 (c)). With this change to the model, the contact between the portions of the wall will still occur at a point, but due to the curvature of their contact surfaces the reaction force would shift towards the centre of the wall.

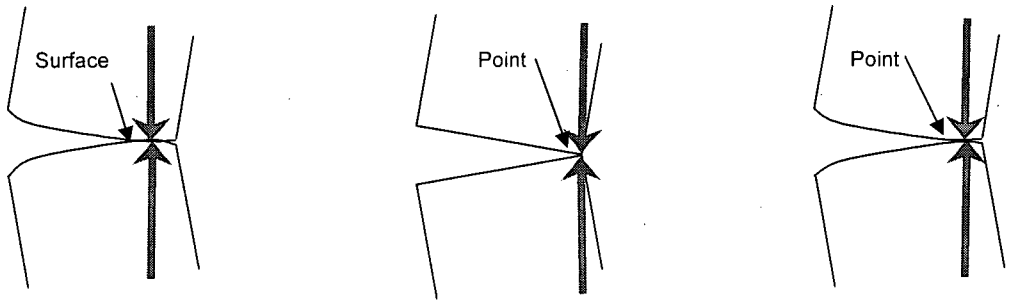


(a) Actual Wall (b) Current Model (c) Proposed Model

**Figure 5.14 Effect of Crack Condition on Reaction Force**

### 5.8.4.3 Variable Crack Location and Multiple Cracks

Working Model could be used to investigate the change in rocking behaviour by varying the crack location and incorporating multiple cracks (i.e. several rigid blocks). In the actual tests, more than one crack formed, possibly decreasing the relative displacements, thereby making the wall more stable. This could be verified through further modeling.

### 5.8.4.4 Boundary Conditions

The previously discussed model used rotational slotted connections as the boundary conditions. As shown in Tests GC5-1.49 through GC7-1.71, the effect of an applied moment greatly increases the walls stability. This could be verified by modifying the boundary condition to include a bearing plate at the top of the wall. The boundary conditions could also be modified to account for diaphragm flexibility, constrained vertical motion due to floors, and vertical gravity loads. Rotational springs and damping could also be included to model possible wall connections and/or retrofitting options.

### 5.8.4.5 Restraint Forces

For engineers designing retrofitting options, Working Model can be used as a tool to generate forces from the restraints. These forces can be used to give an estimation of the required capacity needed in URM wall connections. If the wall is allowed to rotate, rotational demands on restraints can also be estimated.

### 5.8.4.6 Fragility Curves

Once confidence in the accuracy of the model has been developed, fragility curves could be developed using techniques similar to incremental dynamic analysis [Vamvatsikos, 2001]. Wall models could be analyzed using several ground motions that are incrementally scaled to produce instability envelopes, similar to those in Figure 5.13. These results could be used to develop fragility curves that relate the probability of collapse with the ground motion intensity. These curves could be developed for various *h/t* ratios in order to allow designers to carry out a performance based design for the out-of-plane response of a URM building.

# 6 CONCLUSIONS AND RECOMMENDATIONS

## 6.1 Conclusions

The study presented has investigated the sensitivity of the out-of-plane response of multi-wythe URM walls to the type of ground motion and the quality of the wall construction. Analyses based on a nonlinear-elastic SDOF model indicate that, given sufficient anchorage of the walls to the diaphragms, URM buildings located on soft soil sites are more likely to experience out-of-plane wall failures than buildings located on firm ground. On average, the intensity of the site class C ground motions had to be scaled 1.7 times higher than the level of the 2005 NBCC to observe instability; while the site class E ground motions caused instability of the wall just below the level of the 2005 NBCC. Based on the shake table test results, the SDOF model generally provides a conservative estimate of the peak response of multi-wythe URM walls.

Shake table tests were conducted on four full-scale multi-wythe walls with varying construction quality and using three different ground motions. All walls experienced cracking at approximately the PGA of the 2005 NBCC level, but exhibited a stable rocking behaviour without collapse beyond a ground motion 1.5 times greater than the 2005 NBCC level. The quality of the collar joints did not appear to have an impact on the peak response of the walls.

The walls had a height-to-thickness (h/t) ratio of 12, thereby exceeding the h/t limit of 9 specified by current seismic rehabilitation guidelines, (FEMA 356), for the top storey of a multistorey building located in Vancouver, and hence would require extensive retrofit based on these guidelines. Considering the good performance of the walls during the shake table tests, the h/t limits from FEMA 356 appear somewhat conservative for the evaluation of similar walls adequately supported by the floor diaphragms. For a one-storey building, the walls satisfied the h/t limits from FEMA 356 and would not require retrofit.

The walls un-cracked stiffness, maximum force on an un-cracked wall, cracking strength and the maximum total force acting on a cracked wall were calculated with simple analytical techniques and compared very well to the results observed. Results obtained from the shake table were then compared to the SDOF model. In all cases the SDOF model provided a conservative estimate of

the peak response of multi-wythe URM walls. However, as shown by other researchers, modeling the wall as a damped oscillator type system may not be an appropriate representation of rocking bodies. Therefore, a rigid body numerical model was developed using a commercially available software, Working Model. The results obtained using this model compared very well to the full-scale tests, accurately predicting the maximum relative displacement at the crack location for the scaled ground motions used in the testing program.

## 6.2 Recommendations

The following recommendations are made for future research:

- Further testing is required to investigate the sensitivity of these observations to the input motion, including any amplification of input motions for the walls in multi-storey buildings.
- As the results of the full-scale tests consistently showed rigid body rocking once the wall was cracked, it may be possible to perform further tests using scaled models on a 'mini-shaker table.' These models, having similar scaled properties to those of the walls (i.e. unit weight, coefficient of restitution, coefficient of friction), would allow researchers to perform parametric studies to investigate such areas as: ground motion, diaphragm flexibility, *h/t* ratios, and variable crack heights. Results from such tests could be used to calibrate and build confidence in numerical models.
- These tests only considered out-of-plane loading. Further testing is recommended to investigate the walls' response to simultaneous in-plane and out-of-plane excitation.
- During all the tests performed, wall stability was contingent on an adequate connection being in place at the top of the wall. Further tests are required to investigate which types of connections are effective for both inertia and rotational demands, and to develop methodologies to design such connections.
- During Tests GC5-7, the wall experienced interference with the top restraint, applying a moment to the top of the wall leading to reduced crack displacements and increased wall stability. Further research into how this affects the walls' response/performance as well as the demands on restraints is recommended.

- During the tests that underwent rocking with relatively high crack displacements, it was observed that the wall began to rock about a new 'dynamic stability' point, as seen in the oscillations in the crack acceleration versus relative crack displacement plots. Further research into why this occurs is recommended.
- Further work needs to be done to determine a method to calculate the effective rocking acceleration at the crack, how this affects the walls' response, and what influence it has on the inertial force acting on the wall.
- A SDOF model was used to predict the walls' stability assuming a crack at mid-height. The model should be adjusted, taking into account the actual crack locations observed during the tests, and then re-compare these new results to those seen in the test.
- Continue to develop the model used in the Working Model analysis, including the suggested work in Section 5.8.4. This analysis procedure could then possibly be used by practicing engineers carrying out assessment work.
- Since the first dynamic out-of-plane tests were performed by ABK [1981], there have been a significant number of new tests conducted, and various models proposed. These new findings should be incorporated into the assessment criteria of FEMA 356 [ASCE 2000].

# REFERENCES


ABK, 1981, "Methodology for Mitigation of Seismic Hazards in Existing Unreinforced Masonry Buildings: Wall Testing, Out-Of-Plane", *ABK Topical Report 04*.

Abrams, D., 2000, "A Set of Class Notes in Masonry Structures, Third Edition", The Masonry Society, USA.

Adams, J., and Atkinson, G., 2003, "Development of Seismic Hazard Maps for the Proposed 2005 Edition of the National Building Code of Canada", *Canadian Journal of Civil Engineering*, Vol. 30, pp. 255-271.

American Society of Civil Engineers (ASCE), 2000, "Prestandard and Commentary for the Seismic Rehabilitation of Buildings", *FEMA 356*, Federal Emergency Management Agency, Washington, D.C., USA.

American Society for Testing and Materials (ASTM), 2000, "Standard Test Method for Measurement of Masonry Flexural Strength", *ASTM-C1072-00a*, ASTM, USA.

Anderson, C., 1984, "Arching Action in Transverse Laterally Loaded Masonry Wall Panels", *The Structural Engineer*, Vol. 62B, No. 1, pp. 12-23.

Applied Technology Council (ATC), 1998, "Evaluation of Earthquake Damaged Concrete and Masonry Wall Buildings", *FEMA 306*, FEMA, Washington, D.C., USA.

Atkinson,R.H., Amadei, B.P., Saeb, S., Sture, S., 1989, "Response of Masonry Bed Joints in Direct Shear", *Journal of Structural Engineering*, Vol. 115, N0. 9, pp. 2276-2296.

Azevedo, J., Sincraian, G., and Lemos, J., 2000. "Seismic Behaviour of Blocky Masonry Structures", *Earthquake Engineering Spectra,* Vol. 16, No.2, pp. 337-365.

Canadian Standard Association (CSA), 2001, "Method of Testing Compressive Strength of Masonry Prisms", *CAN/CSA-A3 69.1-M90 (R2001)*, CSA, Canada.

CSA, 2003, "Methods of Sampling and Testing Brick, *CAN3-82.2M78(R2003)*, CSA, Canada.

CSA, 2004, "Mortar and Grout for Unit Masonry", *CSA-A179-04*, CSA, Canada.

Cundall, P., 1971, "A Computer Model for Simulating Progressive Large-Scale Movements in Blocky Rock Systems", *Proceedings of the Symposium of the International Society of Rock Mechanics*, France, Vol. 1. Paper No. II-8.

Doherty, K., 2000, "An Investigation of the Weak Links in the Seismic Load Path of Unreinforced Masonry Buildings", *PhD Thesis*, University of Adelaide, Australia.

Doherty, K.T., Griffith, M.C., Lam, N. and Wilson, J., 2002, "Displacement-Based Seismic Analysis for Out-of-Plane Bending of Unreinforced Masonry Walls", *Earthquake Engineering Structural Dynamics*, Vol. 31, pp. 833-850.

ElGawady, M.A., Lsetuzzi, P., Badoux, M., 2004, "A Review of Conventional Seismic Retrofitting Techniques for URM", *Proceedings on the 13th International Brock and Block Masonry Conference*, July.

ElGawady, M.A., Ma, Q., Butterworth, J., and Ingham, J.M., 2006, "The Effect of Interface Material on the Dynamic Behaviour of Free Rocking Blocks" *Proceedings on the 8th US National Conference on Earthquake Engineering,* 2006.

FEMA, 1997, "NEHRP Guidelines for the Seismic Rehabilitation of Buildings", *FEMA 273*, FEMA, Washington, D.C., October 1997.

Griffith, M., Magenes, G., Melis, Giammichele, G., and Picchi, L., 2003, "Evaluation of Out-of-Plane Stability of Unreinforced Masonry Walls Subjected to Seismic Excitations," *Journal of Earthquake Engineering,* Vol. 7, Special Issue 1, pp. 141-169.

Griffith, M., Lam, N., Wilson, J., and Doherty, K., 2004, "Experimental Investigation of Unreinforced Brick Masonry Walls in Flexure", *Journal of Structural Engineering*, 130(3), pp. 423-432.

Gülkan, P. Clough, R. Mayes, R., and Manos, G., 1990, "Seismic Testing of Single-Storey Masonry Houses: Part 1 and 2", *Journal of Structural Engineering*, 116(1), 235-274.

Housner, G. W., 1963, "The Behaviour of Inverted Pendulum Structures during Earthquakes", *Bulletin of the Seismological Society of America*, Vol. 53, No. 2, pp. 403-417.

Kaharrazi, M. 2001. "Vibration Characteristics of Single-Family Wood Frame Buildings", *Master Thesis*, University of British Columbia, Canada.

Knowledge Revolution, 1996, "Working Model 2D, Version 4.0", *Software User Manual*, Knowledge Revolution, California.

Konstantinidis, D., Makris, N., 2005, "Seismic Response Analysis of Multidrum Classical Columns", *Earthquake Engineering and Structural Dynamics,* Vol 34, pp. 1243-1270.

Lemos, J., Azevedo, F., Oliveira, C., and Sincraian, G., 1998, "Three-Dimensional Analysis of a Block Masonry Pillar Using Discrete Elements", *Procedings Monument-98, Workshop on Seismic Performance of Monuments, Lisbon, Portugal,* pp. 117-126.

Makris, N., and Zhang, J., 1999, "Response and Overturning of Anchored Equipment under Seismic Excitation" *Report No. PEER-98/05,* Pacific Earthquake Engineering Research Center, University of California, Berkeley, CA.

Makris, N., and Konstantinidis, D., 2003, "The Rocking Spectrum and the Limitations of Practical Design Methodologies", *Earthquake Engineering and Structural Dynamics*, Vol. 32, pp. 265-289.

Makris, N., and Konstantinidis, D., 2001, "The Rocking Spectrum and the Shortcomings of Design Guidelines", *Report No. PEER-01/07*, Pacific Earthquake Engineering Research Center, University of California, Berkeley, CA.

Martini, K., 1997, "Finite Element Studies in the Out-of-Plane Failure of Unreinforced Masonry", *Proceedings on the International Conference on Computing in Civil and Building Engineering*, Vol. 1., Korea.

Meisl, C., Mattman, D., Elwood, K, White, T, and Ventura, C., 2005, "Out-of-plane Seismic Performance of Unreinforced Clay Brick Masonry Walls", *10th Canadian Masonry Symposium*, Masonry Canada, Banff, Alberta, Canada.

Natural Resources Canada, 2006. "Damage Photographs from the M7.3 Vancouver Island Earthquake of 1946", *Photograph,* http://www.seismo.ca/historic_eq/20th/1946/1946photos_e.php, April.

National Information Service for Earthquake Engineering,(NISEE), April 2006a. "NR409", *The Earthquake Engineering Online Archive, Northridge Collection,* http://nisee.berkeley.edu/elibrary/getimg?id=NR413, NISEE, University of California, Berkeley.

National Information Service for Earthquake Engineering,(NISEE), April 2006b. "NR409" *The Earthquake Engineering Online Archive, Northridge Collection,* http://nisee.berkeley.edu/elibrary/getimg?id=NR409, NISEE, University of California, Berkeley.

Paulay, T., Priestly, J.N., 1992, "Seismic Design of Reinforced Concrete and Masonry Buildings", J. Wiley.

Paquette, J., M. Bruneau, and A. Filiatrault, 2001, "Out-of-Plane Seismic Evaluation and Retrofit of Turn-of-the-Century North American Masonry Walls", *Journal of Structural Engineering*, Vol. 127, No. 5, pp. 561-569.

Priestley, M. J. N., R. J. Evison, and A. J. Carr, 1978, "Seismic Response of Structures Free to Rock on Their Foundations" *Bulletin of the New Zealand National Society for Earthquake Engineering,* 11(3) 14150.

Priestley, J.N., 1985, "Seismic Behaviour of Unreinforced Masonry Walls," *Bulletin of the New Zealand National Society for Earthquake Engineering*, Vol. 18, No. 2, pp 191-205.

Turek, M., 2002, "In-Plane Shake Table Testing of Unreinforced Masonry Walls Strengthened with Fiber Reinforced-Plastics", *Master Thesis*, University of British Columbia, Canada.

Simsir, C., Aschheim, M. and Abrams, D., 2004, "Out-Of-Plane Dynamic Response of Unreinforced Masonry Bearing Walls Attached to Flexible Diaphragms", *13th World Conference on Earthquake Engineering*, Vancouver, BC, Canada.

SEAOC, 1991, "Reflection on the Loma Prieta Earthquake", Structural Engineers Association of California.

Structural Vibration Solutions, 2005, *ARTeMIS Extractor Software*, Structural Vibration Solutions, Denmark.

Taylor, Graham, 2004, "Typical URM School Building in British Columbia, *Photogrph*, TGB Seismic Consultants Ltd.

Vamvatsikos, D., Cornell, A., 2002, "Incremental Dynamic Analysis", *Earthquake Engineering and Structural Dynamics,* Vol. 31, pp. 491-514.

West, W.H., Hodgkinson, H.R., and Webb, W.F., 1973, "The Resistance of Brick Walls to Lateral Loading," *Proceeding of the British Ceramic Society,* Vol. 21, pp. 141-164.

West, W.H., Hodgkinson, H.R., and Haseltine, B.A., 1977, "The resistance of Brickwork to Latral Loading – Part 1 – Experimental Methods and Resuts of Tests on Small Specimens and Full Sized Walls", *The Structural Engineer,* Vol. 55, No. 10, pp. 411-421.

Yokel, F. Y., and R. D. Dickers, 1971, "Strength of Loadbearing Masonry Walls", *Journal of Structural Engineering*, ASCE, Vol. 120, No. ST5, pp. 1593-1608.

Yokel, F. Y., and G. Fattal, 1976, "Failure Hypothesis for Masonry Shear Walls", *Journal of Structural Engineering*, ASCE, Vol. 120, No. ST3, pp. 515-532.

Zhang, J., and Makris, N., 2001, "Rocking Response of Free-Standing Blocks Under Cycloidal Pulses", *Journal of Engineering Mechanics*, ASCE, 127(5)L 47383.

Zirpke, P., 2004, *Verbal Communications*, June.

# APPENDIX A. MATERIAL TESTING AND PROPERTIES

## A.1 Mortar Compression Tests

**Mortar Cube Compression**
**CSA A179-94**

**Project:** **UBC 100 - URM Walls** **Date:** **03-Jun-05**

**Testing Apparatus:**
Batch 1 was tested at the Basilte Material Testing Lab, Batch 3 was tested at the UBC Structures Lab. The Baldwin testing apparatus was used.

**Cube Dimensions:** 51mm x 51mm **Mortar Type:** O

**Mortar Batch:** 1 (Tested at Basilite)

| Age (days) | # Cubes Tested | $f_c$ (MPa) |
|---|---|---|
| 7 | 3 | 2.9 |
| 28 | 6 | 4 |
| 56 | 3 | 3.9 |

**Mix Design:**

| Portland Cement | Lime | Sand |
|---|---|---|
| 1 | 2 | 9 |

**Mortar Batch:** 3 (Tested at UBC)
**Age:** 330 days (11 months)

| Specimen | $f_c$ (MPa) | $E_{elastic}$ (N/mm) |
|---|---|---|
| 1 | Improper load rate - NA | |
| 2 | 5.60 | 12191.1 |
| 3 | 6.79 | 22017.1 |
| 4 | Not level bearing surface - NA | |
| 5 | 6.39 | 30930.1 |
| 6 | Not level bearing surface - NA | |
| 7 | 6.17 | 30508.7 |
| 8 | 5.75 | 30522.5 |
| 9 | 6.12 | 34177.4 |
| **Mean** | 6.14 | 26724.48 |
| **Stand. Dev.** | 0.39 | 7476.15 |
| **Sample Cov.** | 0.06 | 0.28 |

Note: Walls were tested approximately 7.5 months after construction

**Sample Failure (Specimen 8)**

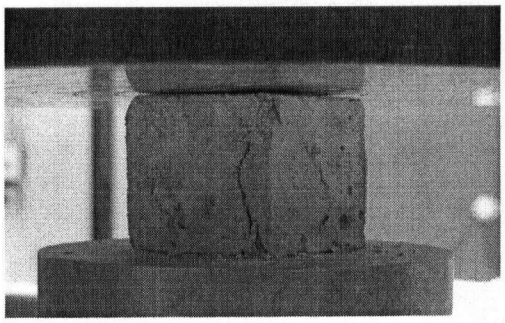

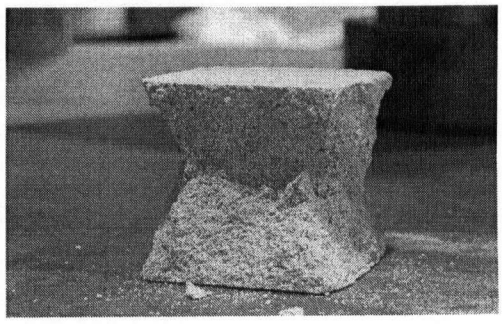

## Mortar Cube Compression
## CSA A179-94

**Project:** UBC 100 - URM Walls **Date:** 03-Jun-05

**Load vs. Displacement:**

Specimen 2

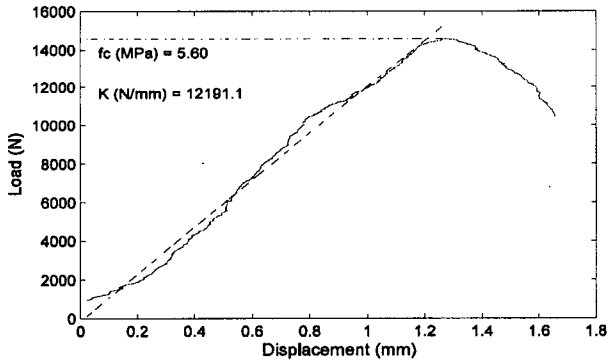


Specimen 3

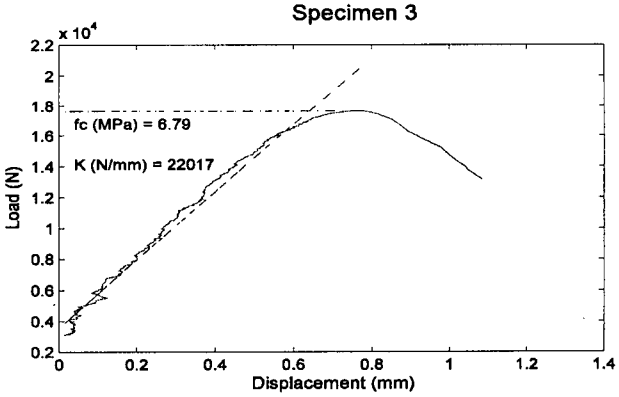


Specimen 5

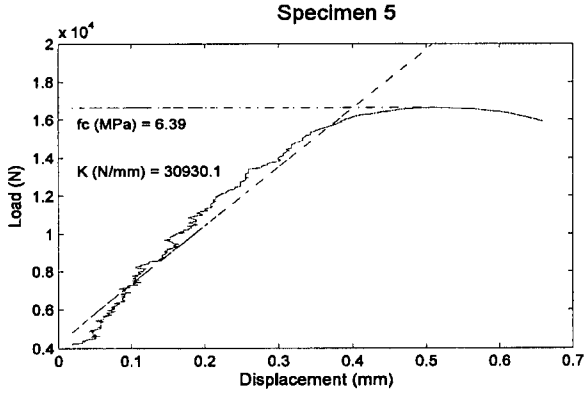


Specimen 7

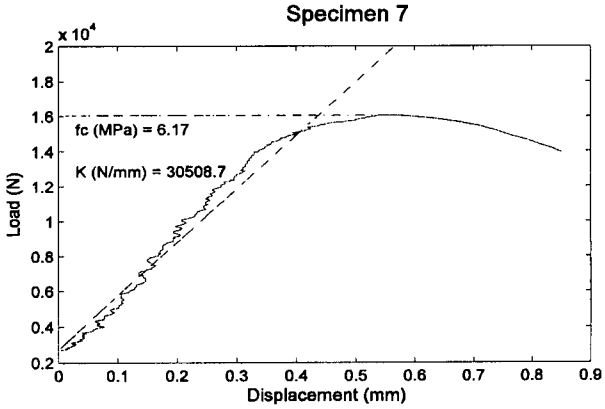


Specimen 8

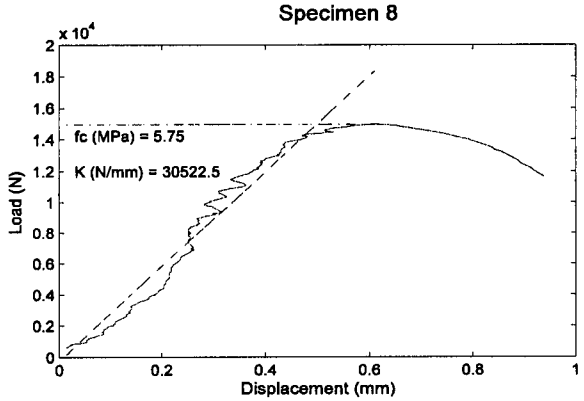


Specimen 9

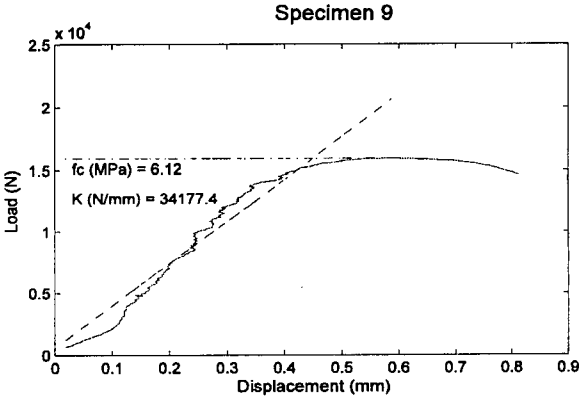

## A.2 Brick Absorption Properties

**Brick Absorption Test**
**CSA A82.2-M78**

**Project:** **UBC 100 - URM Walls** **Date: 03-Jun-05**

**24-Hour Submersion Test**

$W_1$ = Dry mass of specimen

$W_2$ = Saturated mass of the specimen after 24-hour submersion in cold water

$$\textbf{Absorption} = \frac{100(W_2-W_1)}{W_1} \%$$

| Sample | $W_1$ (kg) | $W_2$ (kg) | Absorption (%) |
|---|---|---|---|
| A-1 | 2.880 | 3.134 | 8.82 |
| A-2 | 2.853 | 3.140 | 10.06 |
| A-3 | 2.859 | 3.123 | 9.23 |
| A-4 | 2.887 | 3.174 | 9.94 |
| A-5 | 2.794 | 3.086 | 10.45 |
| A-6 | 2.813 | 3.105 | 10.38 |
| **Mean** | - | - | **9.81** |
| **Stand Dev** | - | - | **0.65** |
| **Sample Cov** | - | - | **0.07** |

**5-Hour Boiling Test**

$W_1$ = Dry mass of specimen

$W_3$ = Saturated mass of the specimen after 5-hour submersion in boiling water

$$\textbf{Absorption} = \frac{100(W_3-W_1)}{W_1} \%$$

| Sample | $W_1$ (kg) | $W_3$ (kg) | Absorption (%) |
|---|---|---|---|
| A-1 | 2.880 | 3.170 | 10.07 |
| A-2 | 2.853 | 3.169 | 11.08 |
| A-3 | 2.859 | 3.149 | 10.14 |
| A-4 | 2.887 | 3.195 | 10.67 |
| A-5 | 2.794 | 3.108 | 11.24 |
| A-6 | 2.813 | 3.133 | 11.38 |
| **Mean** | - | - | **10.76** |
| **Stand Dev** | - | - | **0.56** |
| **Sample Cov** | - | - | **0.05** |

**Average Absorption: 24hr and 5hr Boiling =** **10.29** %

## A.3 Brick Compression Tests

**Brick Compression Tests**
**CSA 82.2 - M78 / ASTM C140**

**Project:** **UBC 100 - URM Walls** **Date:** **03-Jun-05**

**Testing Apparatus:**
Testing was performed at the UBC Structures Lab. The Baldwin testing apparatus was used. All specimens were capped with hydrostone to ensure a level bearing surface. The load was applied at approximately 500lb/s.

**Notes:**
The brick specimens were initially tested flat, (i.e. A = l x w), but were not able to fail as the specimen height was not enough to form a failure plane. There for the bricks were tested on their edge, (i.e. A = l x t). This can be considered equivalent as the bricks are solid and homogeneous.

**Results:**

| Specimen | l (mm) | w (mm) | t (mm) | Area (mm) | $f_b$ (MPa) | $E_{elastic}$ (N/mm) |
|---|---|---|---|---|---|---|
| 1 | 218 | 110 | 60 | 13080 | 18.01 | 280953 |
| 2 | 218 | 110 | 60 | 13080 | 18.23 | 306064 |
| 3 | 218 | 110 | 59 | 12862 | 12.22 | 205575 |
| 4 | 219 | 110 | 60 | 13140 | 21.04 | 349069 |
| 5 | 218 | 110 | 59 | 12862 | 11.58 | 164327 |
| 6 | 218 | 109 | 59 | 12862 | 11.22 | 145651 |
| **Mean** | 218.17 | 109.83 | 59.50 | 12981.00 | 15.38 | 241940 |
| **Stand. Dev.** | 0.37 | 0.37 | 0.50 | 120.67 | 3.85 | 74976 |
| **Sample Cov.** | 0.00 | 0.00 | 0.01 | 0.01 | 0.25 | 0.31 |

**Typical Failures:**

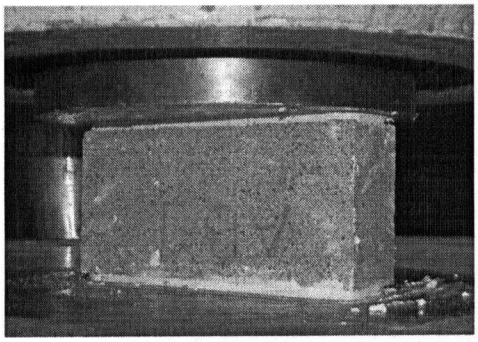

Specimen 1

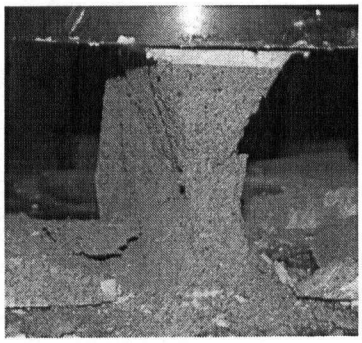

Specimen 5

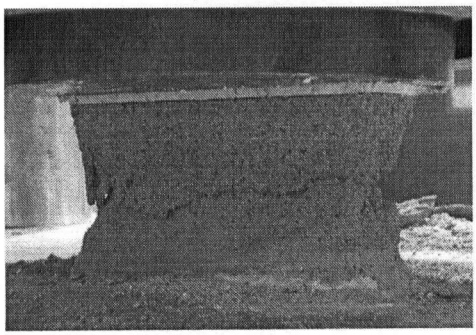

Specimen 1

Specimen 9

**Brick Compression Tests**
**CSA 82.2 - M78 / ASTM C140**

**Project:** **UBC 100 - URM Walls** **Date:** **03-Jun-05**

**Load vs. Displacement:**

Specimen 1

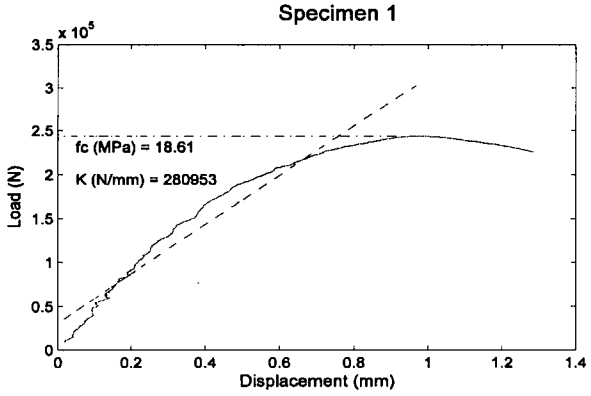


Specimen 2

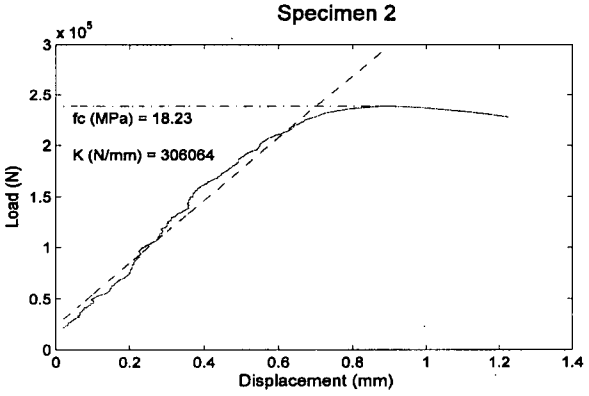


Specimen 3

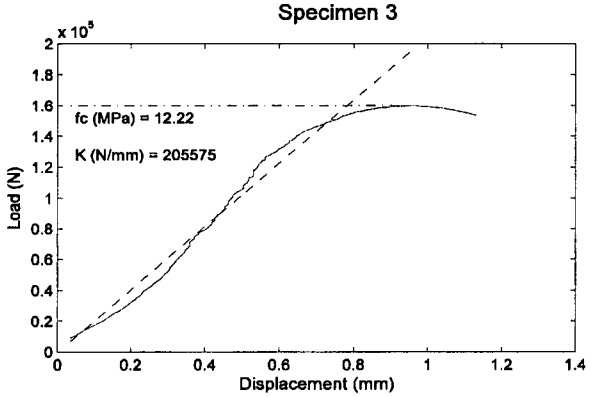


Specimen 4

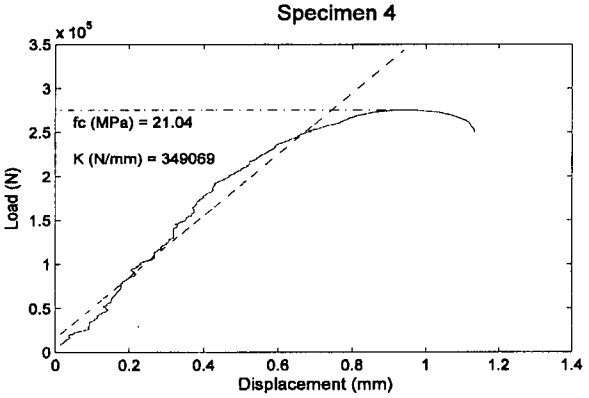


Specimen 5

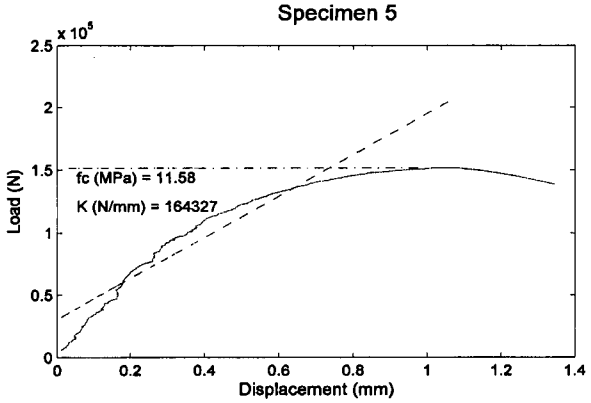


Specimen 6

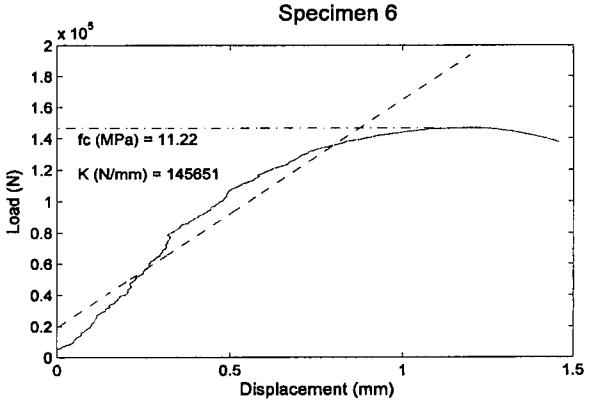

## A.4 Masonry Compression Tests

**Masonry Prism Compression Tests**
**CSA-A-3 69.1-M90 (R 2001)**

**Project:** **UBC 100 - URM Walls** **Date:** **04-Nov-05**

**Testing Apparatus:**
Testing was performed at the UBC Structures Lab. The Baldwin testing apparatus was used.
Specimens All specimens were capped with hydrostone to ensure a level bearing surface.
The load was applied at approximately 500lb/s.

**Correction Factor:**

| Prism h/t | 1.30 | 1.50 | 2.00 | 2.25 | 3.00 | 4.00 | 5.00 |
|---|---|---|---|---|---|---|---|
| Factor | 0.75 | 0.86 | 1.00 | 1.04 | 1.07 | 1.15 | 1.22 |

**Results:**

| | | | | | | | | | Factored | | |
|---|---|---|---|---|---|---|---|---|---|---|---|
| Specimen | Mortar Batch | Age[1] (months) | $A_g$ ($mm^2$) | # Bricks in Stack | h (mm) | t (mm) | h/t (mm) | Cor. Fac. | $f_m$ (MPa) | $E_{elastic}$[2] (N/mm) | $E_m$[3] (MPa) |
| 1 | 1 | 15.5 | 24090 | 2 | 137 | 110 | 1.25 | 0.72 | 10.36 | 233176 | 1326 |
| 2 | 1 | 15.5 | 24090 | 3 | 210 | 110 | 1.91 | 0.97 | 16.14 | 367730 | 3206 |
| 3 | 1 | 15.5 | 24090 | 3 | 215 | 110 | 1.95 | 0.99 | 11.79 | 196922 | 1758 |
| 4 | 3 | 15.5 | 24090 | 3 | 214 | 110 | 1.95 | 0.99 | 16.47 | 291468 | 2589 |
| 5 | 2 | 15.5 | 24090 | 4 | 287 | 110 | 2.61 | 1.05 | 10.63 | 141074 | 1681 |
| 6 | 2 | 15.5 | 24090 | 4 | 289 | 110 | 2.63 | 1.06 | 12.40 | 176060 | 2112 |
| Mean | | - | - | - | - | - | - | - | 12.97 | 234405 | 2112 |
| Stand. Dev. | | - | - | - | - | - | - | - | 2.46 | 75887 | 626 |
| Sample Cov. | | - | - | - | - | - | - | - | 0.19 | 0.32 | 0.30 |

**Note:** [1] Walls tested approximately 7.5 months after construction

[2] $E_{elastic}$ is the stiffness of the entire masonry prism

[3] $E_m$ is the elastic modulus of the entire prism

**Typical Failures:**

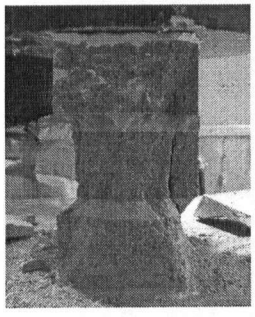

Specimen 2

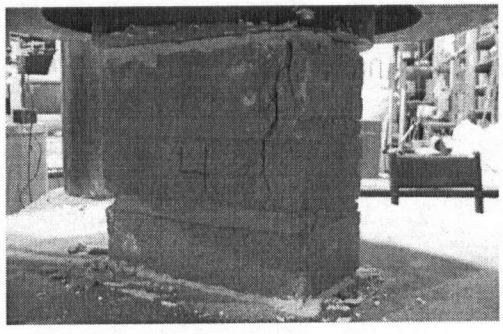

Specimen 4

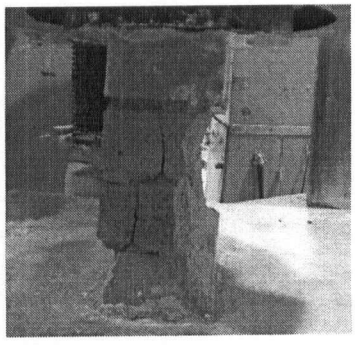

Specimen 6

## Masonry Prism Compression Tests
## CSA-A-3 69.1-M90 (R 2001)

**Project:** UBC 100 - URM Walls **Date:** 04-Nov-05

**Load vs. Displacement (Un-Factored):**

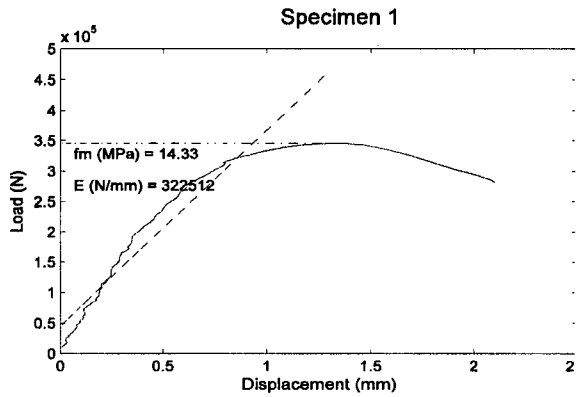


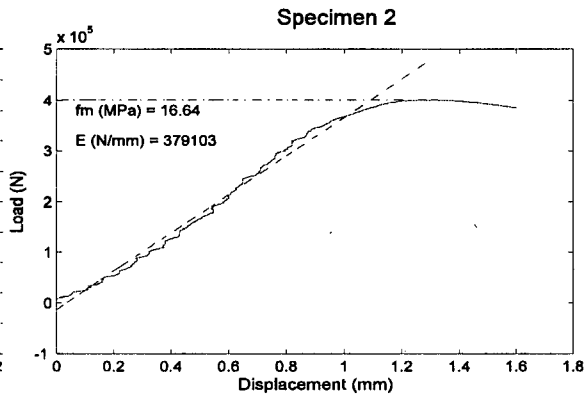


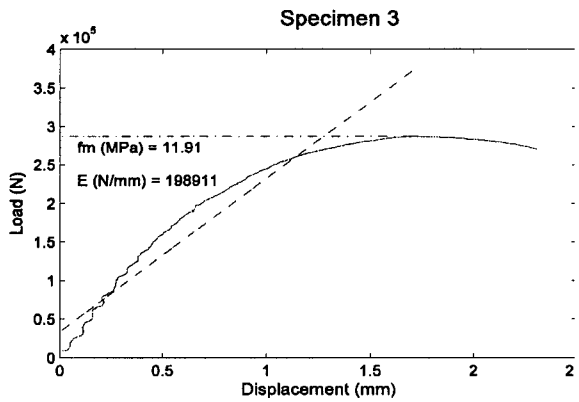


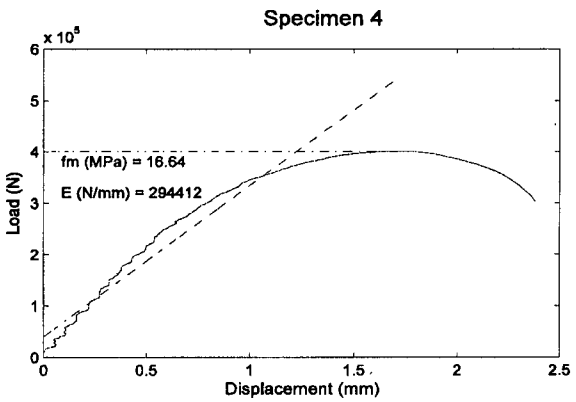


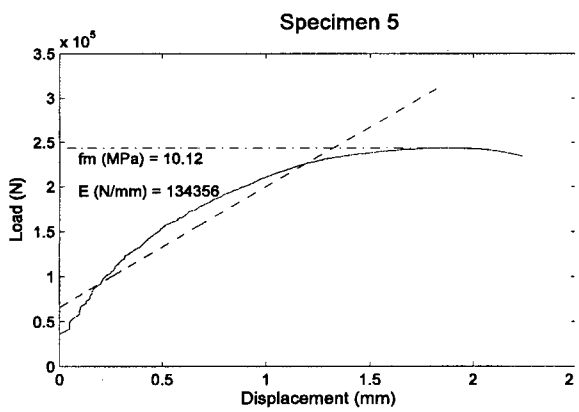


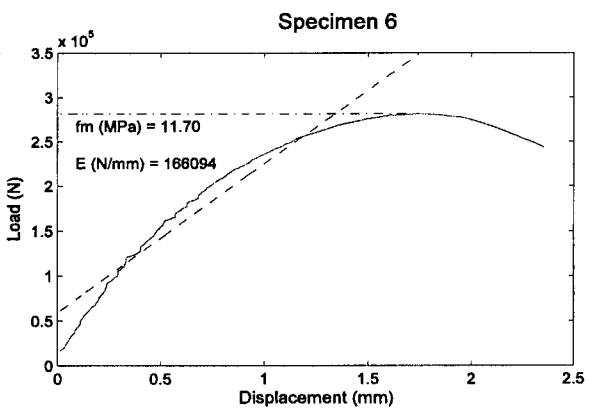

## A.5 Masonry Bond Wrench Tests

**Bond Wrench Test - Calculations**
**ASTM C 1072 - 99**

**Project: UBC 100 - URM Walls** **Date: 28-Apr-05**

**Testing Apparatus:**
Testing was performed at Basilte Concrete Products Lab in Vancouver. Their in-house bond wrench machine was used. The load is applied by use of a pneumatic jack which applies a load to the loading arm.

**Calculations:**

$$F_g = \frac{6(PL + P_l l_l)}{bd^2} - \frac{(P+P_l)}{bd}$$

where:

$F_g$ = gross area flexural tensile strength, MPa
$P$ = maximum applied load, N
$P_l$ = weight of loading arm, N
$L$ = distance from center of prism to loading point, mm
$L_l$ = distance from center of prism to centroid of loading arm, mm
$b$ = average width of cross section of the specified mortar bedded area (perpendicular to loading), mm
$d$ = average thickness of cross section of the specified mortar bedded area (parallel to loading), mm

| | | | | |
|---|---|---|---|---|
| b = | 219 mm | (Full bed of mortar) | r = | 43 mm |
| d = | 110 mm | (Full bed of mortar) | d/2 = | 55 mm |
| L = | 427 mm | | $L_l$ = | 13 mm |

Mass of loading Arm = 17.88 kg $P_l$ = 175.4028 N

P = 0.292*(Jack Force) N (from sum of moments about 'O')
P = 2.987*(Jack Reading) - 226.799 N

**Bond Wrench Testing Apparatus**

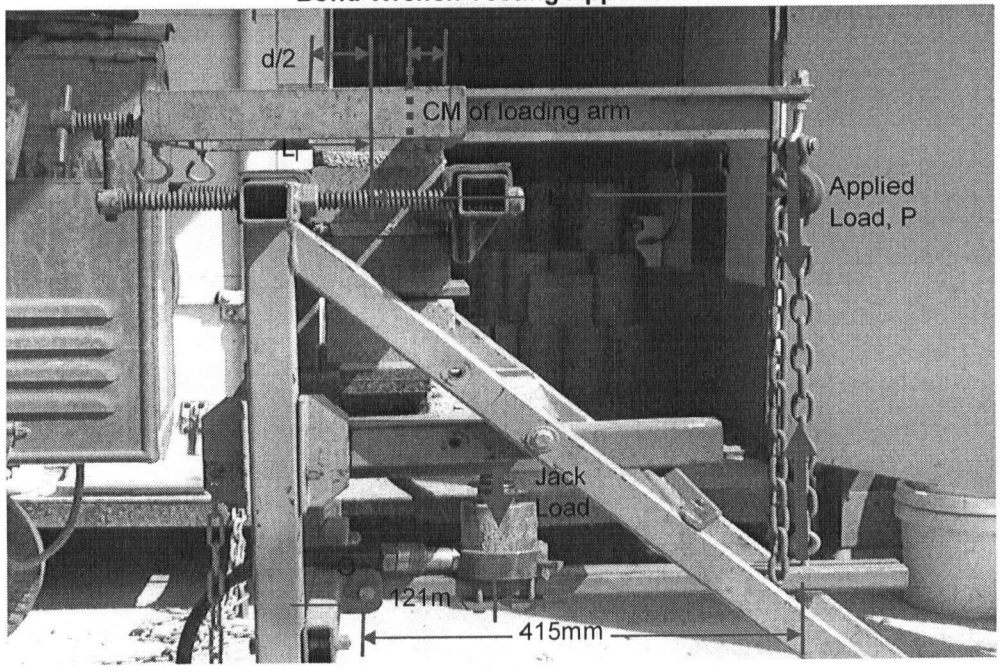

## Bond Wrench Test - Loading Jack Calibration

**Project: UBC 100 - URM Walls** **Date: 28-Apr-05**

| Trial 1 | | Trial 2 | | Trail 3 | |
|---|---|---|---|---|---|
| Guage [PSI] | Dial [LBS] | Guage [PSI] | Dial [LBS] | Guage [PSI] | Dial [LBS] |
| 50 | 90 | 37.5 | 0 | 37.5 | 0 |
| 120 | 125 | 60 | 0 | 60 | 0 |
| 150 | 175 | 90 | 25 | 90 | 25 |
| 180 | 251 | 120 | 75 | 120 | 100 |
| 210 | 326 | 150 | 150 | 150 | 175 |
| 240 | 376 | 180 | 226 | 180 | 251 |
| 270 | 452 | 210 | 301 | 210 | 326 |
| 300 | 527 | 240 | 351 | 240 | 376 |
| | | 270 | 427 | 270 | 452 |
| | | 300 | 502 | 300 | 527 |

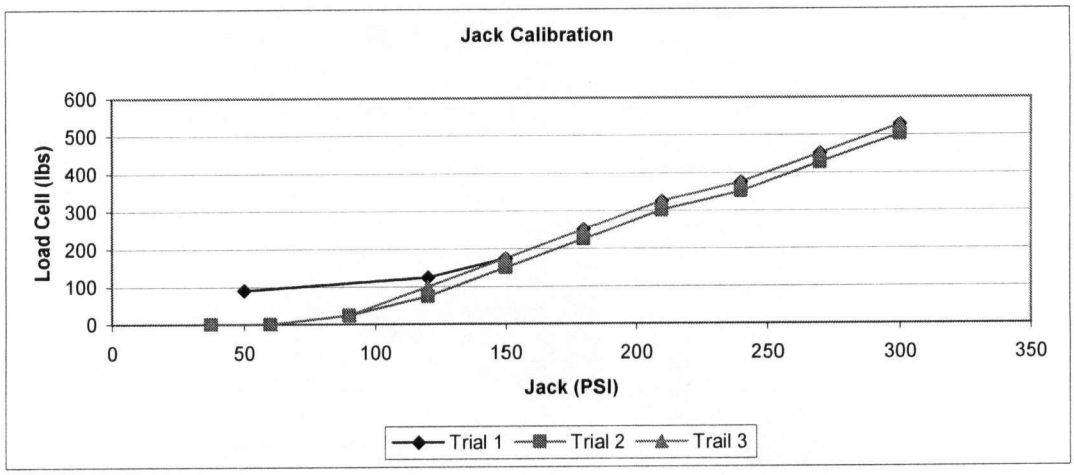


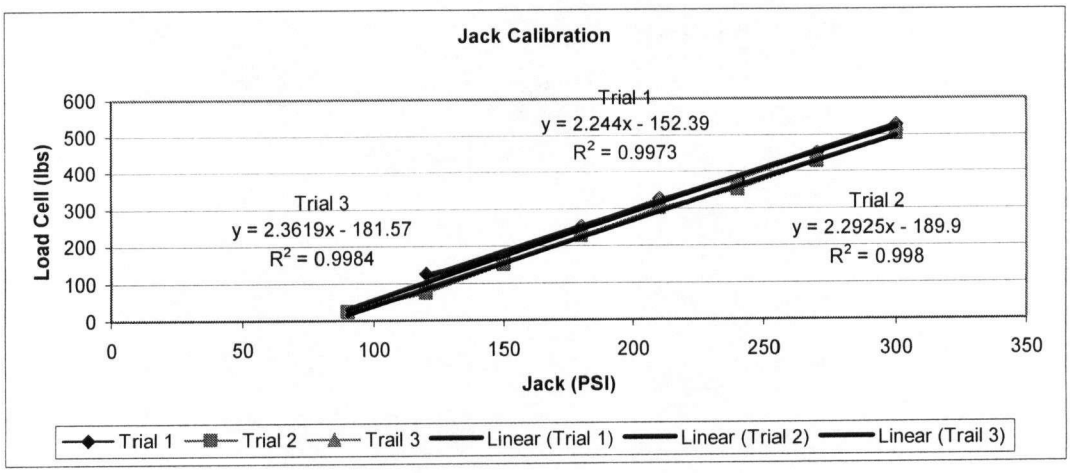


**Jack Conversion:** **Applied Load = 2.2995*(Jack Reading) - 174.62**
**Applied Load = 10.228*(Jack Reading) - 776.710**

## Bond Wrench Test
## ASTM C 1072 - 99

**Project: UBC 100 - URM Walls** **Date: 28-Apr-05**

**Calculation:**

Flexural Tensile Strength: $F_g = \frac{6(PL + P_l L_l)}{bd^2} - \frac{(P+P_l)}{bd}$ MPa

| | | | |
|---|---|---|---|
| b = | 219 mm | L = | 427 mm |
| d = | 110 mm | $L_l$ = | 13 mm |
| Pl = | 175.4028 N | P = | 2.987*(Jack Reading) - 226.799 N |

**Data:**

Note: Gauge limit is 300psi, any values greater than 300psi are estimates

**Mortar Batch:** 1
**Age:** 290 days (9.5 months)

Specimen: BW2-B1

| Brick | Jack Gauge (psi) | | P | $F_g$ |
|---|---|---|---|---|
| | Initial | Final | (N) | (MPa) |
| 1 | 72 | 115 | 116.706 | 0.106 |
| 2 | 72 | 170 | 280.991 | 0.258 |
| 3 | 72 | 239 | 487.094 | 0.449 |

| $F_g$ (MPa) | | |
|---|---|---|
| Average | Standard Deviation | Sample COV |
| 0.271 | 0.172 | 0.634 |

Specimen: BW3-B1

| Brick | Jack Gauge (psi) | | P | $F_g$ |
|---|---|---|---|---|
| | Initial | Final | (N) | (MPa) |
| 1 | 72 | 241 | 493.068 | 0.454 |
| 2 | 72 | 206 | 388.523 | 0.357 |
| 3 | 72 | 185 | 325.796 | 0.299 |
| 4 | 72 | 245 | 505.016 | 0.465 |
| 5 | 72 | 226 | 448.263 | 0.413 |

| $F_g$ (MPa) | | |
|---|---|---|
| Average | Standard Deviation | Sample COV |
| 0.398 | 0.069 | 0.174 |

**Batch 1 Flexural Strength (MPa)**

| Average | Standard Deviation | Sample COV |
|---|---|---|
| 0.350134 | 0.124477 | 0.3555124 |

**Mortar Batch:** 2
**Age:** 291 days (9.5 months)

Specimen: BW2-B2

| Brick | Jack Gauge (psi) | | P | $F_g$ |
|---|---|---|---|---|
| | Initial | Final | (N) | (MPa) |
| 1 | 72 | 260 | 549.821 | 0.507 |
| 2 | 72 | 245 | 505.016 | 0.465 |
| 3 | 72 | 310 | 699.171 | 0.645 |
| 4 | 72 | 238 | 484.107 | 0.446 |
| 5 | 72 | 335 | 773.846 | 0.714 |

| $F_g$ (MPa) | | |
|---|---|---|
| Average | Standard Deviation | Sample COV |
| 0.555 | 0.118 | 0.212 |

**Bond Wrench Test**
**ASTM C 1072 - 99**

**Project: UBC 100 - URM Walls** **Date: 28-Apr-05**

Specimen: BW3-B2

| Brick | Jack Gauge (psi) | | P | $F_g$ |
|---|---|---|---|---|
| | Initial | Final | (N) | (MPa) |
| 1 | 72 | 261 | 552.808 | 0.509 |
| 2 | 72 | 219 | 427.354 | 0.393 |
| 3 | 72 | 320 | 729.041 | 0.672 |
| 4 | 72 | 265 | 564.756 | 0.520 |
| 5 | 72 | 236 | 478.133 | 0.440 |

| $F_g$ (MPa) | | |
|---|---|---|
| Average | Standard Deviation | Sample COV |
| 0.507 | 0.106 | 0.209 |

**Batch 2 Flexural Strength (MPa)**

| Average | Standard Deviation | Sample COV |
|---|---|---|
| 0.53124 | 0.108718 | 0.2046493 |

---

**Mortar Batch:** 3
**Age:** 292 days (9.5 months)

Specimen: BW1-B3

| Brick | Jack Gauge (psi) | | P | $F_g$ |
|---|---|---|---|---|
| | Initial | Final | (N) | (MPa) |
| 1 | 72 | 199 | 367.614 | 0.338 |
| 2 | 72 | 190 | 340.731 | 0.313 |
| 3 | 72 | 199 | 367.614 | 0.338 |
| 4 | 72 | 198 | 364.627 | 0.335 |

| $F_g$ (MPa) | | |
|---|---|---|
| Average | Standard Deviation | Sample COV |
| 0.331 | 0.012 | 0.036 |

Specimen: BW2-B3

| Brick | Jack Gauge (psi) | | P | $F_g$ |
|---|---|---|---|---|
| | Initial | Final | (N) | (MPa) |
| 1 | 72 | 154 | 233.199 | 0.214 |
| 2 | 72 | 224 | 442.289 | 0.407 |
| 3 | 72 | 320 | 729.041 | 0.672 |
| 4 | 72 | 181 | 313.848 | 0.288 |

| $F_g$ (MPa) | | |
|---|---|---|
| Average | Standard Deviation | Sample COV |
| 0.395 | 0.201 | 0.509 |

**Batch 3 Flexural Strength (MPa)**

| Average | Standard Deviation | Sample COV |
|---|---|---|
| 0.363262 | 0.136331 | 0.375297 |

---

**Summary**

| Batch | Average | Standard Deviation | Sample COV |
|---|---|---|---|
| 1 | 0.350 | 0.124 | 0.356 |
| 2 | 0.531 | 0.109 | 0.205 |
| 3 | 0.363 | 0.136 | 0.375 |
| All | 0.424 | 0.146 | 0.345 |

**FEMA 356 Recommended Values**

| | | |
|---|---|---|
| Good | 20 psi | 0.14 Mpa |
| Fair | 10 psi | 0.07 MPa |
| Poor | 0 psi | 0 MPa |

**Bond Wrench Test**
**ASTM C 1072 - 99**

**Project: UBC 100 - URM Walls** **Date: 28-Apr-05**

**Typical Failures**

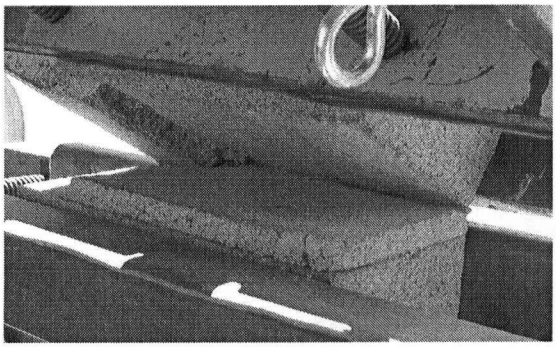

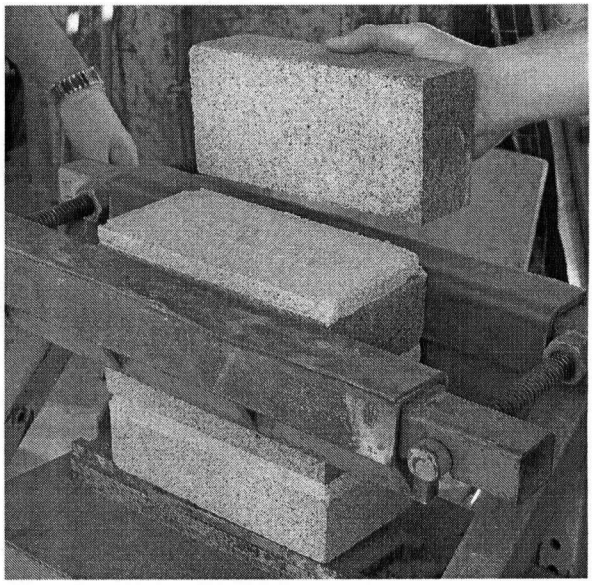

**Typical Specimens**

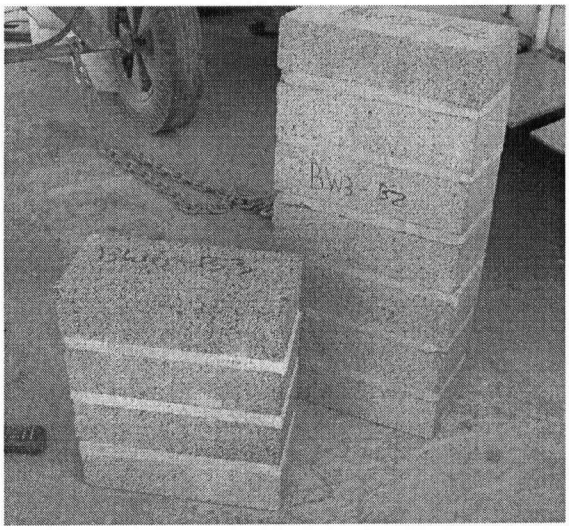

# APPENDIX B. WALL MASS AND DIMENSIONS

## B.1 Wall GC

**URM Wall Properties**

**Wall Number:** GC **Joint Quality:** Good **Date:** 05-Jan-05
**Bond:** Running **Age at Date Tested:** 5.5 months

**Weight:**

| | | |
|---|---|---|
| A. URM Wall + Lifting Rig + Base Channel | = | 49.8 kN |
| B. Lifting Rig | = | 3.122 kN |
| C. Base Channel | = | 2.656 kN |
| **URM Wall Weight** | = | **44.022 kN** |
| **URM Wall Mass** | = | **4487.462 kg** |

**Geometry:**

| Location | Elevation [1] [mm] | | Dimension [mm] | | | | Area |
|---|---|---|---|---|---|---|---|
| | S | N | N | S | E | W | [mm$^2$] |
| Base | 0 | 0 | 360 | 355 | 1500 | 1508 | 537680 |
| Header Course[2] 1 | 466 | 460 | 354 | 349 | 1504 | 1505 | 528832 |
| Header Course 2 | 453 | 455 | 354 | 348 | 1504 | 1505 | 528080 |
| Header Course 3 | 453 | 447 | 352 | 352 | 1501 | 1505 | 529056 |
| Header Course 4 | 460 | 460 | 352 | 351 | 1499 | 1507 | 528305 |
| Header Course 5 | 461 | 454 | 354 | 350 | 1499 | 1502 | 528176 |
| Header Course 6 | 460 | 459 | 355 | 350 | 1499 | 1500 | 528574 |
| Header Course 7 | 449 | 460 | 355 | 348 | 1500 | 1501 | 527426 |
| Header Course 8 | 461 | 451 | 354 | 350 | 1497 | 1502 | 527824 |
| Header Course 9 | 532 | 535 | 358 | 353 | 1490 | 1496 | 530762 |
| Header 9 Elevation | 4195 | 4048 | | | | | - |
| Top | 4188 | 4188 | - | - | - | - | - |
| Average | 420 | 418 | 355 | 351 | 1499 | 1503 | 529471 |
| Overall Dimensions | 4188 | | 353 | | 1501 | | 529473 |

| | | | | |
|---|---|---|---|---|
| **URM Wall Volume** | = | **2.22E+09 mm$^3$** | = | **2.22 m$^3$** |
| **URM Wall Density** | = | **19.85 kN/m$^3$** | = | **2023.72 kg/m$^3$** |

**Notes:**

[1] Elevation measured from base of wall

[2] Elevation between header courses (between bottom brick of header course's)

**Height From Wall Base to Centre of Top Rubber Restraint:**

| Location | S | N |
|---|---|---|
| Average (mm) | 4088 | 4177.5 |

## B.2 Wall PC

### URM Wall Properties

**Wall Number:** PC **Joint Quality:** Poor **Date:** 24-Feb-05

**Bond:** Running **Age at Date Tested:** 7.25 months

**Weight:**

| | | |
|---|---|---|
| A. URM Wall + Lifting Rig + Base Channel | = | 45 kN |
| B. Lifting Rig | = | 3.122 kN |
| C. Base Channel | = | 3.337 kN |
| **URM Wall Weight** | = | **38.541 kN** |
| **URM Wall Mass** | = | **3928.746 kg** |

**Geometry:**

| Location | Elevation [1] [mm] | | Dimension [mm] | | | | Area |
|---|---|---|---|---|---|---|---|
| | S | N | N | S | E | W | [mm$^2$] |
| **Base** | 0 | 0 | 357 | 357 | 1495 | 1494 | 533537 |
| **Header Course[2] 1** | 400 | 400 | 355 | 356 | 1493 | 1495 | 531117 |
| **Header Course 2** | 458 | 465 | 354 | 356 | 1497 | 1497 | 531435 |
| **Header Course 3** | 458 | 453 | 356 | 355 | 1498 | 1497 | 532361 |
| **Header Course 4** | 459 | 460 | 354 | 356 | 1503 | 1494 | 531968 |
| **Header Course 5** | 455 | 449 | 356 | 354 | 1500 | 1497 | 531968 |
| **Header Course 6** | 448 | 459 | 354 | 352 | 1503 | 1495 | 529147 |
| **Header Course 7** | 448 | 445 | 355 | 354 | 1502 | 1496 | 531396 |
| **Header Course 8** | 458 | 457 | 355 | 358 | 1501 | 1501 | 535107 |
| **Header Course 9** | 454 | 457 | 359 | 354 | 1504 | 1500 | 535463 |
| **Header 9 Elevation** | 4036 | 4049 | - | - | - | - | - |
| **Top Elevation** | 4175 | 4190 | - | - | - | - | - |
| **Average** | 1021 | 1024 | 356 | 355 | 1500 | 1497 | 532350 |
| **Overall Dimensions** | **4183** | | **355** | | **1498** | | **532350** |

**URM Wall Volume** = **2.23E+09 mm$^3$** = **2.226553 m$^3$**

**URM Wall Density** = **17.30971 kN/m$^3$** = **1764.497 kg/m$^3$**

**Notes:**

[1] Elevation measured from base of wall

[2] Elevation between header courses (between bottom brick of header course's)

**Height From Wall Base to Centre of Top Rubber Restraint:**

| Location | N | S |
|---|---|---|
| | 4160 | 4145 |
| **Average (mm)** | 4153 | |

**Wall Out of Plumb:**

Wall tilts towards the South 28mm

## B.3 Wall GD

### URM Wall Properties

**Wall Number:** GD **Joint Quality:** Good **Date:** 30-Mar-05

**Bond:** Running **Age at Date Tested:** 8.5 months

**Weight:**

| | | |
|---|---|---|
| A. URM Wall + Lifting Rig + Base Channel | = | 44.675 kN |
| B. Lifting Rig | = | 3.122 kN |
| C. Base Channel | = | 3.337 kN |
| **URM Wall Weight** | = | **38.216 kN** |
| **URM Wall Mass** | = | **3895.617 kg** |

**Geometry:**

| Location | Elevation [1] [mm] | | Dimension [mm] | | | | Area |
|---|---|---|---|---|---|---|---|
| | S | N | N | S | E | W | [mm$^2$] |
| Base | 0 | 0 | 358 | 358 | 1501 | 1494 | 536105 |
| Header Course [2] 1 | 395 | 397 | 360 | 358 | 1498 | 1497 | 537603 |
| Header Course 2 | 450 | 449 | 355 | 359 | 1498 | 1499 | 534965 |
| Header Course 3 | 455 | 454 | 358 | 357 | 1505 | 1502 | 537501 |
| Header Course 4 | 461 | 461 | 351 | 351 | 1507 | 1502 | 528080 |
| Header Course 5 | 451 | 450 | 352 | 350 | 1501 | 1501 | 526851 |
| Header Course 6 | 465 | 462 | 356 | 351 | 1501 | 1502 | 530780 |
| Header Course 7 | 462 | 459 | 349 | 351 | 1498 | 1495 | 523775 |
| Header Course 8 | 450 | 452 | 349 | 348 | 1493 | 1500 | 521530 |
| Header Course 9 | 457 | 456 | 352 | 349 | 1494 | 1497 | 524173 |
| Header 9 Elevation | 4047 | 4055 | | | | | - |
| Top Elevation | 4188 | 4191 | - | - | - | - | - |
| Average | 1023 | 1024 | 354 | 353 | 1500 | 1499 | 530136 |
| Overall Dimensions | 4190 | | 354 | | 1499 | | 530135 |

| | | | | |
|---|---|---|---|---|
| **URM Wall Volume** | = | **2.22E+09 mm$^3$** | = | **2.221 m$^3$** |
| **URM Wall Density** | = | **17.20667 kN/m$^3$** | = | **1753.992 kg/m$^3$** |

**Notes:**

[1] Elevation measured from base of wall

[2] Elevation between header courses (between bottom brick of header course's)

**Height From Wall Base to Centre of Top Rubber Restraint:**

| Location | S | | N | |
|---|---|---|---|---|
| | E | W | E | W |
| | 4078 | 4079 | 4085 | 4085 |
| Average | 4078.5 | | 4085 | |

## B.4 Wall PD

### URM Wall Properties

**Wall Number:** PD **Joint Quality:** Poor **Date:** 14-Mar-05

**Bond:** Running **Age at Date Tested:** 8 months

**Weight:**

| | | |
|---|---|---|
| A. URM Wall + Lifting Rig + Base Channel | = | 44.8451 kN |
| B. Lifting Rig | = | 3.122 kN |
| C. Base Channel | = | 2.656 kN |
| **URM Wall Weight** | = | **39.0671 kN** |
| **URM Wall Mass** | = | **3982.376 kg** |

* Mass of wall determined from measuring samples of Wall

**Geometry:**

| Location | Elevation [1] [mm] | | Dimension [mm] | | | | Area |
|---|---|---|---|---|---|---|---|
| | S | N | N | S | E | W | [mm$^2$] |
| **Base** | 0 | 0 | 355 | 355 | 1500 | 1495 | 531613 |
| **Header Course[2] 1** | 380 | 388 | 355 | 353 | 1500 | 1500 | 531000 |
| **Header Course 2** | 440 | 446 | 355 | 353 | 1501 | 1495 | 530292 |
| **Header Course 3** | 455 | 455 | 345 | 350 | 1500 | 1495 | 520381 |
| **Header Course 4** | 460 | 458 | 351 | 351 | 1499 | 1496 | 525623 |
| **Header Course 5** | 455 | 457 | 356 | 350 | 1501 | 1496 | 528971 |
| **Header Course 6** | 460 | 460 | 349 | 354 | 1501 | 1495 | 526547 |
| **Header Course 7** | 478 | 469 | 355 | 352 | 1500 | 1498 | 529897 |
| **Header Course 8** | 455 | 460 | 351 | 353 | 1500 | 1500 | 528000 |
| **Header Course 9** | 452 | 455 | 355 | 355 | 1502 | 1505 | 533743 |
| **Header 9 Elevation** | 4035 | 4048 | | | | | - |
| **Top Elevation** | 4171 | 4184 | - | - | - | - | - |
| **Average** | 404 | 405 | 353 | 353 | 1500 | 1498 | 528606 |
| **Overall Dimensions** | **4178** | | **353** | | **1499** | | **528605** |

| | | | | |
|---|---|---|---|---|
| **URM Wall Volume** | = | **2.21E+09 mm$^3$** | = | **2.208246 m$^3$** |
| **URM Wall Density** | = | **17.69146 kN/m$^3$** | = | **1801.575 kg/m$^3$** |

**Notes:**

[1] Elevation measured from base of wall

[2] Elevation between header courses (between bottom brick of header course's)

**Height From Wall Base to Centre of Top Rubber Restraint:**

| Location | S | | N | |
|---|---|---|---|---|
| | E | W | E | W |
| | 4058 | 4075 | 4085 | 4070 |
| **Average** | 4066.5 | | 4077.5 | |

# APPENDIX C. SHAKE TABLE TEST DRAWINGS

## C.1 URM Wall Construction Drawings

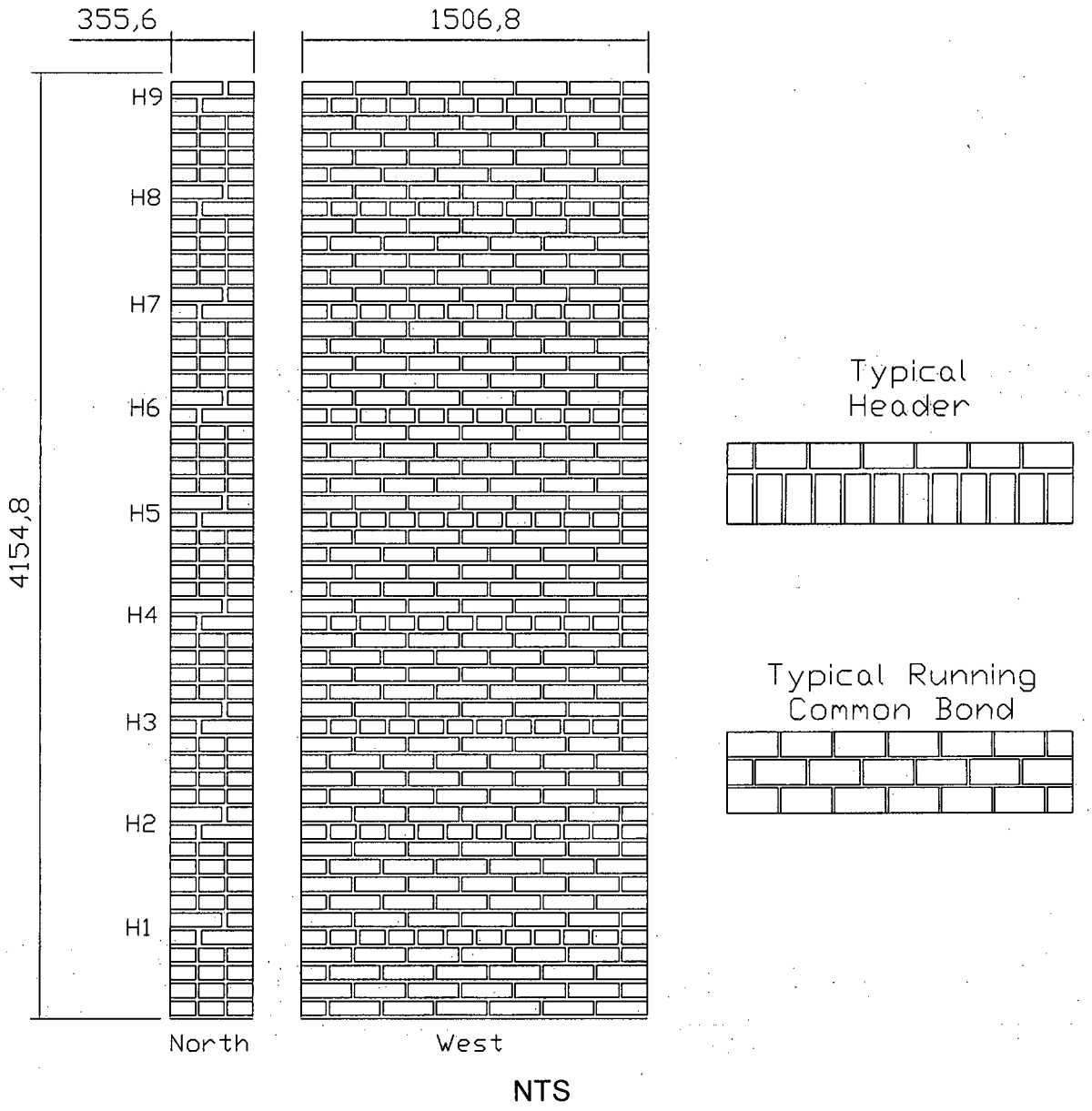

## C.2 Test Set-Up Elevation View

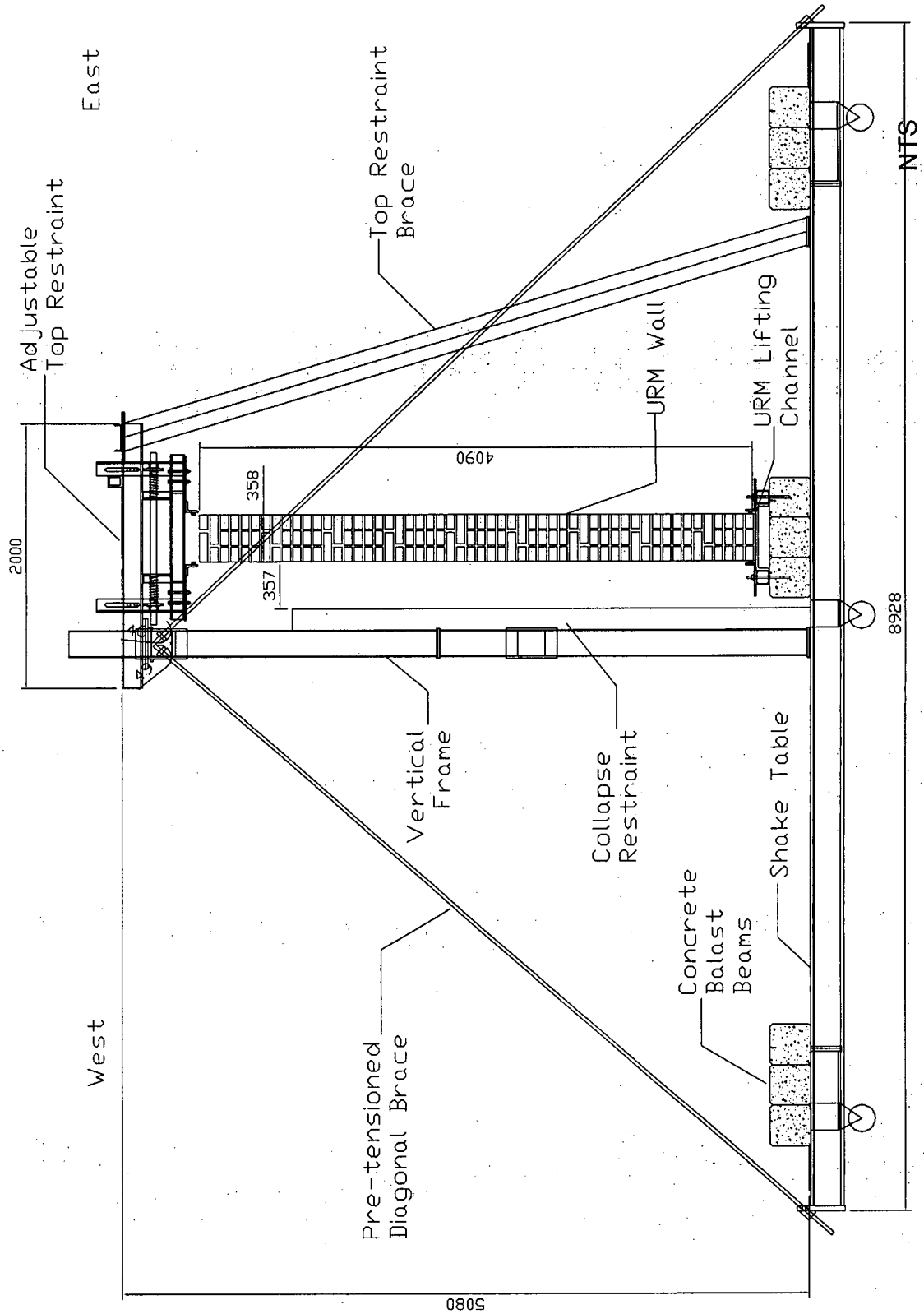

## C.3 Test Set-Up Plan View

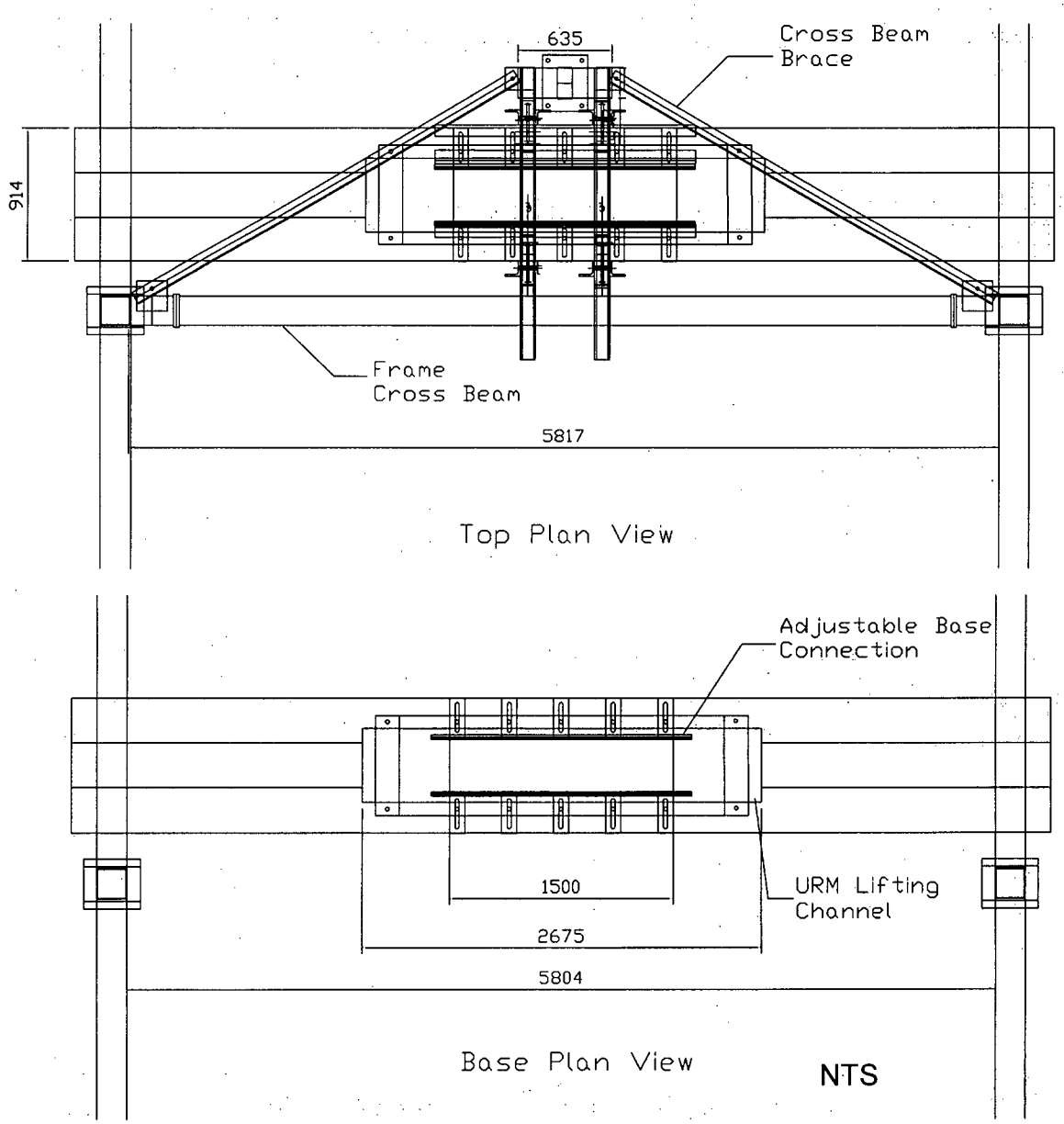

## C.4 Top Restraint Fabrication Drawings

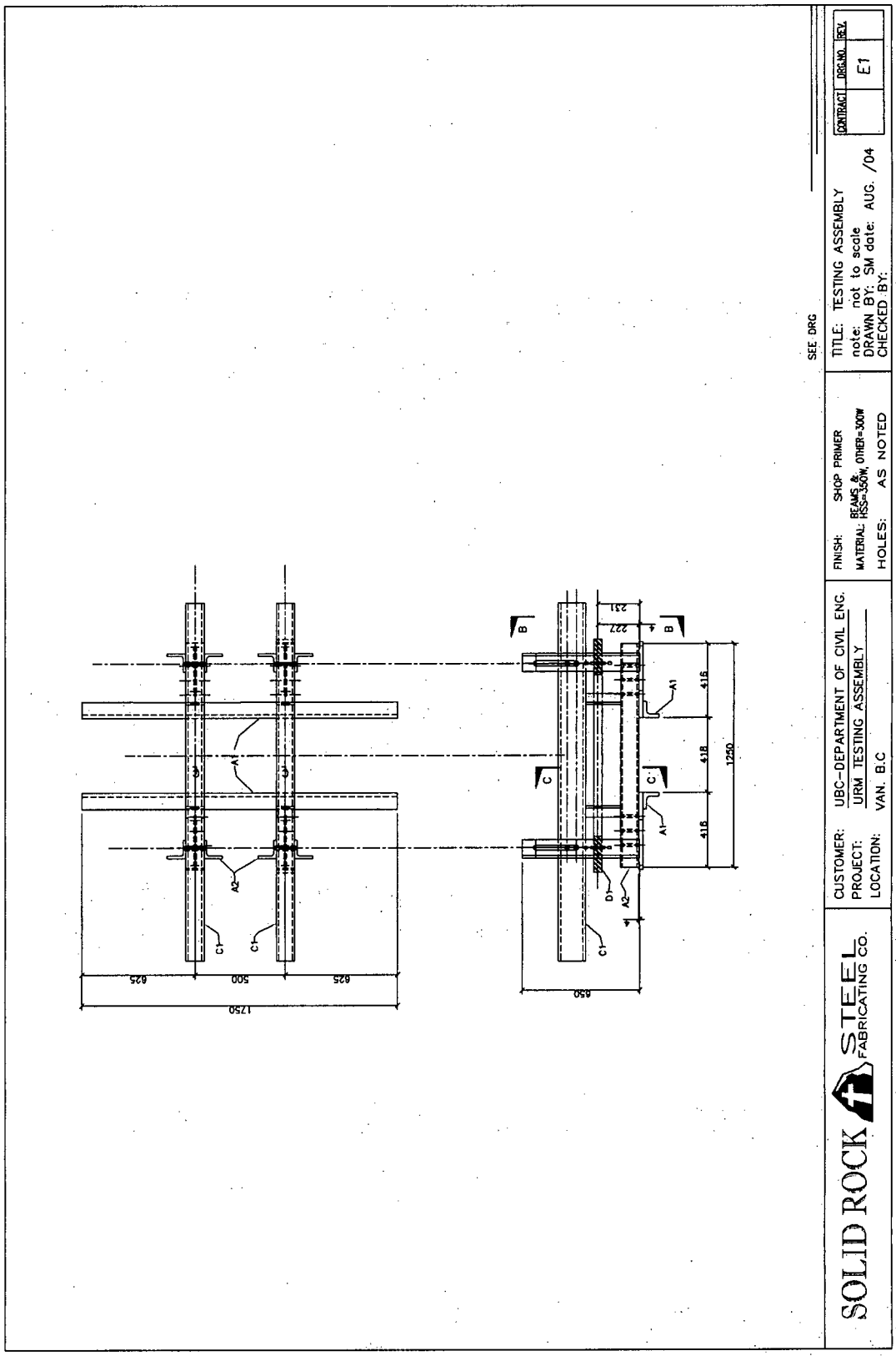

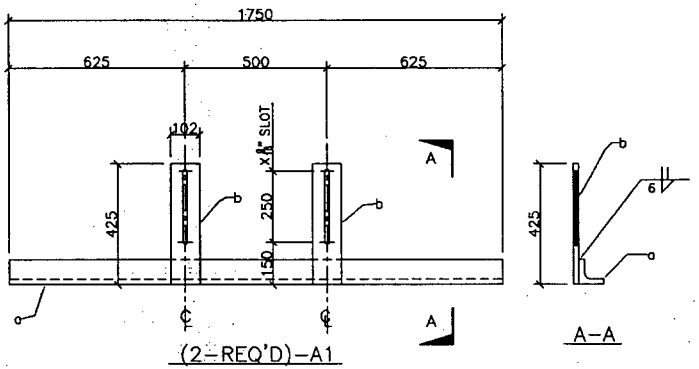


(2-REQ'D)-A1




A-A

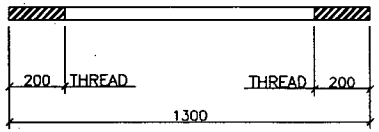


(2-REQ'D)-D1

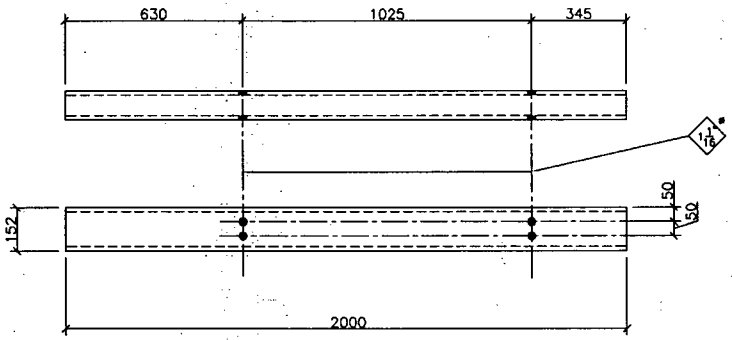


(2-REQ'D)-C1

BILL OF MATERIAL

| MK | QTY | MATERIAL | LENGTH | REMARKS | WEIGHT |
|---|---|---|---|---|---|
| | | 2-A1 | | | |
| a | 2 | L89X89X13 | 1750 | | |
| b | 4 | BAR 13X102 | 425 | | |
| | | 2-C1 | | | |
| | 2 | HSS 152X102X13 | 2000 | | |
| | | 2-D1 | | | |
| | 2 | 1 1/2"ø ROD | 1300 | THREAD AS SHOWN | |

FIELD BOLTS:
8-1" ø A 325 X 6½" LG.

SEE DRG

SOLID ROCK STEEL FABRICATING CO.

CUSTOMER: UBC-DEPARTMENT OF CIVIL ENG.
PROJECT: URM TESTING ASSEMBLY
LOCATION: VAN. B.C

FINISH: SHOP PRIMER
MATERIAL: BEAMS & HSS=350W, OTHER=300W
HOLES: AS NOTED

TITLE: TESTING ASSEMBLY
note: not to scale
DRAWN BY: SM date: AUG. /04
CHECKED BY:

| CONTRACT | DRG.NO. | REV. |
|---|---|---|
| | 1 | |

| BILL OF MATERIAL | | | | | |
|---|---|---|---|---|---|
| MK | QTY | MATERIAL | LENGTH | REMARKS | WEIGHT |
| | | 2-A2 | | | |
| c | 2 | HSS 102X102X9.5 | 1250 | | |
| $d^R$ | 4 | L102X102X13 | 650 | | |
| $d^L$ | 4 | L102X102X13 | 650 | | |
| e | 4 | BAR 13X102 | 200 | | |
| g | 8 | BAR 13X51 | 200 | | |
| h | 4 | BAR 13X102 | 150 | | |

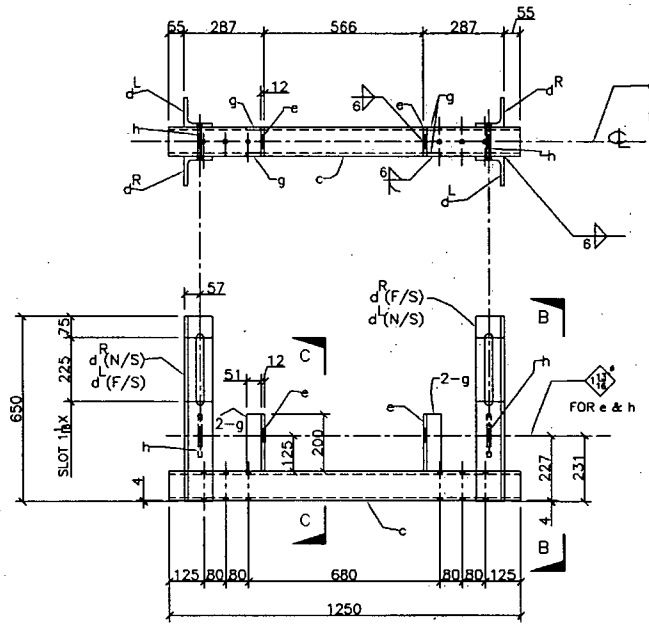


(2-REQ'D)-A2

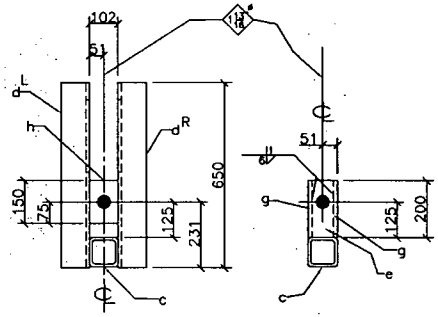


B-B C-C

FIELD BOLTS:
12-$\frac{1}{2}$" ø A 325 X 5$\frac{1}{4}$"LG.

SEE DRG

| | | | |
|---|---|---|---|
| SOLID ROCK STEEL FABRICATING CO. | CUSTOMER: UBC-DEPARTMENT OF CIVIL ENG.<br>PROJECT: URM TESTING ASSEMBLY<br>LOCATION: VAN. B.C | FINISH: SHOP PRIMER<br>MATERIAL: BEAMS & HSS=350W, OTHER=300W<br>HOLES: AS NOTED | TITLE: TESTING ASSEMBLY<br>note: not to scale<br>DRAWN BY: SM date: AUG. /04<br>CHECKED BY: |

| CONTRACT | DRG.NO. | REV. |
|---|---|---|
| | 2 | |

## C.5 Support Frame Stiffness

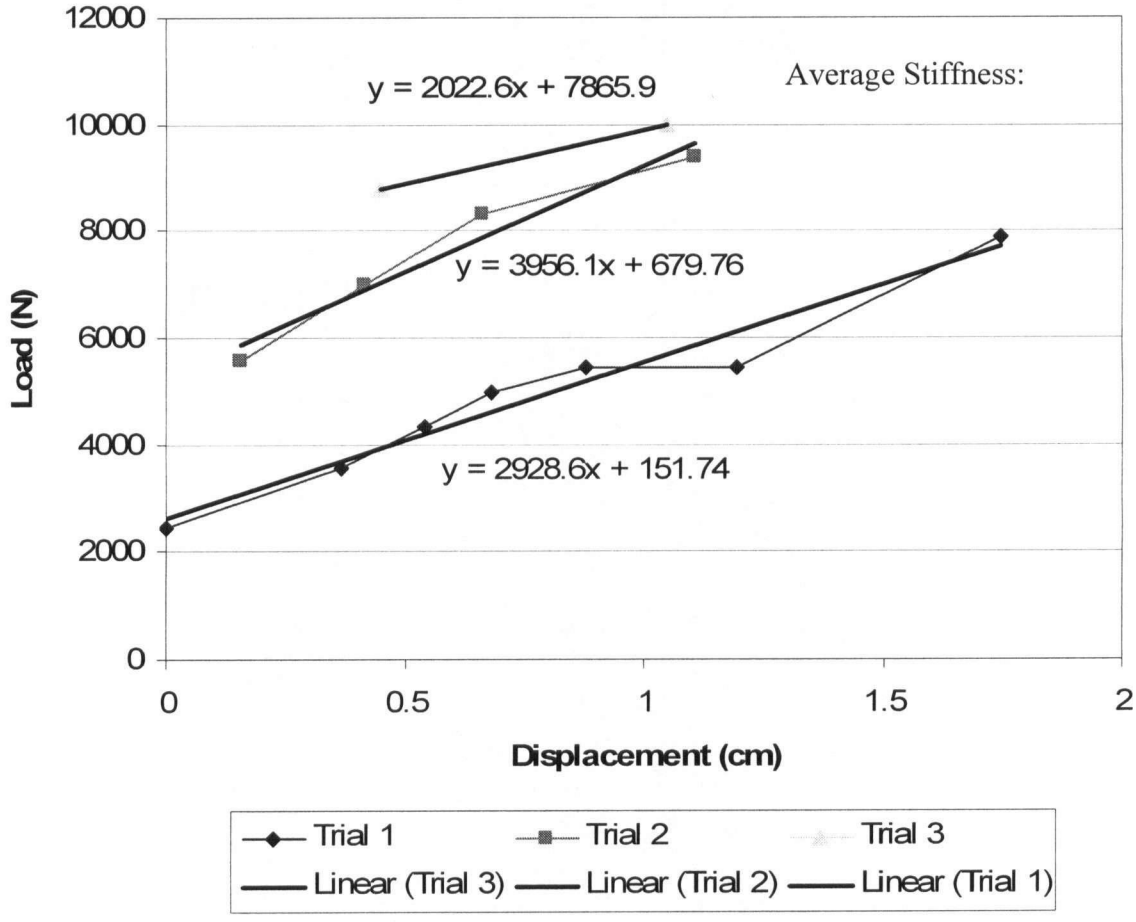

# APPENDIX D. INSTRUMENTATION

## D.1 List of Instrumentation

| Channel | Code | Data Acquisition Module | | Experiment Location |
|---|---|---|---|---|
| 1 | Load Cell | 1520 #4 | | Linear Table Actuator |
| 2 | SP18 | 1100 #3 | 0 | Top Brace - S |
| 3 | SP19 | 1100 #3 | 1 | Top Brace - Middle |
| 4 | SP20 | 1100 #3 | 2 | Conc Beam - Middle |
| 5 | SP22 | 1100 #3 | 3 | Top Connection - Vertical - relative to table |
| 6 | SP4 | 1100 #3 | 4 | Top Brace - N - relative to table |
| 10 | SP2 | 1100 #3 | 8 | Wall - Base - relative to table |
| 11 | SP3 | 1100 #3 | 9 | Wall - H1 - relative to table |
| 12 | SP10 | 1100 #3 | 10 | Wall - H2 |
| 13 | SP12 | 1100 #3 | 11 | Wall - H3 |
| 14 | SP15 | 1100 #3 | 12 | Wall - H4 |
| 15 | SP17 | 1100 #3 | 13 | Wall - H5 |
| 16 | SP16 | 1100 #3 | 14 | Wall - H6 |
| 17 | SP14 | 1100 #3 | 15 | Wall - H7 |
| 18 | SP13 | 1100 #3 | 16 | Wall - H8 |
| 19 | SP1 | 1100 #3 | 17 | Wall - H9 - relative to table |
| 25 | LP12 | 1520 #9 | 0 | Table Corner Wheel - SE |
| 26 | LP11 | 1521 #9 | 1 | Table Corner Wheel - NE |
| 27 | LP5 | 1522 #9 | 2 | Concrete Beam - W |
| 28 | LP6 | 1523 #9 | 3 | Concrete Beam - E |
| 29 | LP9 | 1524 #9 | 4 | Bottom URM -E |
| 30 | LP10 | 1525 #9 | 5 | Bottom URM -W |
| 31 | LP7 | 1526 #9 | 6 | Top URM Wall - W |
| 32 | LP8 | 1527 #9 | 7 | Top URM Wall - E |
| 38 | A1D-21 | 1100 | 18 | Concrete Beam |
| 39 | A1D-20 | 1100 | 19 | Top Restraint |
| 40 | A3D-3-X | 1520 #4 | 1 | Wall - Base |
| 41 | A3D-3-Y | 1521 #4 | 2 | Wall - Base |
| 42 | A3D-3-Z | 1522 #4 | 3 | Wall - Base |
| 43 | A3D-2-X | 1523 #4 | 4 | Wall - H1 |
| 44 | A3D-2-Y | 1524 #4 | 5 | Wall - H2 |
| 45 | A3D-2-Z | 1525 #4 | 6 | Wall - H3 |
| 46 | A1D-8 | 1520 #5 FB | 0 | Wall - H2 |
| 47 | A1D-7 | 1521 #5 FB | 1 | Wall - H3 |
| 48 | A1D-6 | 1522 #5 FB | 2 | Wall - H4 |
| 49 | A1D-5 | 1523 #5 FB | 3 | Wall - H5 |
| 50 | A1D-4 | 1524 #5 FB | 4 | Wall - H6 |
| 51 | A1D-3 | 1525 #5 FB | 5 | Wall - H7 |
| 52 | A1D-2 | 1526 #5 FB | 6 | Wall - H8 |
| 53 | A1D-1 | 1527 #5 FB | 7 | Wall - H9 |
| 54 | A3D-1-X | 1520 #6 | 0 | Top of Wall |
| 55 | A3D-1-Y | 1521 #6 | 1 | Top of Wall |
| 56 | A3D-1-Z | 1522 #6 | 2 | Top of Wall |
| 57 | Impact Hammer | Mod #3 | 20 | |
| 58 | Displ. Fbk. | Mod #4 | 21 | |
| 59 | Displ. Cntrl. | Mod #5 | 22 | |
| 62 | SG1 | 1520 #7 1/4B | | Top Restraint -SES |
| 63 | SG2 | 1521 #7 1/4B | | Top Restraint -SEN |
| 64 | SG3 | 1522 #7 1/4B | | Top Restraint -SWS |
| 65 | SG4 | 1523 #7 1/4B | | Top Restraint -SWN |
| 66 | SG5 | 1524 #7 1/4B | | Top Restraint -NES |
| 67 | SG6 | 1525 #7 1/4B | | Top Restraint -NEN |
| 68 | SG7 | 1526 #7 1/4B | | Top Restraint -NWS |
| 69 | SG8 | 1527 #7 1/4B | | Top Restraint -NWN |

## D.2 Instrument Locations

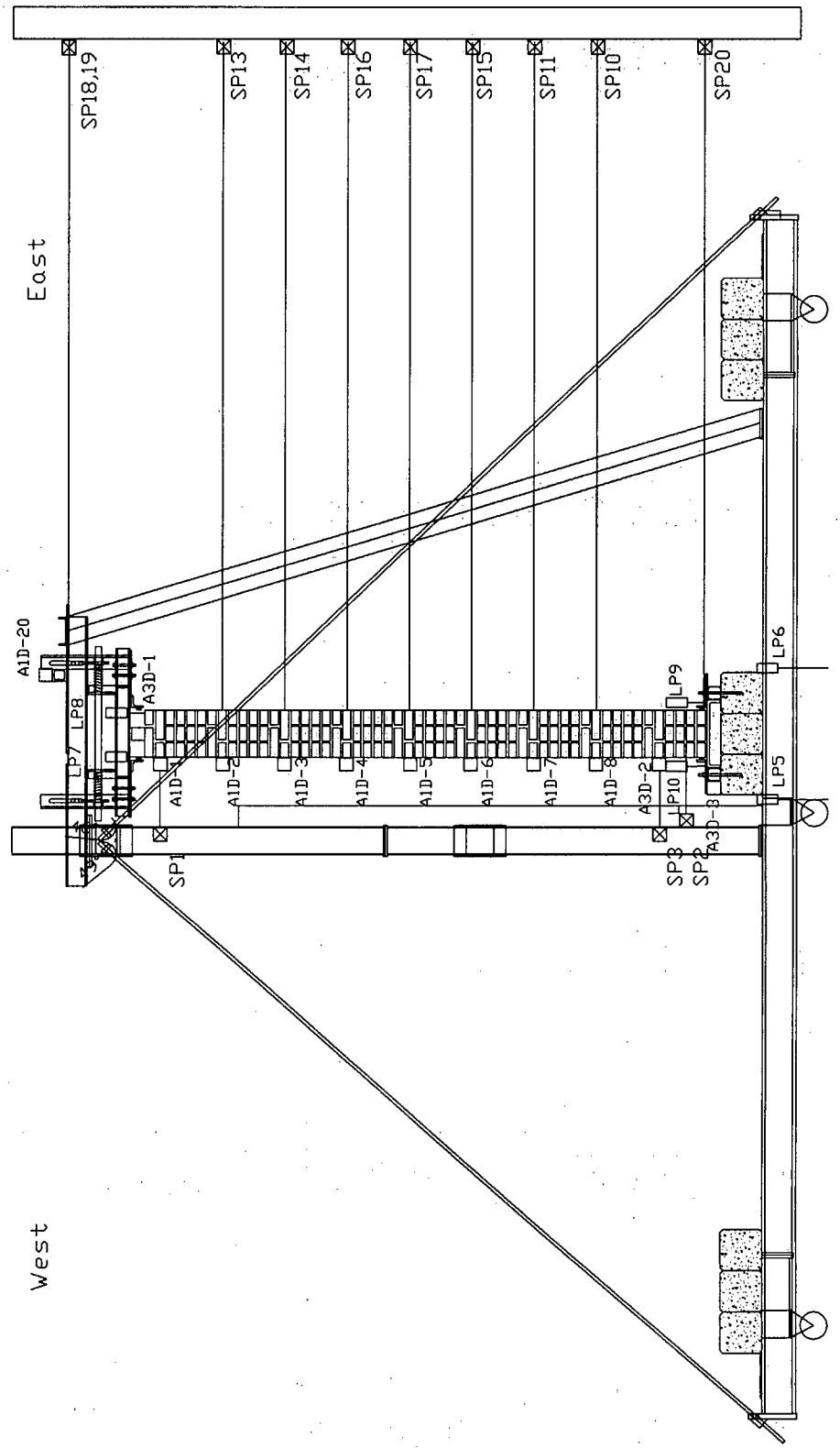

# APPENDIX E. VISUAL OBSERVATIONS

## E1. Wall GC

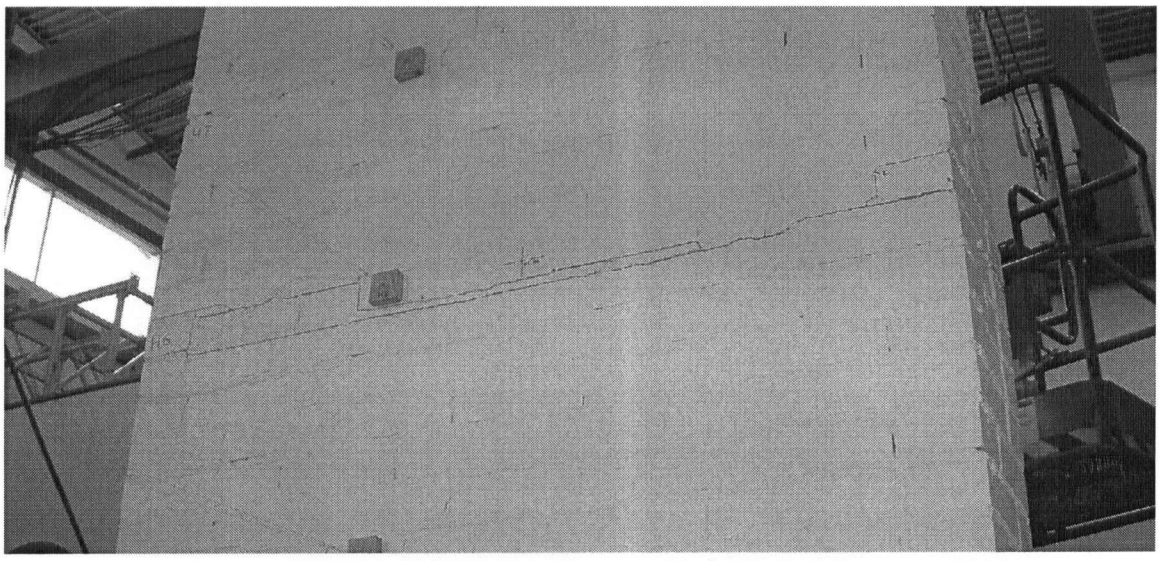

Crack Formed at Header 6 (Test GC2-1.32*)

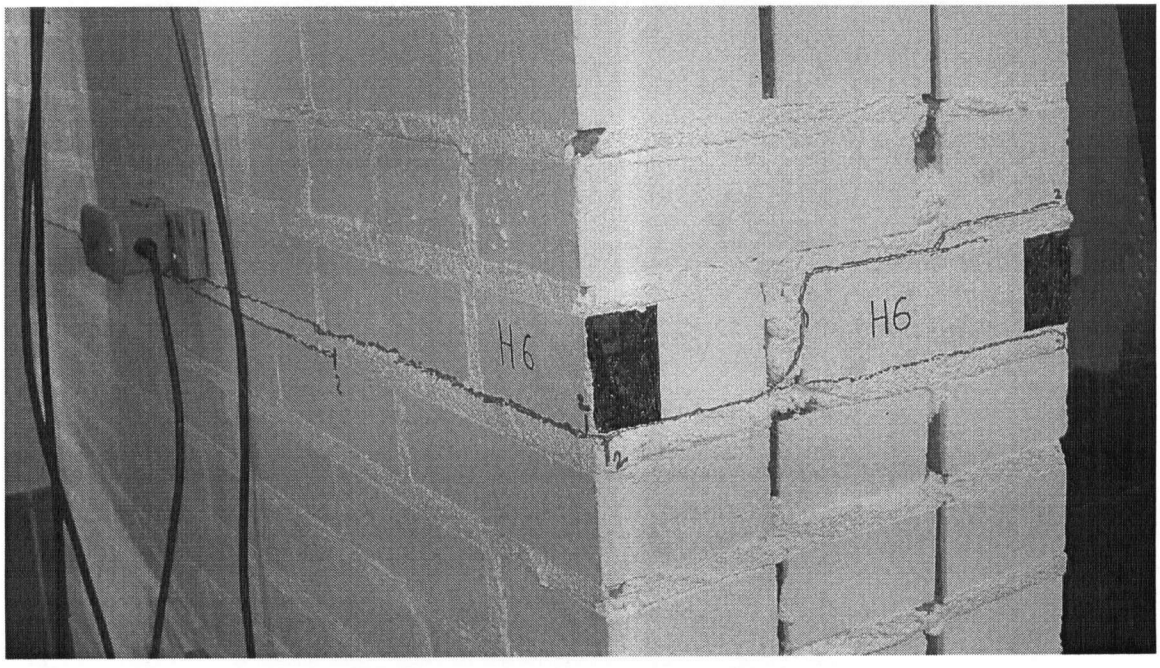


Crack Formed at Header 6 (Test GC2-1.32*)

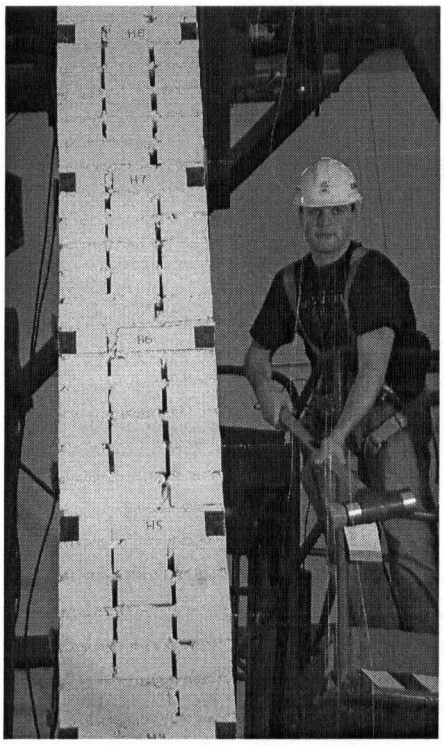

Hammer Test (Test GC2-1.32*)

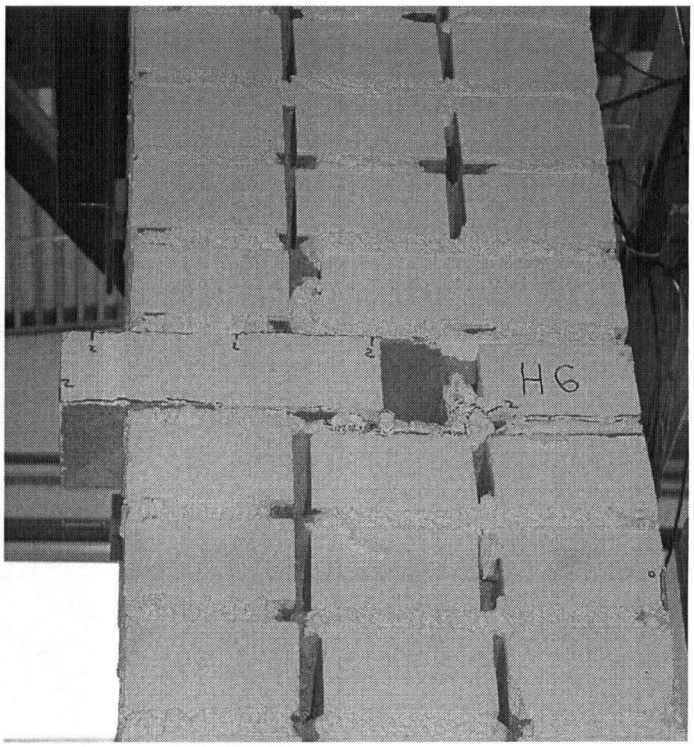


Dislodged Brick at Header 6 (Test GC3-0.60)

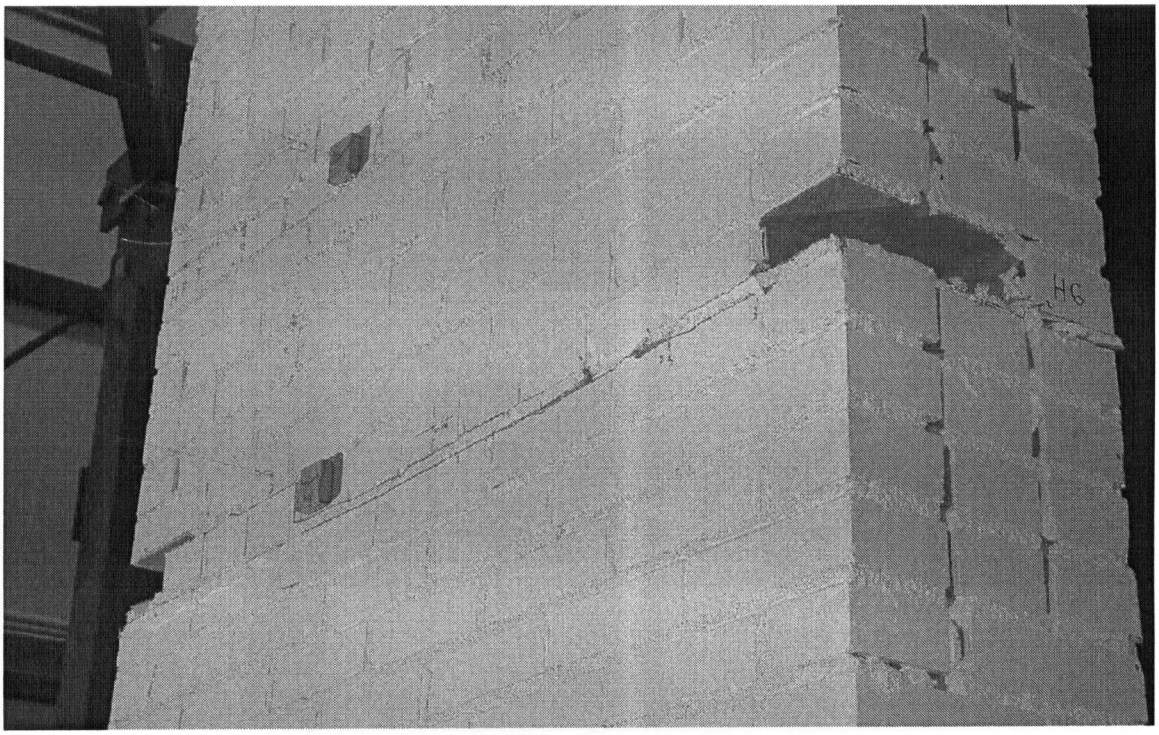


Loss of Bricks at Header 6 (Test GC4-1.21)

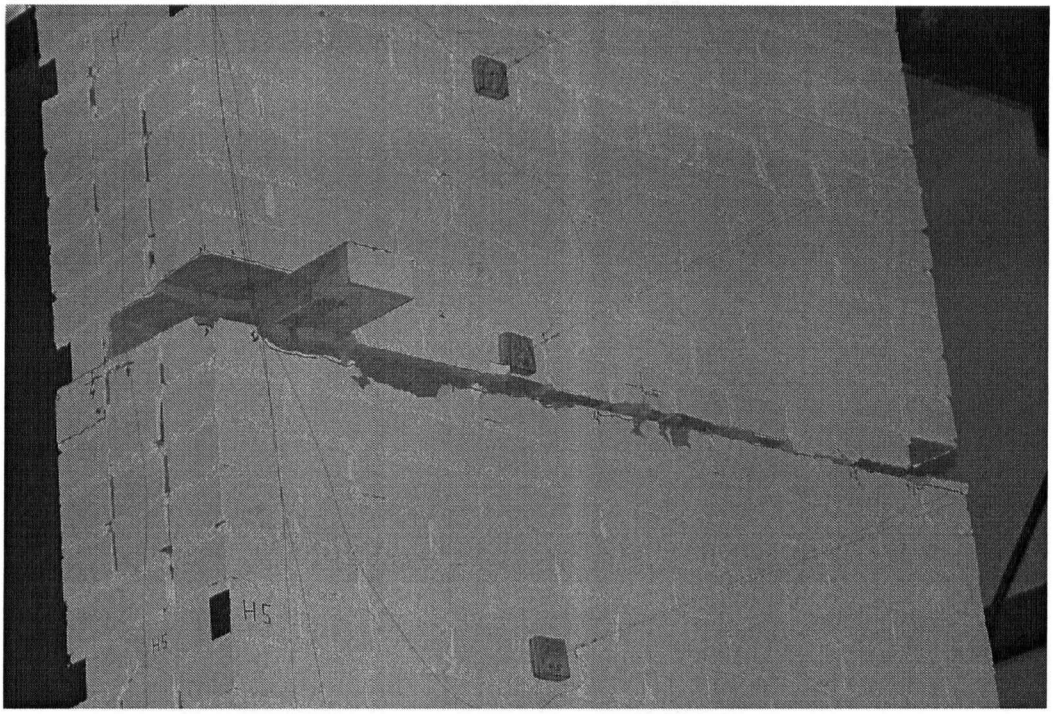


Loss and Crushing of Bricks at Header 6 (Test GC5-1.49)

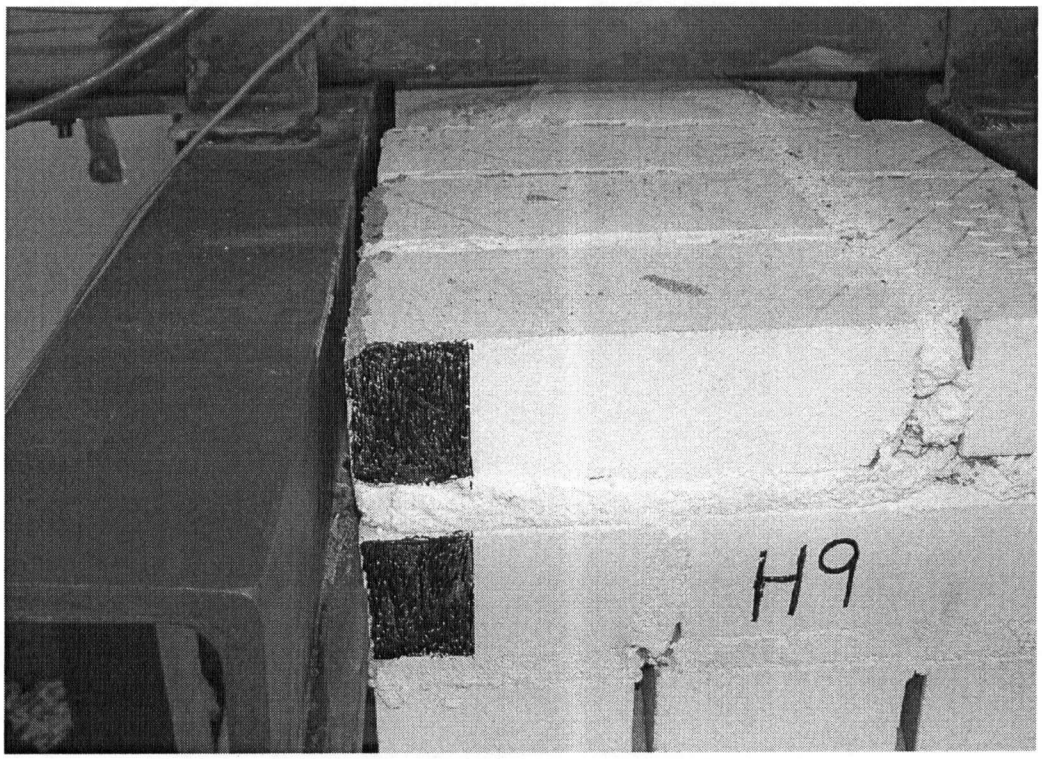


Bearing Contact at Top of Wall (Test GC6-1.57)

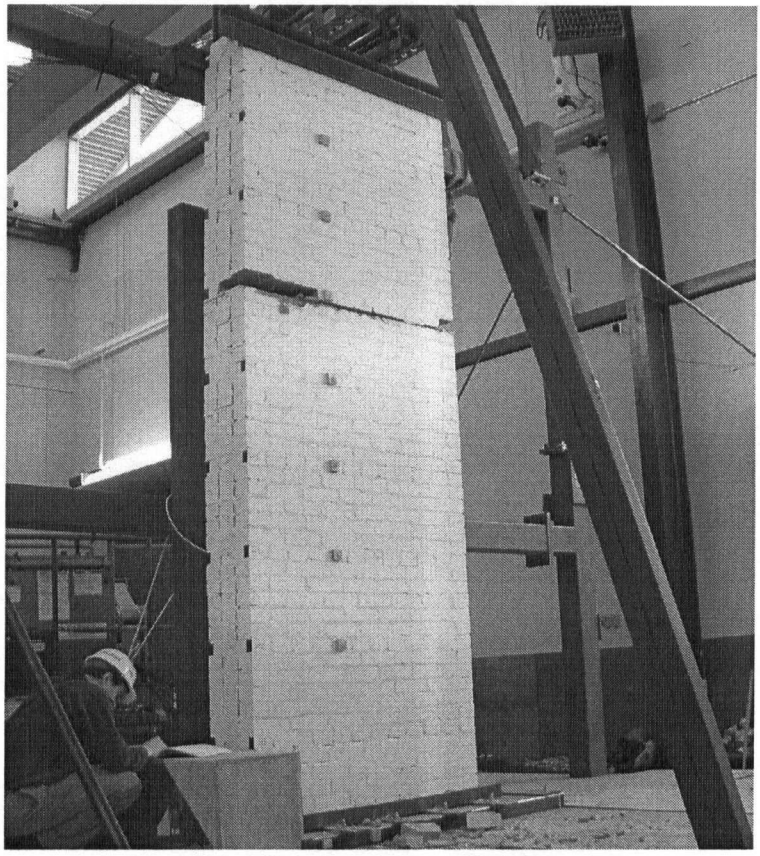

Damage at Header 6 (Test GC6-1.57)

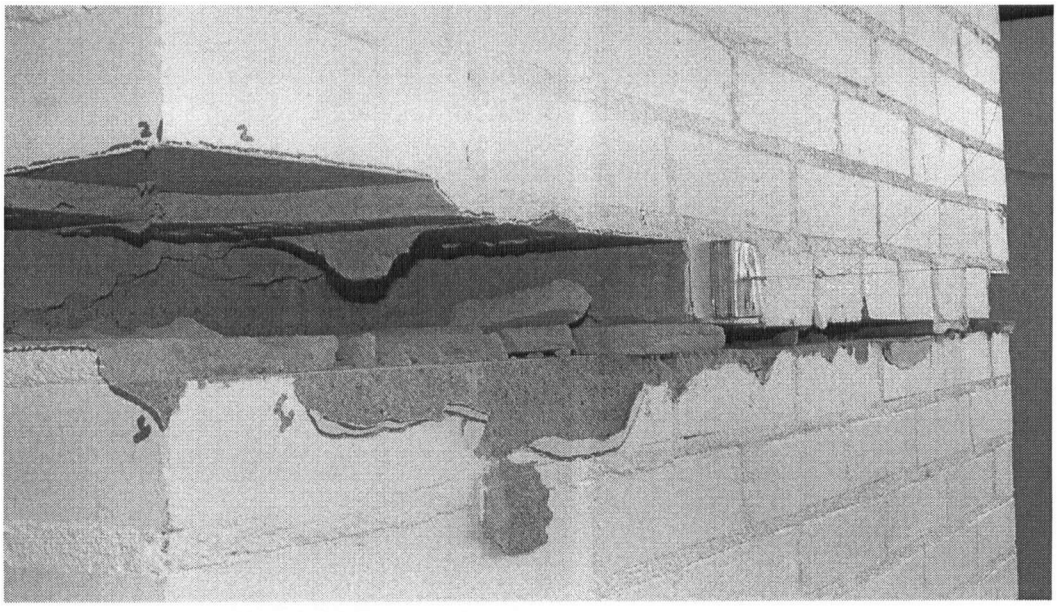


Damage at Header 6 (Test GC6-1.57)

## E.2 Wall PC

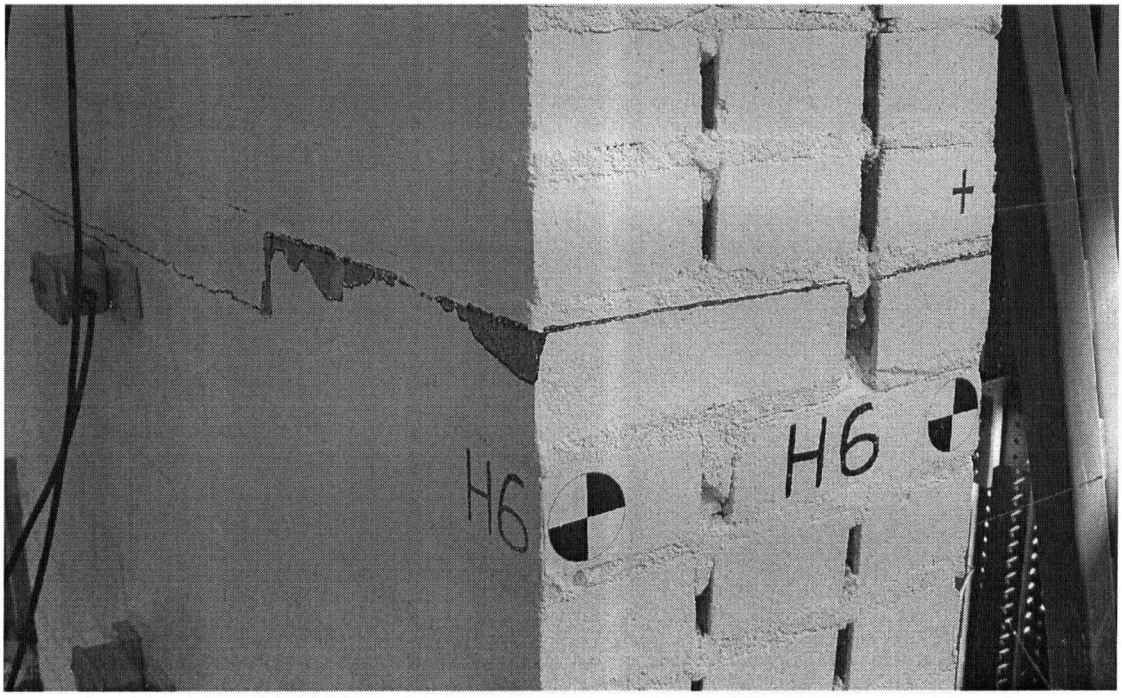


Crack and Brick Crushing at Header 6 (Test PD2-0.59*)

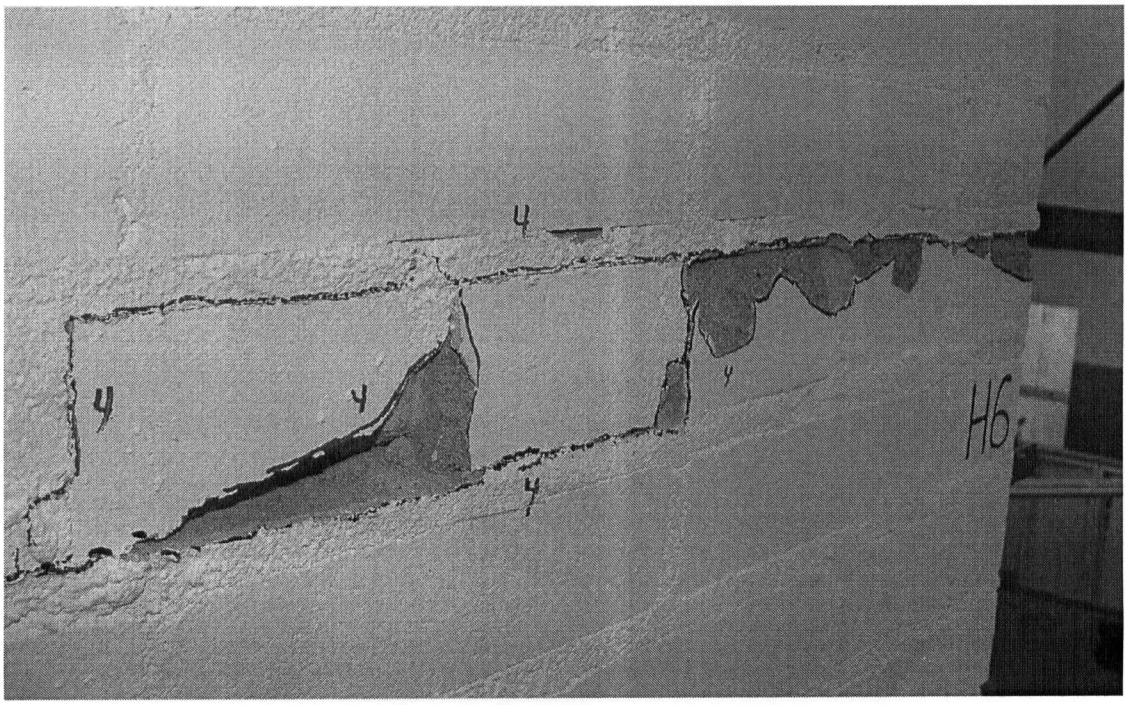


Crack and Brick Crushing at Header 6 (Test PD4-1.40)

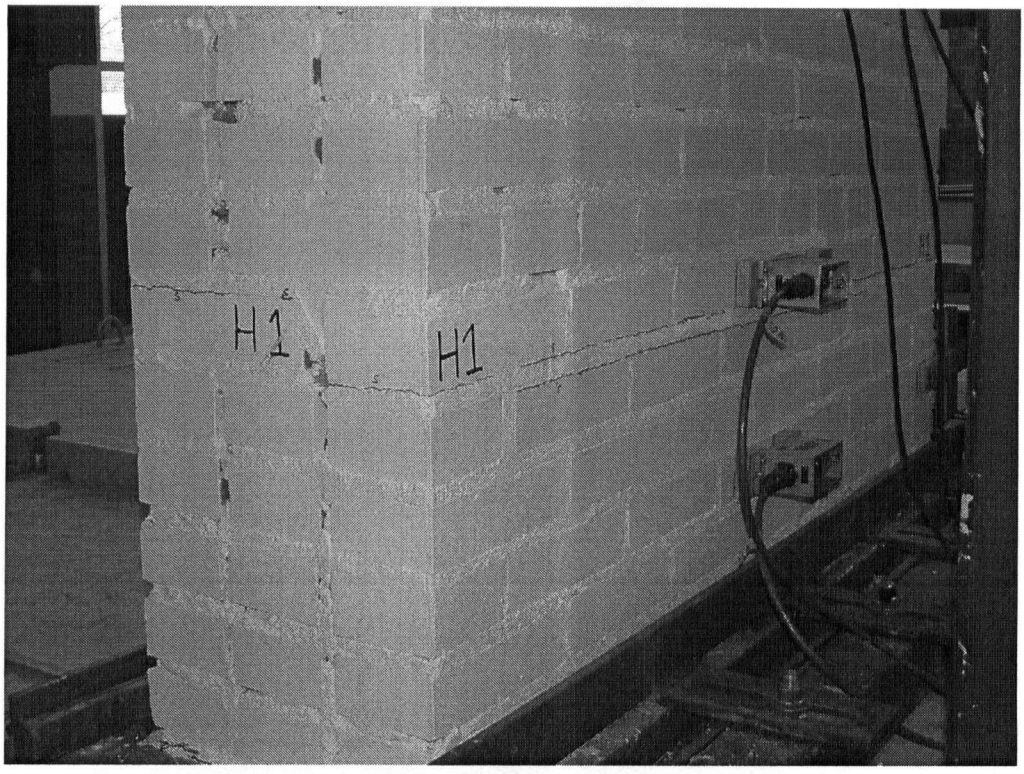


Crack at Header 1 (Test PD5-1.55)


Crack and Brick Crushing at Header 6 (Test PD5-1.55)

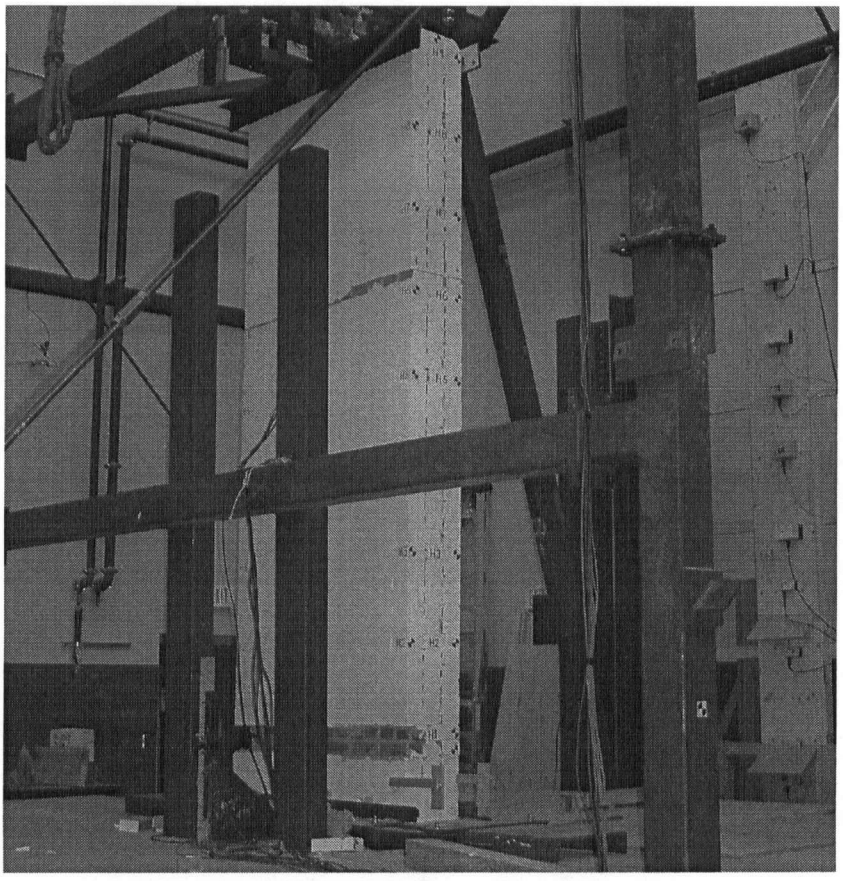

Wall Damaged at Header 1 and 6 (Test PD6-1.57)

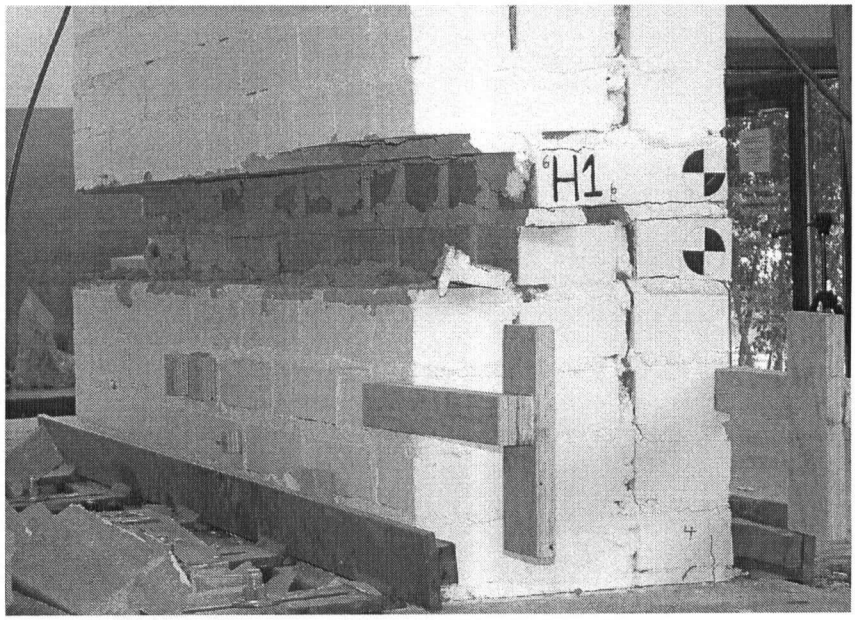


Loss of One Wythe at Header 1 (Test PD6-1.57)

## E.3 Wall GD

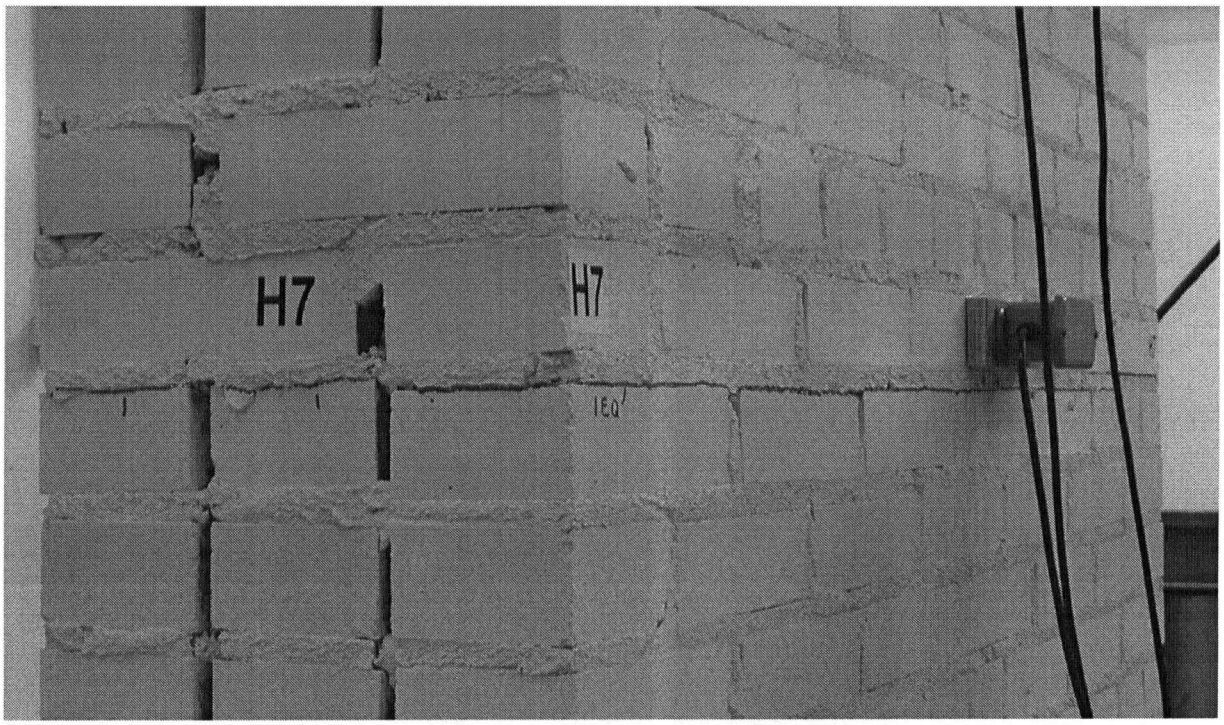


Crack at Header 7 (Test GD1-0.75*)

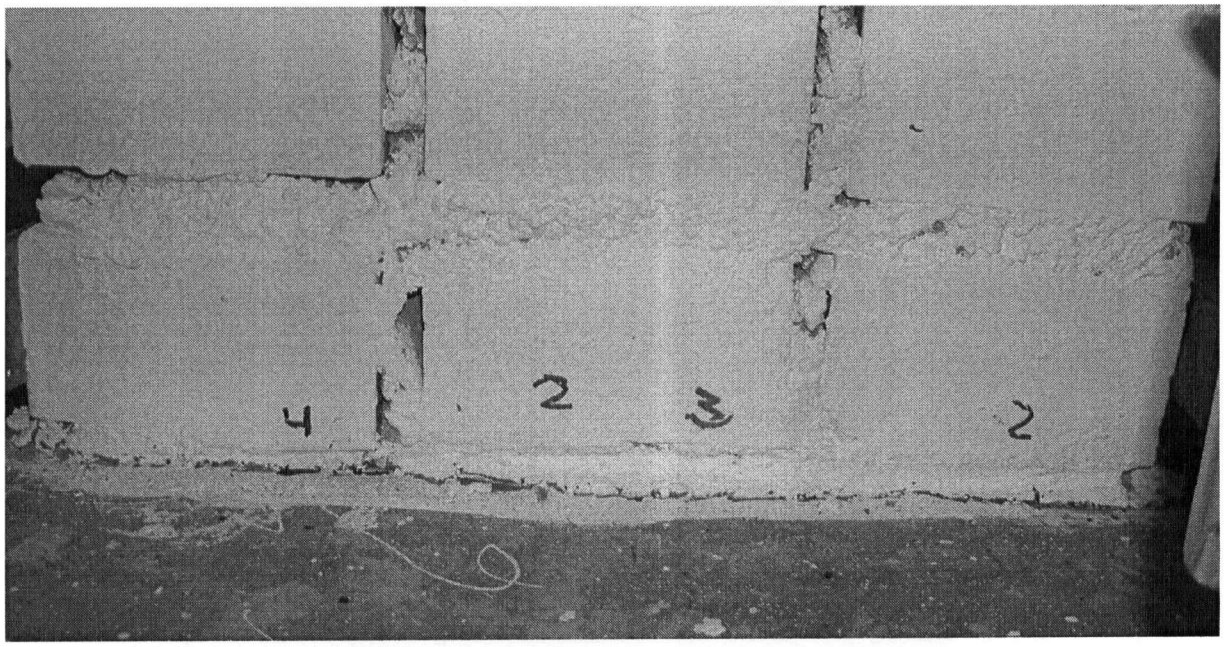


Crack at Wall Base (Test GD4-1.24)

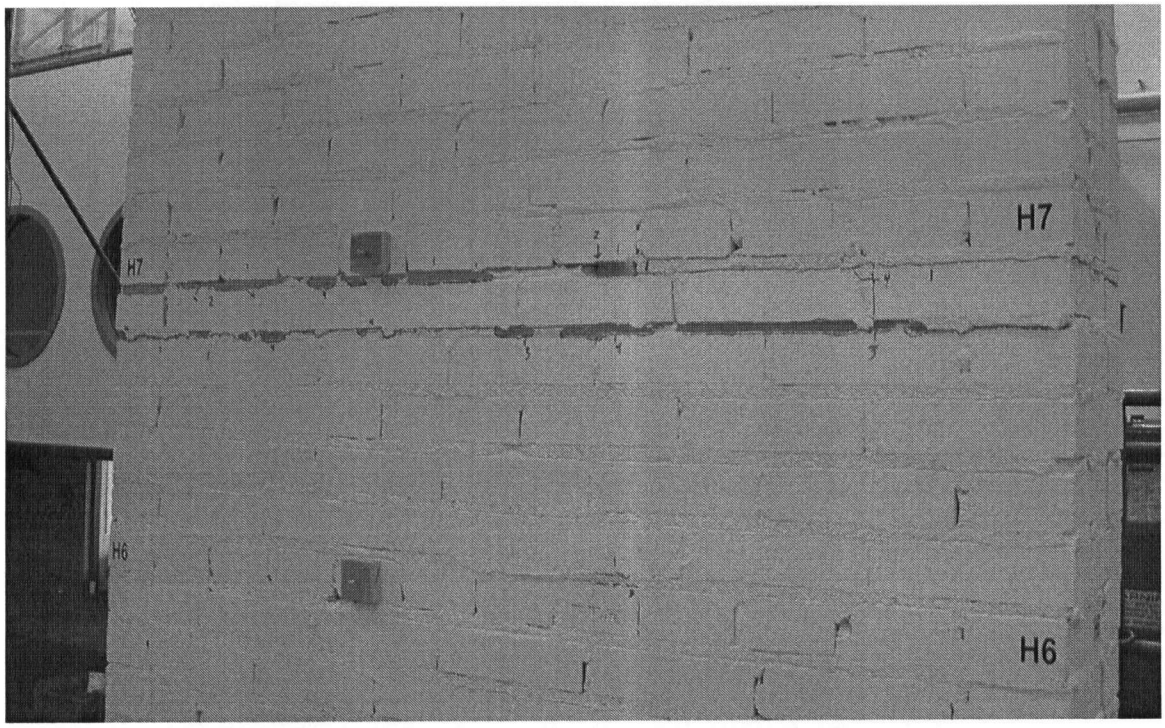


Crack at Header 7 with Mortar Spalling (Test GD4-1.24)

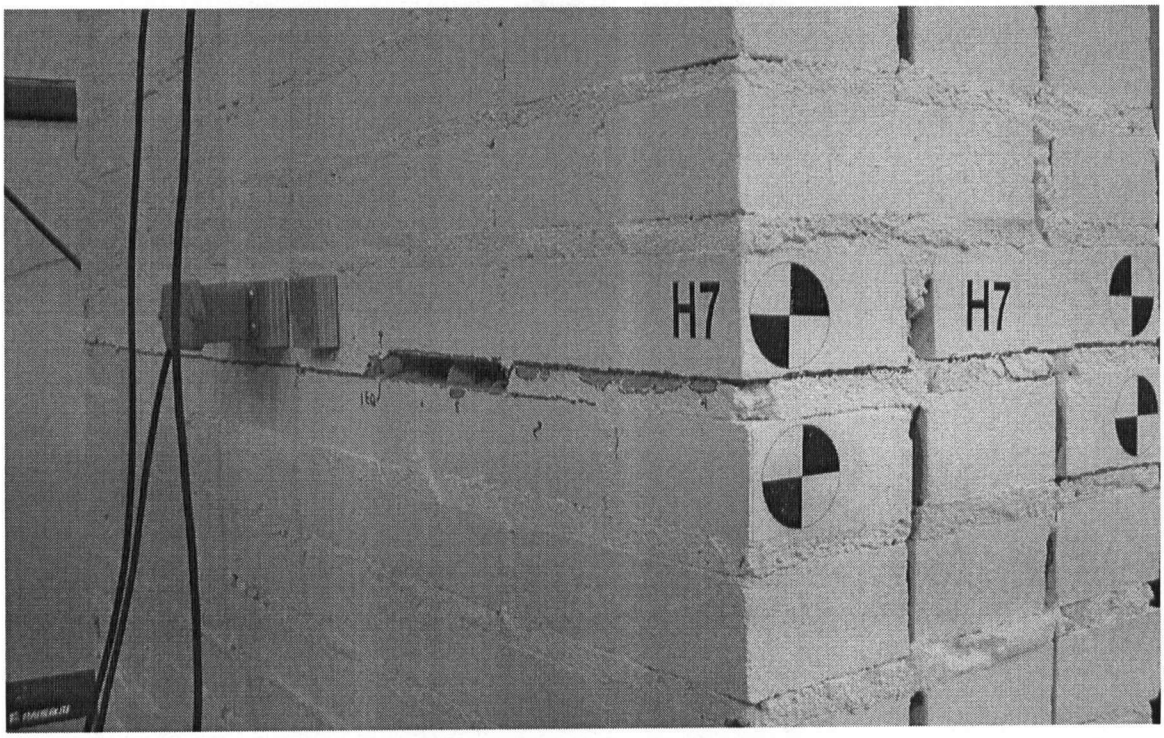


Crack at Header 7 with Mortar Loss (Test GD4-1.24)

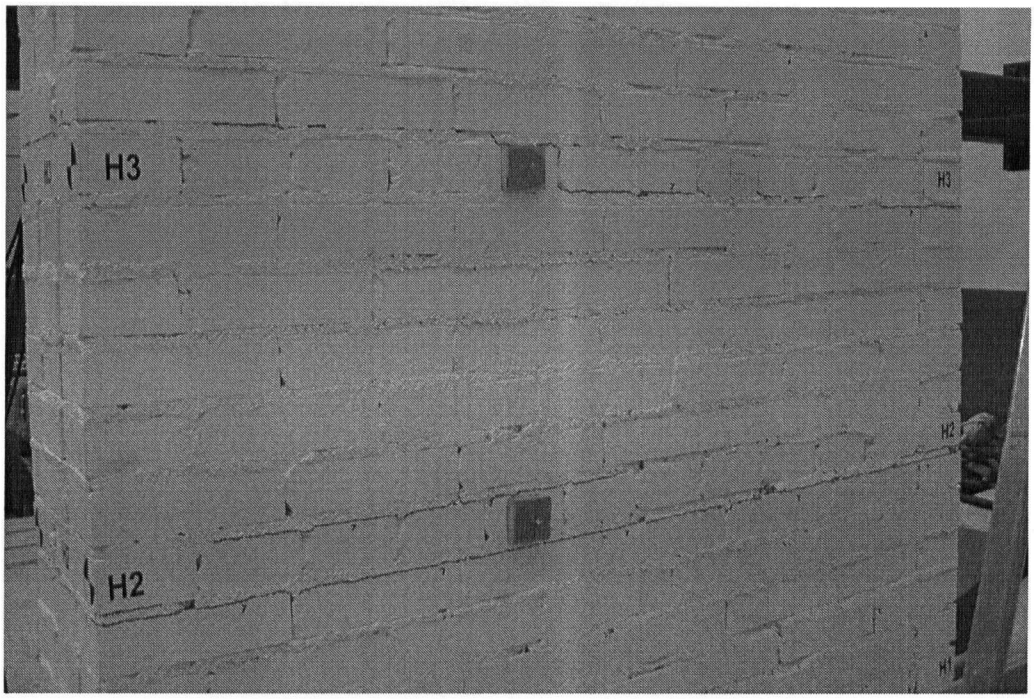


Crack at Headers 2 and 3 (Test GD5-1.65)

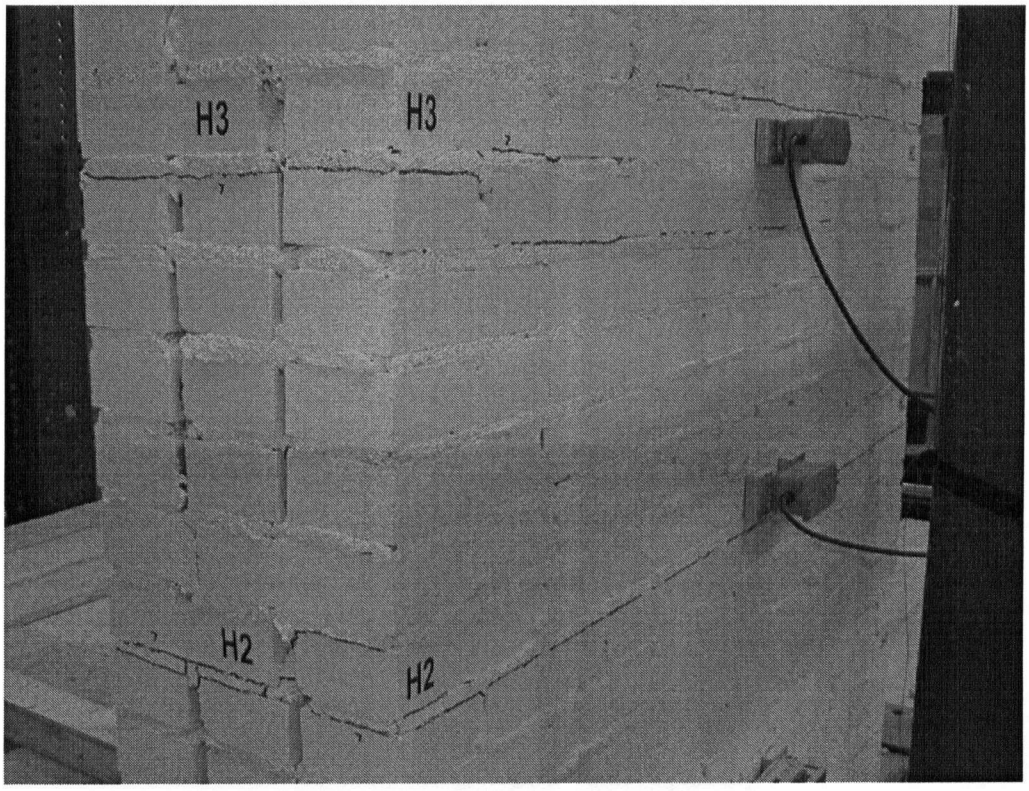


Crack at Headers 2 and 3 (Test GD5-1.65)

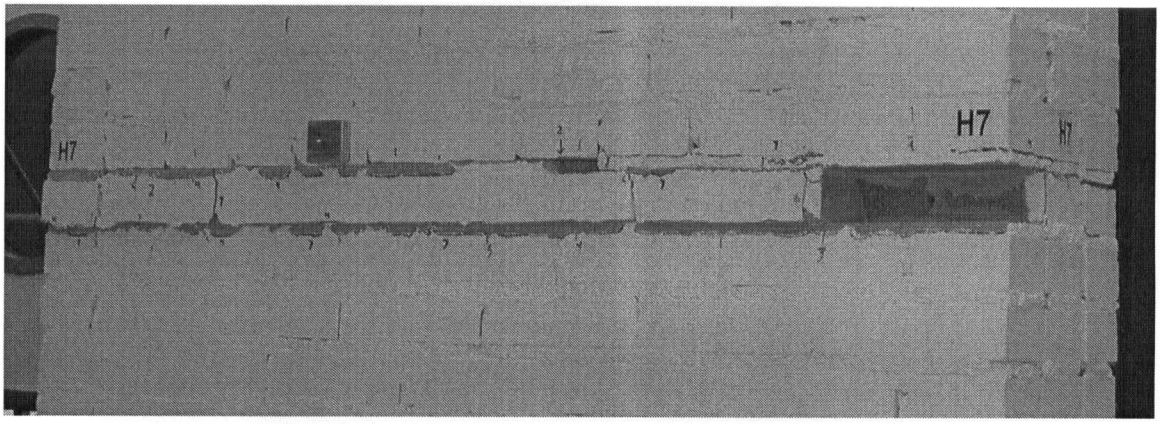


Loss of Brick and Mortar Crushing at Headers 7 (Test GD5-1.65)

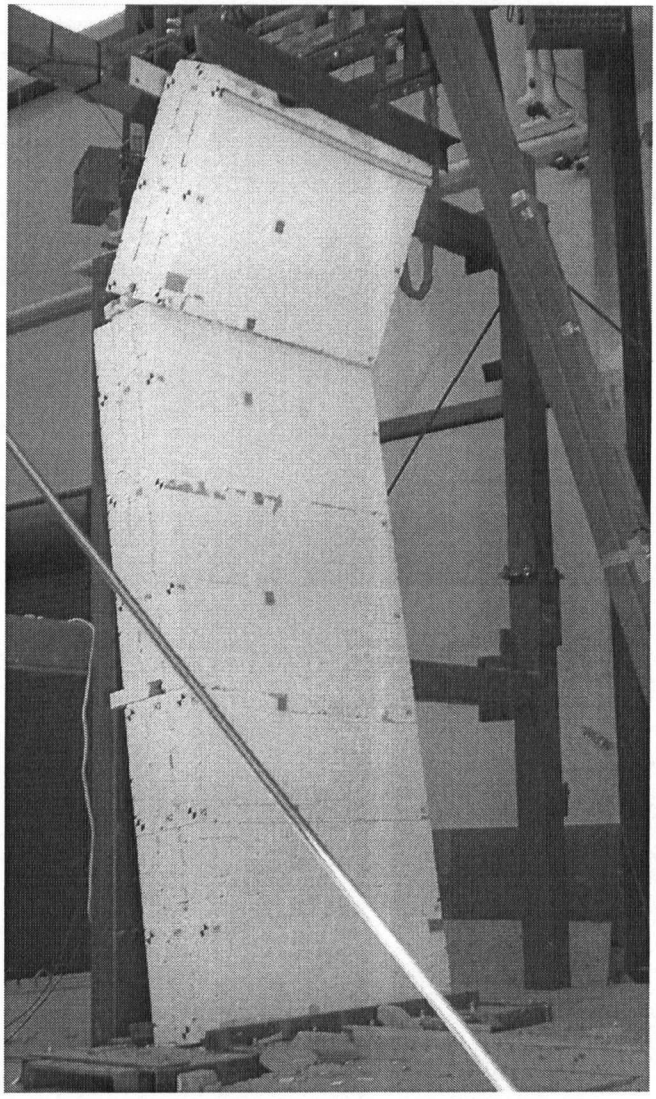

Collapsed Wall (Test GD6-1.83)

## E.4 Wall PD

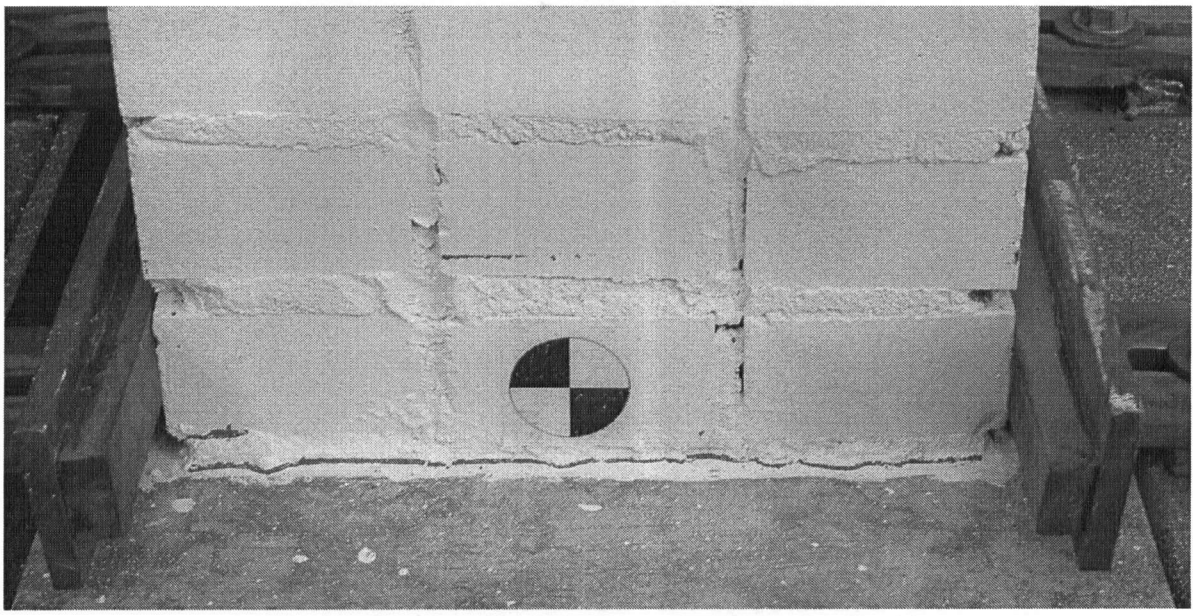

Crack at Wall Base (Test PD1-0.79*)

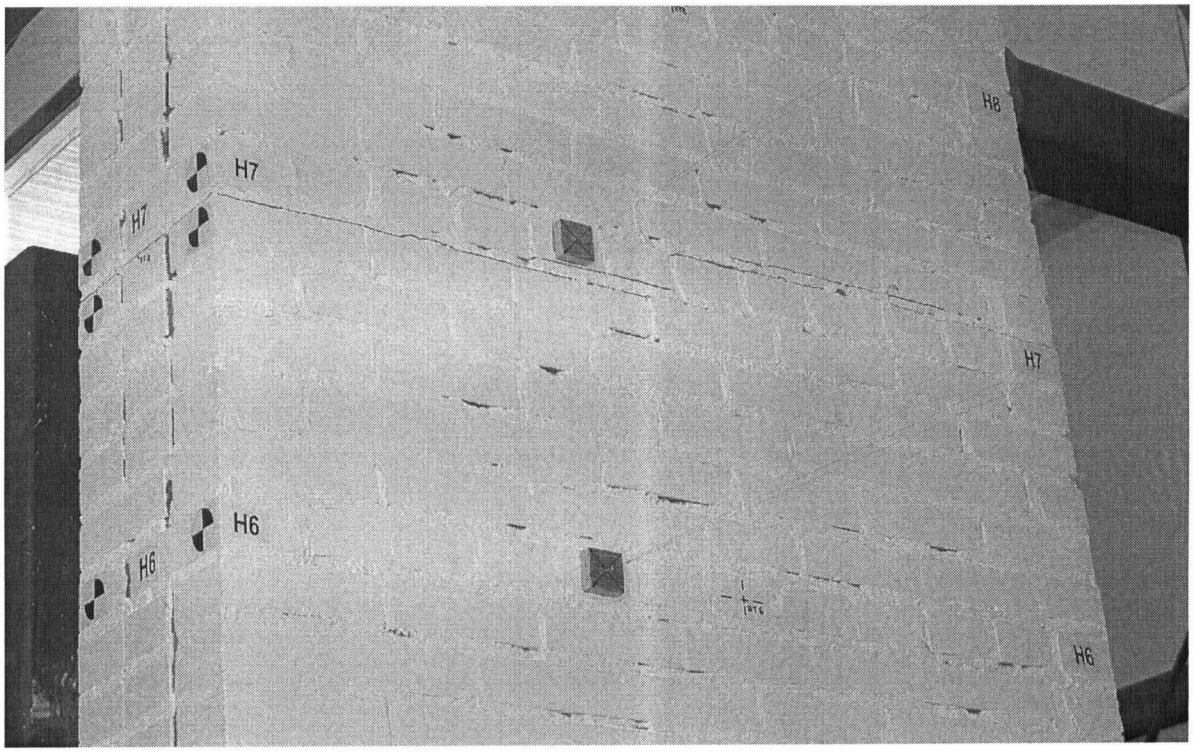


Crack at Header 7 (Test PD1-0.79*)

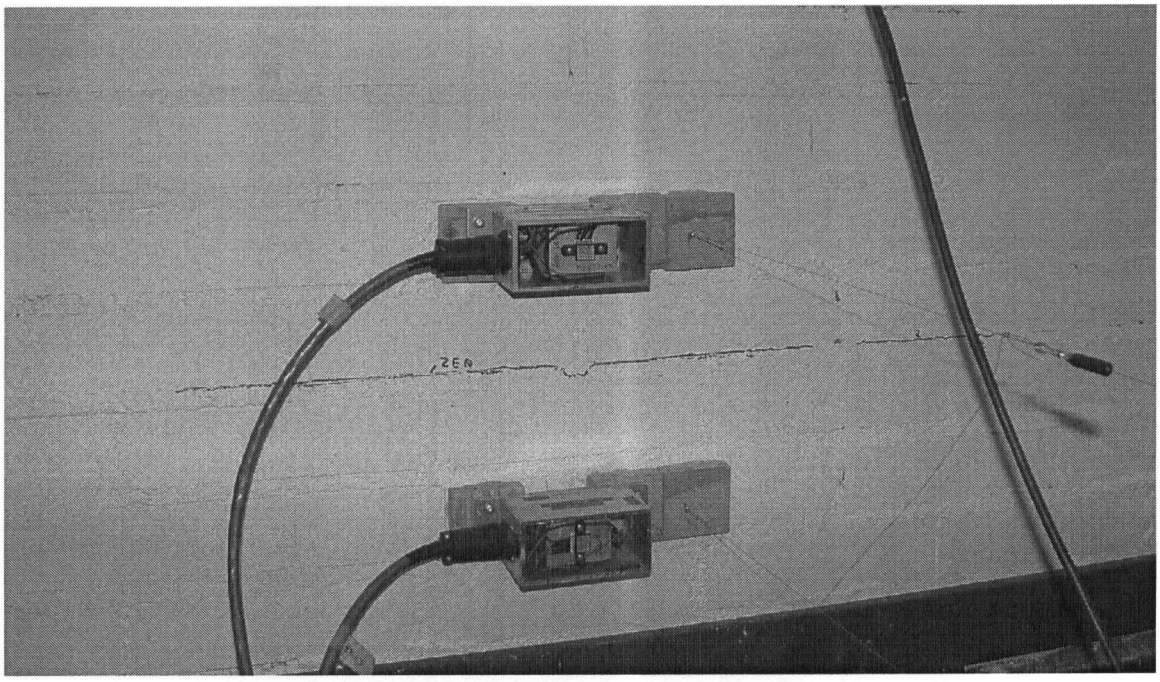

Crack at Header 1 (Test PD2-0.78)

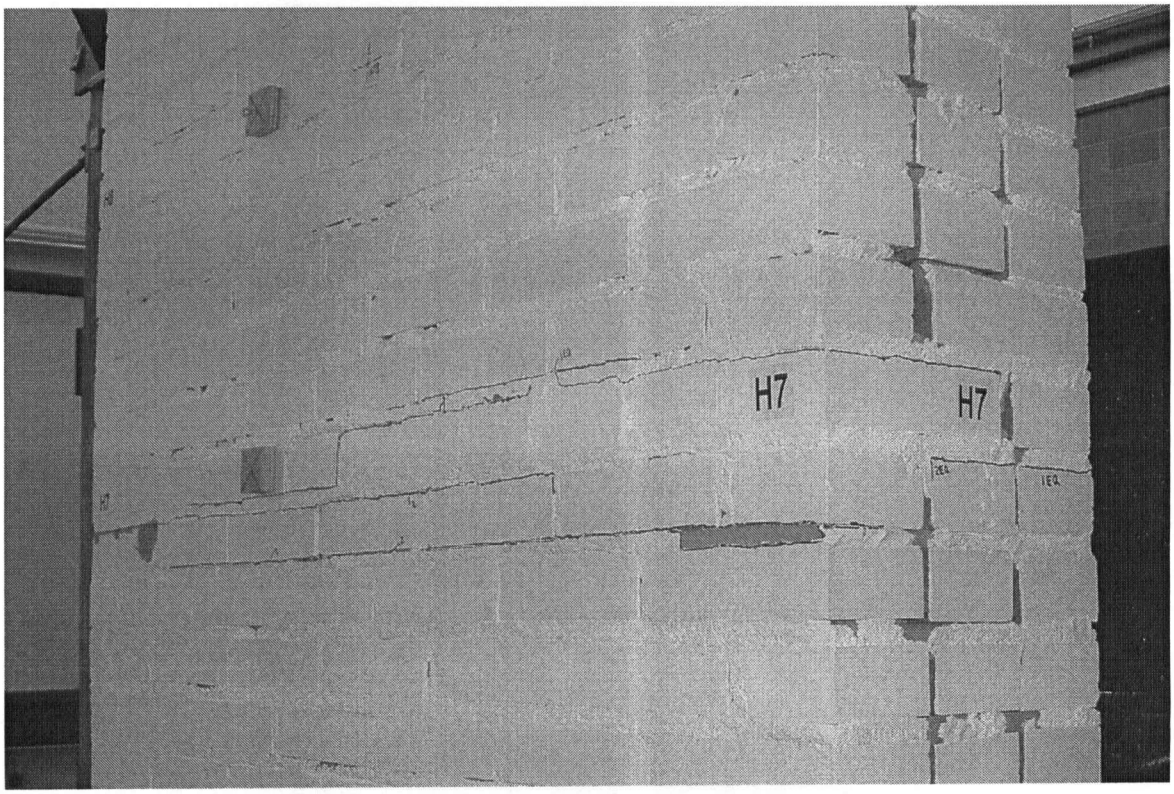


Crack at Header 7 (Test PD2-0.78)

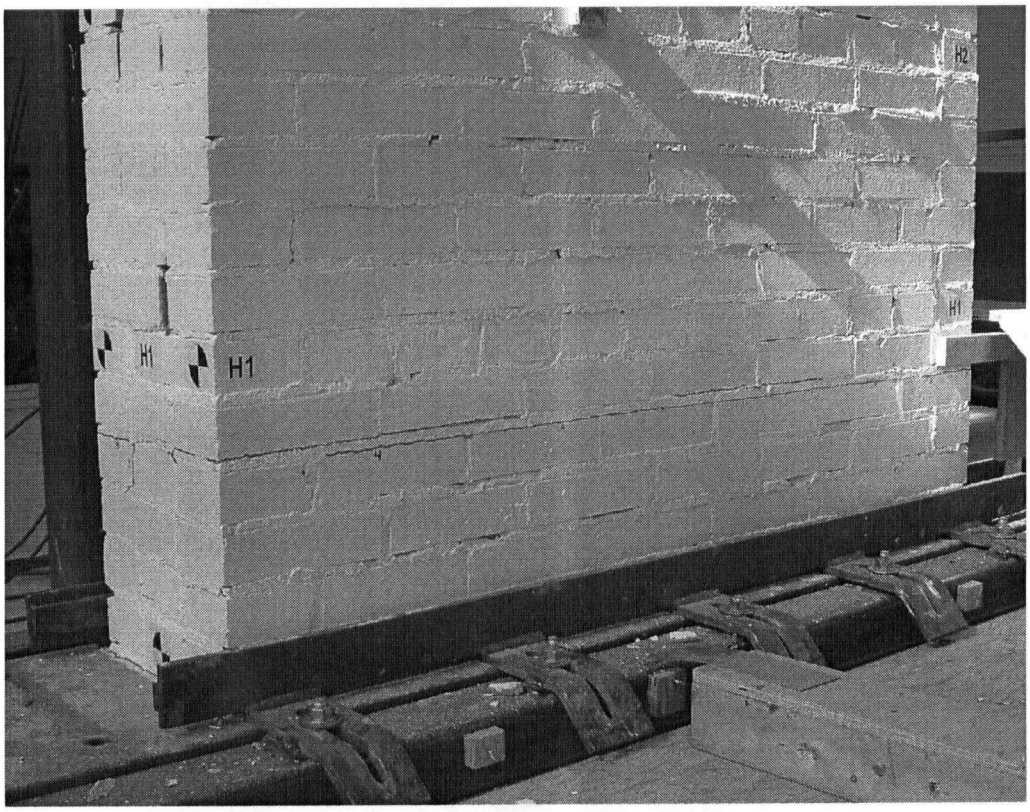


Cracks at Header 1 (Test PD4-1.20)

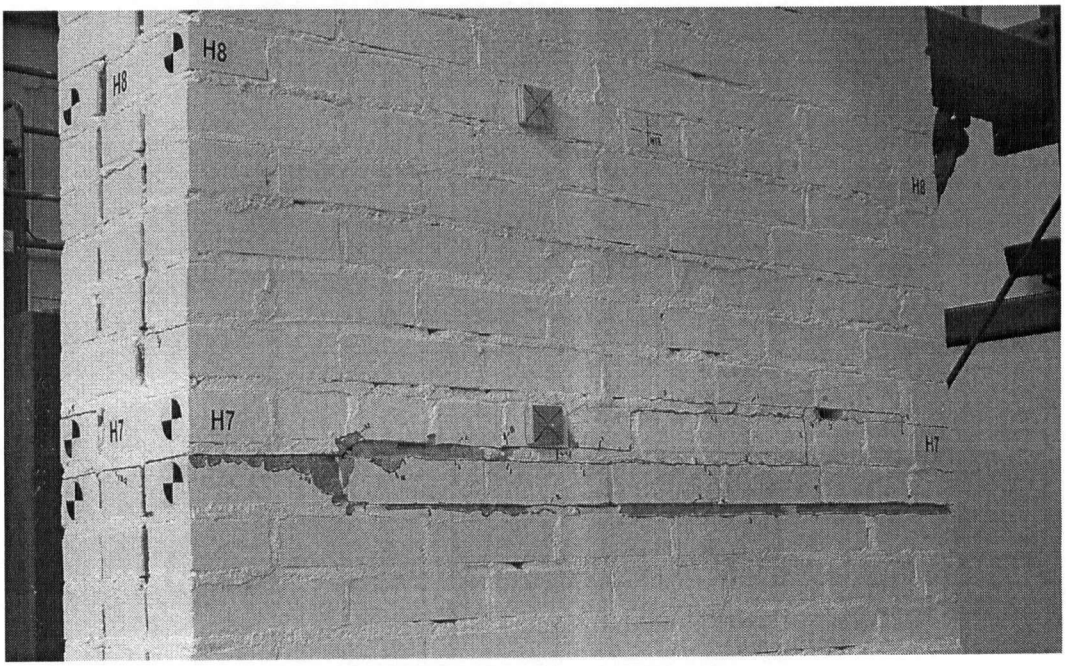


Crack at Header 7 (Test PD4-1.20)

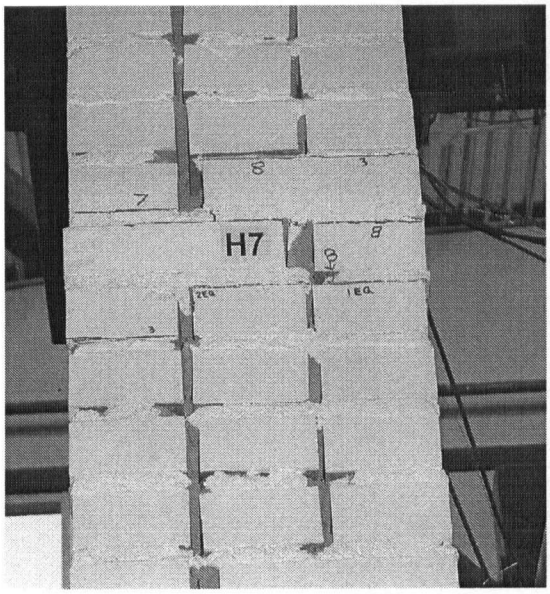


Wall Offset at Header 7
(Test PD5-1.66)

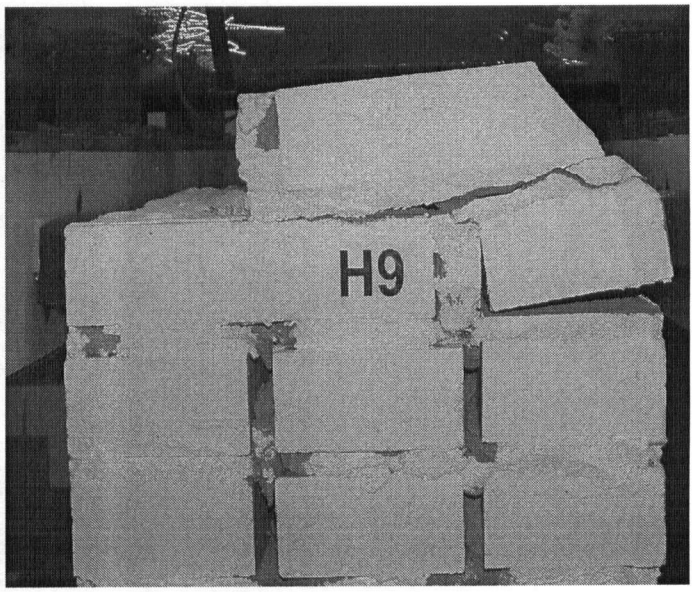


Crack at Header 9 (Test PD5-1.66)

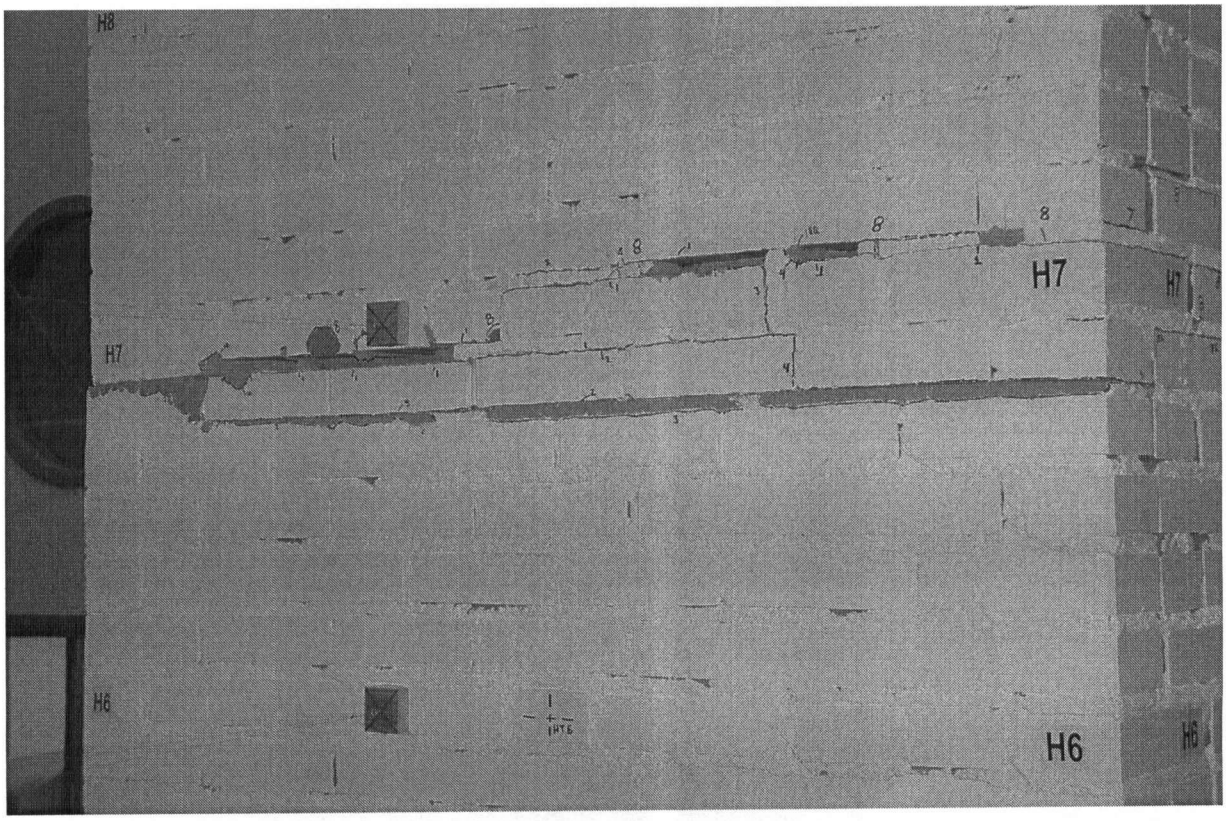


Crack at Header 7 with Mortar Loss and Brick Crushing (Test PD5-1.66)

Collapsed Wall (Test PD6-2.22)

C



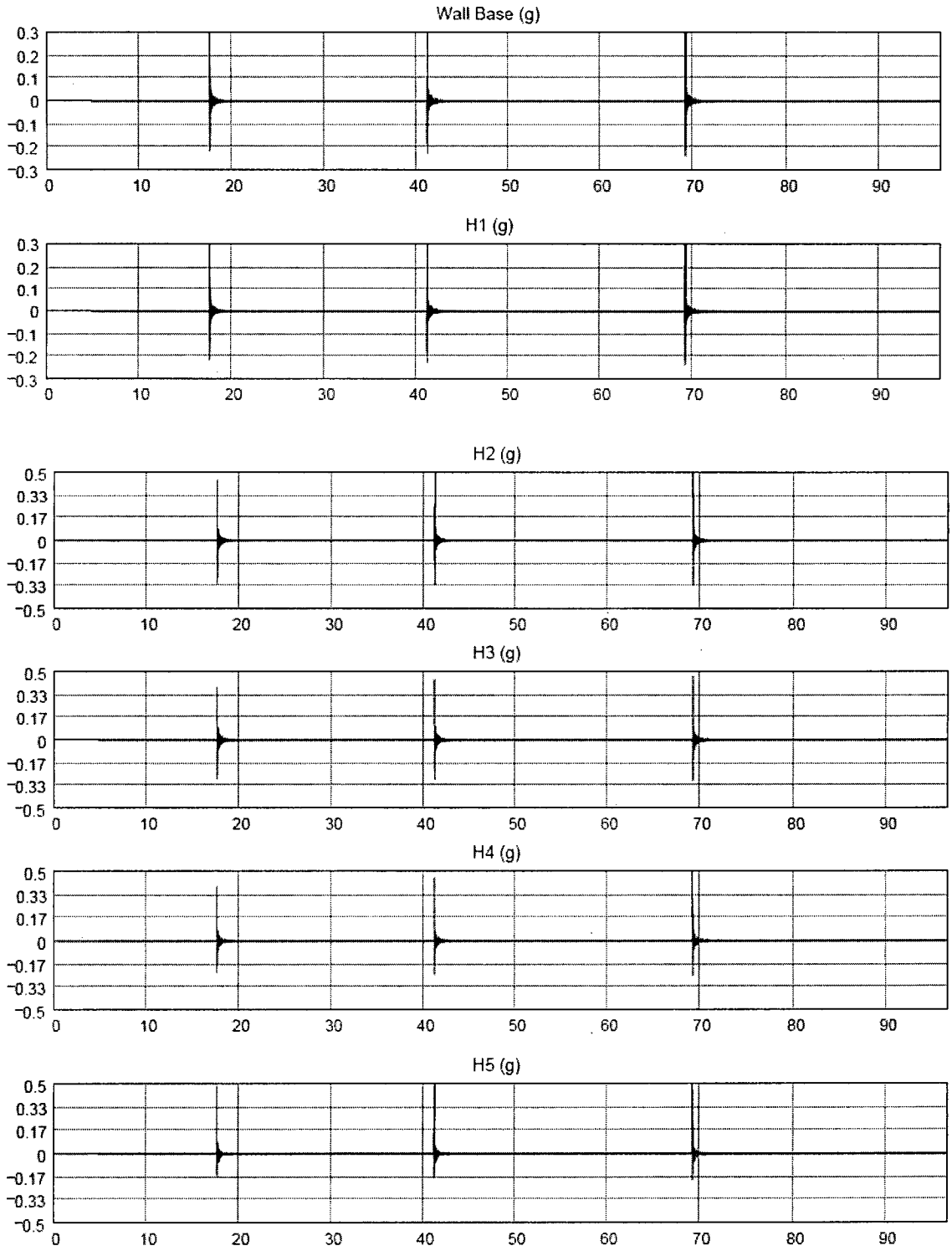


**Developed by C.E. Ventura** **Last Update: 16 April 04** **File: FD Analysis of Impact Records (Accels)**

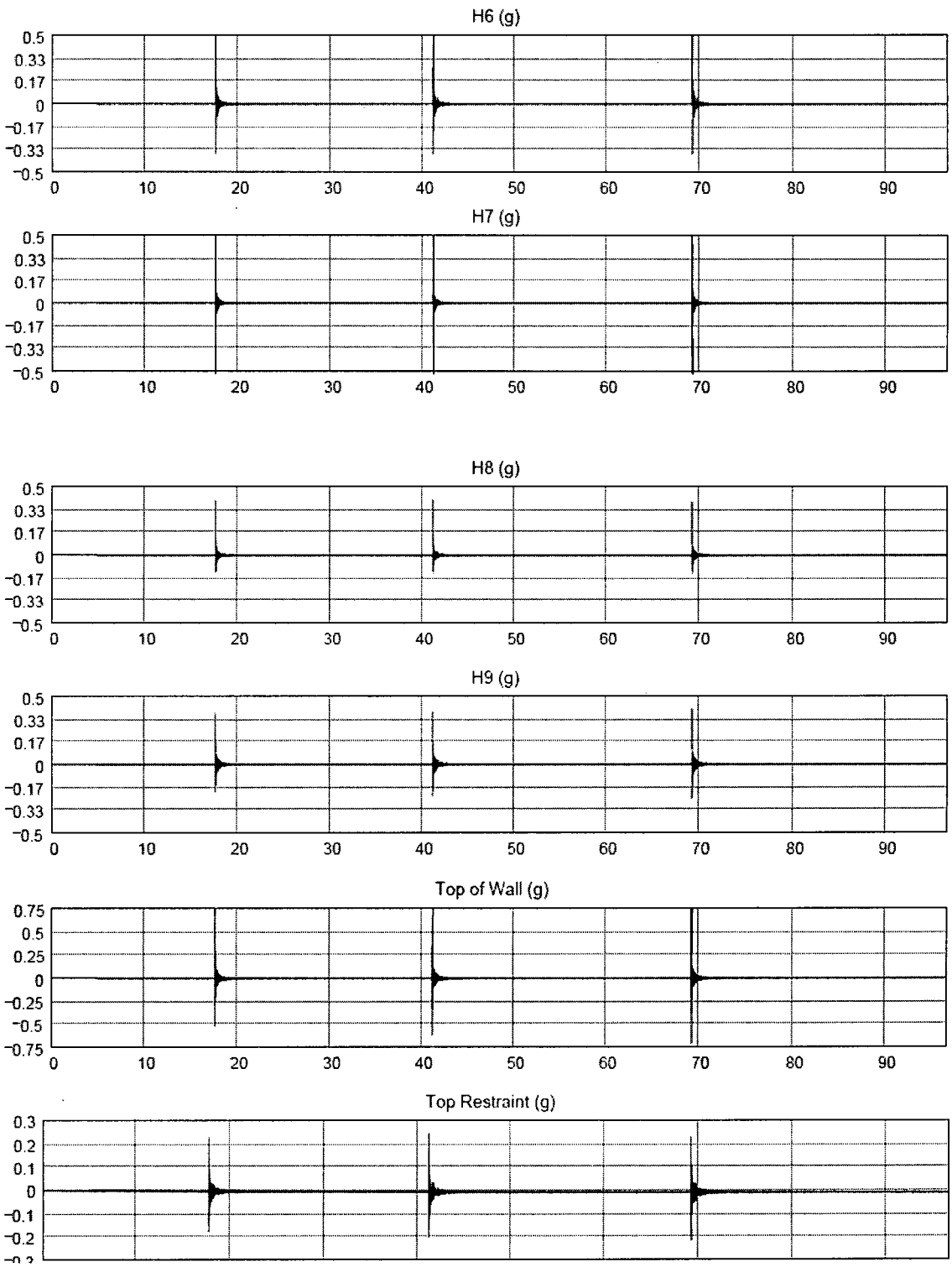
H6 (g)
H7 (g)
H8 (g)
H9 (g)
Top of Wall (g)
Top Restraint (g)

Store record and remove linear trends:

$H := \text{detrend}(\text{table}^{\langle 14 \rangle})$ $Hm := \max(|H|)$ $H4 := \text{detrend}(\text{table}^{\langle 7 \rangle})$ $H4m := \max(|H4|)$

$Table := \text{detrend}(\text{table}^{\langle 1 \rangle})$ $Tablem := \max(|Table|)$ $H5 := \text{detrend}(\text{table}^{\langle 8 \rangle})$ $H5m := \max(|H5|)$

$TopRest := \text{detrend}(\text{table}^{\langle 2 \rangle})$ $TopRestm := \max(|TopRest|)$ $H6 := \text{detrend}(\text{table}^{\langle 9 \rangle})$ $H6m := \max(|H6|)$

$Base := \text{detrend}(\text{table}^{\langle 3 \rangle})$ $Basem := \max(|Base|)$ $H7 := \text{detrend}(\text{table}^{\langle 10 \rangle})$ $H7m := \max(|H7|)$

$H1 := \text{detrend}(\text{table}^{\langle 4 \rangle})$ $H1m := \max(|H1|)$ $H8 := \text{detrend}(\text{table}^{\langle 11 \rangle})$ $H8m := \max(|H8|)$

$H2 := \text{detrend}(\text{table}^{\langle 5 \rangle})$ $H2m := \max(|H2|)$ $H9 := \text{detrend}(\text{table}^{\langle 12 \rangle})$ $H9m := \max(|H9|)$

$H3 := \text{detrend}(\text{table}^{\langle 6 \rangle})$ $H3m := \max(|H3|)$ $Top := \text{detrend}(\text{table}^{\langle 13 \rangle})$ $Topm := \max(|Top|)$

Compute Power Spectrum for each signal and display it:

No. of overlapping segments (>2): nos := 3 Overlapping factor (0<of<1): of := .1 Smooth factor: sm := 11

$PH := \text{movavg}(\text{pspectrum}(H, nos, of), sm)$ $PH5 := \text{movavg}(\text{pspectrum}(H5, nos, of), sm)$

$PBase := \text{movavg}(\text{pspectrum}(Base, nos, of), sm)$ $PH6 := \text{movavg}(\text{pspectrum}(H6, nos, of), sm)$

$PH1 := \text{movavg}(\text{pspectrum}(H1, nos, of), sm)$ $PH7 := \text{movavg}(\text{pspectrum}(H7, nos, of), sm)$

$PH2 := \text{movavg}(\text{pspectrum}(H2, nos, of), sm)$ $PH8 := \text{movavg}(\text{pspectrum}(H8, nos, of), sm)$

$PH3 := \text{movavg}(\text{pspectrum}(H3, nos, of), sm)$ $PH9 := \text{movavg}(\text{pspectrum}(H9, nos, of), sm)$

$PH4 := \text{movavg}(\text{pspectrum}(H4, nos, of), sm)$ $PTop := \text{movavg}(\text{pspectrum}(Top, nos, of), sm)$

$PTable := \text{movavg}(\text{pspectrum}(Table, nos, of), sm)$ $PTopRest := \text{movavg}(\text{pspectrum}(TopRest, nos, of), sm)$

$\text{length}(PH) = 17279$ $k := 0 .. 0.50 \cdot \text{length}(PH)$ $\Delta f := [(\text{length}(PH) - 1) \cdot \Delta]^{-1}$ $\Delta f = 0.0289$

Frequency Range to Display: Flow := 0 Fhigh := 50

DATA1 = "3-H6-HammerTestDataWallB"

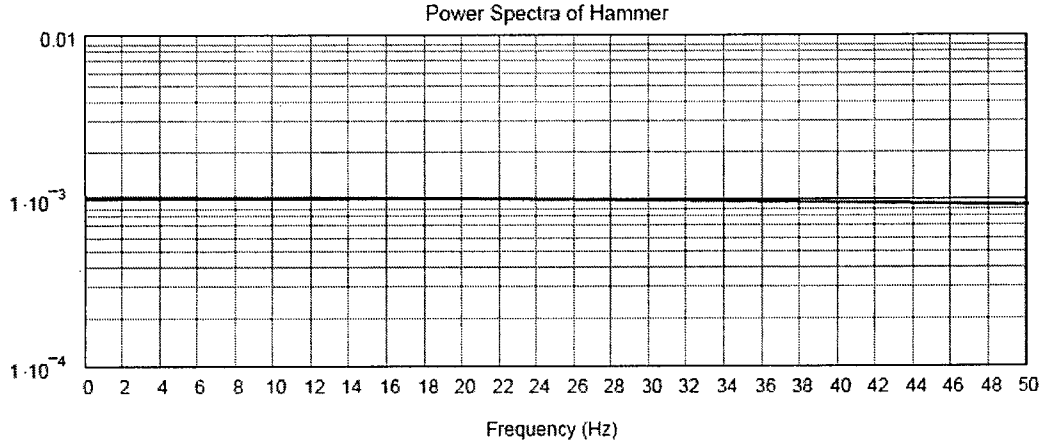


**Developed by C.E. Ventura** **Last Update: 16 April 04** **File: FD Analysis of Impact Records (Accels)**

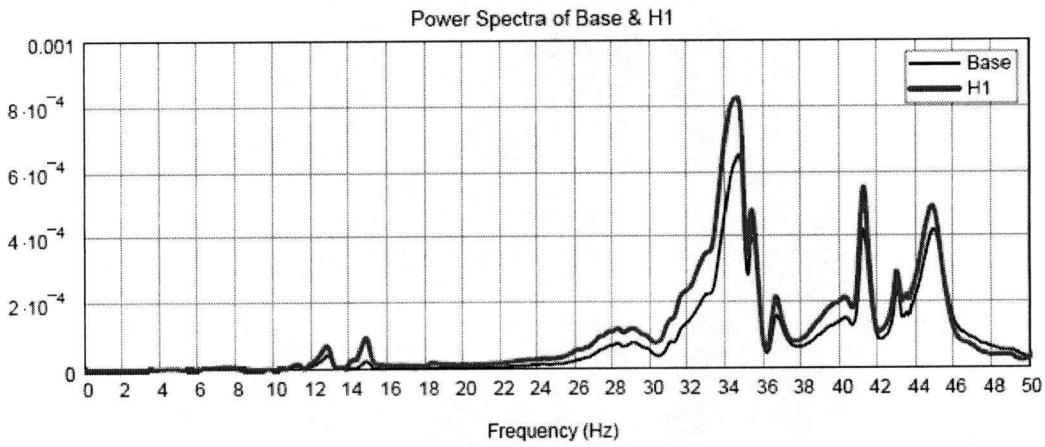


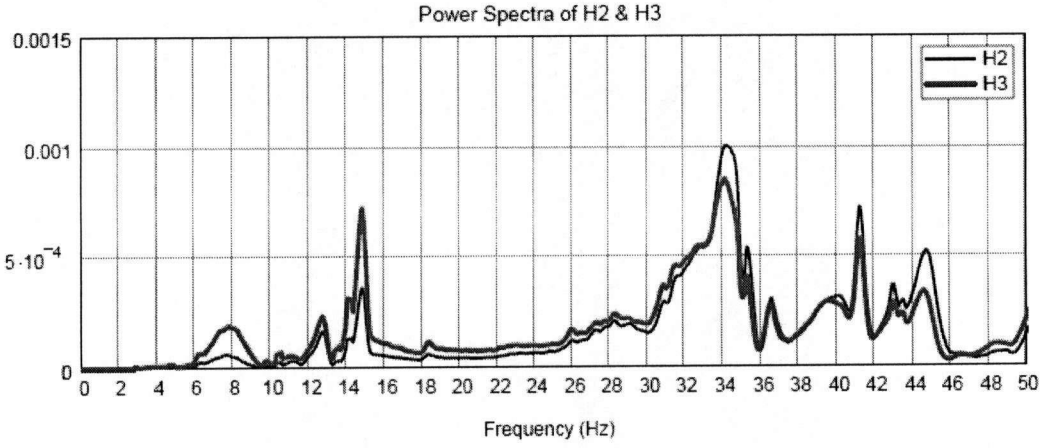


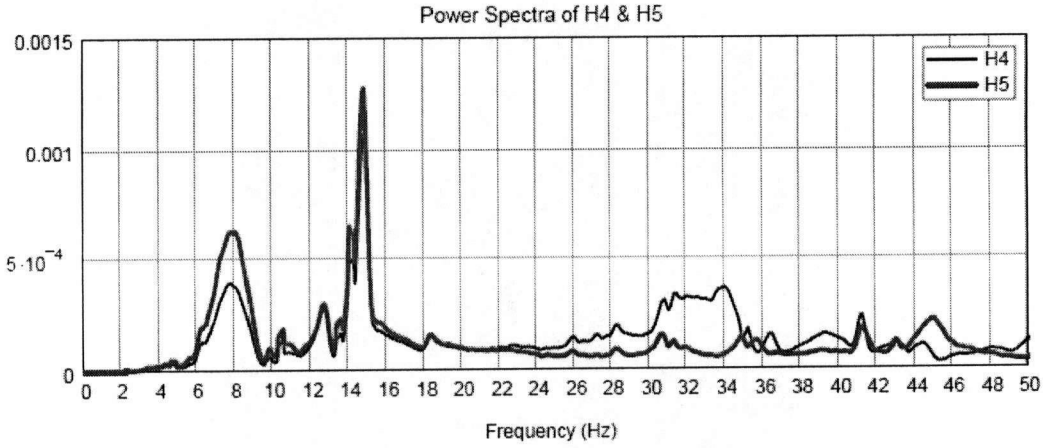


**Developed by C.E. Ventura** **Last Update: 16 April 04** **File: FD Analysis of Impact Records (Accels)**

D



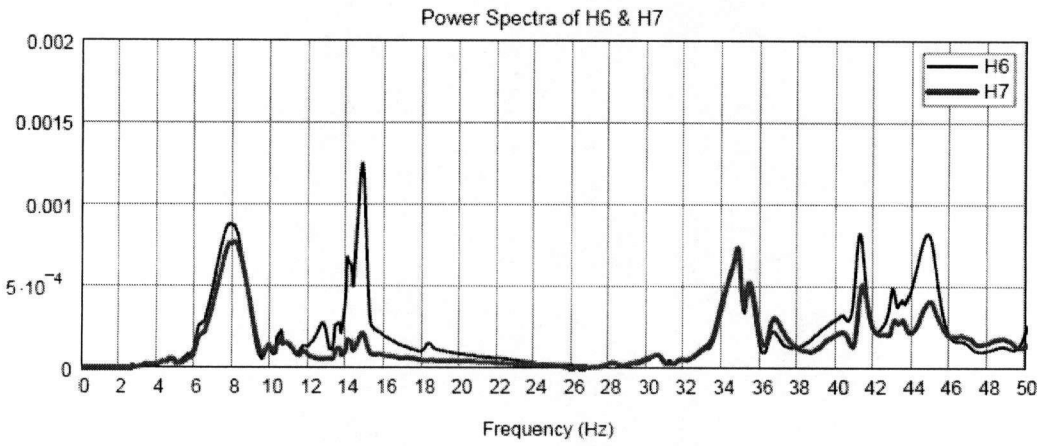


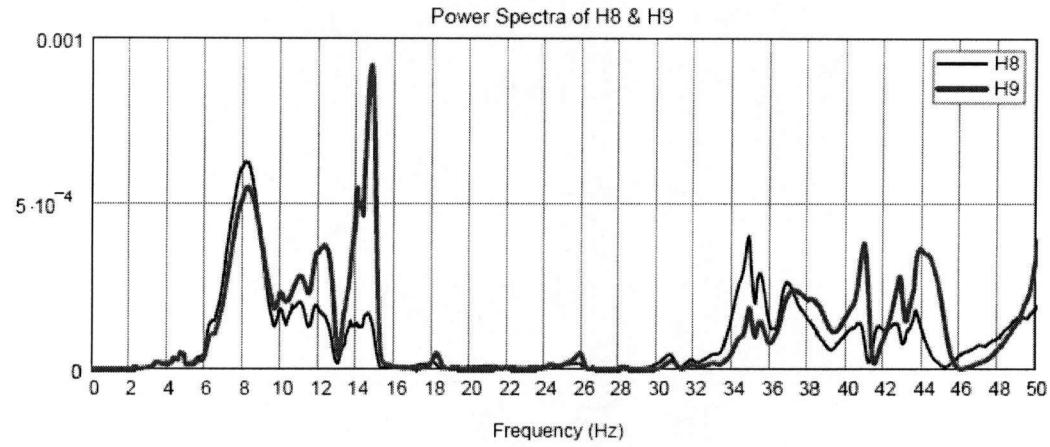


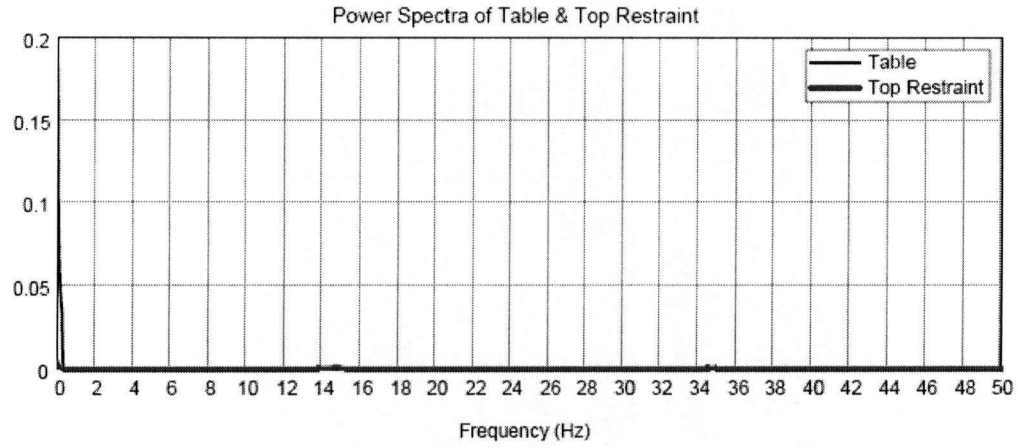


**Developed by C.E. Ventura** **Last Update: 16 April 04** **File: FD Analysis of Impact Records (Accels)**

Date: 2/5/2006 Page 7

**Compute FRF, Phase Angle, Coherence and Cross-Spectrum:** I := H O := H1 Ts := T

Reference:D:\Projects\UBC100 project\Shake Table tests\UBC 100 Hammer Tests\FD Spectral ratios-subroutine - ver 2.mcd(R)

length(FRF) = 17279 $j := 0 .. 0.50 \cdot \text{length}(FRF)$ $\Delta f := [(\text{length}(FRF) - 1) \cdot \Delta]^{-1}$ ==> $\Delta f = 0.0289$

FRF1 := FRF $\phi 1 := \phi$ CO1 := CO O := H2

Reference:D:\Projects\UBC100 project\Shake Table tests\UBC 100 Hammer Tests\FD Spectral ratios-subroutine - ver 2.mcd(R)

FRF2 := FRF $\phi 2 := \phi$ CO2 := CO O := H3

Reference:D:\Projects\UBC100 project\Shake Table tests\UBC 100 Hammer Tests\FD Spectral ratios-subroutine - ver 2.mcd(R)

FRF3 := FRF $\phi 3 := \phi$ CO3 := CO O := H4

Reference:D:\Projects\UBC100 project\Shake Table tests\UBC 100 Hammer Tests\FD Spectral ratios-subroutine - ver 2.mcd(R)

FRF4 := FRF $\phi 4 := \phi$ CO4 := CO O := H5

Reference:D:\Projects\UBC100 project\Shake Table tests\UBC 100 Hammer Tests\FD Spectral ratios-subroutine - ver 2.mcd(R)

FRF5 := FRF $\phi 5 := \phi$ CO5 := CO O := H6

Reference:D:\Projects\UBC100 project\Shake Table tests\UBC 100 Hammer Tests\FD Spectral ratios-subroutine - ver 2.mcd(R)

FRF6 := FRF $\phi 6 := \phi$ CO6 := CO O := H7

Reference:D:\Projects\UBC100 project\Shake Table tests\UBC 100 Hammer Tests\FD Spectral ratios-subroutine - ver 2.mcd(R)

FRF7 := FRF $\phi 7 := \phi$ CO7 := CO O := H8

Reference:D:\Projects\UBC100 project\Shake Table tests\UBC 100 Hammer Tests\FD Spectral ratios-subroutine - ver 2.mcd(R)

FRF8 := FRF $\phi 8 := \phi$ CO8 := CO O := H9

Reference:D:\Projects\UBC100 project\Shake Table tests\UBC 100 Hammer Tests\FD Spectral ratios-subroutine - ver 2.mcd(R)

FRF9 := FRF $\phi 9 := \phi$ CO9 := CO O := Base

Reference:D:\Projects\UBC100 project\Shake Table tests\UBC 100 Hammer Tests\FD Spectral ratios-subroutine - ver 2.mcd(R)

FRFBase := FRF $\phi Base := \phi$ COBase := CO O := Table

Reference:D:\Projects\UBC100 project\Shake Table tests\UBC 100 Hammer Tests\FD Spectral ratios-subroutine - ver 2.mcd(R)

FRFTable := FRF $\phi Table := \phi$ COTable := CO O := Top

Reference:D:\Projects\UBC100 project\Shake Table tests\UBC 100 Hammer Tests\FD Spectral ratios-subroutine - ver 2.mcd(R)

FRFTop := FRF $\phi Top := \phi$ COTop := CO O := TopRest

Reference:D:\Projects\UBC100 project\Shake Table tests\UBC 100 Hammer Tests\FD Spectral ratios-subroutine - ver 2.mcd(R)

FRFTR := FRF $\phi TopRest := \phi$ COTR := CO

**Developed by C.E. Ventura** **Last Update: 16 April 04** **File: FD Analysis of Impact Records (Accels)**

Date: 2/5/2006 Page 8

**RESULTS FOR ANALYSIS OF DATA FOR:** DTA = "Wall B, Test 3, Hammer H6"
from dataset: DATA1 = "3-H6-HammerTestDataWallB"

Frequency range (in Hz) to be displayed (F0=minimum, FH=maximum): F0 = 0 FH = 50

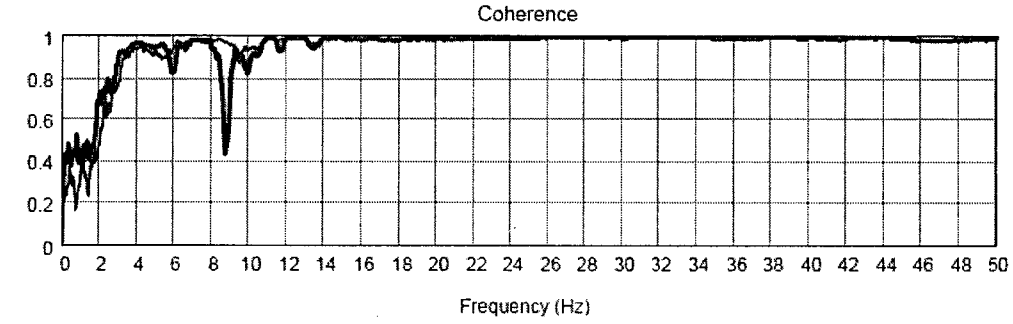


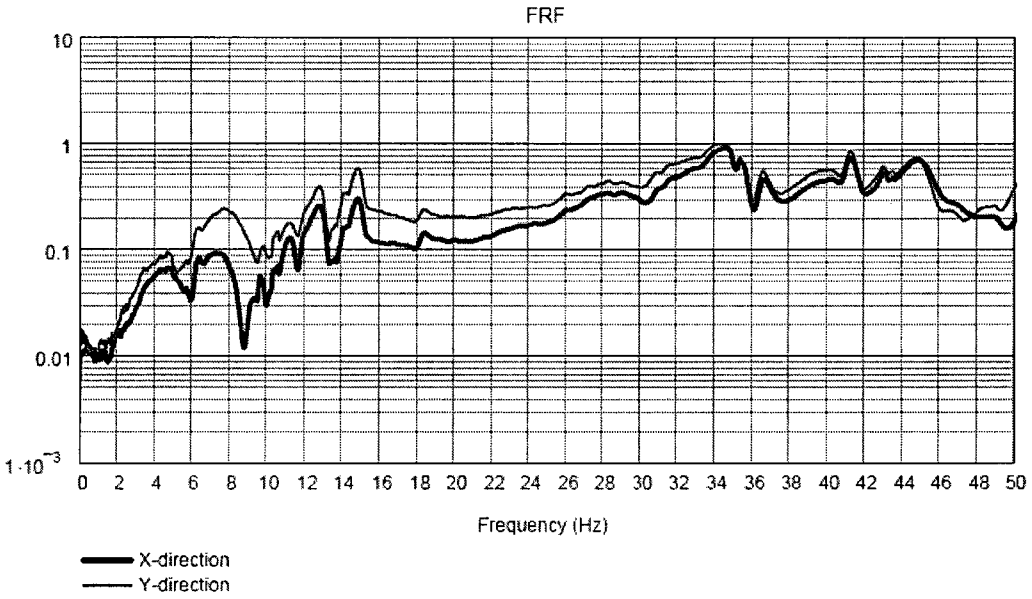

Date: 2/5/2006 Page 9

Frequency range (in Hz) to be displayed (F0=minimum, FH=maximum): F0 := 1 FH := 26

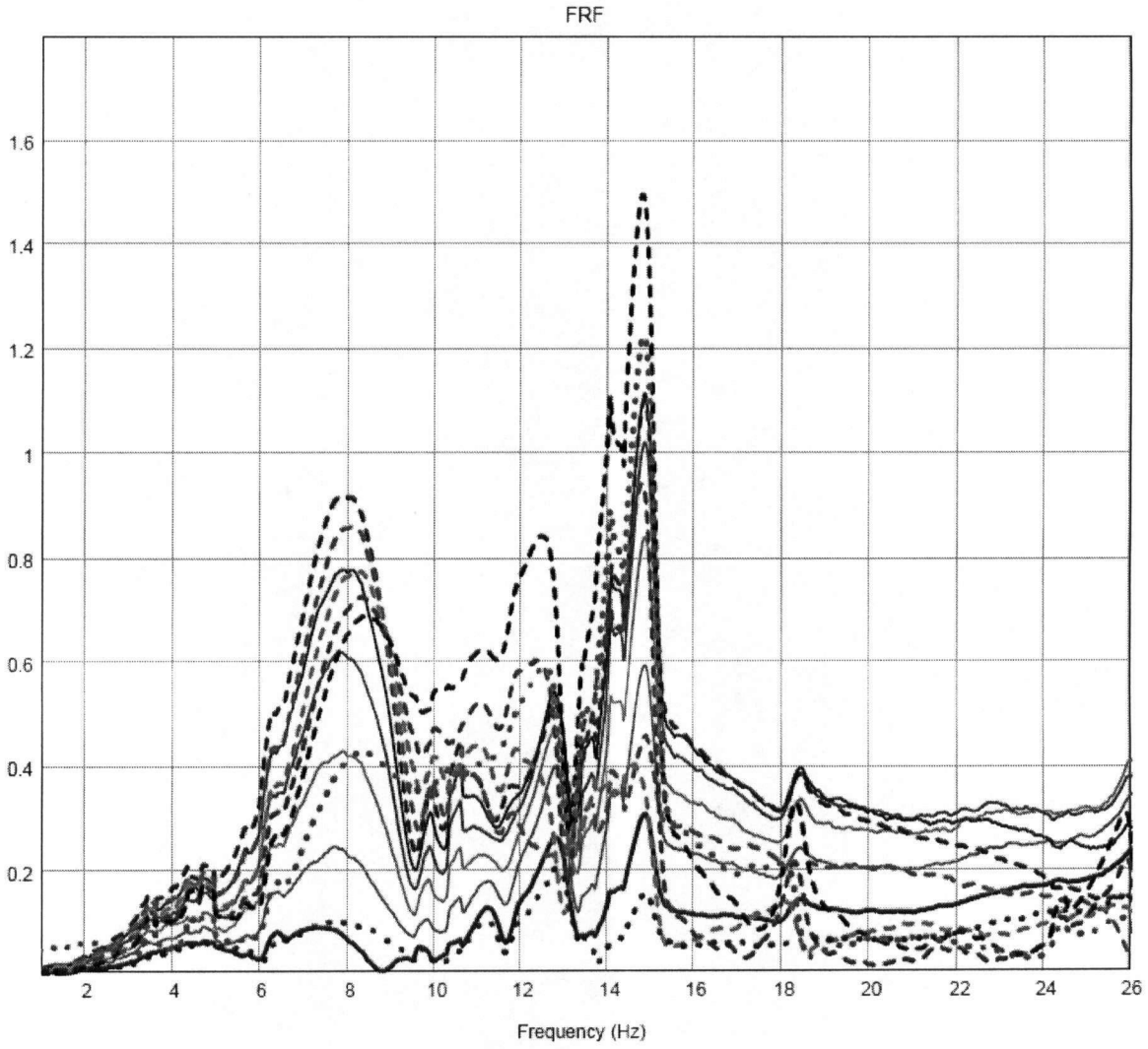


**Developed by C.E. Ventura** **Last Update: 16 April 04** **File: FD Analysis of Impact Records (Accels)**

# APPENDIX G. SHAKE TABLE TEST RESULTS

# G.1 Wall GC

## G.1.1 Test GC1-0.71*

| | | | | | | | | | |
|---|---|---|---|---|---|---|---|---|---|
| **Wall:** | Good Quality Collar Joint | **Test Sequence:** | 1 | | | **Test Number:** | GC1-0.71 | | |
| **Earthquake Record:** | Gilroy | **Scale:** | 0.71* | **Site Class:** | C | **PGA:** | 0.34g | **PGD:** | 1.91cm |
| **Wall Condition:** | No visible damage | | | | | | | | |
| **Height:** | 4133mm | **Thickness:** | 353mm | **h/t:** | 11.7 | **Width:** | 1501mm | **Density:** | 2024kg/m$^3$ |
| **Header Location:** | | **H3:** | 1368mm | **H6:** | 2744mm | **H8:** | 3655mm | | |

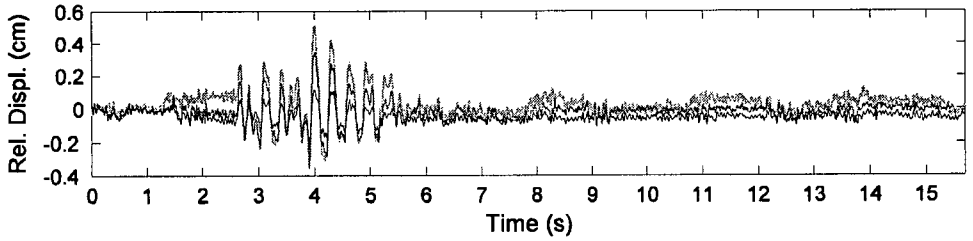


**Relative Displacement Time History (..... H8, — H6, — H3)**

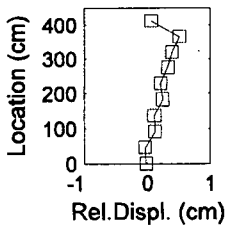


**Profile (t = 4.0s)**

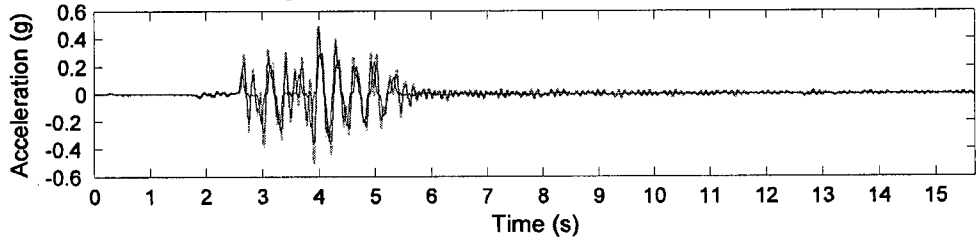


**Acceleration Time History (..... H8, — H6, — H3)**

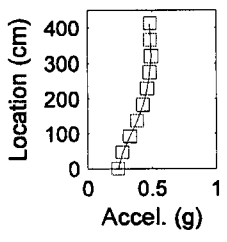


**Profile (t = 4.0s)**

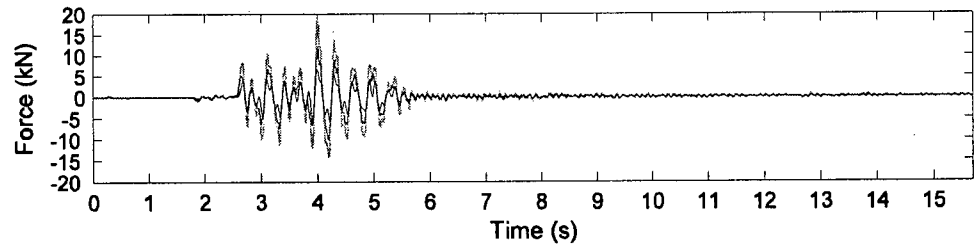


**Force Time History (..... Total, — Lower, — Upper)**

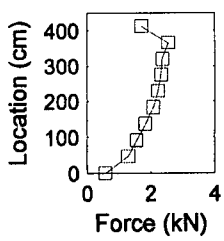


**Profile (t = 4.0s)**

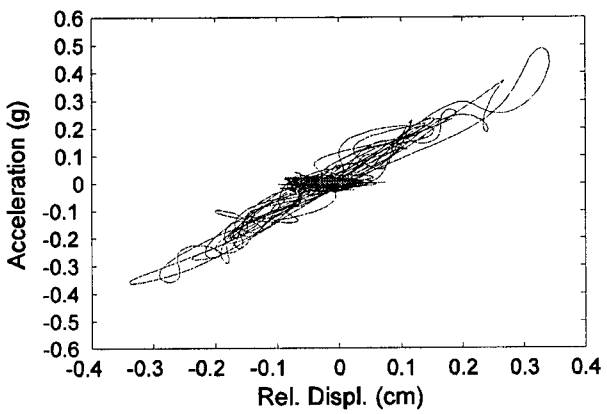


**Crack Acceleration vs. Relative Crack Displacement**

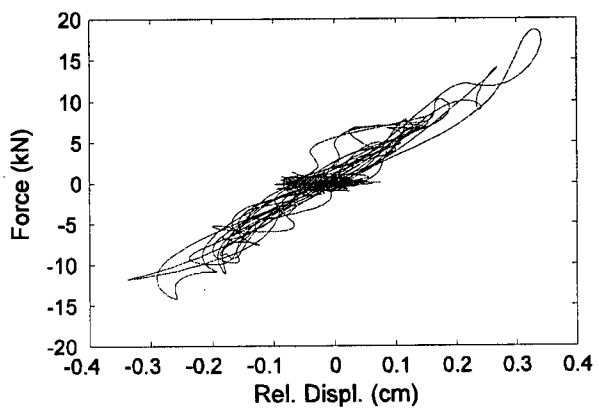


**Total Force vs. Relative Crack Displacement**

| | | | |
|---|---|---|---|
| **Initial Period:** | 0.095s | **Initial Stiffness:** | 44.3kN/cm |

* Scaled to PGA

## G.1.2 Wall GC2-1.32*

| | | | | | | | | | |
|---|---|---|---|---|---|---|---|---|---|
| **Wall:** | Good Quality Collar Joint | **Test Sequence:** | 2 | | | **Test Number:** | GC2-1.32 | | |
| **Earthquake Record:** | Gilroy | **Scale:** | 1.32* | **Site Class:** | C | **PGA:** | 0.63g | **PGD:** | 3.90cm |
| **Wall Condition:** | Crack formed at H6 | | | | | | | | |
| **Height:** | 4133mm | **Thickness:** | 353mm | **h/t:** | 11.7 | **Width:** | 1501mm | **Density:** | 2024kg/m$^3$ |
| **Header Location:** | | **H3:** | 1368mm | **H6:** | 2744mm | **H8:** | 3655mm | | |

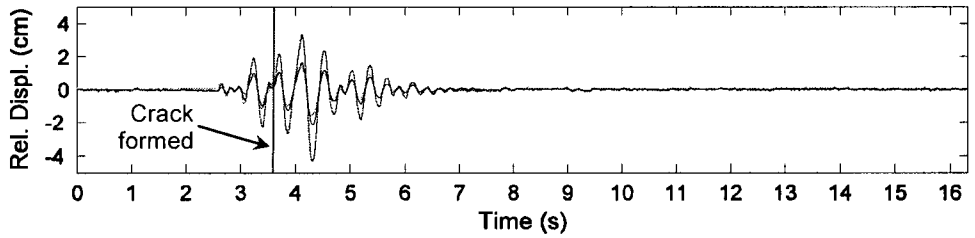


**Relative Displacement Time History (···· H8, —— H6, — H3)**

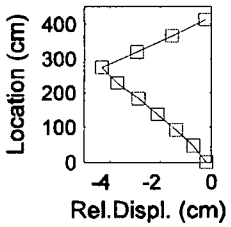


**Profile (t = 4.0s)**

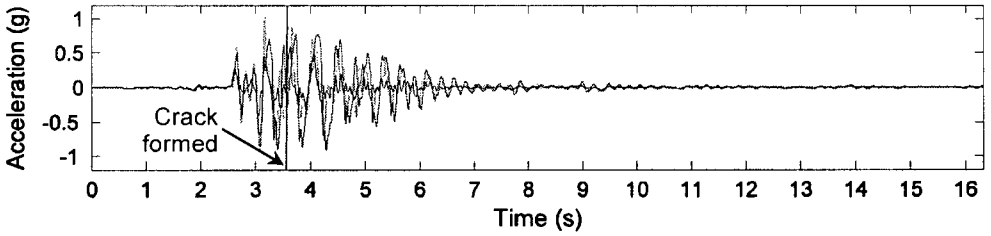


**Acceleration Time History (···· H8, —— H6, — H3)**

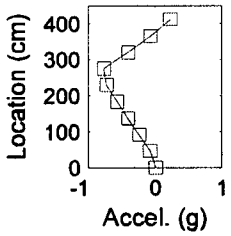


**Profile (t = 4.0s)**

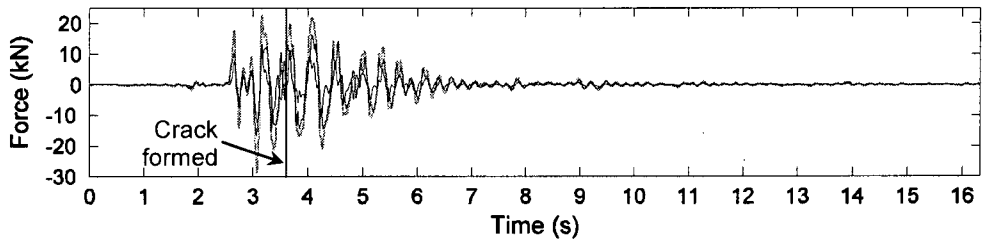


**Force Time History (···· Total, —— Lower, — Upper)**

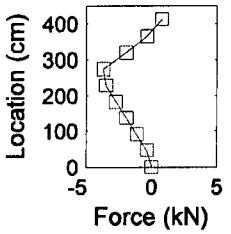


**Profile (t = 4.0s)**

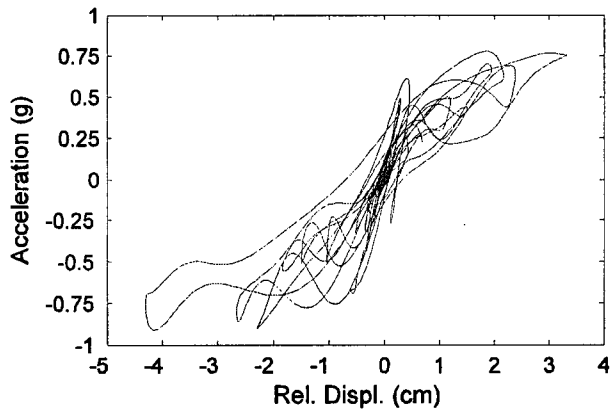


**Crack Acceleration vs. Relative Crack Displacement**

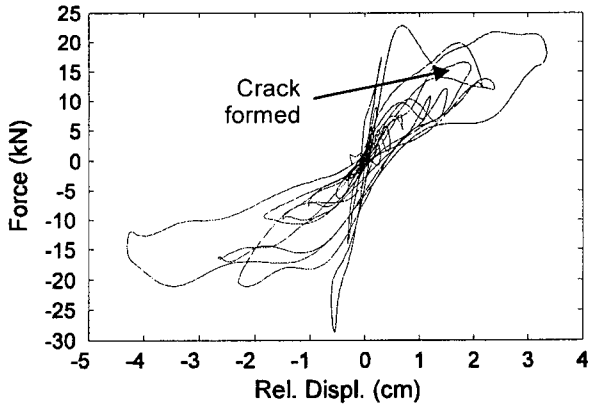


**Total Force vs. Relative Crack Displacement**

| | | | |
|---|---|---|---|
| **Initial Period:** | 0.15s | **Initial Stiffness:** | 46.4kN/cm |

* Scaled to PGA

## G.1.3 Test GC3-0.64

| | | | | | | | | | |
|---|---|---|---|---|---|---|---|---|---|
| **Wall:** | Good Quality Collar Joint | | **Test Sequence:** | 3 | | **Test Number:** | GC3-0.64 | | |
| **Earthquake Record:** | Gilroy | | **Scale:** | 0.64 | **Site Class:** | C | **PGA:** | 0.71g | **PGD:** 4.96cm |
| **Wall Condition:** | Crack at H6 | | | | | | | | |
| **Height:** | 4133mm | **Thickness:** | 353mm | **h/t:** | 11.7 | **Width:** | 1501mm | **Density:** | 2024kg/m$^3$ |
| **Header Location:** | | **H3:** | 1368mm | **H6:** | 2744mm | **H8:** | 3655mm | | |

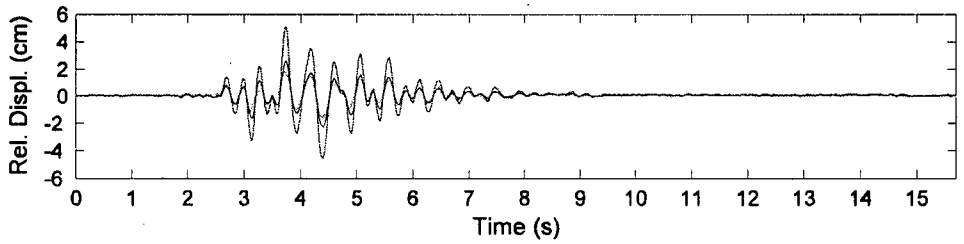


**Relative Displacement Time History (····· H8, —— H6, —— H3)**

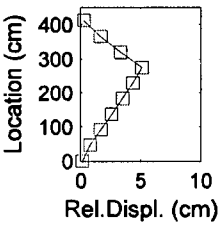


**Profile (t = 3.74s)**

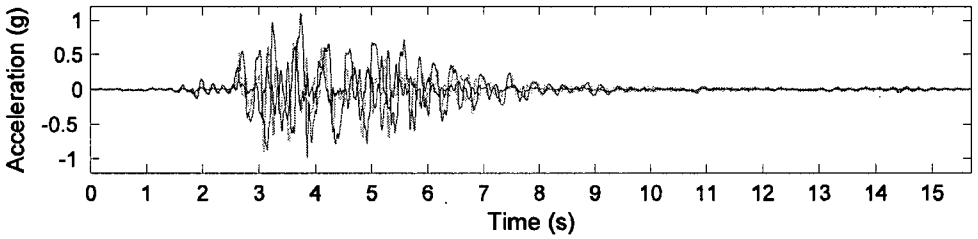


**Acceleration Time History (····· H8, —— H6, —— H3)**

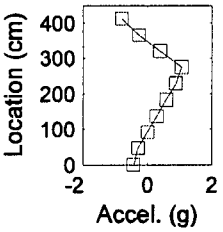


**Profile (t = 3.74s)**

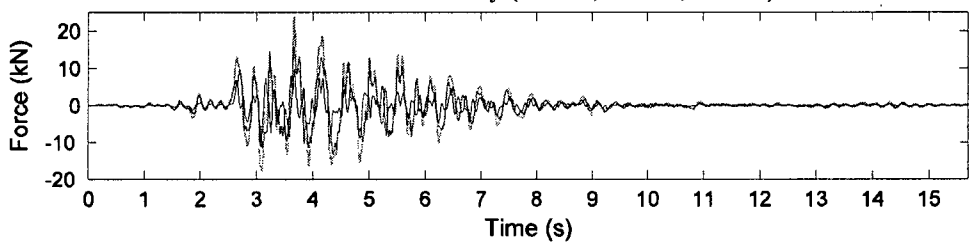


**Force Time History (····· Total, —— Lower, —— Upper)**

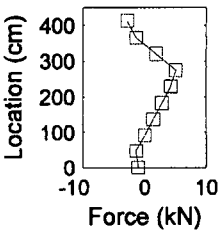


**Profile (t = 3.74s)**

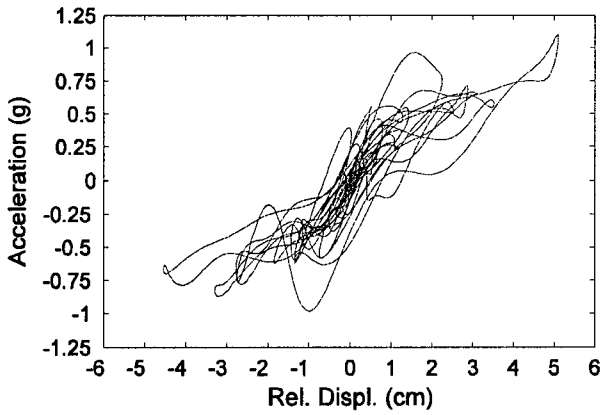


**Crack Acceleration vs. Relative Crack Displacement**

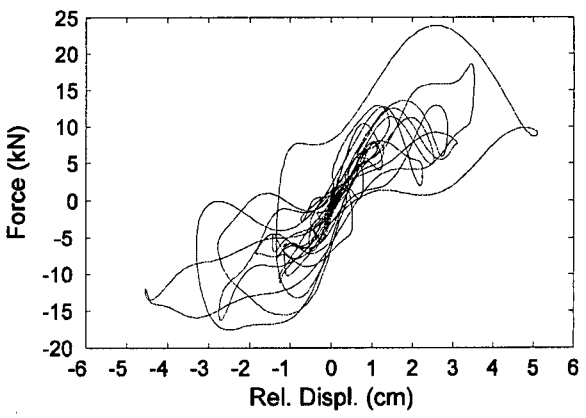


**Total Force vs. Relative Crack Displacement**

| | | | |
|---|---|---|---|
| **Initial Period:** | 0.18s | **Initial Stiffness:** | 10.274kN/cm |

## G.1.4 Test GC4-1.21

| | | | | | | | | | |
|---|---|---|---|---|---|---|---|---|---|
| **Wall:** | Good Quality Collar Joint | | **Test Sequence:** | 4 | | **Test Number:** | GC4-1.21 | | |
| **Earthquake Record:** | Gilroy | | **Scale:** | 1.21 | **Site Class:** | C | **PGA:** | 1.18g | **PGD:** 9.42cm |
| **Wall Condition:** | Crack at H6 | | | | | | | | |
| **Height:** | 4133mm | **Thickness:** | 353mm | **h/t:** | 11.7 | **Width:** | 1501mm | **Density:** | 2024kg/m$^3$ |
| **Header Location:** | **H3:** | 1368mm | **H6:** | 2744mm | **H8:** | 3655mm | | | |

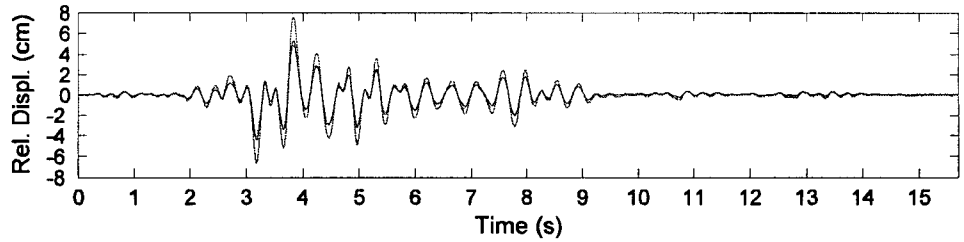


**Relative Displacement Time History (..... H7, ---- H6, — H4)**

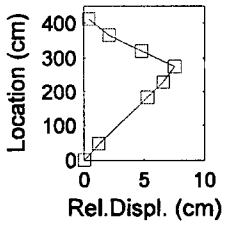


**Profile (t = 3.83s)**

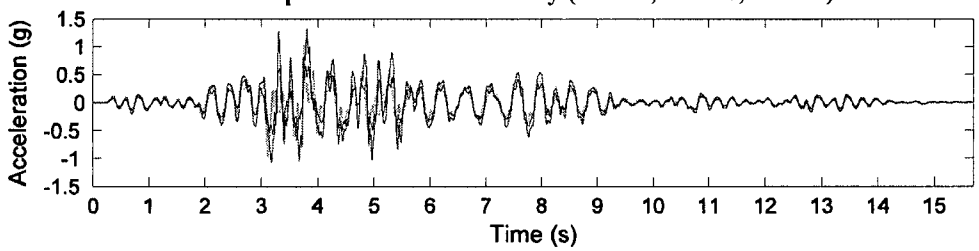


**Acceleration Time History (..... H7, ---- H6, — H4)**

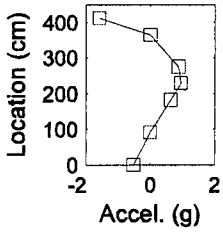


**Profile (t = 3.83s)**

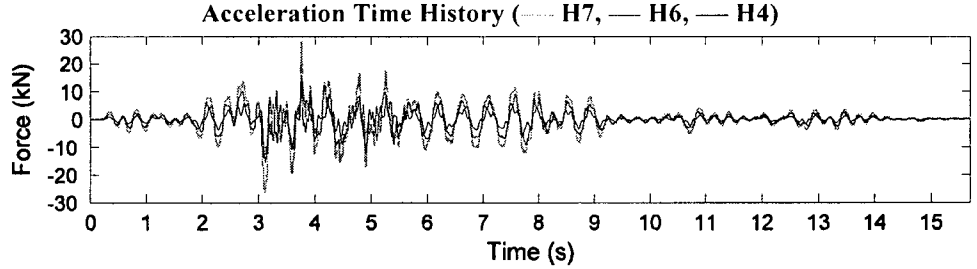


**Force Time History (..... Total, ---- Lower, — Upper)**

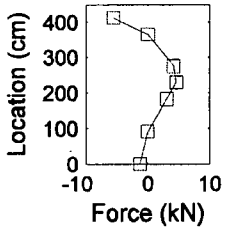


**Profile (t = 3.83s)**

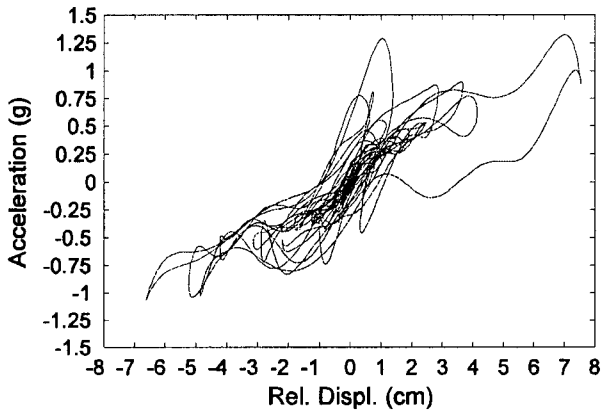


**Crack Acceleration vs. Relative Crack Displacement**

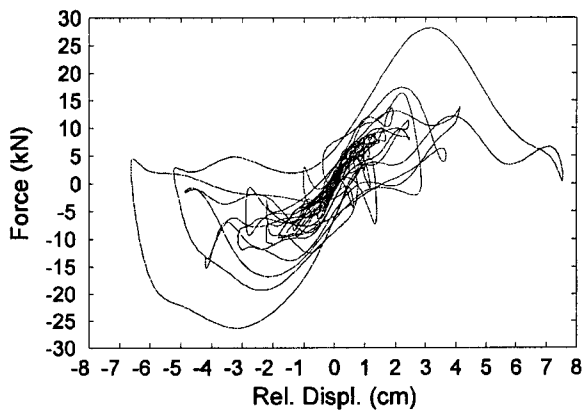


**Total Force vs. Relative Crack Displacement**

| | | | |
|---|---|---|---|
| **Initial Period:** | 0.21s | **Initial Stiffness:** | 11.47kN/cm |

## G.1.5 Test GC5-1.49

| | | | | | | | | | |
|---|---|---|---|---|---|---|---|---|---|
| **Wall:** | Good Quality Collar Joint | | **Test Sequence:** | 5 | | **Test Number:** | GC5-1.49 | | |
| **Earthquake Record:** | Gilroy | | **Scale:** | 1.49 | **Site Class:** | C | **PGA:** | 1.15g | **PGD:** 11.6cm |
| **Wall Condition:** | Crack at H6, *Bearing at top* | | | | | | | | |
| **Height:** | 4133mm | **Thickness:** | 353mm | **h/t:** | 11.7 | **Width:** | 1501mm | **Density:** | 2024kg/m$^3$ |
| **Header Location:** | | **H3:** | 1368mm | **H6:** | 2744mm | **H8:** | 3655mm | | |

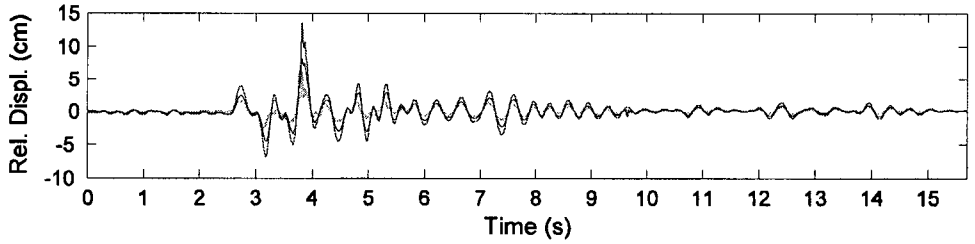


**Relative Displacement Time History (..... H4, ..... H6, — H8)**

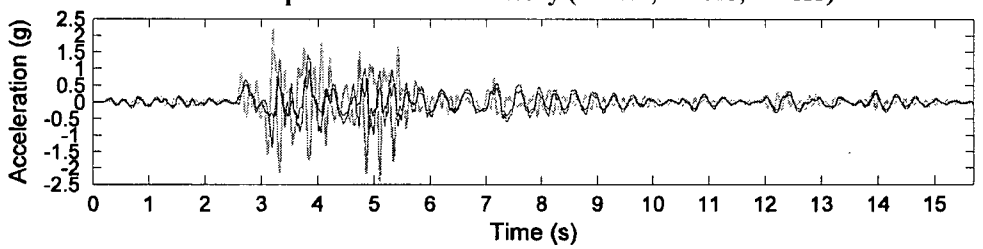


**Acceleration Time History (..... H9, — H6, — H4)**

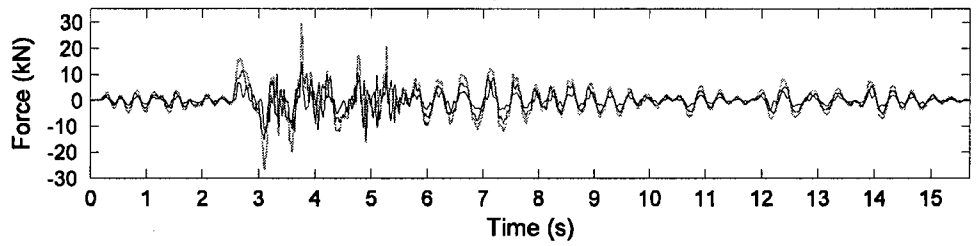


**Force Time History (..... Total, — Lower, — Upper)**

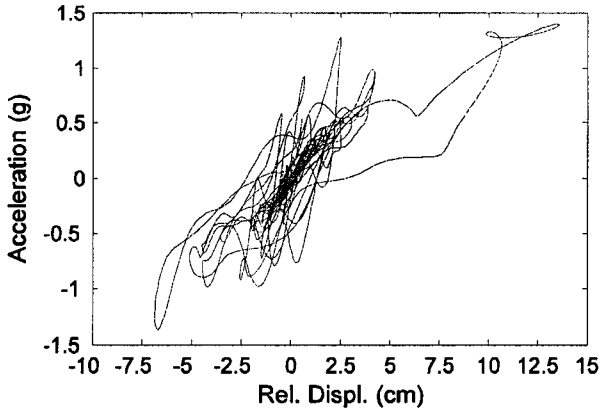


**Crack Acceleration vs. Relative Crack Displacement**

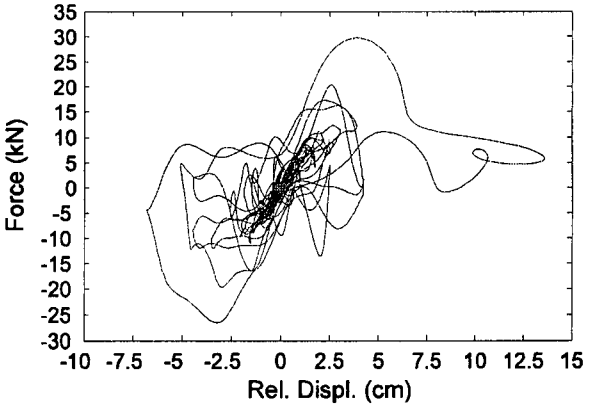


**Total Force vs. Relative Crack Displacement**

## G.1.6 Test GC6-1.57

| | | | | | | | | | |
|---|---|---|---|---|---|---|---|---|---|
| **Wall:** | Good Quality Collar Joint | **Test Sequence:** | 6 | | | **Test Number:** | GC6-1.57 | | |
| **Earthquake Record:** | Gilroy | **Scale:** | 1.57 | **Site Class:** | C | **PGA:** | 1.13g | **PGD:** | 14.3cm |
| **Wall Condition:** | Crack at H6, *Bearing at top* | | | | | | | | |
| **Height:** | 4133mm | **Thickness:** | 353mm | **h/t:** | 11.7 | **Width:** | 1501mm | **Density:** | 2024kg/m$^3$ |
| **Header Location:** | | **H3:** | 1368mm | **H6:** | 2744mm | **H8:** | 3655mm | | |

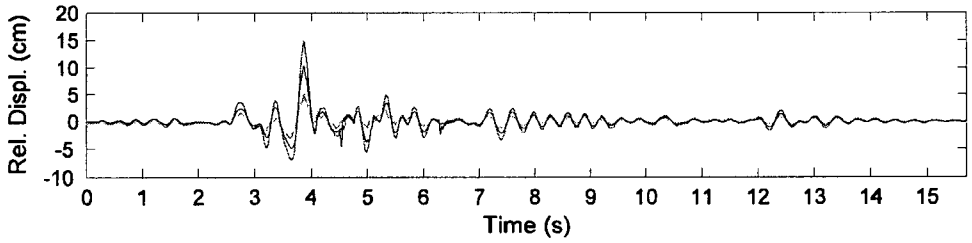


**Relative Displacement Time History (..... H4, ..... H6, — H8)**

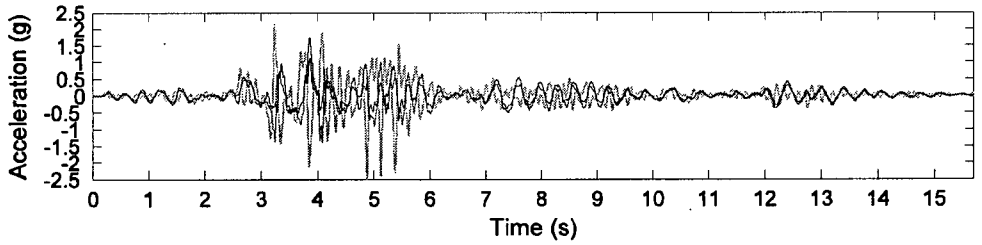


**Acceleration Time History (..... H9, — H6, — H4)**

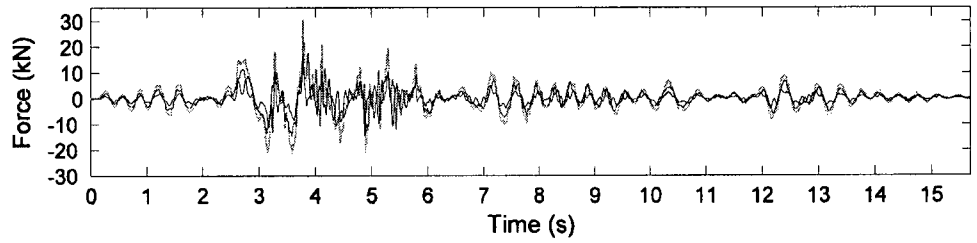


**Force Time History (..... Total, ..... Lower, — Upper)**

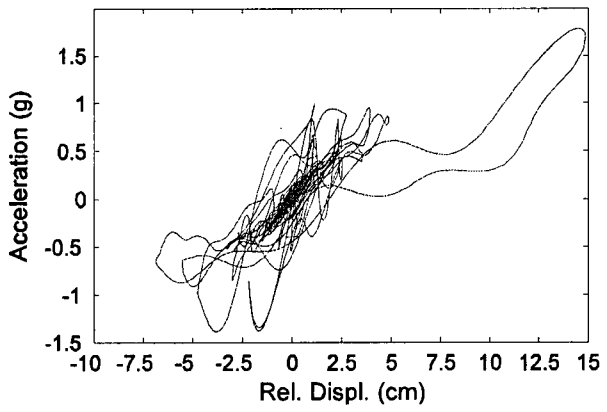


**Crack Acceleration vs. Relative Crack Displacement**

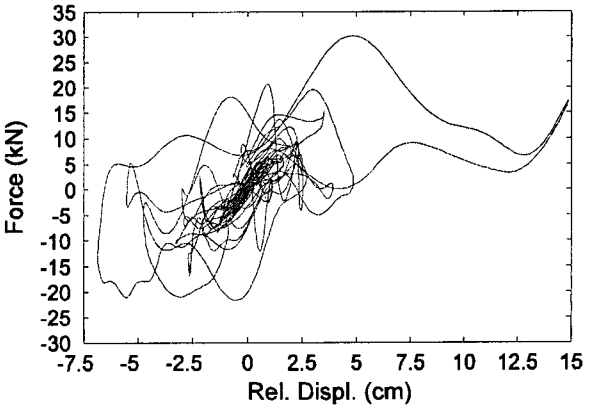


**Total Force vs. Relative Crack Displacement**

## G.1.7 Test GC7-1.61

| | | | | | | | | | |
|---|---|---|---|---|---|---|---|---|---|
| **Wall:** | Good Quality Collar Joint | | **Test Sequence:** | 7 | | **Test Number:** | GC7-1.61 | | |
| **Earthquake Record:** | Gilroy | | **Scale:** | 1.61 | **Site Class:** | C | **PGA:** | 1.21g | **PGD:** 14.3cm |
| **Wall Condition:** | Crack at H6, *Bearing at top* | | | | | | | | |
| **Height:** | 4133mm | **Thickness:** | 353mm | **h/t:** | 11.7 | **Width:** | 1501mm | **Density:** | 2024kg/m$^3$ |
| **Header Location:** | | **H3:** | 1368mm | **H6:** | 2744mm | **H8:** | 3655mm | | |

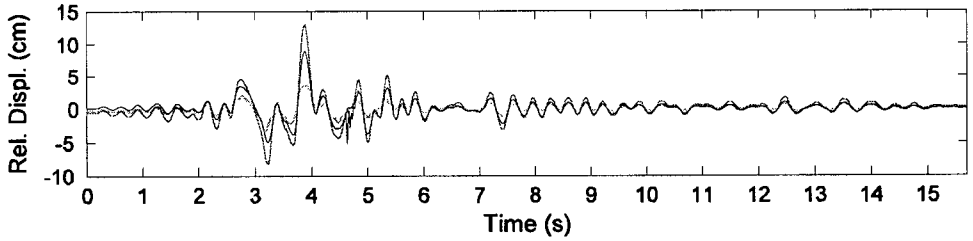


**Relative Displacement Time History (..... H4, — H6, — H8)**

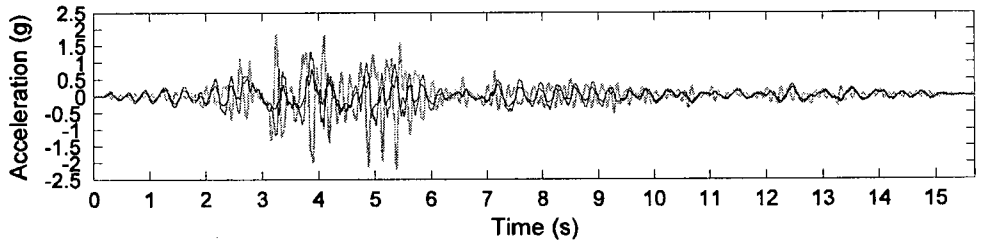


**Acceleration Time History (..... H9, — H6, — H4)**

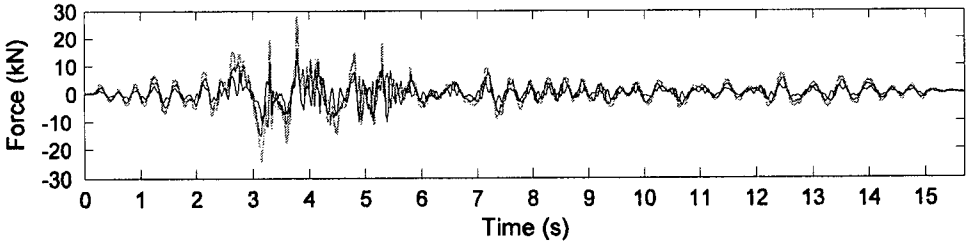


**Force Time History (..... Total, — Lower, — Upper)**

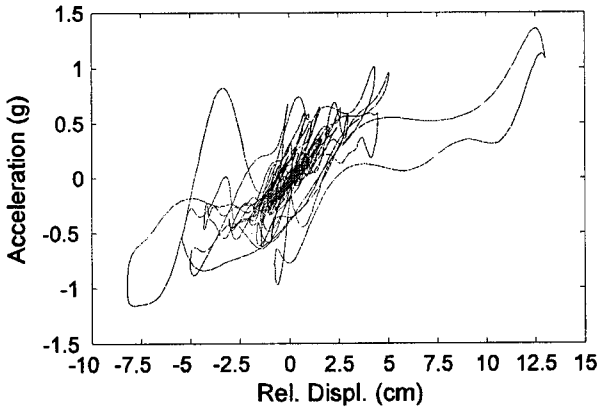


**Crack Acceleration vs. Relative Crack Displacement**

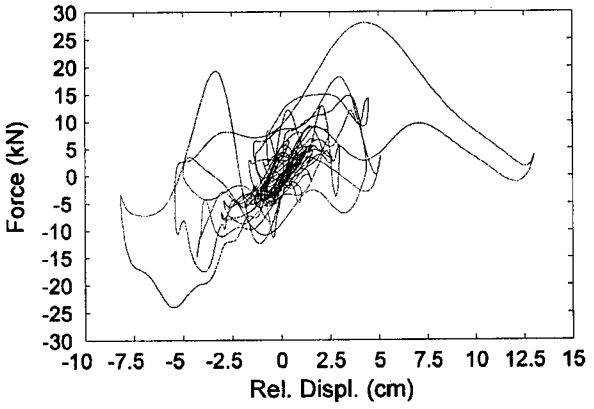


**Total Force vs. Relative Crack Displacement**

## G.2 Wall PC

### G.2.1 Test PC1-0.73*

| | | | | | | | | | |
|---|---|---|---|---|---|---|---|---|---|
| **Wall:** | Poor Quality Collar Joint | **Test Sequence:** | 1 | | | **Test Number:** | PC1-0.73 | | |
| **Earthquake Record:** | Gilroy | **Scale:** | 0.73* | **Site Class:** | C | **PGA:** | 0.35g | **PGD:** | 1.89cm |
| **Wall Condition:** | No visible damage | | | | | | | | |
| **Height:** | 4153mm | **Thickness:** | 355mm | **h/t:** | 11.7 | **Width:** | 1498mm | **Density:** | 1764.5kg/m$^3$ |
| **Header Location:** | | **H3:** | 1317mm | **H6:** | 2682mm | **H8:** | 3586mm | | |

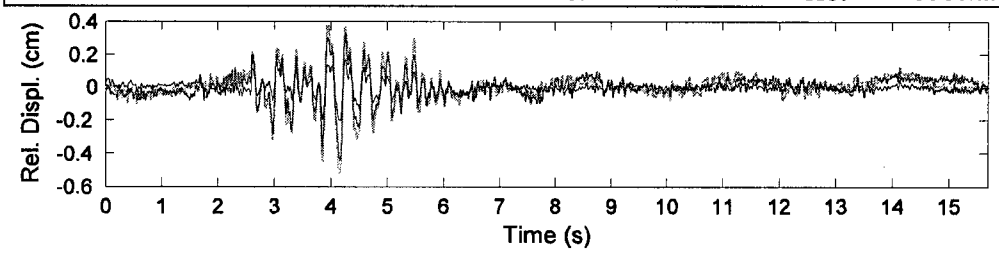


**Relative Displacement Time History (..... H8, ---- H6, — H3)**

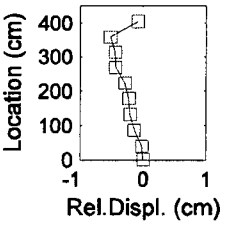


**Profile (t = 4.162)**

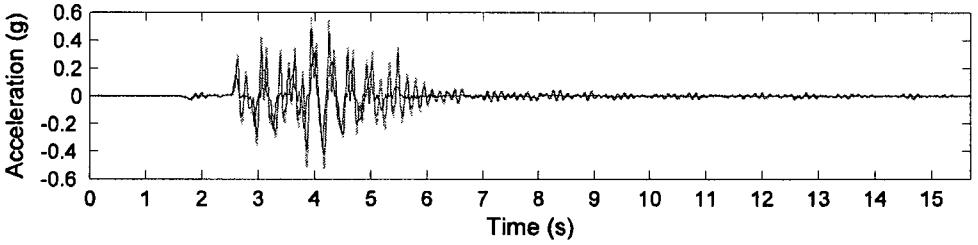


**Acceleration Time History (..... H8, ---- H6, — H3)**

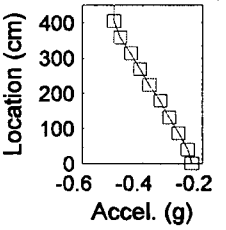


**Profile (t = 4.162)**

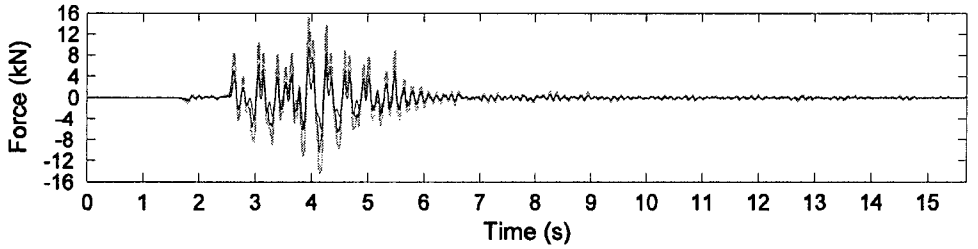


**Force Time History (..... Total, ---- Lower, — Upper)**

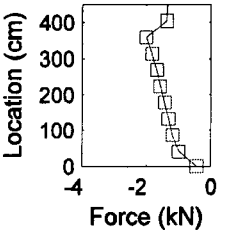


**Profile (t = 4.162)**

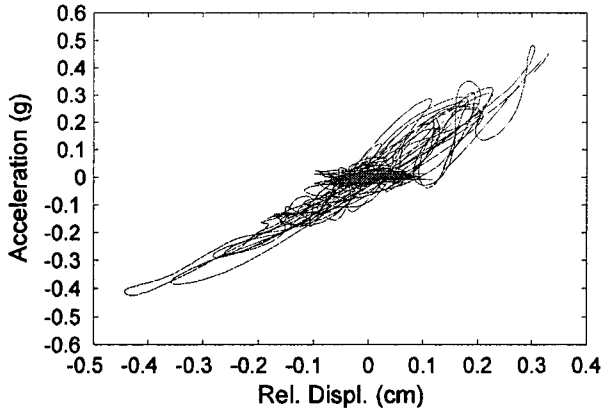


**Crack Acceleration vs. Relative Crack Displacement**

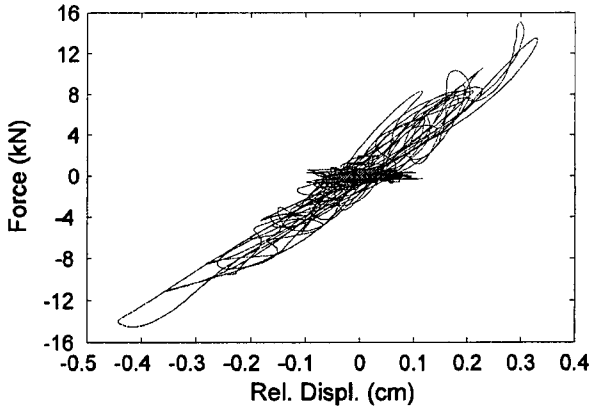


**Total Force vs. Relative Crack Displacement**

| | | | |
|---|---|---|---|
| **Initial Period:** | 0.11s | **Initial Stiffness:** | 43.9kN/cm |

*Scaled to UHS PGA

## G.2.2 Test PC2-1.10*

| | | | | | | | |
|---|---|---|---|---|---|---|---|
| **Wall:** | Poor Quality Collar Joint | **Test Sequence:** | 2 | | **Test Number:** | PC2-1.10 | |
| **Earthquake Record:** | Gilroy | **Scale:** | 1.10* | **Site Class:** C | **PGA:** | 0.53g | **PGD:** 3.84cm |
| **Wall Condition:** | Crack formed at Header 6 during test | | | | | | |
| **Height:** | 4153mm | **Thickness:** | 355mm | **h/t:** 11.7 | **Width:** | 1498mm | **Density:** 1764.5kg/m$^3$ |
| **Header Location:** | | **H3:** | 1317mm | **H6:** 2682mm | **H8:** | 3586mm | |

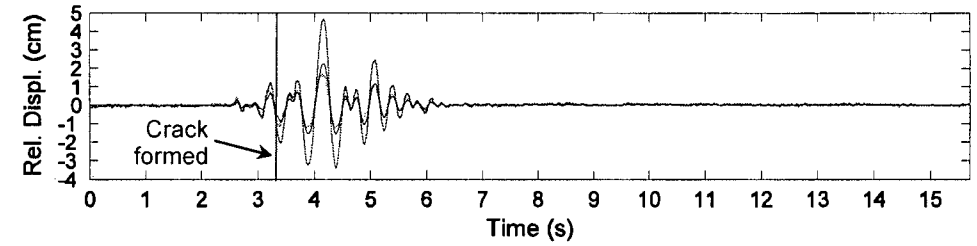


**Relative Displacement Time History (..... H8, ..... H6, — H3)**

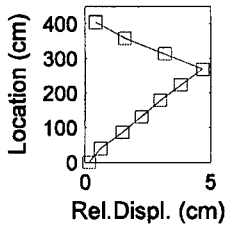


**Profile (t = 4.162)**

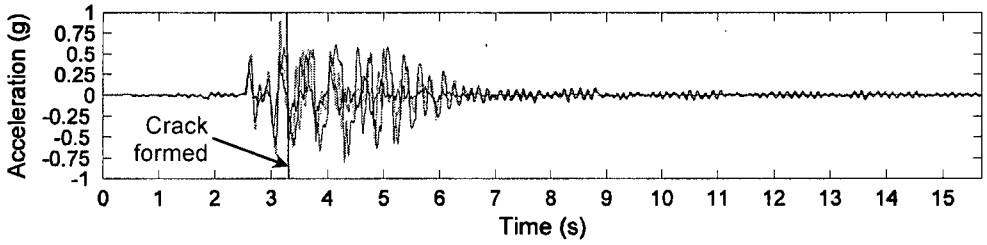


**Acceleration Time History (..... H8, — H6, — H3)**

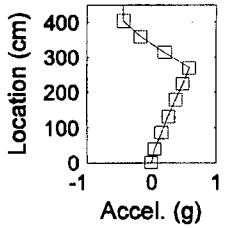


**Profile (t = 4.162)**

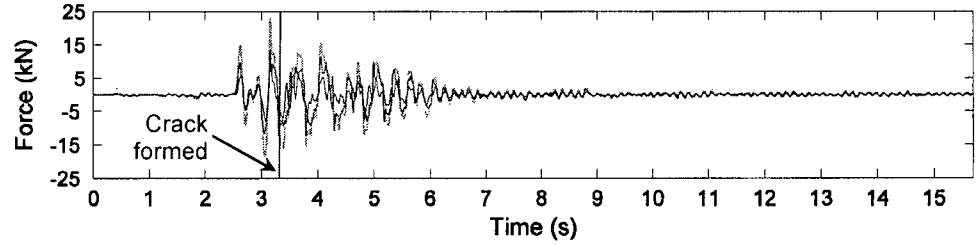


**Force Time History (..... Total, — Lower, — Upper)**

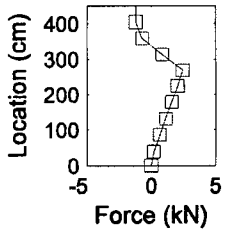


**Profile (t = 4.162)**

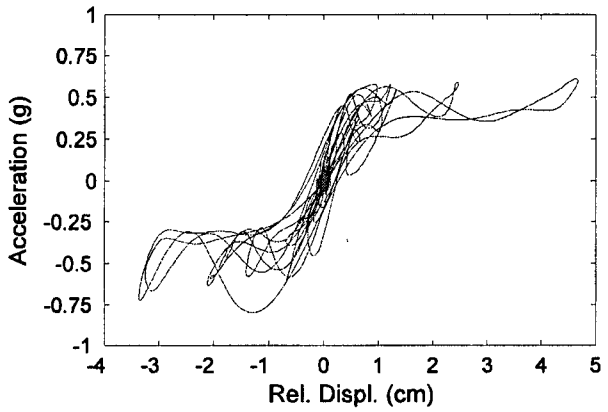


**Crack Acceleration vs. Relative Crack Displacement**

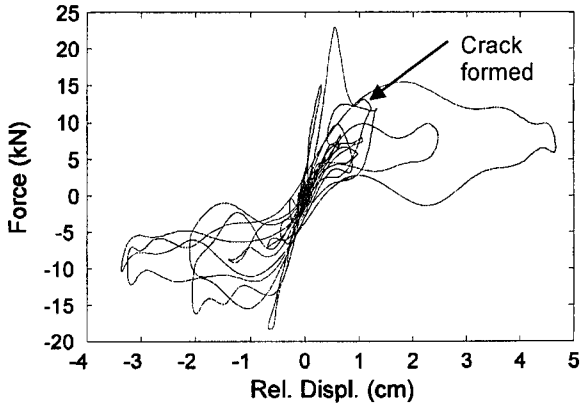


**Total Force vs. Relative Crack Displacement**

| | | | |
|---|---|---|---|
| **Initial Period:** | 0.11s | **Initial Stiffness:** | 37.1kN/cm |

*Scaled to UHS PGA

## G.2.3 Test PC3-0.75

| | | | | | | | | | |
|---|---|---|---|---|---|---|---|---|---|
| **Wall:** | Poor Quality Collar Joint | | **Test Sequence:** | 3 | | **Test Number:** | PC3-0.75 | | |
| **Earthquake Record:** | Gilroy | **Scale:** | 0.75 | **Site Class:** | C | **PGA:** | 0.73g | **PGD:** | 4.87cm |
| **Wall Condition:** | Crack at Header 6 | | | | | | | | |
| **Height:** | 4153mm | **Thickness:** | 355mm | **h/t:** | 11.7 | **Width:** | 1498mm | **Density:** | 1764.5kg/m$^3$ |
| **Header Location:** | | **H3:** | 1317mm | **H6:** | 2682mm | **H8:** | 3586mm | | |

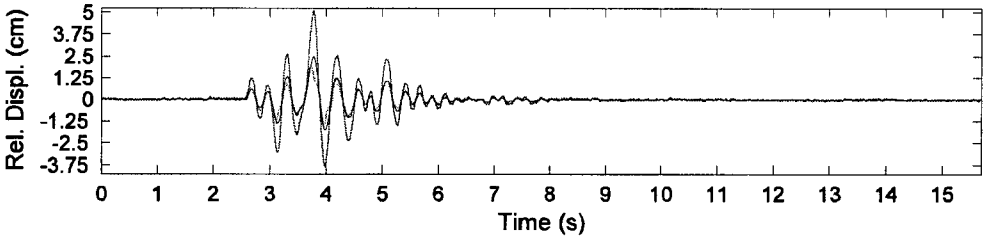


**Relative Displacement Time History (···· H8, — H6, — H3)**

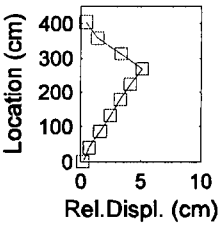


**Profile (t = 3.778s)**

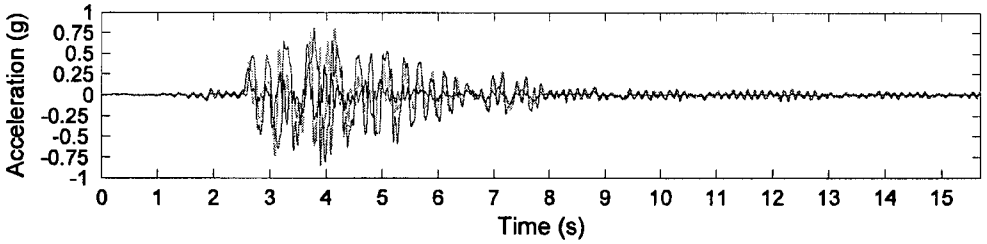


**Acceleration Time History (···· H8, — H6, — H3)**

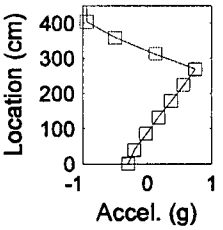


**Profile (t = 3.778s)**

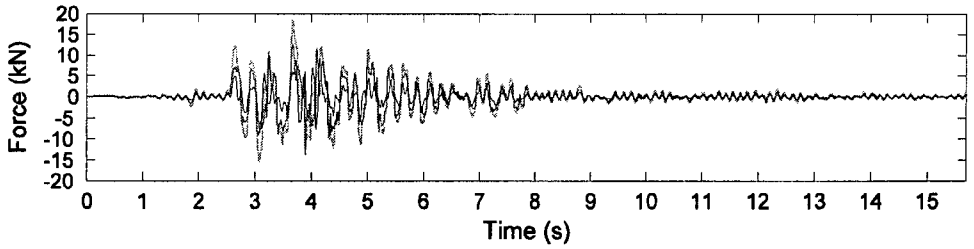


**Force Time History (···· Total, — Lower, — Upper)**

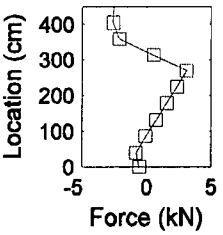


**Profile (t = 3.778s)**

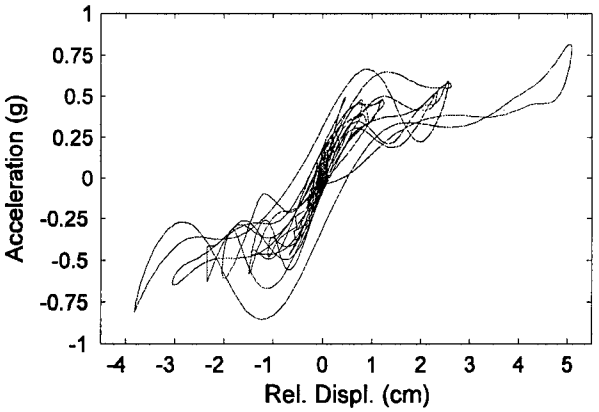


**Crack Acceleration vs. Relative Crack Displacement**

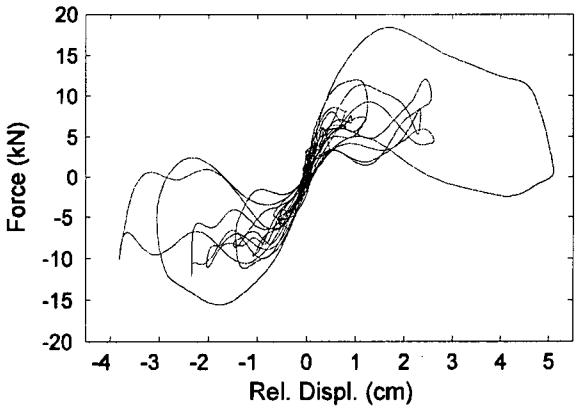


**Total Force vs. Relative Crack Displacement**

| | | | |
|---|---|---|---|
| **Initial Period:** | 0.13s | **Initial Stiffness:** | 19.7kN/cm |

## G.2.4 Test PC4-1.40

| | | | | | | | | | |
|---|---|---|---|---|---|---|---|---|---|
| **Wall:** | Poor Quality Collar Joint | | **Test Sequence:** | 4 | | | **Test Number:** | PC4-1.40 | |
| **Earthquake Record:** | Gilroy | | **Scale:** | 1.40 | **Site Class:** | C | **PGA:** | 1.3g | **PGD:** 9.25cm |
| **Wall Condition:** | Crack at Header 6 | | | | | | | | |
| **Height:** | 4153mm | **Thickness:** | 355mm | **h/t:** | 11.7 | **Width:** | 1498mm | **Density:** | 1764.5kg/m$^3$ |
| **Header Location:** | **H3:** | 1317mm | **H6:** | 2682mm | | **H8:** | 3586mm | | |

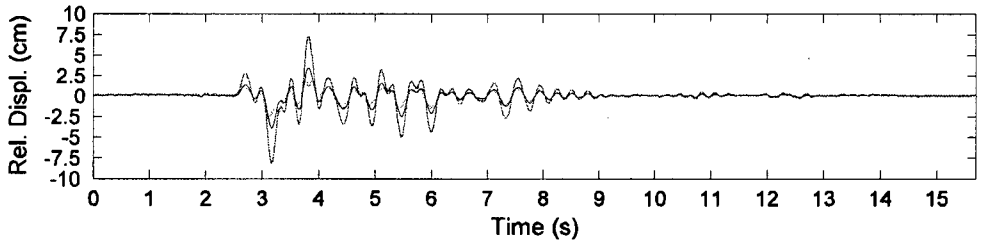


**Relative Displacement Time History (..... H8, ---- H6, — H3)**

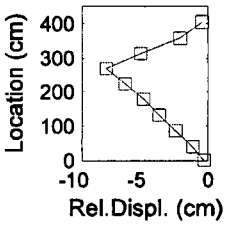


**Profile (t = 3.164s)**

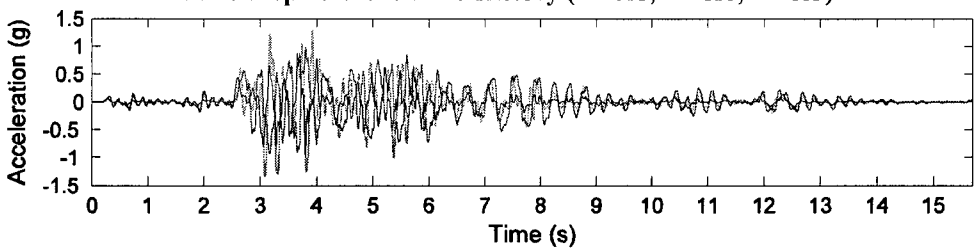


**Acceleration Time History (..... H8, ---- H6, — H3)**

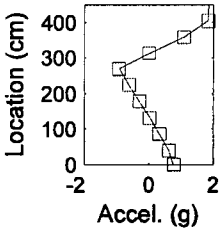


**Profile (t = 3.164s)**

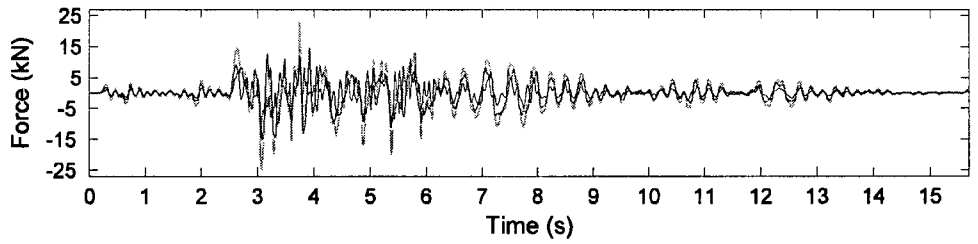


**Force Time History (..... Total, ---- Lower, — Upper)**

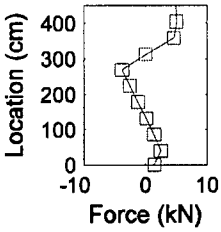


**Profile (t = 3.164s)**

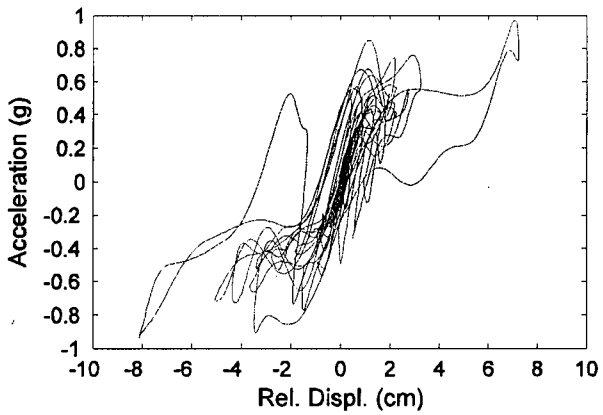


**Crack Acceleration vs. Relative Crack Displacement**

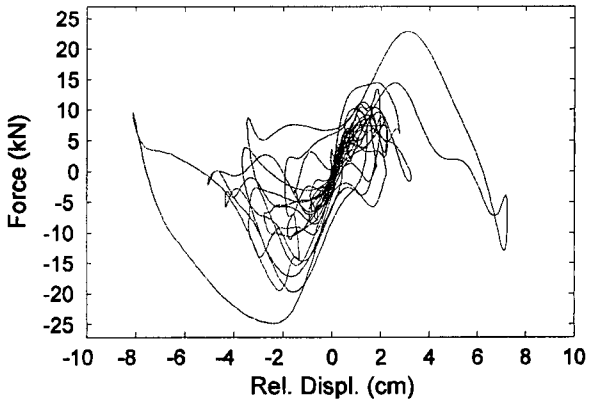


**Total Force vs. Relative Crack Displacement**

| | | | |
|---|---|---|---|
| **Initial Period:** | 0.13s | **Initial Stiffness:** | 12.7kN/cm |

## G.2.5 Test PC5-1.55

| | | | | | | | | | |
|---|---|---|---|---|---|---|---|---|---|
| **Wall:** | Poor Quality Collar Joint | | **Test Sequence:** | 5 | | **Test Number:** | PC5-1.55 | | |
| **Earthquake Record:** | Gilroy | | **Scale:** | 1.55 | **Site Class:** | C | **PGA:** | 1.4g | **PGD:** | 11.44cm |
| **Wall Condition:** | Crack at Header 6, Crack formed at Header 1 | | | | | | | | |
| **Height:** | 4153mm | **Thickness:** | 355mm | **h/t:** | 11.7 | **Width:** | 1498mm | **Density:** | 1764.5kg/m$^3$ | |
| **Header Location:** | **H3:** | 1317mm | **H6:** | 2682mm | **H8:** | 3586mm | | | | |

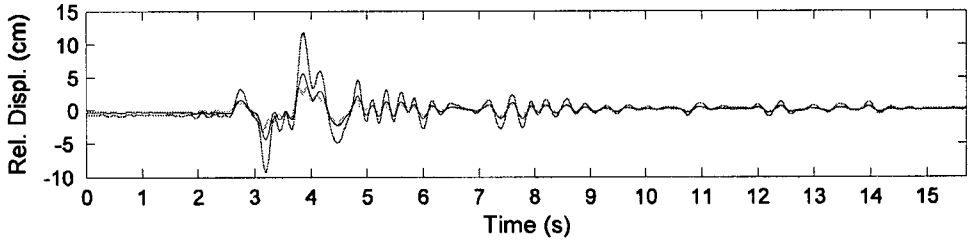


**Relative Displacement Time History (—— H8, —— H6, — H3)**

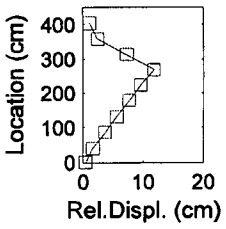


**Profile (t = 3.864s)**

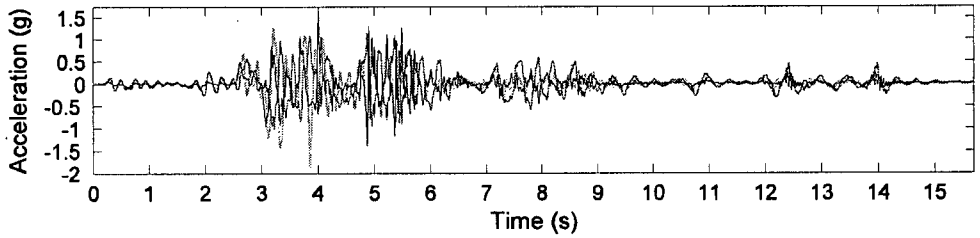


**Acceleration Time History (—— H8, —— H6, — H3)**

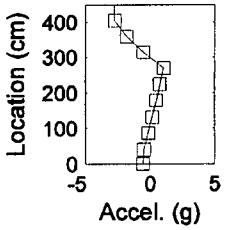


**Profile (t = 3.864s)**

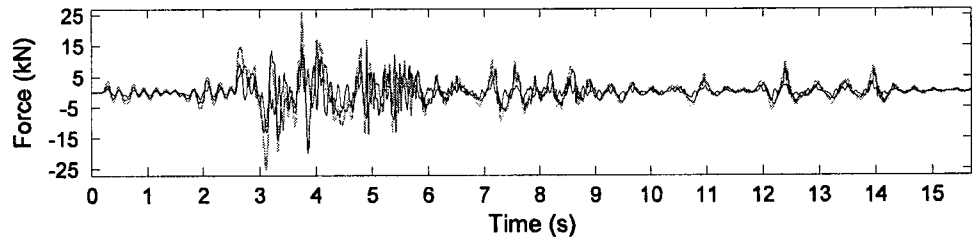


**Force Time History (—— Total, — Lower, — Upper)**

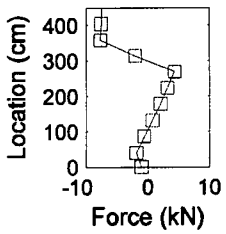


**Profile (t = 3.864s)**

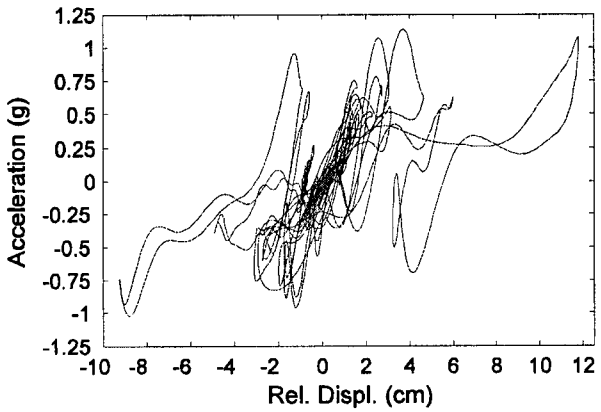


**Crack Acceleration vs. Relative Crack Displacement**

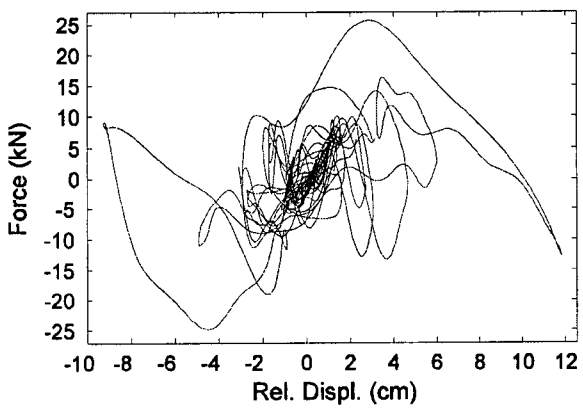


**Total Force vs. Relative Crack Displacement**

| | | | |
|---|---|---|---|
| **Initial Period:** | 0.15s | **Initial Stiffness:** | 7.9kN/cm |

## G.2.6 Test PC6-1.57

| | | | | | | | | | |
|---|---|---|---|---|---|---|---|---|---|
| **Wall:** | Poor Quality Collar Joint | | **Test Sequence:** | 6 | | **Test Number:** | PC6-1.57 | | |
| **Earthquake Record:** | Gilroy | | **Scale:** | 1.57 | **Site Class:** | C | **PGA:** | 1.8g | **PGD:** 14.08cm |
| **Wall Condition:** | Crack at Header 6 and Header 1 | | | | | | | | |
| **Height:** | 4153mm | **Thickness:** | 355mm | **h/t:** | 11.7 | **Width:** | 1498mm | **Density:** | 1764.5kg/m$^3$ |
| **Header Location:** | **H3:** | 1317mm | **H6:** | 2682mm | **H8:** | 3586mm | | | |

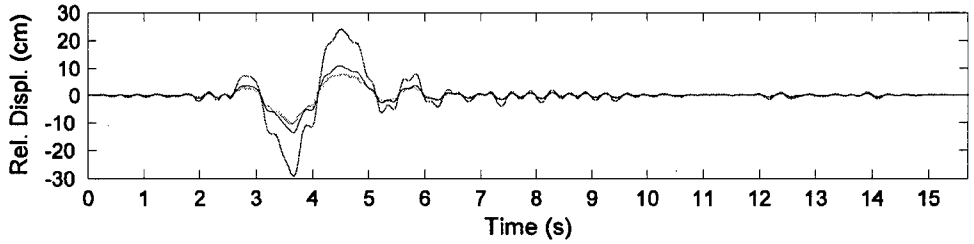


**Relative Displacement Time History (..... H8, ..... H6, — H3)**

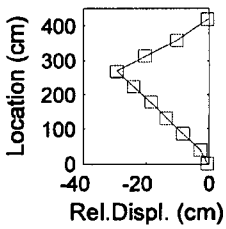


**Profile (t = 3.662s)**

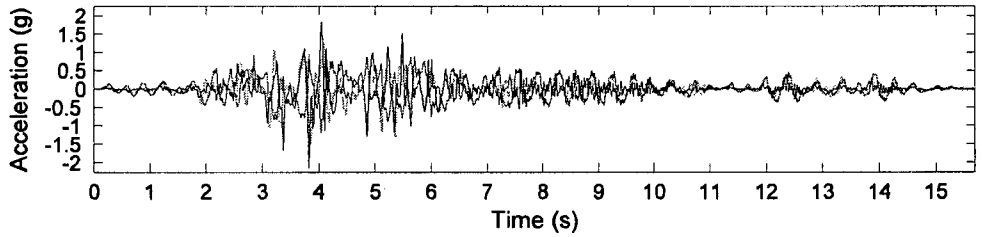


**Acceleration Time History (..... H8, — H6, — H3)**

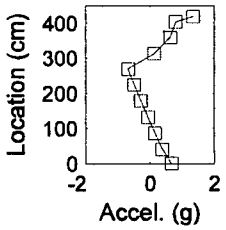


**Profile (t = 3.662s)**

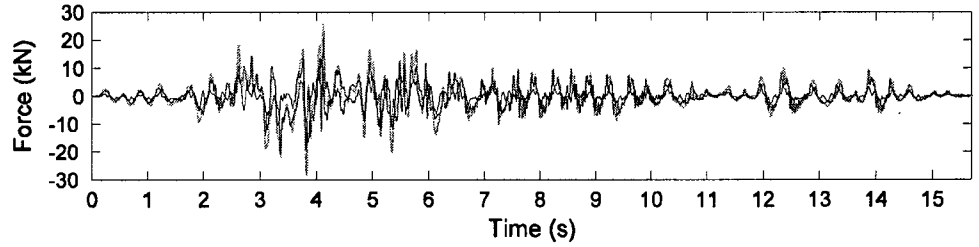


**Force Time History (..... Total, — Lower, — Upper)**

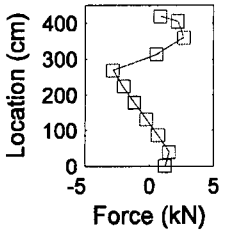


**Profile (t = 3.662s)**

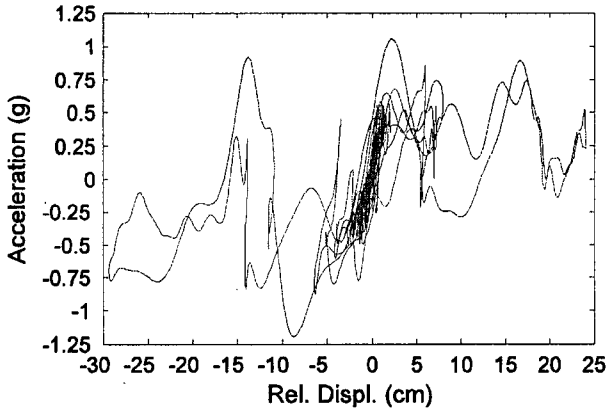


**Crack Acceleration vs. Relative Crack Displacement**

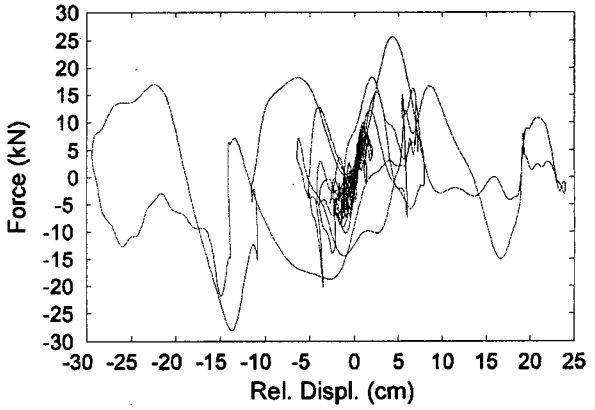


**Total Force vs. Relative Crack Displacement**

| | | | |
|---|---|---|---|
| **Initial Period:** | 0.25s | **Initial Stiffness:** | 8.29kN/cm |

## G.2.7 Test PC7-1.75

| | | | | | | | | | |
|---|---|---|---|---|---|---|---|---|---|
| **Wall:** | Poor Quality Collar Joint | **Test Sequence:** | 7 | | | **Test Number:** | PC7-1.75 | | |
| **Earthquake Record:** | Gilroy | **Scale:** | 1.75 | **Site Class:** | C | **PGA:** | 1.5g | **PGD:** | 16.03cm |
| **Wall Condition:** | Crack at Header 6, two layers of outer wythe bricks at Header 1 lost during test. | | | | | | | | |
| **Height:** | 4153mm | **Thickness:** | 355mm | **h/t:** | 11.7 | **Width:** | 1498mm | **Density:** | 1764.5kg/m$^3$ |
| **Header Location:** | | **H4:** | 1777mm | **H6:** | 2682mm | **H8:** | 3586mm | | |

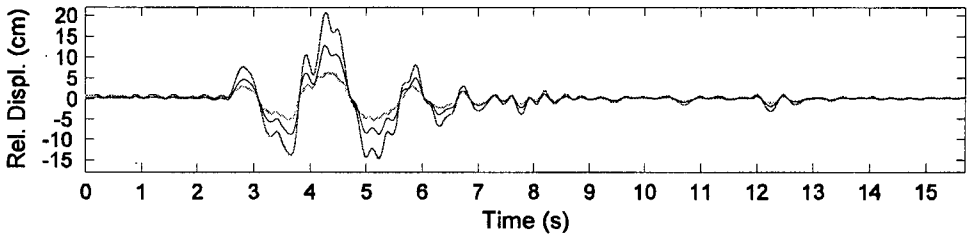


**Relative Displacement Time History (..... H8, ..... H6, — H4)**

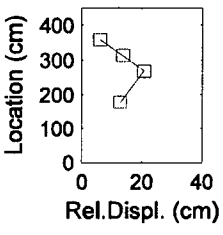


**Profile (t = 4.274s)**

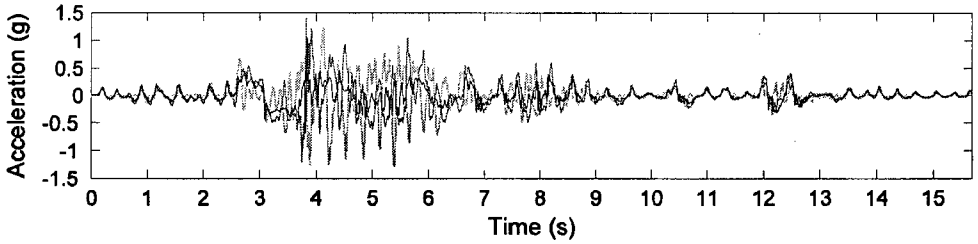


**Acceleration Time History (..... H8, ..... H6, — H4)**

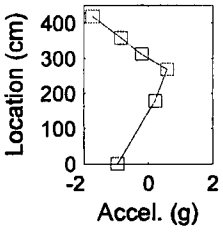


**Profile (t = 4.274s)**

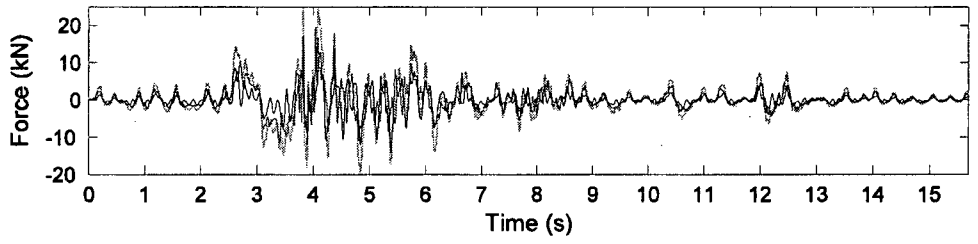


**Force Time History (— Total, — Lower, — Upper)**

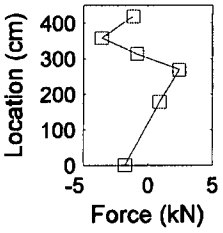


**Profile (t = 4.274s)**

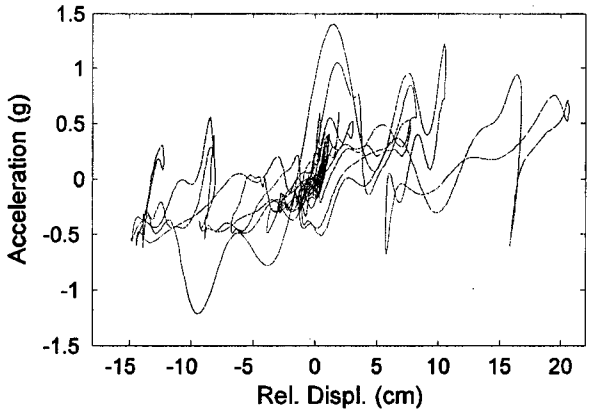


**Crack Acceleration vs. Relative Crack Displacement**

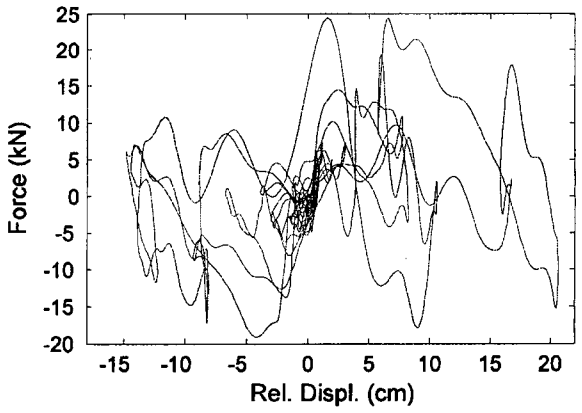


**Total Force vs. Relative Crack Displacement**

| | | | |
|---|---|---|---|
| **Initial Period:** | 0.21s | **Initial Stiffness:** | 14.19kN/cm |
| **Note:** Instrumentation removed before test. | | | |

## G.3 Wall GD

### G.3.1 Test GD1-0.75*

| | | | | | | | | | |
|---|---|---|---|---|---|---|---|---|---|
| **Wall:** | Good Quality Collar Joint | **Test Number:** | 1 | | | **Test Number:** | GD1-0.75 | | |
| **Earthquake Record:** | Hayward | **Scale:** | 0.75* | **Site Class:** | D | **PGA:** | 0.40g | **PGD:** | 3.09cm |
| **Wall Condition:** | Crack formed at Header 7 | | | | | | | | |
| **Height:** | 4082mm | **Thickness:** | 354mm | **h/t:** | 11.5 | **Width:** | 1499mm | **Density:** | 1754kg/m$^3$ |
| **Header Location:** | | **H4:** | 1761mm | **H7:** | 3136mm | **H8:** | 3587mm | | |

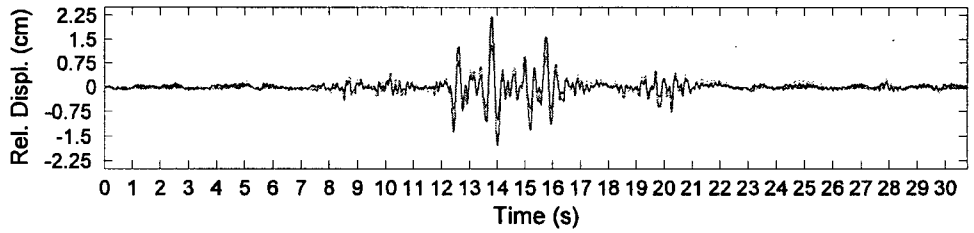


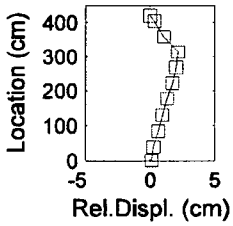


**Relative Displacement Time History (..... H8, ..... H7, — H4)** **Profile (t = 13.8s)**

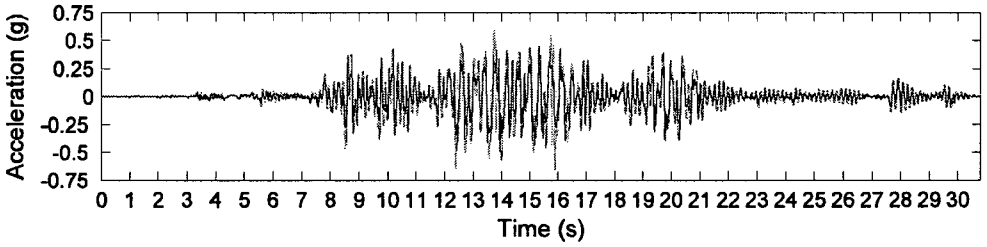


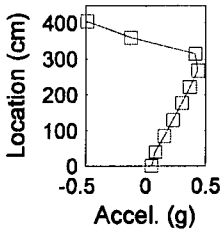


**Acceleration Time History (..... H8, — H7, — H4)** **Profile (t = 13.8s)**

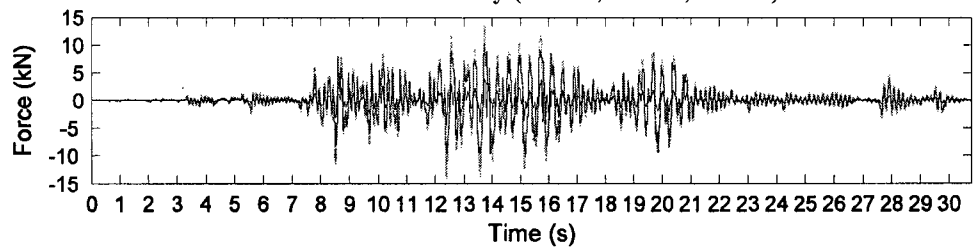


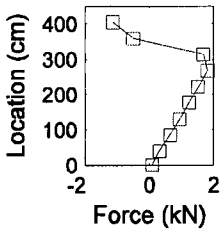


**Force Time History (..... Total, ..... Lower, — Upper)** **Profile (t = 13.8s)**

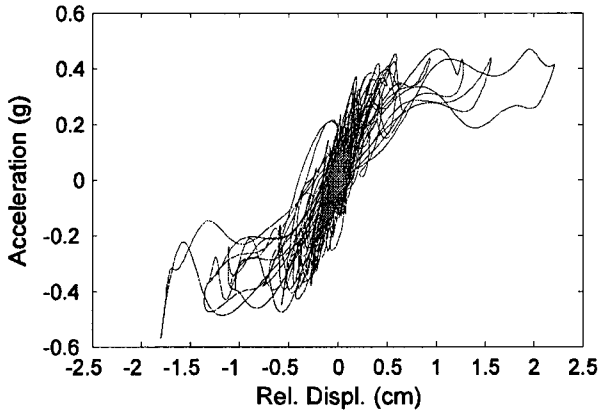


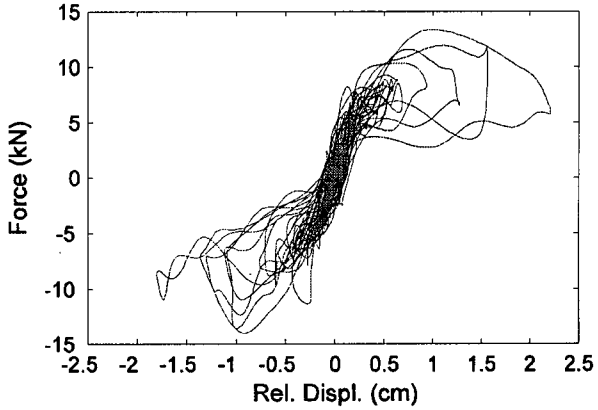


**Crack Acceleration vs. Relative Crack Displacement** **Total Force vs. Relative Crack Displacement**

| | | | | | |
|---|---|---|---|---|---|
| **Initial Period:** | 0.11s | **Un-Cracked Stiffness:** | 39.7kN/cm | **Cracked Stiffness:** | 17.5kN/cm |

*Scaled to UHS PGA

## G.3.2 Test GD2-0.81

| | | | | | | | | | |
|---|---|---|---|---|---|---|---|---|---|
| **Wall:** | Good Quality Collar Joint | | **Test Sequence:** | 2 | | **Test Number:** | GD2-0.81 | | |
| **Earthquake Record:** | Hayward | | **Scale:** | 0.81 | **Site Class:** | D | **PGA:** | 0.52g | **PGD:** 3.83cm |
| **Wall Condition:** | Crack at Header 7 | | | | | | | | |
| **Height:** | 4082mm | **Thickness:** | 354mm | **h/t:** | 11.5 | **Width:** | 1499mm | **Density:** | 1754kg/m$^3$ |
| **Header Location:** | **H4:** | 1761mm | **H7:** | 3136mm | **H8:** | 3587mm | | | |

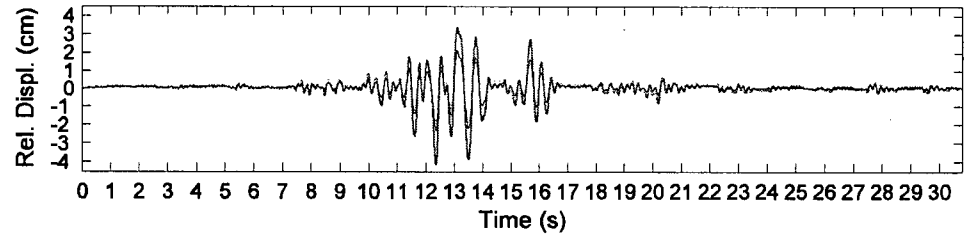


**Relative Displacement Time History (┈ H8, ── H7, — H4)**

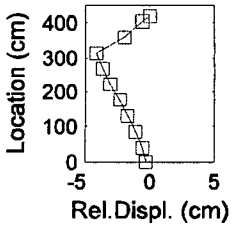


**Profile (t = 12.36s)**

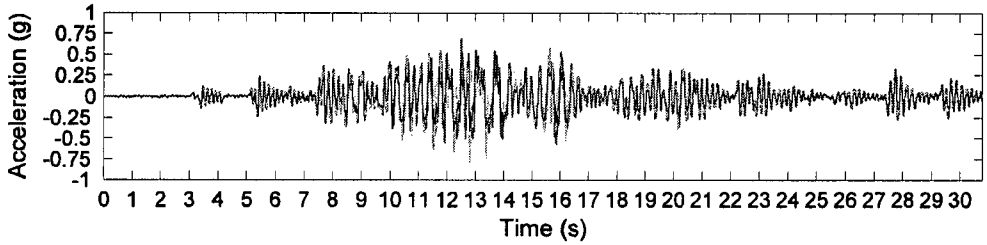


**Acceleration Time History (┈ H8, ── H7, — H4)**

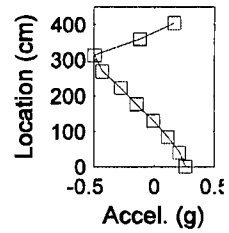


**Profile (t = 12.36s)**

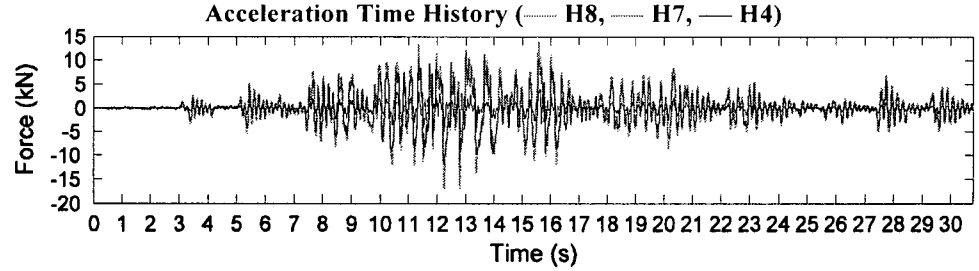


**Force Time History (┈ Total, ── Lower, — Upper)**

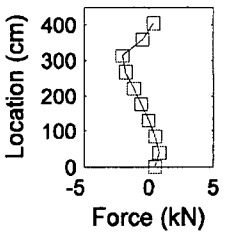


**Profile (t = 12.36s)**

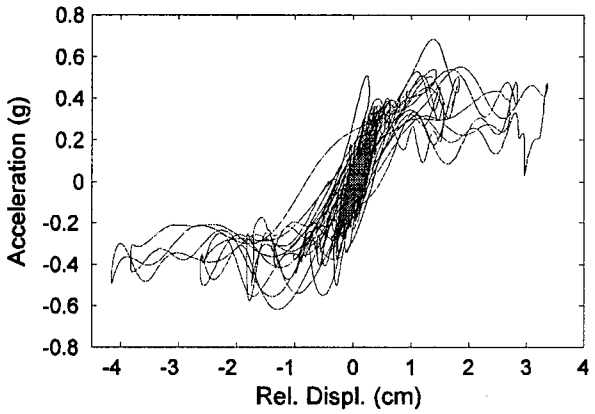


**Crack Acceleration vs. Relative Crack Displacement**

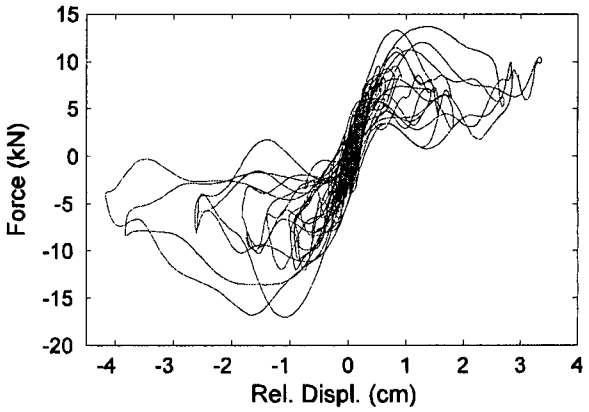


**Total Force vs. Relative Crack Displacement**

| | | | |
|---|---|---|---|
| **Initial Period:** | 0.13s | **Cracked Stiffness:** | 18.8kN/cm |

## G.3.3 Test GD3-1.00

| | | | | | | | | | |
|---|---|---|---|---|---|---|---|---|---|
| **Wall:** | Good Quality Collar Joint | | **Test Sequence:** | 3 | | **Test Number:** | GD3-1.00 | | |
| **Earthquake Record:** | Hayward | | **Scale:** | 1.00 | **Site Class:** | D | **PGA:** | 0.76g | **PGD:** 5.4cm |
| **Wall Condition:** | Crack at Header 7 | | | | | | | | |
| **Height:** | 4082mm | **Thickness:** | 354mm | **h/t:** | 11.5 | **Width:** | 1499mm | **Density:** | 1754kg/m$^3$ |
| **Header Location:** | **H4:** | 1761mm | **H7:** | 3136mm | **H8:** | 3587mm | | | |

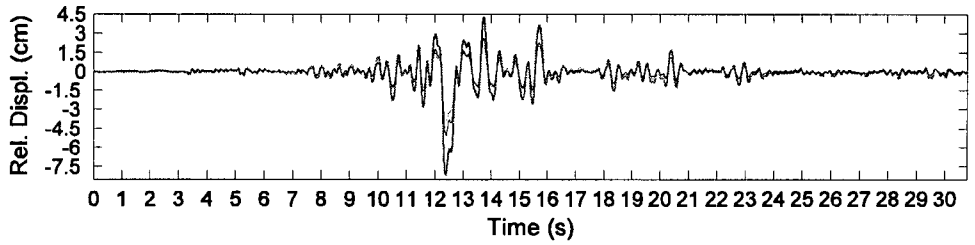


**Relative Displacement Time History (···· H8, — H7, — H4)**

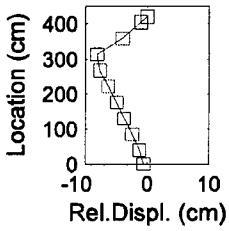


**Profile (t = 12.39s)**

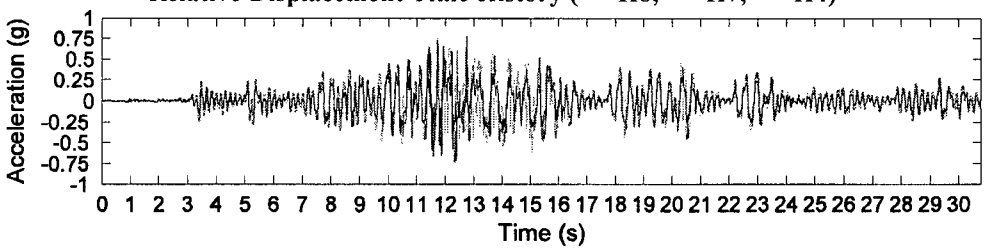


**Acceleration Time History (···· H8, — H7, — H4)**

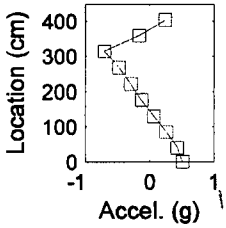


**Profile (t = 12.39s)**

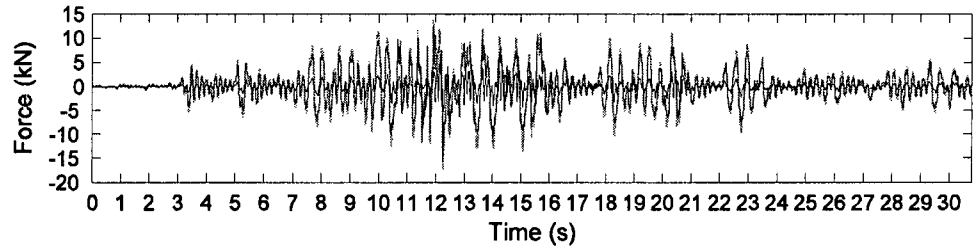


**Force Time History (···· Total, — Lower, — Upper)**

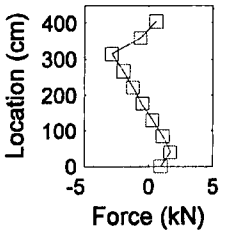


**Profile (t = 12.39s)**

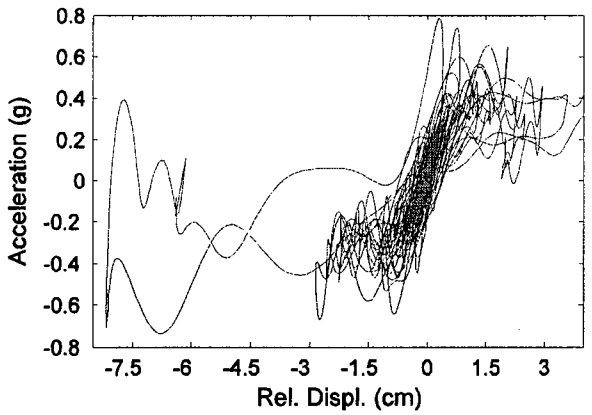


**Crack Acceleration vs. Relative Crack Displacement**

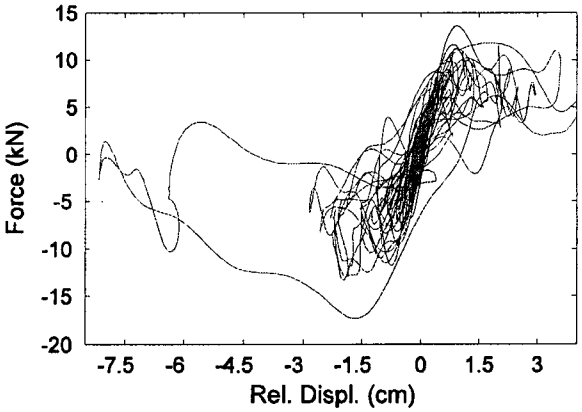


**Total Force vs. Relative Crack Displacement**

| | | | |
|---|---|---|---|
| **Initial Period:** | 0.13s | **Cracked Stiffness:** | 17.4kN/cm |

## G.3.4 Test GD4-1.24

| | | | | | | | | | |
|---|---|---|---|---|---|---|---|---|---|
| **Wall:** | Good Quality Collar Joint | **Test Number:** | 4 | | | **Test Number:** | GD4-1.24 | | |
| **Earthquake Record:** | Hayward | **Scale:** | 1.24 | **Site Class:** | D | **PGA:** | 1.0g | **PGD:** | 6.50 cm |
| **Wall Condition:** | Crack at Header 7 | | | | | | | | |
| **Height:** | 4082mm | **Thickness:** | 354mm | **h/t:** | 11.5 | **Width:** | 1499mm | **Density:** | 1754kg/m$^3$ |
| **Header Location:** | | **H4:** | 1761mm | **H7:** | 3136mm | **H8:** | 3587mm | | |

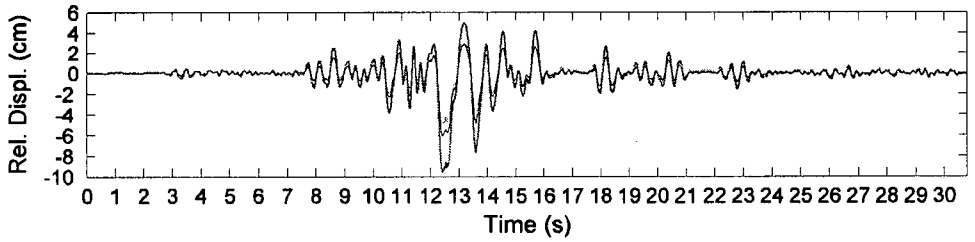


**Relative Displacement Time History (— H8, — H7, — H4)**

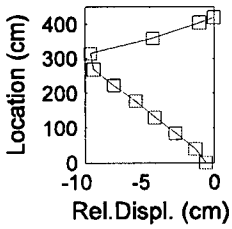


**Profile (t = 12.42s)**

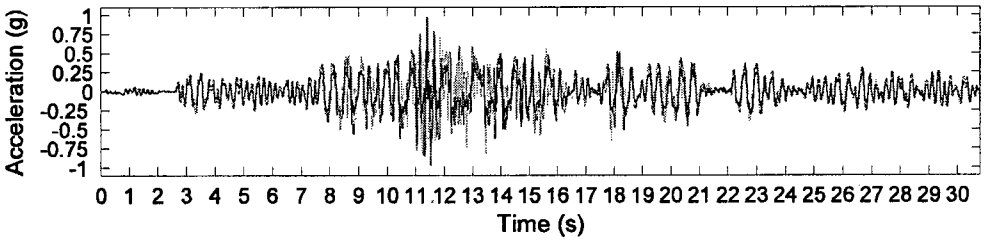


**Acceleration Time History (— H8, — H7, — H4)**

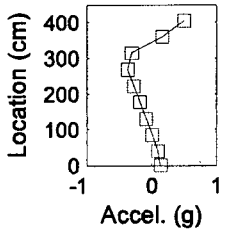


**Profile (t = 12.42s)**

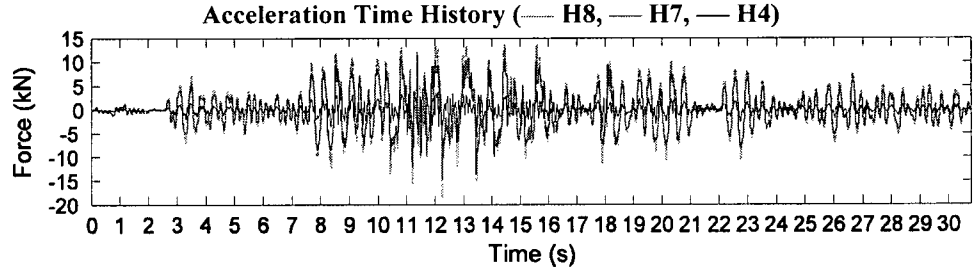


**Force Time History (— Total, — Lower,— Upper)**

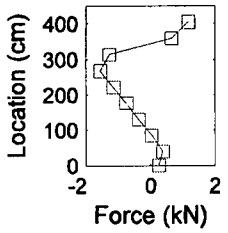


**Profile (t = 12.42s)**

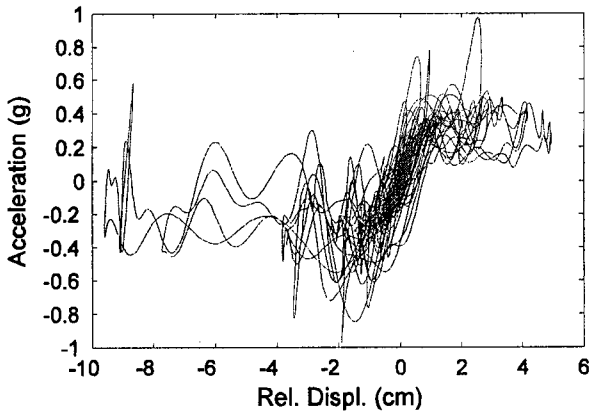


**Crack Acceleration vs. Relative Crack Displacement**

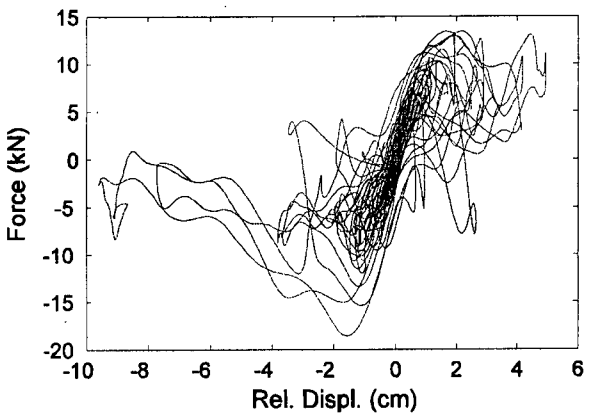


**Total Force vs. Relative Crack Displacement**

| | | | |
|---|---|---|---|
| **Initial Period:** | 0.14s | **Cracked Stiffness:** | 10.3kN/cm |

## G.3.5 Test GD5-1.65

| | | | | | | | | | |
|---|---|---|---|---|---|---|---|---|---|
| **Wall:** | Good Quality Collar Joint | **Test Sequence:** | 7 | | | **Test Number:** | | GD5-1.65 | |
| **Earthquake Record:** | Hayward | **Scale:** | 1.65 | **Site Class:** | D | **PGA:** | 1.51g | **PGD:** | 9.16cm |
| **Wall Condition:** | Crack at Header 7, new cracks formed at H2 and H3 | | | | | | | | |
| **Height:** | 4082mm | **Thickness:** | 354mm | **h/t:** | 11.5 | **Width:** | 1499mm | **Density:** | 1754kg/m$^3$ |
| **Header Location:** | **H5:** | 2212mm | **H7:** | 3136mm | | **H8:** | 3587mm | | |

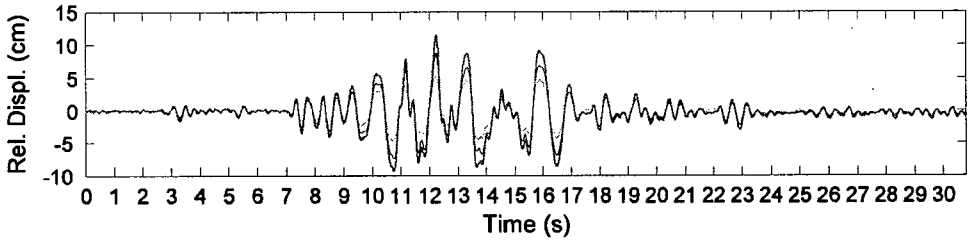


**Relative Displacement Time History (— H8, — H7, — H5)**

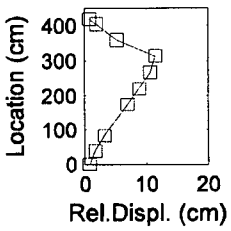


**Profile (t = 12.24s)**

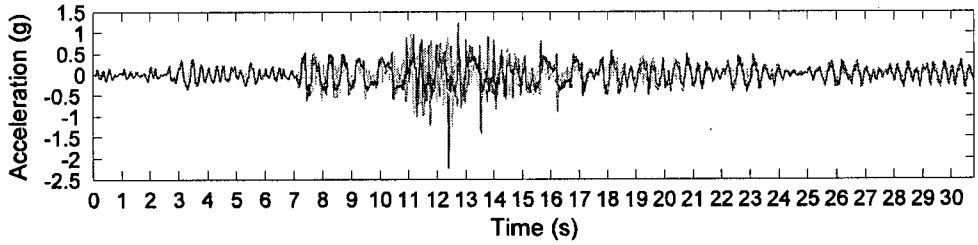


**Acceleration Time History (— H8, — H7, — H5)**

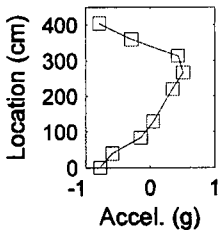


**Profile (t = 12.24s)**

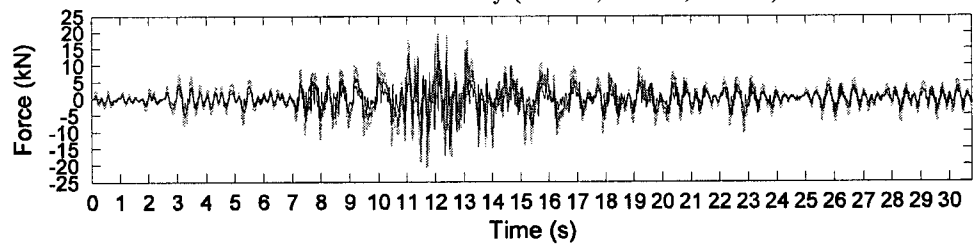


**Force Time History (— Total, — Lower, — Upper)**

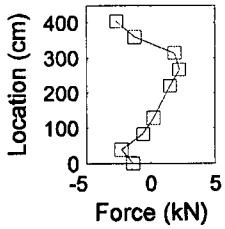


**Profile (t = 12.24s)**

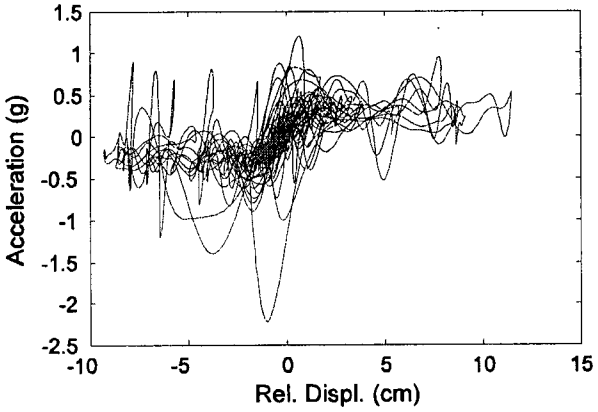


**Crack Acceleration vs. Relative Crack Displacement**

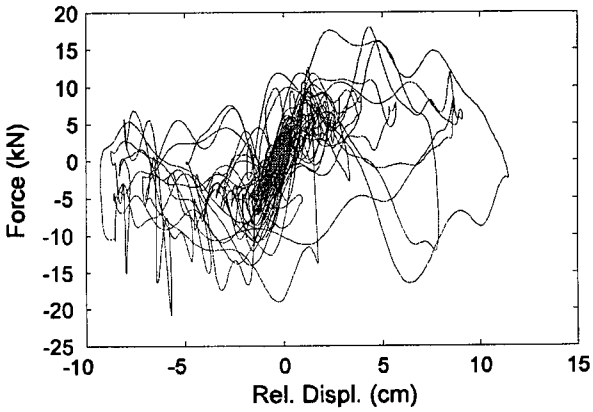


**Total Force vs. Relative Crack Displacement**

| | | | |
|---|---|---|---|
| **Initial Period:** | 0.21s | **Cracked Stiffness:** | 8.1kN/cm |

## G.3.6 Test GD6-1.19

| | | | | | | | | | |
|---|---|---|---|---|---|---|---|---|---|
| **Wall:** | Good Quality Collar Joint | **Test Sequence:** | 8 | | | **Test Number:** | | GD6-1.19 | |
| **Earthquake Record:** | Hayward | **Scale:** | 1.19 | **Site Class:** | D | **PGA:** | 1.16g | **PGD:** | 6.62cm |
| **Wall Condition:** | Cracks at Header 2, 3 and 7 | | | | | | | | |
| **Height:** | 4082mm | **Thickness:** | 354mm | **h/t:** | 11.5 | **Width:** | 1499mm | **Density:** | 1754kg/m$^3$ |
| **Header Location:** | | **H5:** | 2212mm | **H7:** | 3136mm | **H8:** | 3587mm | | |

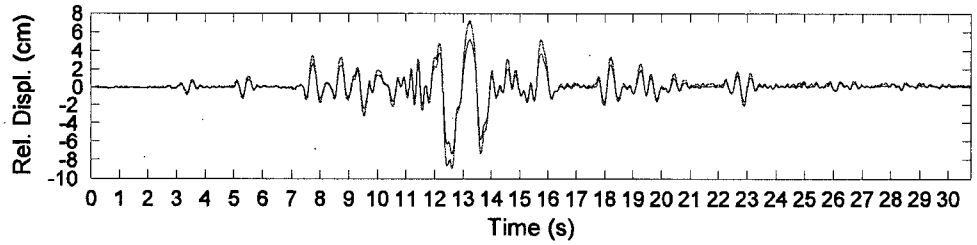


**Relative Displacement Time History (..... H8, ---- H7, — H5)**

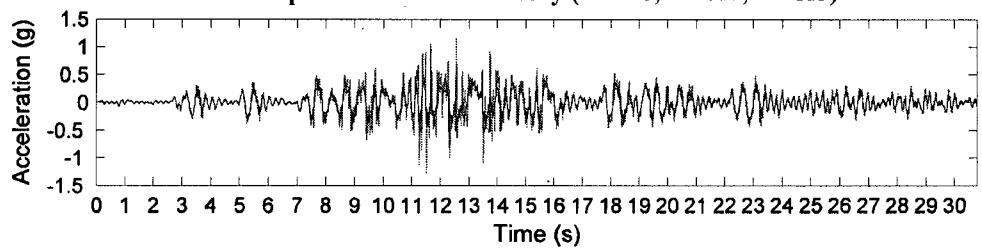


**Acceleration Time History (..... H8, ---- H7, — H5)**

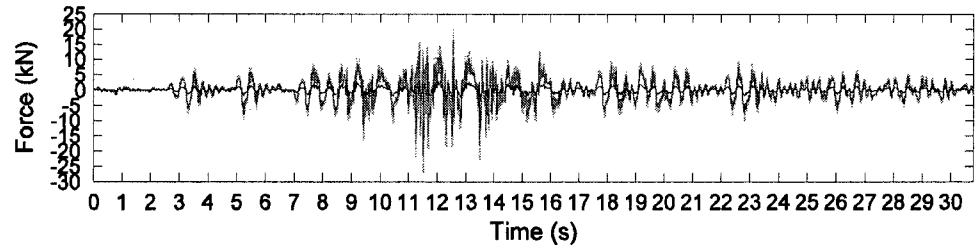


**Force Time History (..... Total, ---- Lower, — Upper)**

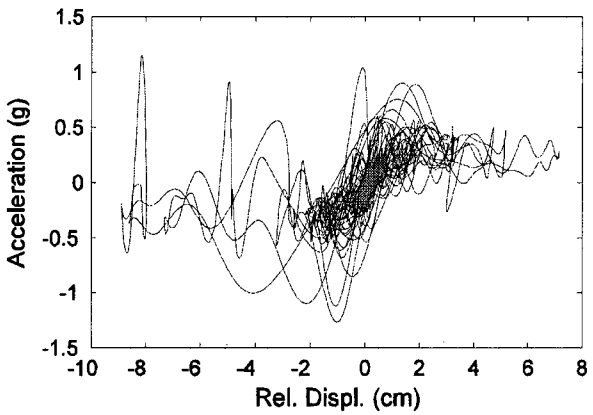


**Crack Acceleration vs. Relative Crack Displacement**

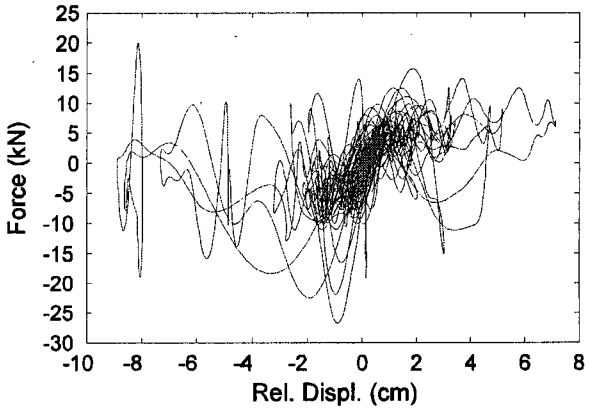


**Total Force vs. Relative Crack Displacement**

| | | | |
|---|---|---|---|
| **Initial Period:** | 0.20s | **Cracked Stiffness:** | Difficult to determine |

## G.3.7 Test GD7-1

| | | | | | | | | | |
|---|---|---|---|---|---|---|---|---|---|
| **Wall:** | Good Quality Collar Joint | | **Test Sequence:** | 9 (Collapse) | | **Test Number:** | | GD7-1.83 | |
| **Earthquake Record:** | Hayward | | **Scale:** | 1.83 | **Site Class:** | D | **PGA:** | 1.40g | **PGD:** 11.2cm |
| **Wall Condition:** | Cracks at Header 2, 3 and 7. Wall Collapse. | | | | | | | | |
| **Height:** | 4082mm | **Thickness:** | 354mm | **h/t:** | 11.5 | **Width:** | 1499mm | **Density:** | 1754kg/m$^3$ |
| **Header Location:** | **H5:** | 2212mm | **H7:** | 3136mm | | **H8:** | 3587mm | | |

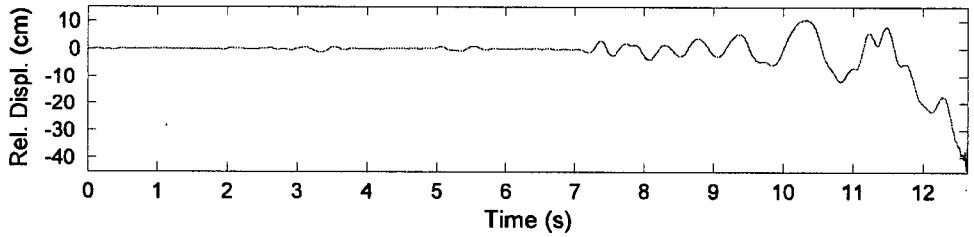


**Relative Displacement Time History (— H7)**

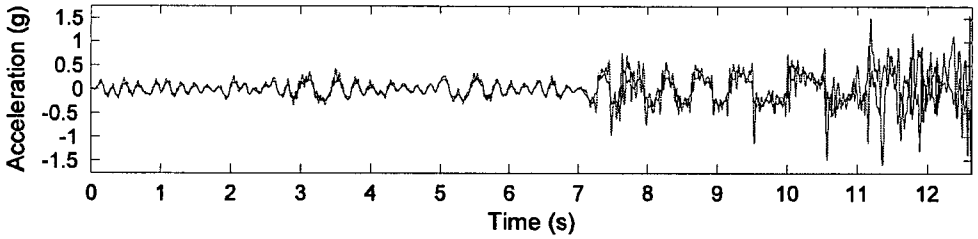


**Acceleration Time History (— H7, — H5)**

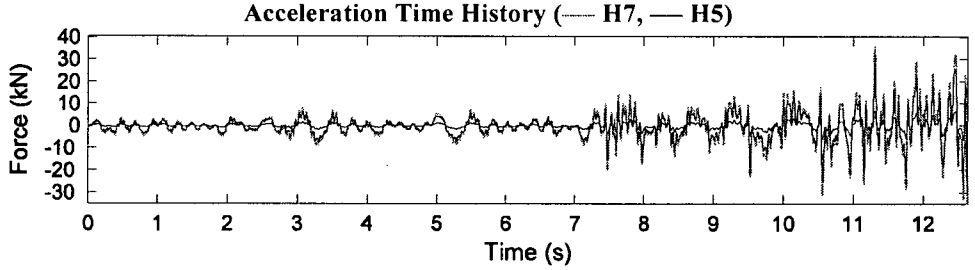


**Force Time History (— Total, — Lower, — Upper)**

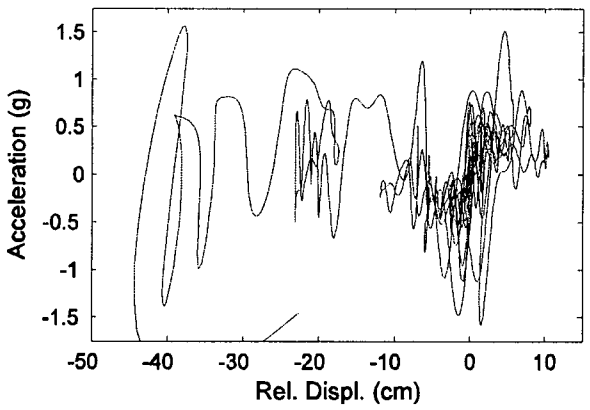


**Crack Acceleration vs. Relative Crack Displacement**

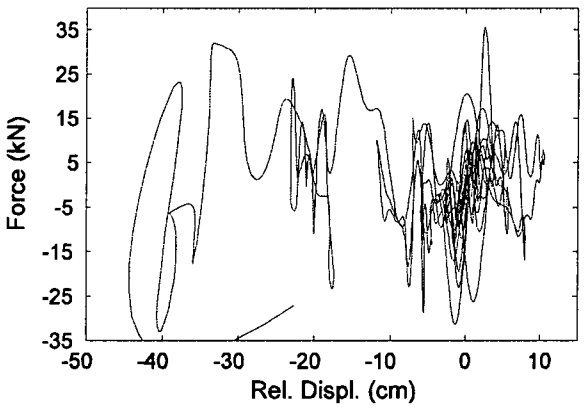


**Total Force vs. Relative Crack Displacement**

| | |
|---|---|
| **Cracked Stiffness:** | 17.7kN/cm (not too reliable due to lack of instrumentation) |

## G.3.8 Test GD(Sub1)1-1.01

| | | | | | | | | | |
|---|---|---|---|---|---|---|---|---|---|
| **Wall:** | Good Quality Collar Joint | | | **Test Number:** | 5 (Subduction) | **Test Number:** | GD(Sub1)1-1.01 | | |
| **Earthquake Record:** | HKD 109 | | **Scale:** | 1.01 | **Site Class:** | D | **PGA:** | 0.76g | **PGD:** 11.3cm |
| **Wall Condition:** | Crack at Header 7 | | | | | | | | |
| **Height:** | 4082mm | **Thickness:** | 354mm | **h/t:** | 11.5 | **Width:** | 1499mm | **Density:** | 1754kg/m$^3$ |
| **Header Location:** | **H5:** | 2212mm | **H7:** | 3136mm | **H8:** | 3587mm | | | |

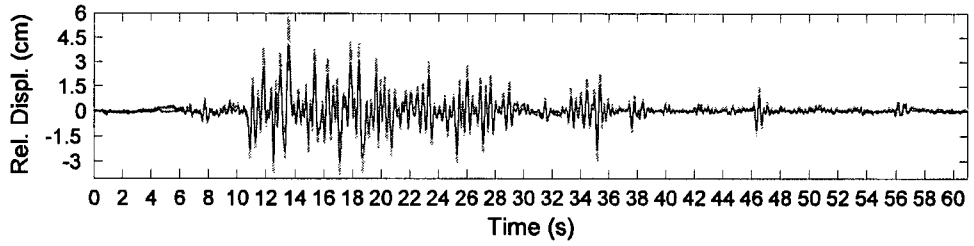


**Relative Displacement Time History (— H8, — H7, — H5)**

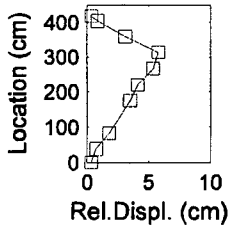


**Profile (t = 13.55s)**

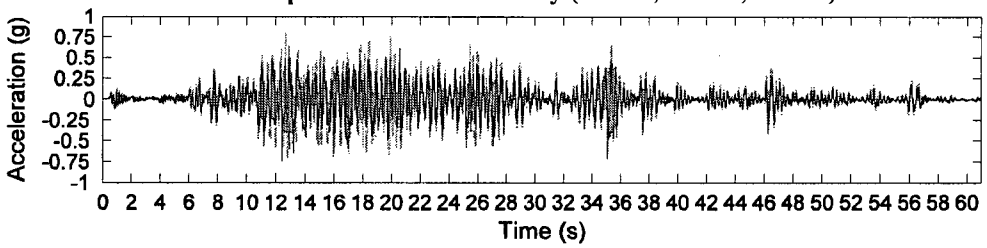


**Acceleration Time History (— H8, — H7, — H5)**

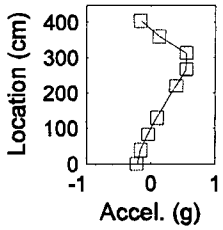


**Profile (t = 13.55s)**

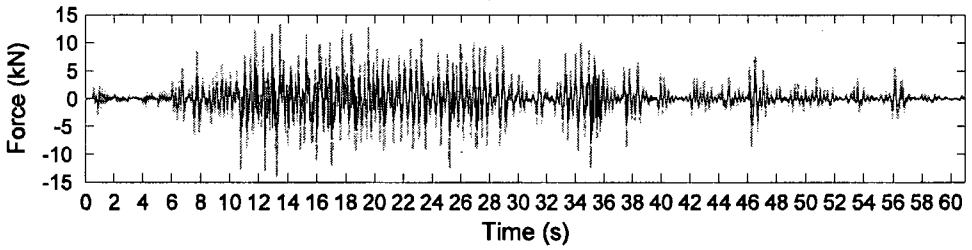


**Force Time History (— Total, — Lower, — Upper)**

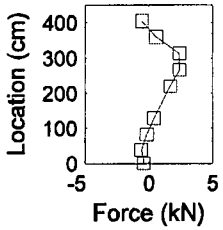


**Profile (t = 13.55s)**

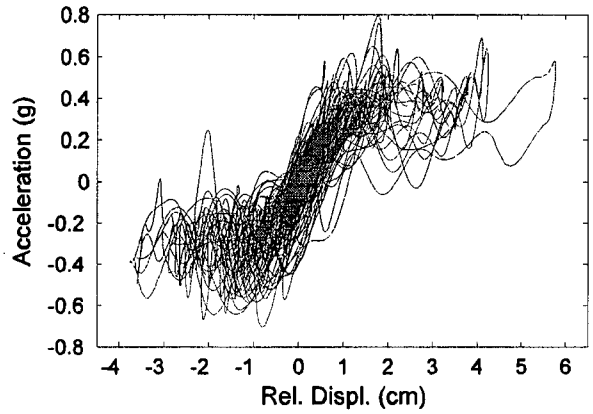


**Crack Acceleration vs. Relative Crack Displacement**

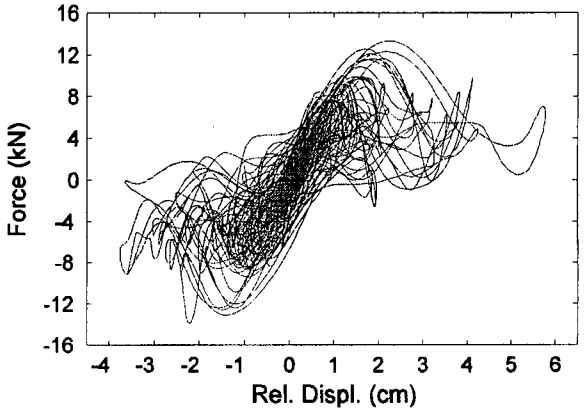


**Total Force vs. Relative Crack Displacement**

| | | | |
|---|---|---|---|
| **Initial Period:** | 0.15s | **Cracked Stiffness:** | 8.4kN/cm |

## G.3.8 Test GD(Sub1)2-1.26

| | | | | | | | | | |
|---|---|---|---|---|---|---|---|---|---|
| **Wall:** | Good Quality Collar Joint | | | **Test Number:** | 6 (Subduction) | **Test Number:** | GD(Sub1)2-1.26 | | |
| **Earthquake Record:** | HKD 109 | **Scale:** | 1.26 | **Site Class:** | D | **PGA:** | 0.78g | **PGD:** | 14.1cm |
| **Wall Condition:** | Crack at Header 7 | | | | | | | | |
| **Height:** | 4082mm | **Thickness:** | 354mm | **h/t:** | 11.5 | **Width:** | 1499mm | **Density:** | 1754kg/m$^3$ |
| **Header Location:** | **H5:** | 2212mm | **H7:** | 3136mm | **H8:** | 3587mm | | | |

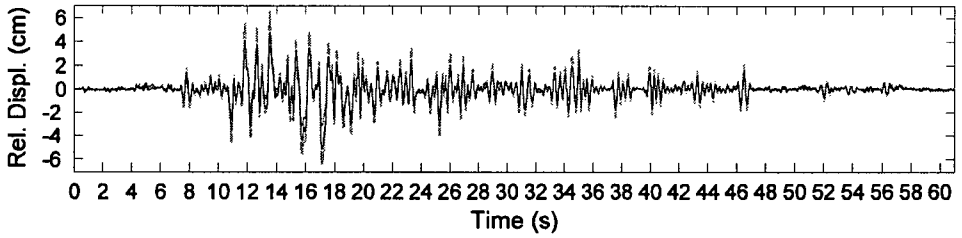


**Relative Displacement Time History (—— H8, —— H7, —— H5)**

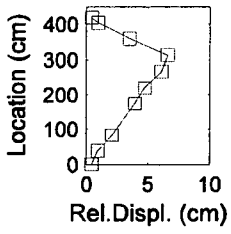


**Profile (t = 13.55s)**

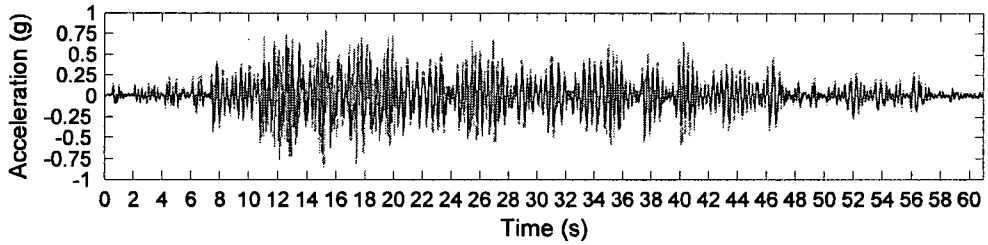


**Acceleration Time History (—— H8, —— H7, —— H5)**

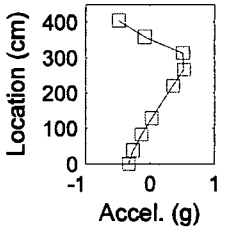


**Profile (t = 13.55s)**

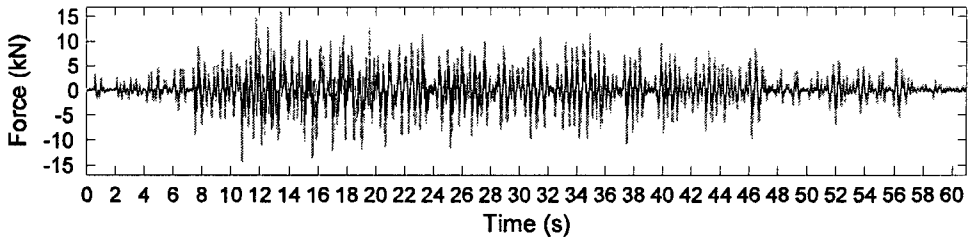


**Force Time History (—— Total, —— Lower, —— Upper)**

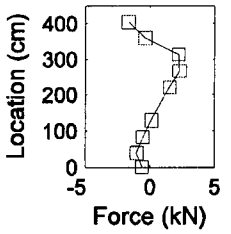


**Profile (t = 13.55s)**

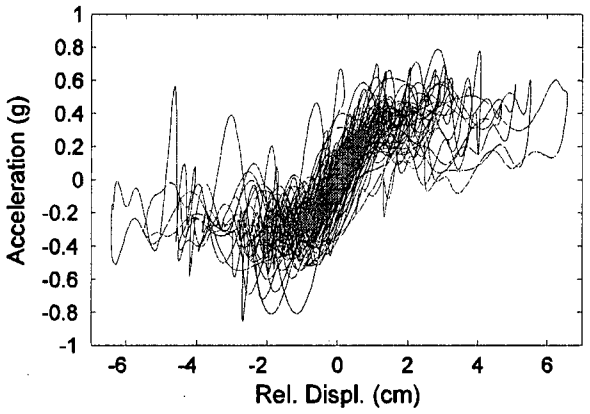


**Crack Acceleration vs. Relative Crack Displacement**

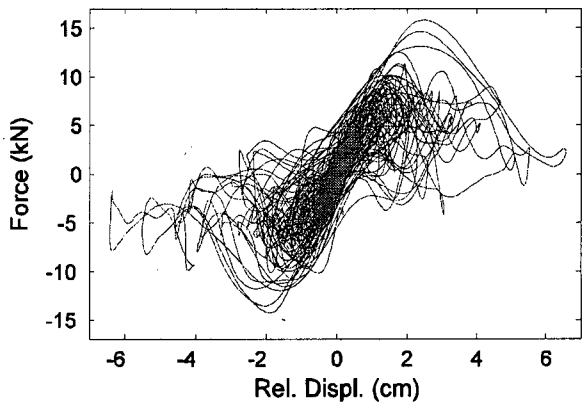


**Total Force vs. Relative Crack Displacement**

| | | | |
|---|---|---|---|
| **Initial Period:** | 0.24s | **Cracked Stiffness:** | 7.4kN/cm |

## G.4 Wall PD

### G.4.1 Test PD1-0.79*

| | | | | | | | | | |
|---|---|---|---|---|---|---|---|---|---|
| **Wall:** | Poor Quality Collar Joint | **Test Sequence:** | I | | **Test Number:** | PD1-0.79 | | | |
| **Earthquake Record:** | Hayward | **Scale:** | 0.79* | **Site Class:** | D | **PGA:** | 0.42g | **PGD:** | 3.25cm |
| **Wall Condition:** | Crack formed at Header 7 | | | | | | | | |
| **Height:** | 4072mm | **Thickness:** | 353mm | **h/t:** | 11.5 | **Width:** | 1499mm | **Density:** | 1803kg/m$^3$ |
| **Header Location:** | **H4:** | 1741mm | **H7:** | 3131mm | **H8:** | 3589mm | | | |

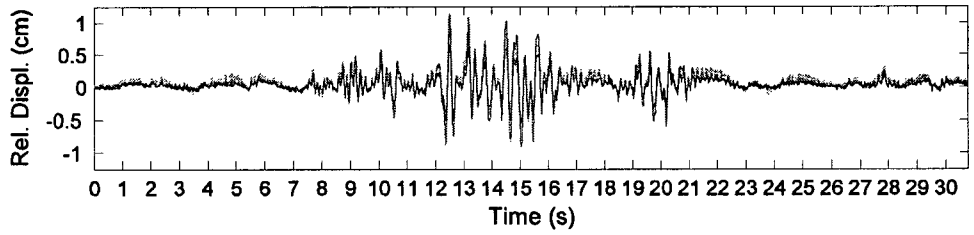


**Relative Displacement Time History (—— H8, —— H7, — H4)**

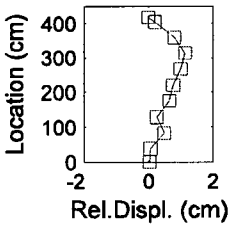


**Profile (t = 12.5s)**

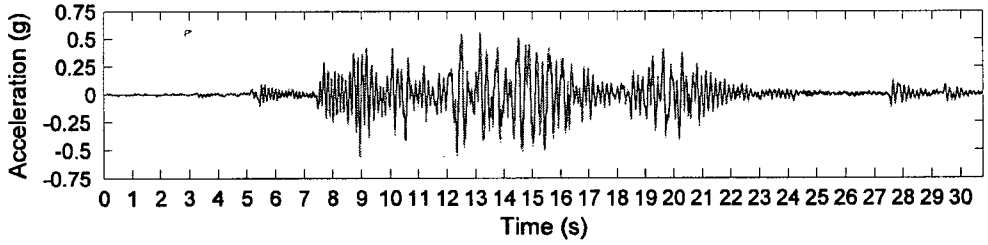


**Acceleration Time History (—— H8, —— H7, — H4)**

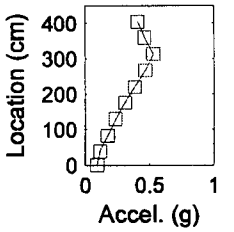


**Profile (t = 12.5s)**

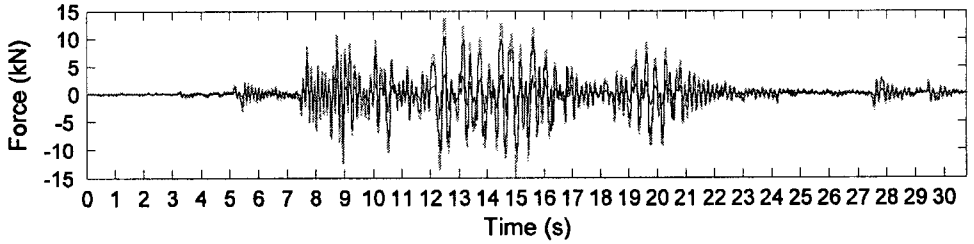


**Force Time History (—— Total, — Lower, — Upper)**

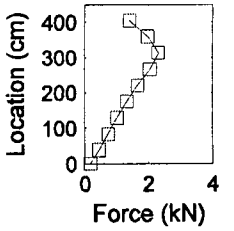


**Profile (t = 12.5s)**

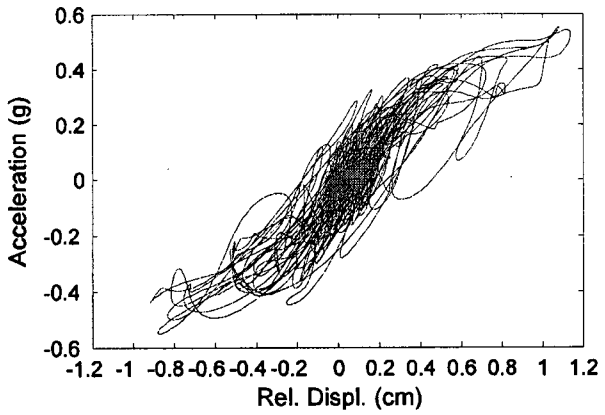


**Crack Acceleration vs. Relative Crack Displacement**

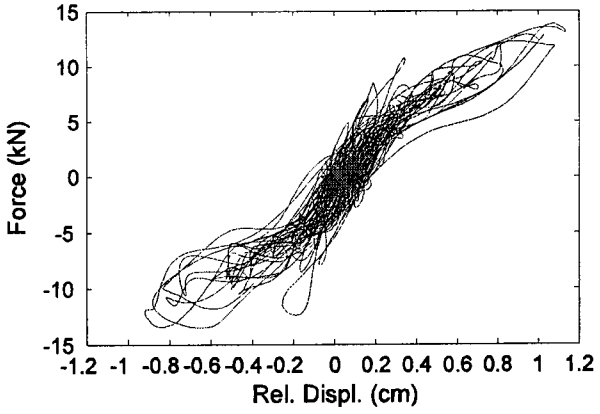


**Total Force vs. Relative Crack Displacement**

| | | | | | |
|---|---|---|---|---|---|
| **Initial Period:** | 0.11s | **Un-Cracked Stiffness:** | 42.40kN/cm | **Cracked Stiffness:** | 27.69kN/cm |

*Scaled to UHS PGA

## G.4.2 Test PD2-0.78

| | | | | | | | | | |
|---|---|---|---|---|---|---|---|---|---|
| **Wall:** | Poor Quality Collar Joint | **Test Sequence:** | 2 | | **Test Number:** | PD2-0.78 | | | |
| **Earthquake Record:** | Hayward | **Scale:** | 0.78 | **Site Class:** | D | **PGA:** | 0.49g | **PGD:** | 3.94cm |
| **Wall Condition:** | Crack at Header 7, new crack formed at H1 | | | | | | | | |
| **Height:** | 4072mm | **Thickness:** | 353mm | **h/t:** | 11.5 | **Width:** | 1499mm | **Density:** | 1803kg/m$^3$ |
| **Header Location:** | | **H4:** | 1741mm | **H7:** | 3131mm | **H8:** | 3589mm | | |

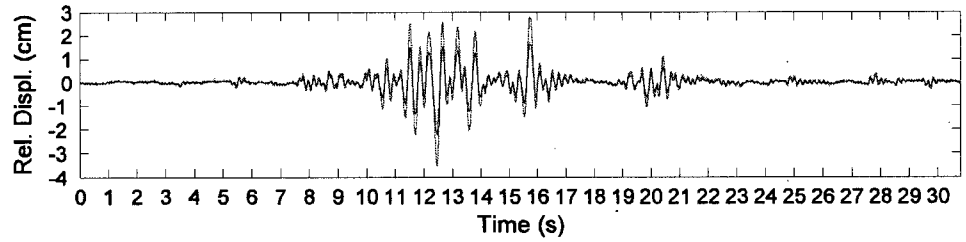


**Relative Displacement Time History (—— H8, —— H7, — H4)**

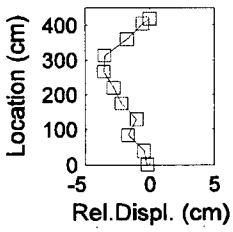


**Profile (t = 12.46s)**

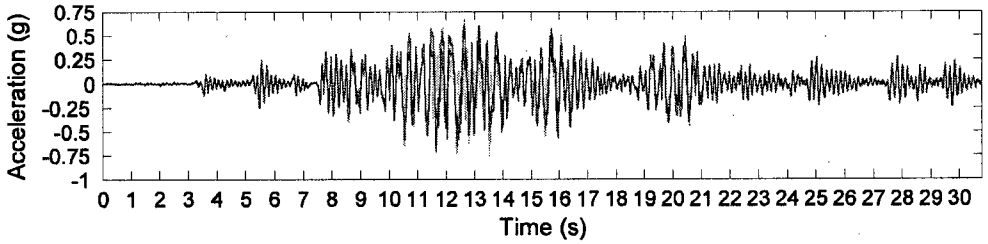


**Acceleration Time History (—— H8, —— H7, — H4)**

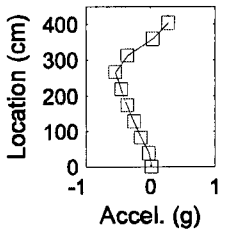


**Profile (t = 12.46s)**

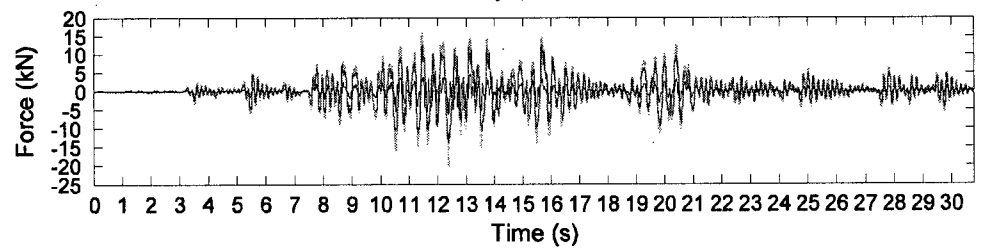


**Force Time History (—— Total, —— Lower, — Upper)**

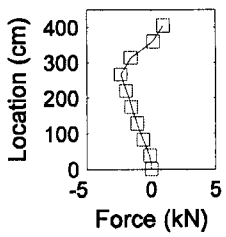


**Profile (t = 12.46s)**

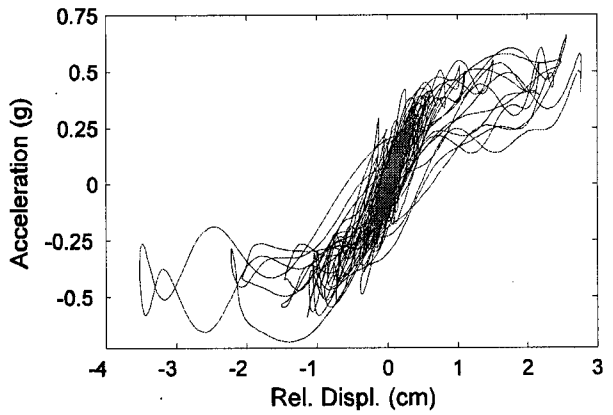


**Crack Acceleration vs. Relative Crack Displacement**

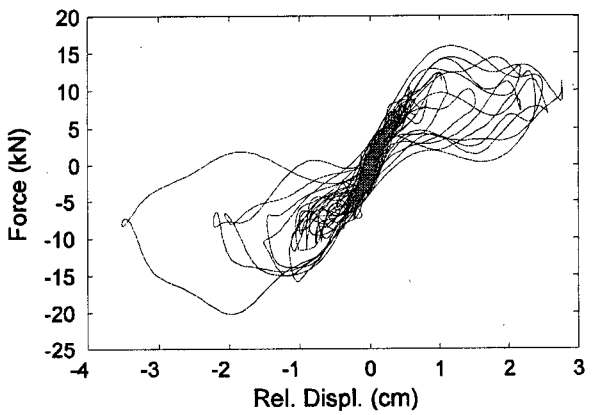


**Total Force vs. Relative Crack Displacement**

| | | | |
|---|---|---|---|
| **Initial Period:** | 0.13s | **Initial Stiffness:** | 19.81kN/cm |

## G.4.3 Test PD3-0.97

| | | | | | | | | | |
|---|---|---|---|---|---|---|---|---|---|
| **Wall:** | Poor Quality Collar Joint | | **Test Sequence:** | 3 | | **Test Number:** | PD3-0.97 | | |
| **Earthquake Record:** | Hayward | | **Scale:** | 0.97 | **Site Class:** | D | **PGA:** | 0.77g | **PGD:** 5.19cm |
| **Wall Condition:** | Crack at Header 7 and 1 | | | | | | | | |
| **Height:** | 4072mm | **Thickness:** | 353mm | **h/t:** | 11.5 | **Width:** | 1499mm | **Density:** | 1803kg/m$^3$ |
| **Header Location:** | **H4:** | 1741mm | **H7:** | 3131mm | **H8:** | 3589mm | | | |

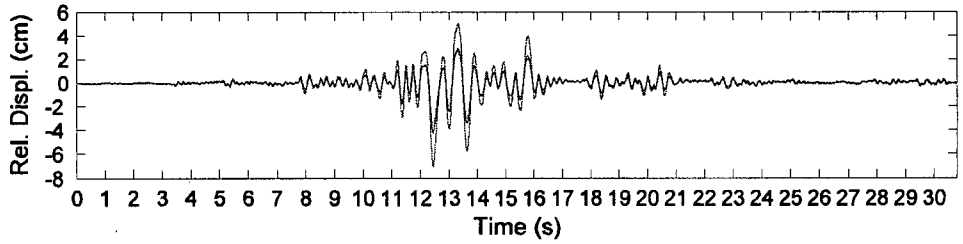


**Relative Displacement Time History (—— H8, —— H7, —— H4)**

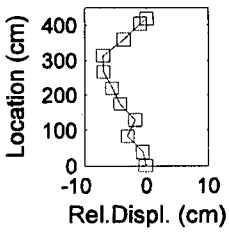


**Profile (t = 12.45s)**

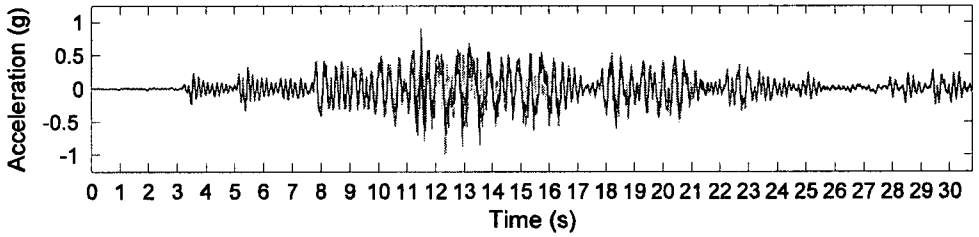


**Acceleration Time History (—— H8, —— H7, —— H4)**

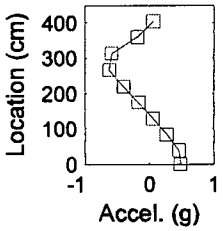


**Profile (t = 12.45s)**

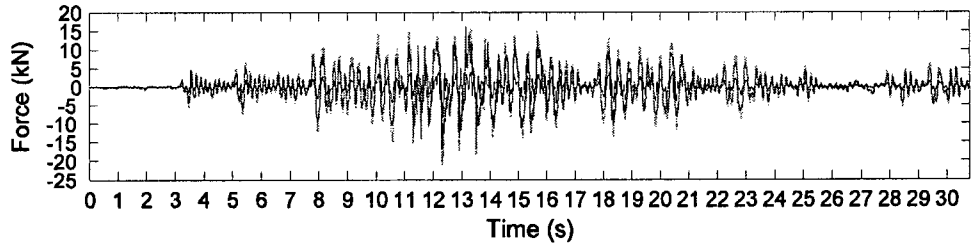


**Force Time History (—— Total, —— Lower, —— Upper)**

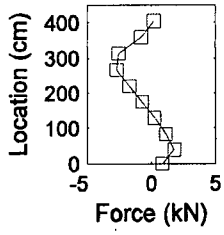


**Profile (t = 12.45s)**

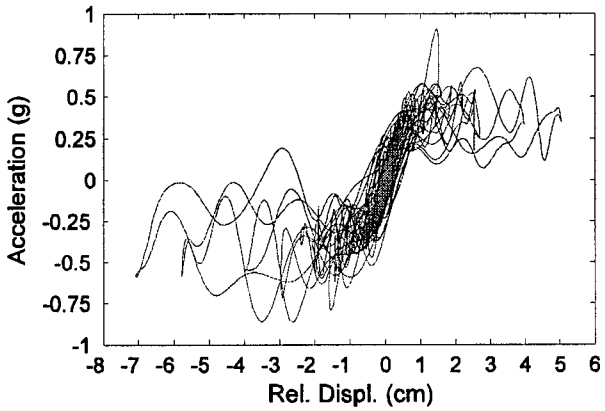


**Crack Acceleration vs. Relative Crack Displacement**

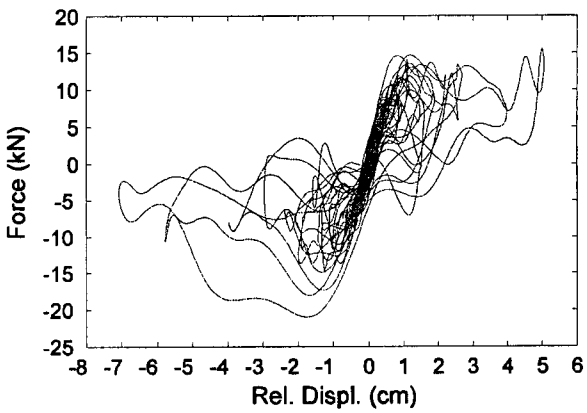


**Total Force vs. Relative Crack Displacement**

| | | | |
|---|---|---|---|
| **Initial Period:** | 0.13s | **Initial Stiffness:** | 18.57kN/cm |

## G.4.4 Test PD4-1.20

| | | | | | | | | | |
|---|---|---|---|---|---|---|---|---|---|
| **Wall:** | Poor Quality Collar Joint | | **Test Sequence:** | 4 | | **Test Number:** | PD4-1.20 | | |
| **Earthquake Record:** | Hayward | | **Scale:** | 1.20 | **Site Class:** | D | **PGA:** | 1.1g | **PGD:** | 6.25cm |
| **Wall Condition:** | Crack at Header 7 and 1 | | | | | | | | | |
| **Height:** | 4072mm | **Thickness:** | 353mm | **h/t:** | 11.5 | **Width:** | 1499mm | | **Density:** | 1803kg/m$^3$ |
| **Header Location:** | **H4:** | 1741mm | **H7:** | 3131mm | **H8:** | 3589mm | | | | |

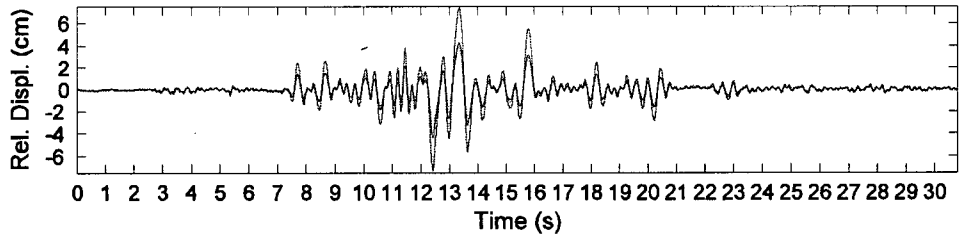


**Relative Displacement Time History (..... H8, ---- H7, — H4)**

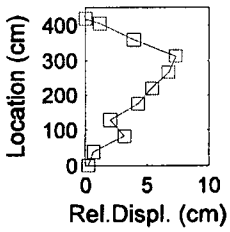


**Profile (t = 13.35s)**

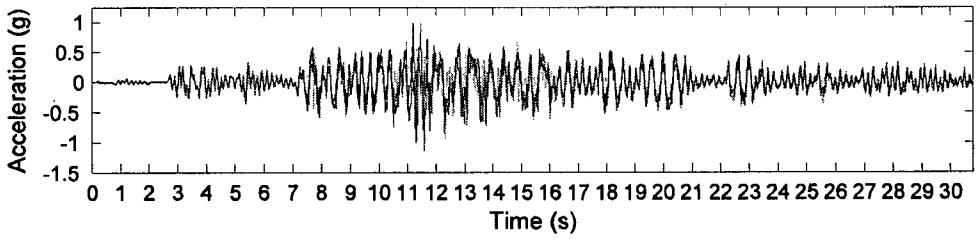


**Acceleration Time History (..... H8, ---- H7, — H4)**

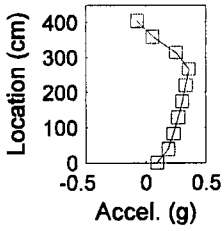


**Profile (t = 13.35s)**

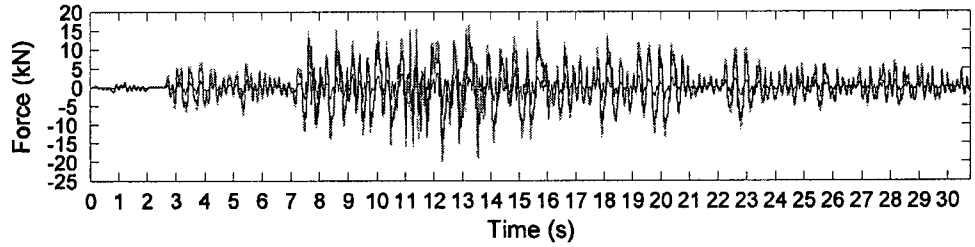


**Force Time History (..... Total, ---- Lower, — Upper)**

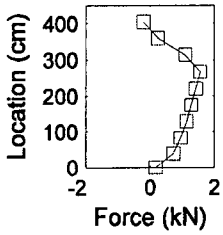


**Profile (t = 13.35s)**

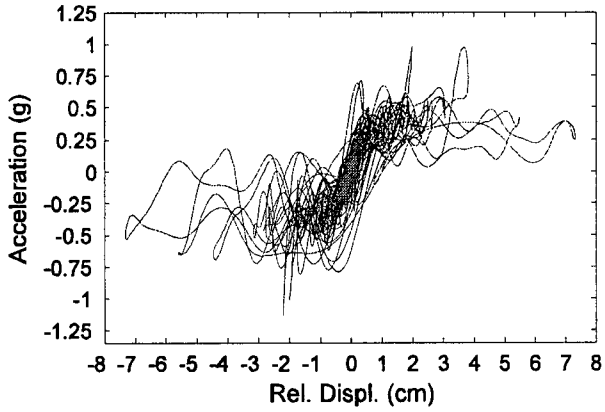


**Crack Acceleration vs. Relative Crack Displacement**

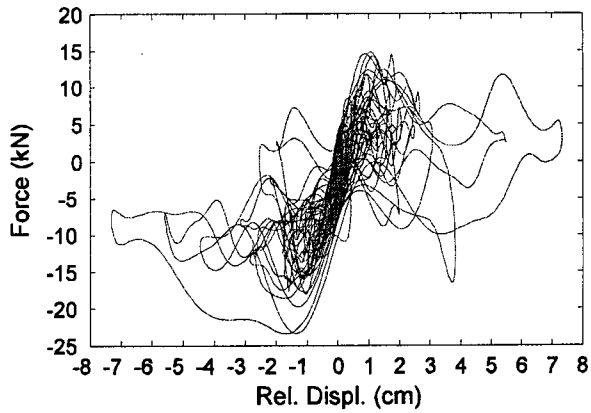


**Total Force vs. Relative Crack Displacement**

| | | | |
|---|---|---|---|
| **Initial Period:** | 0.14s | **Initial Stiffness:** | 27.79kN/cm |

## G.4.5 Test PD5-1.66

| | | | | | | | | | |
|---|---|---|---|---|---|---|---|---|---|
| **Wall:** | Poor Quality Collar Joint | | **Test Sequence:** | 8 | | **Test Number:** | PD5-1.66 | | |
| **Earthquake Record:** | Hayward | | **Scale:** | 1.66 | **Site Class:** | D | **PGA:** | 1.25g | **PGD:** 9.11cm |
| **Wall Condition:** | Crack at Header 7 and 1 | | | | | | | | |
| **Height:** | 4072mm | **Thickness:** | 353mm | **h/t:** | 11.5 | **Width:** | 1499mm | **Density:** | 1803kg/m$^3$ |
| **Header Location:** | **H4:** | 1741mm | **H7:** | 3131mm | **H8:** | 3589mm | | | |

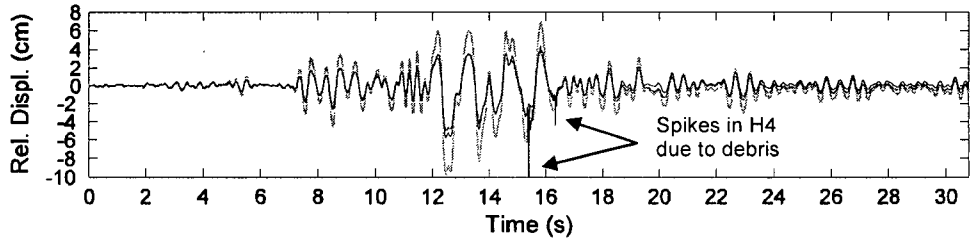


**Relative Displacement Time History (···· H8, ---- H7, — H4)**

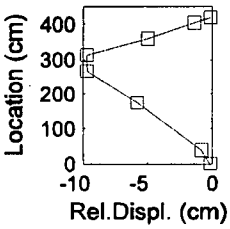


**Profile (t = 12.47s)**

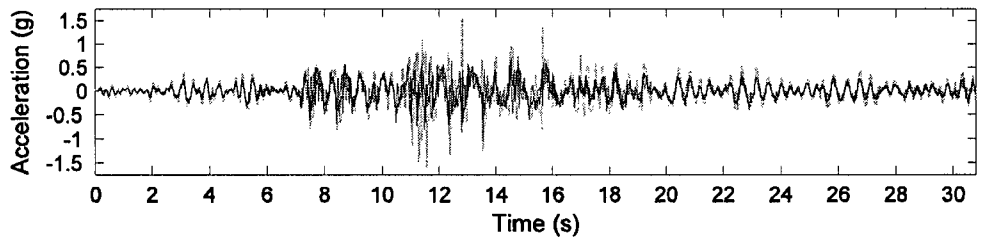


**Acceleration Time History (···· H8, ---- H7, — H4)**

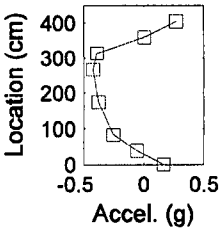


**Profile (t = 12.47s)**

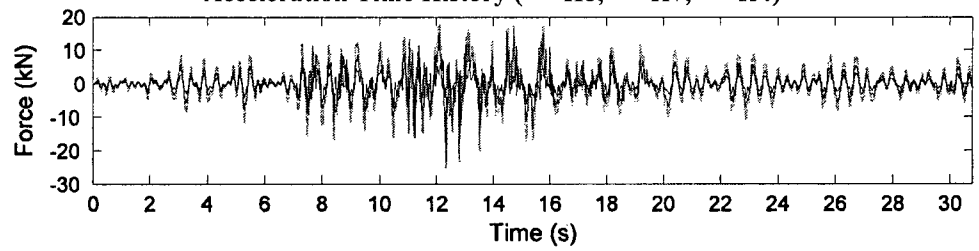


**Force Time History (···· Total, ---- Lower, — Upper)**

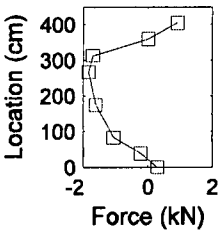


**Profile (t = 12.47s)**

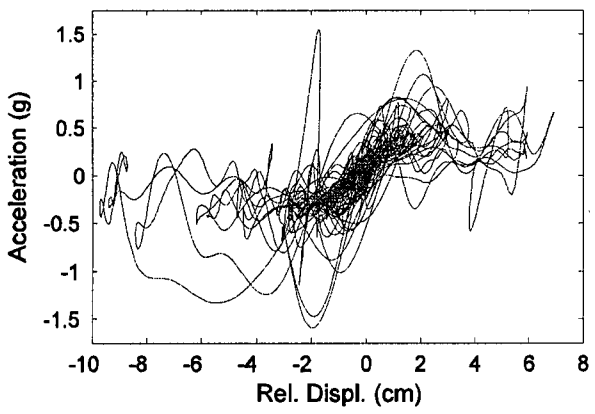


**Crack Acceleration vs. Relative Crack Displacement**

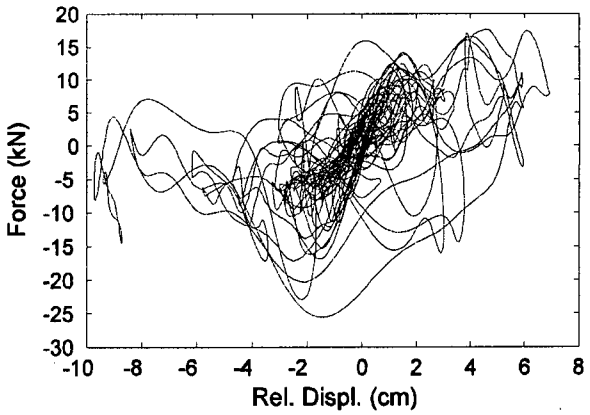


**Total Force vs. Relative Crack Displacement**

| | | | | | |
|---|---|---|---|---|---|
| **Initial Period:** | 0.22s | **Initial Stiffness:** | 10.95kN/cm | **Second Stiffness:** | 8.32kN/cm |

## G.4.6 Test PD6-2.22

| | | | | | | | | | |
|---|---|---|---|---|---|---|---|---|---|
| **Wall:** | Poor Quality Collar Joint | **Test Sequence:** | 10 (Wall Collapse) | | **Test Number:** | PD6-2.22 | | | |
| **Earthquake Record:** | Hayward | **Scale:** | 2.22 | **Site Class:** | D | **PGA:** | 1.55g | **PGD:** | 13cm |
| **Wall Condition:** | Crack at Header 7 and 1, only instrumentation on wall at H7, Wall Collapse | | | | | | | | |
| **Height:** | 4072mm | **Thickness:** | 353mm | **h/t:** | 11.5 | **Width:** | 1499mm | **Density:** | 1803kg/m$^3$ |
| **Header Location:** | | | | **H7:** | 3131mm | | | | |

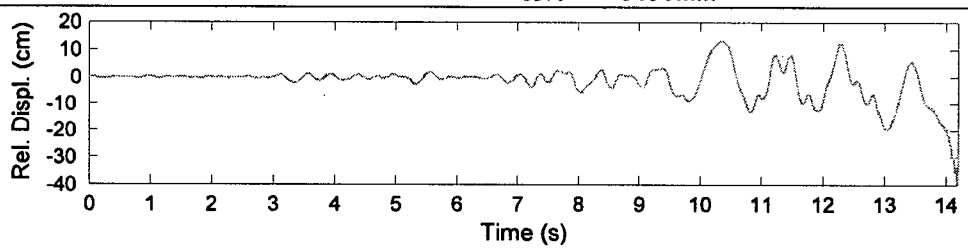


**Relative Displacement Time History (—— H7)**

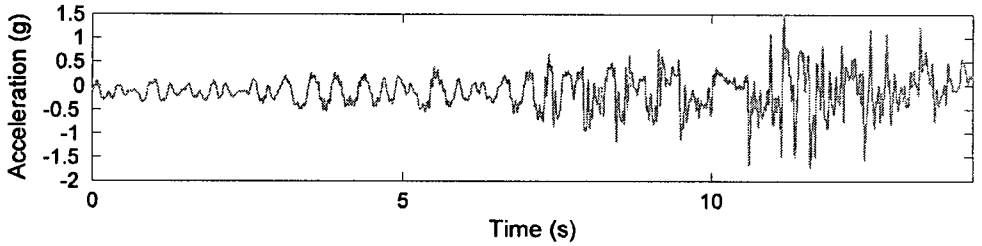


**Acceleration Time History (—— H7)**

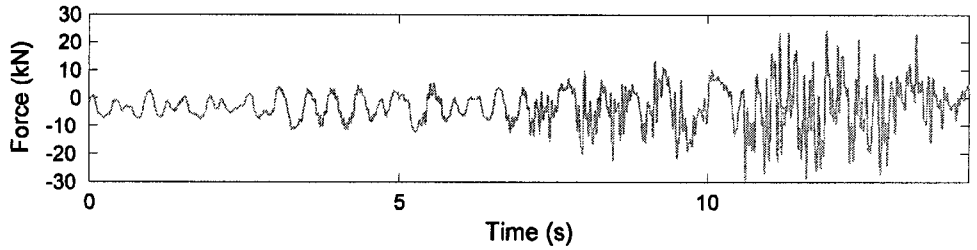


**Force Time History (—— Total)**

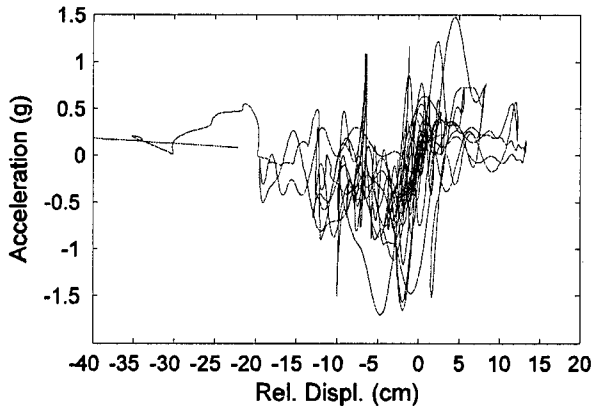


**Crack Acceleration vs. Relative Crack Displacement**

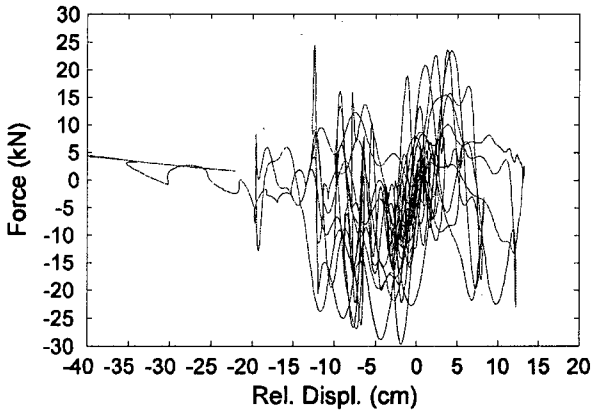


**Total Force vs. Relative Crack Displacement**

**Initial Stiffness:** 9.5kN/cm

## G.4.7 Test PD(Sub1)1-1.02

| | | | | | | | | | |
|---|---|---|---|---|---|---|---|---|---|
| **Wall:** | Poor Quality Collar Joint | **Test Sequence:** | 5 (Subduction) | **Test Number:** | PD(Sub1)1-1.02 | | | | |
| **Earthquake Record:** | HKD 109 | **Scale:** | 1.02 | **Site Class:** | D | **PGA:** | 0.64g | **PGD:** | 11.4cm |
| **Wall Condition:** | Crack at Header 7 and 1 | | | | | | | | |
| **Height:** | 4072mm | **Thickness:** | 353mm | **h/t:** | 11.5 | **Width:** | 1499mm | **Density:** | 1803kg/m$^3$ |
| **Header Location:** | **H1:** | 384mm | **H7:** | 3131mm | **H8:** | 3589mm | | | |

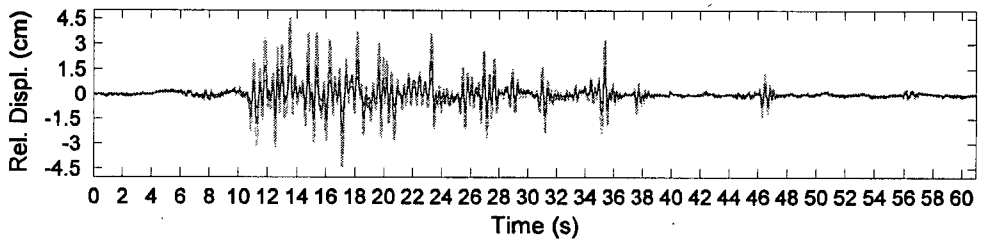


**Relative Displacement Time History (—— H7, —— H8, —— H1)**

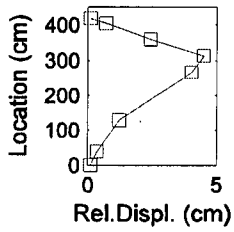


**Profile (t = 13.55s)**

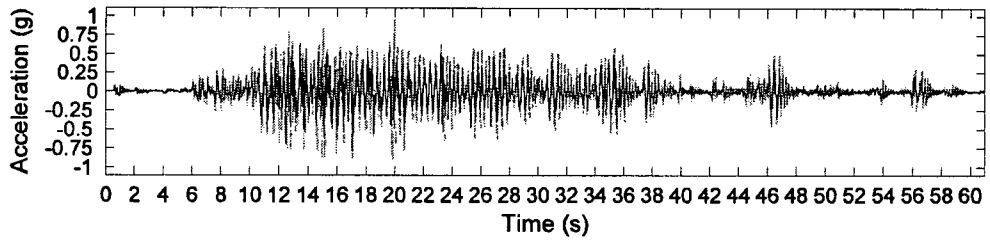


**Acceleration Time History (—— H7, —— H8, —— H1)**

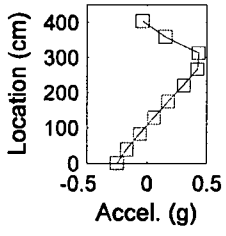


**Profile (t = 13.55s)**

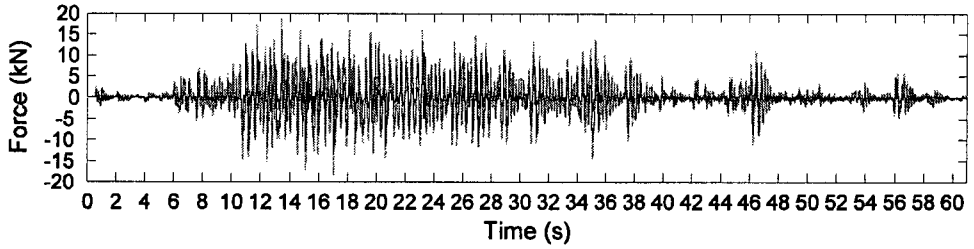


**Force Time History (—— Total, —— Lower, —— Upper)**

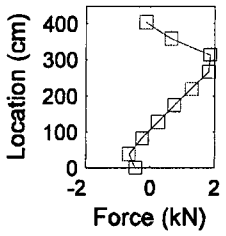


**Profile (t = 13.55s)**

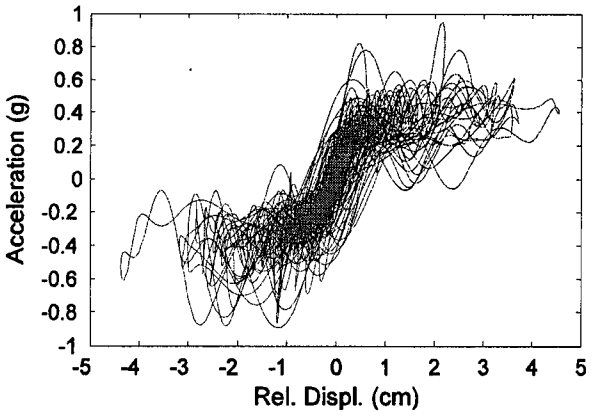


**Crack Acceleration vs. Relative Crack Displacement**

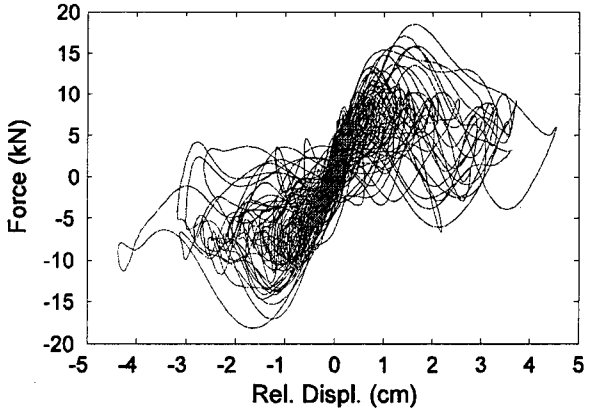


**Total Force vs. Relative Crack Displacement**

| | | | |
|---|---|---|---|
| **Initial Period:** | 0.14s | **Initial Stiffness:** | 16.1kN/cm |

## G.4.8 Test PD(Sub1)2-1.11

| | | | | | | | | | |
|---|---|---|---|---|---|---|---|---|---|
| **Wall:** | Poor Quality Collar Joint | **Test Sequence:** | 6 (Subduction) | **Test Number:** | PD(Sub1)2-1.11 | | | | |
| **Earthquake Record:** | HKD 109 | **Scale:** | 1.11 | **Site Class:** | D | **PGA:** | 0.80g | **PGD:** | 12.4cm |
| **Wall Condition:** | Crack at Header 7 and 1 | | | | | | | | |
| **Height:** | 4072mm | **Thickness:** | 353mm | **h/t:** | 11.5 | **Width:** | 1499mm | **Density:** | 1803kg/m$^3$ |
| **Header Location:** | | **H4:** | 174mm | **H7:** | 3131mm | **H8:** | 3589mm | | |

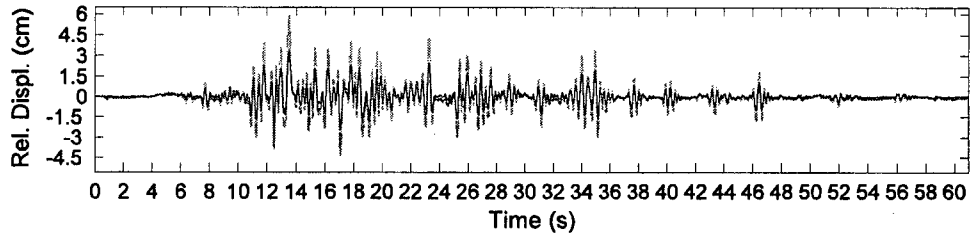


Relative Displacement Time History (..... H7, ..... H8, — H4)

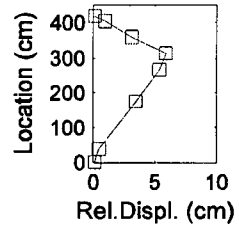


Profile (t = 13.51s)

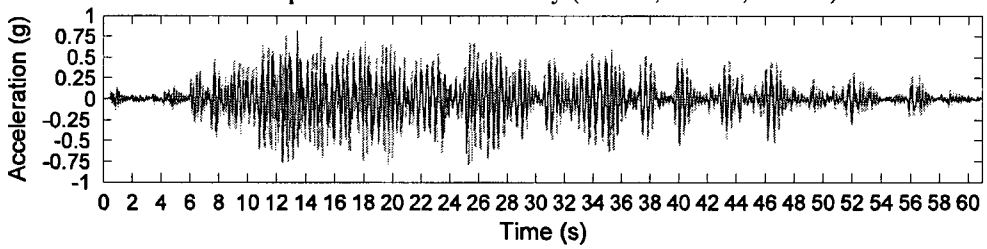


Acceleration Time History (..... H7, ..... H8, — H1)

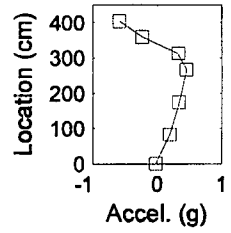


Profile (t = 13.51s)

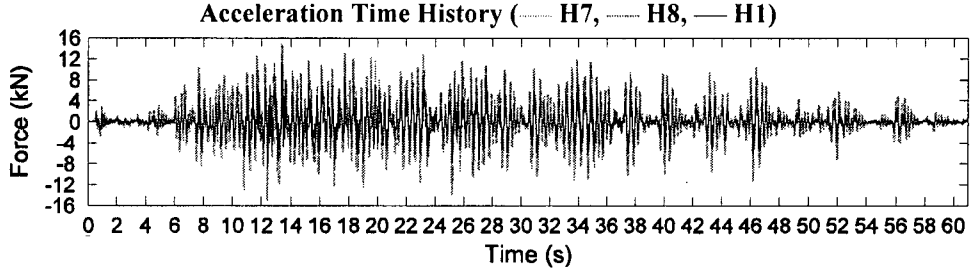


Force Time History (..... Total, ..... Lower, — Upper)

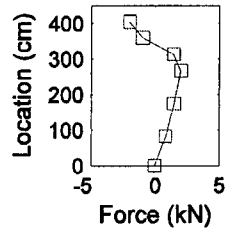


Profile (t = 13.51s)

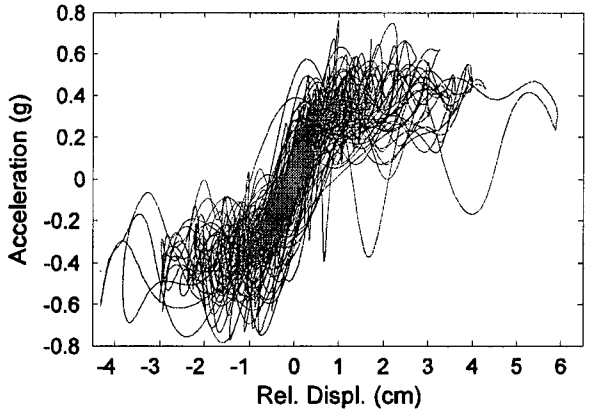


Crack Acceleration vs. Relative Crack Displacement

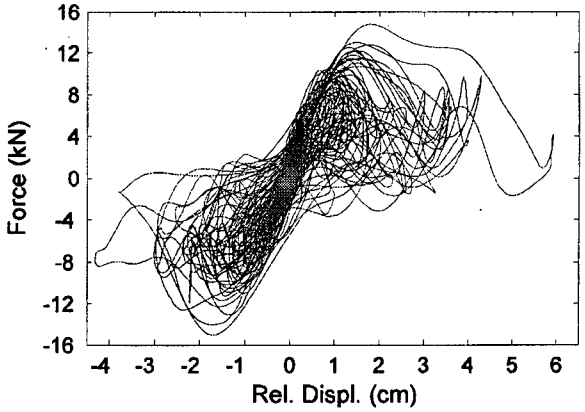


Total Force vs. Relative Crack Displacement

| | | | |
|---|---|---|---|
| **Initial Period:** | 0.13s | **Initial Stiffness:** | 10.9kN/cm |

## G.4.9 Test PD(Sub1)3-1.25

| | | | | | | | | | |
|---|---|---|---|---|---|---|---|---|---|
| **Wall:** | Poor Quality Collar Joint | | **Test Sequence:** | 7 (Subduction) | | **Test Number:** | PD(Sub1)3-1.25 | | |
| **Earthquake Record:** | HKD 109 | **Scale:** | 1.25 | **Site Class:** | D | **PGA:** | 0.86g | **PGD:** | 14.0cm |
| **Wall Condition:** | Crack at Header 7 and 1 | | | | | | | | |
| **Height:** | 4072mm | **Thickness:** | 353mm | **h/t:** | 11.5 | **Width:** | 1499mm | **Density:** | 1803kg/m$^3$ |
| **Header Location:** | | **H4:** | 174mm | **H7:** | 3131mm | **H8:** | 3589mm | | |

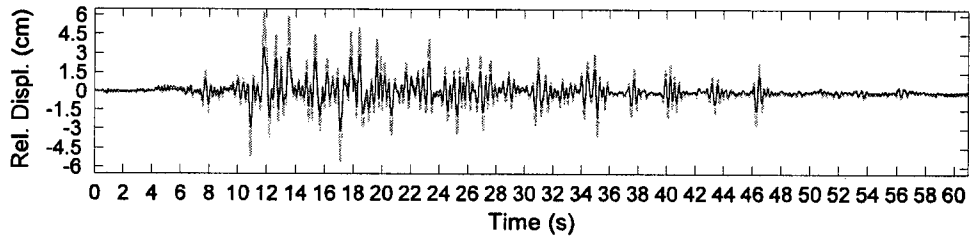


**Relative Displacement Time History (— H7, — H8, — H4)**

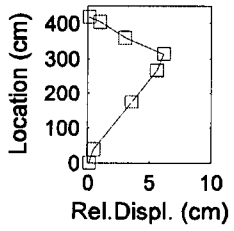


**Profile (t = 11.8s)**

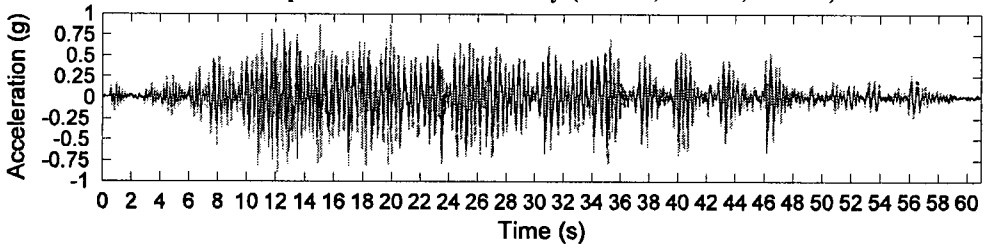


**Acceleration Time History (— H7, — H8, — H1)**

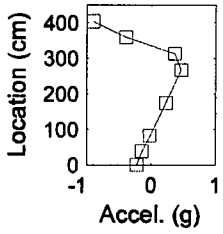


**Profile (t = 11.8s)**

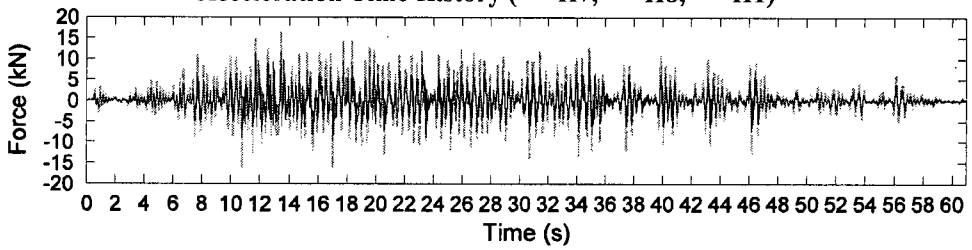


**Force Time History (— Total, — Lower, — Upper)**

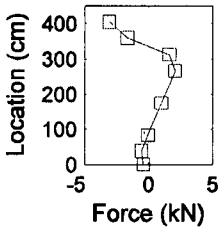


**Profile (t = 11.8s)**

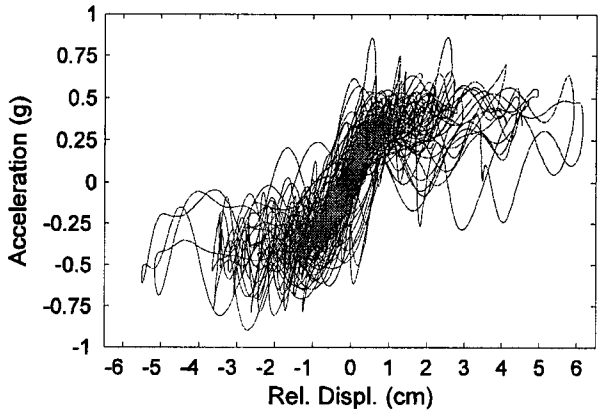


**Crack Acceleration vs. Relative Crack Displacement**

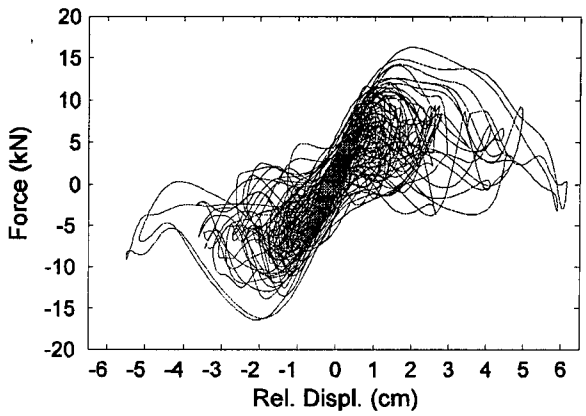


**Total Force vs. Relative Crack Displacement**

| | | | |
|---|---|---|---|
| **Initial Period:** | 0.19s | **Initial Stiffness:** | 9.58kN/cm |

## G.4.10 Test PD(Sub2)1-1.10

| | | | | | | | | | |
|---|---|---|---|---|---|---|---|---|---|
| **Wall:** | Poor Quality Collar Joint | **Test Sequence:** | 9 (Subduction) | | | **Test Number:** | PD(Sub2)1-1.10 | | |
| **Earthquake Record:** | HKD 085 | **Scale:** | 1.10 | **Site Class:** | D | **PGA:** | 0.76g | **PGD:** | 15.4cm |
| **Wall Condition:** | Crack at Header 7 and 1, only instrumentation on wall at H7 | | | | | | | | |
| **Height:** | 4072mm | **Thickness:** | 353mm | **h/t:** | 11.5 | **Width:** | 1499mm | **Density:** | 1803kg/m$^3$ |
| **Header Location:** | | | | **H7:** | 3131mm | | | | |

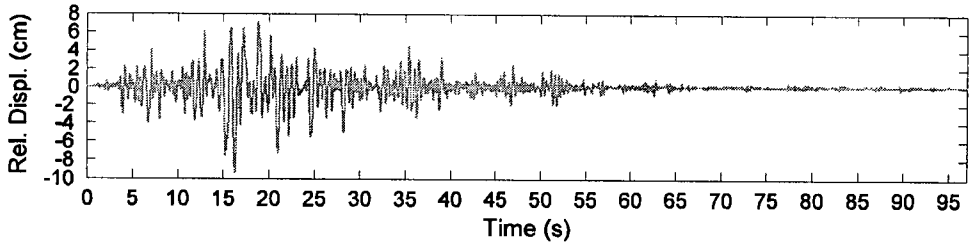


**Relative Displacement Time History (—— H7)**

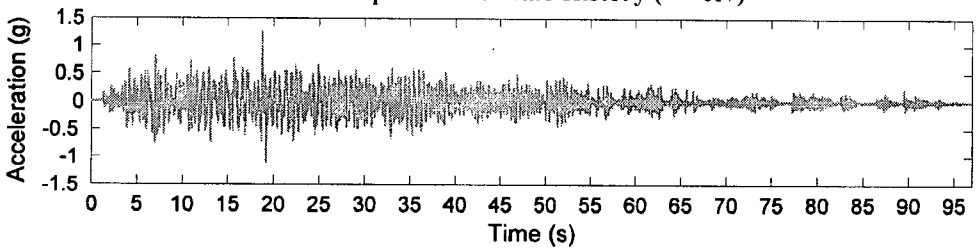


**Acceleration Time History (—— H7)**

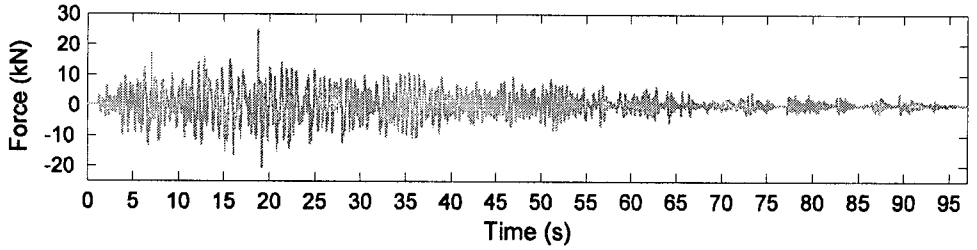


**Force Time History (—— Total)**

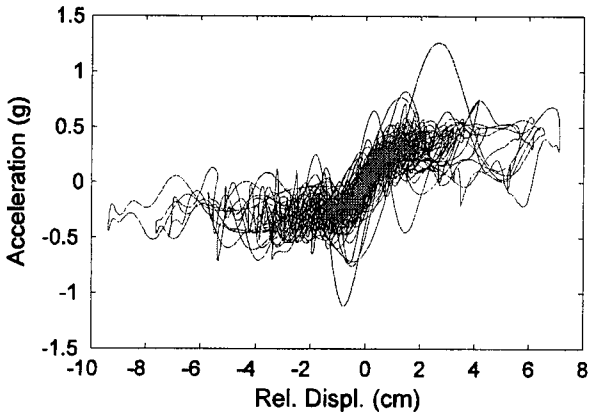


**Crack Acceleration vs. Relative Crack Displacement**

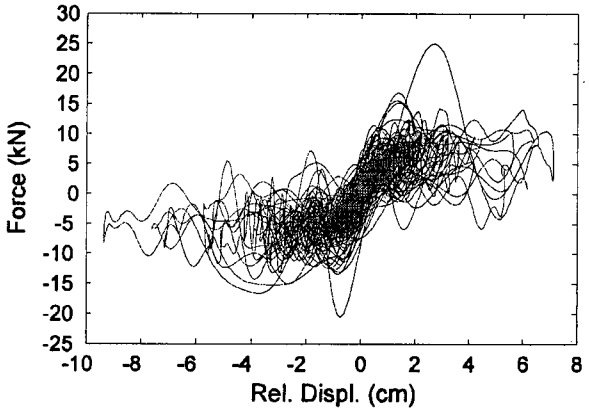


**Total Force vs. Relative Crack Displacement**

| | | | |
|---|---|---|---|
| **Initial Period:** | 0.22s | **Initial Stiffness:** | 11.0kN/cm |

# APPENDIX H. WORKING MODEL RESULTS AND COMPARISIONS

# H.1 Wall PC

## H.1.1 Test PC1-0.73*

| | | | | | | | | | | | |
|---|---|---|---|---|---|---|---|---|---|---|---|
| **Wall:** | Poor Quality Collar Joint | | | **Test Sequence:** | 1 | | | **Test Number:** | | PC1-0.73 | |
| **Earthquake Record:** | Gilroy | | | **Scale:** | 0.73* | **Site Class:** | C | **PGA:** | 0.35g | **PGD:** | 1.89cm |
| **Wall Condition:** | No visible damage | | | | | | | | | | |
| **Height:** | 4153mm | **Thickness:** | 355mm | **h/t:** | 11.7 | **Width:** | 1498mm | **Density:** | 1764.5kg/m$^3$ | | |
| **Header Location:** | | **H3:** | 1317mm | **H6:** | 2682mm | **H8:** | 3586mm | | | | |

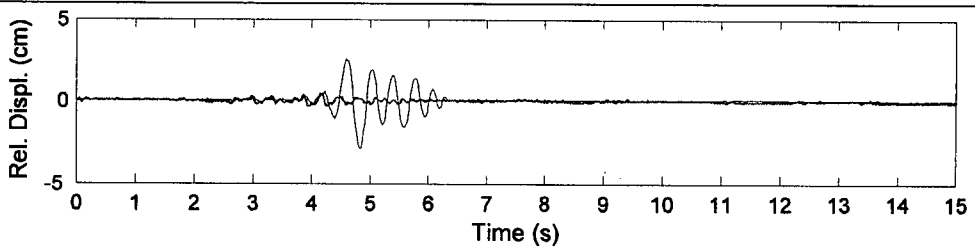


**Relative Displacement Time History at Crack**

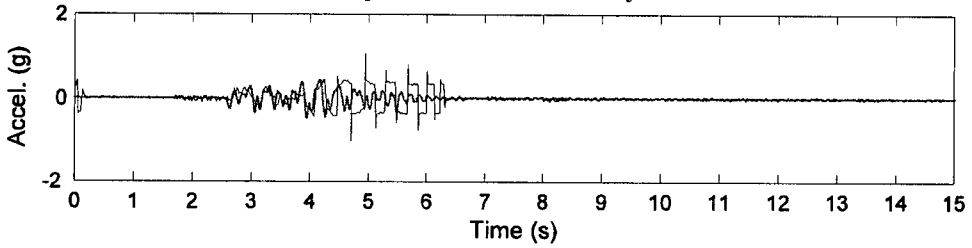


**Acceleration Time History at Crack**

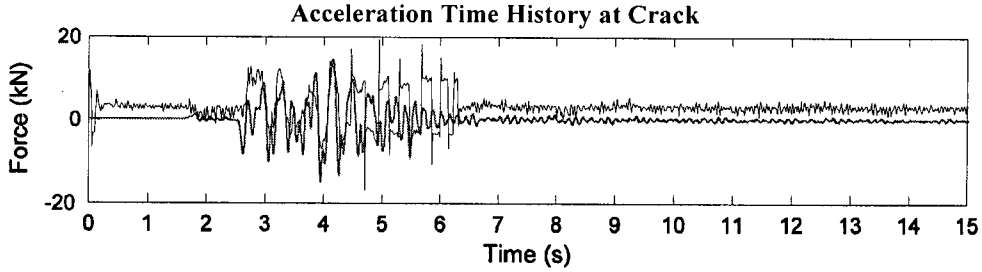


**Force Time History**

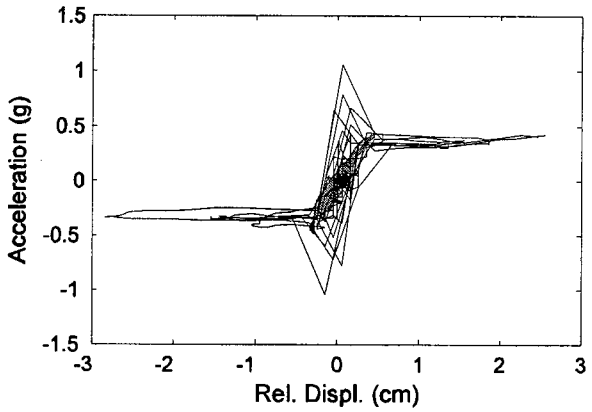


**Crack Acceleration vs. Relative Crack Displacement**

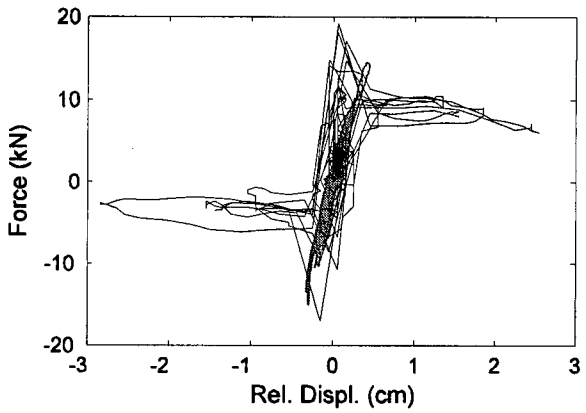


**Total Force vs. Relative Crack Displacement**

( —— Full Scale Test, — Working Model)

***Note:*** *WM assumes a previously cracked wall*

## H.1.2 Test PC2-1.10*

| | | | | | | | | | |
|---|---|---|---|---|---|---|---|---|---|
| **Wall:** | Poor Quality Collar Joint | **Test Sequence:** | 2 | | | **Test Number:** | | PC2-1.10 | |
| **Earthquake Record:** | Gilroy | **Scale:** | 1.10* | **Site Class:** | C | **PGA:** | 0.53g | **PGD:** | 3.84cm |
| **Wall Condition:** | Crack formed at Header 6 during test | | | | | | | | |
| **Height:** | 4153mm | **Thickness:** | 355mm | **h/t:** | 11.7 | **Width:** | 1498mm | **Density:** | 1764.5kg/m$^3$ |
| **Header Location:** | | **H3:** | 1317mm | **H6:** | 2682mm | **H8:** | 3586mm | | |

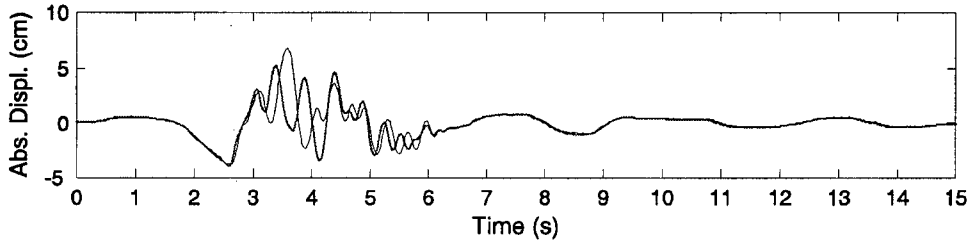


**Relative Displacement Time History**

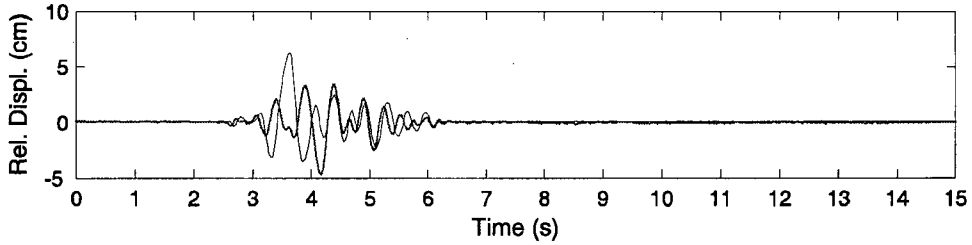


**Acceleration Time History**

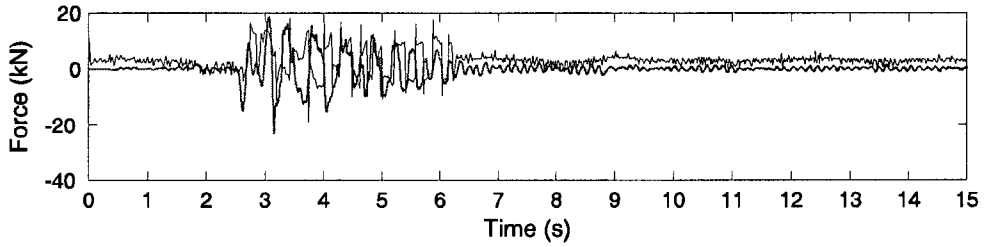


**Force Time History**

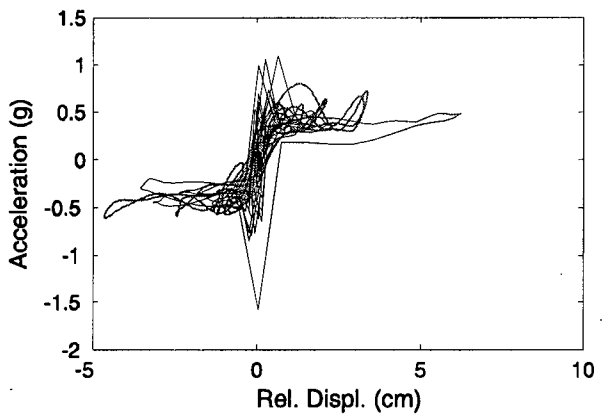


**Crack Acceleration vs. Relative Crack Displacement**

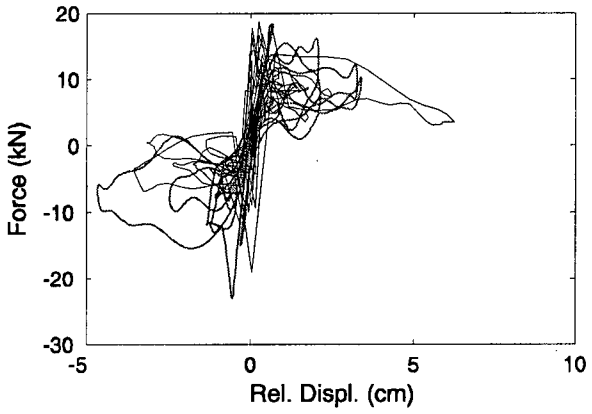


**Total Force vs. Relative Crack Displacement**

**( ..... Full Scale Test, — Working Model)**

*Note: WM assumes a pre-cracked wall*

## H.1.3 Test PC3-0.75

| | | | | | | | | | |
|---|---|---|---|---|---|---|---|---|---|
| **Wall:** | Poor Quality Collar Joint | | **Test Sequence:** | 3 | | **Test Number:** | PC3-0.75 | | |
| **Earthquake Record:** | Gilroy | | **Scale:** | 0.75 | **Site Class:** | C | **PGA:** | 0.73g | **PGD:** 4.87cm |
| **Wall Condition:** | Crack at Header 6 | | | | | | | | |
| **Height:** | 4153mm | **Thickness:** | 355mm | **h/t:** | 11.7 | **Width:** | 1498mm | **Density:** | 1764.5kg/m$^3$ |
| **Header Location:** | | **H3:** | 1317mm | **H6:** | 2682mm | **H8:** | 3586mm | | |

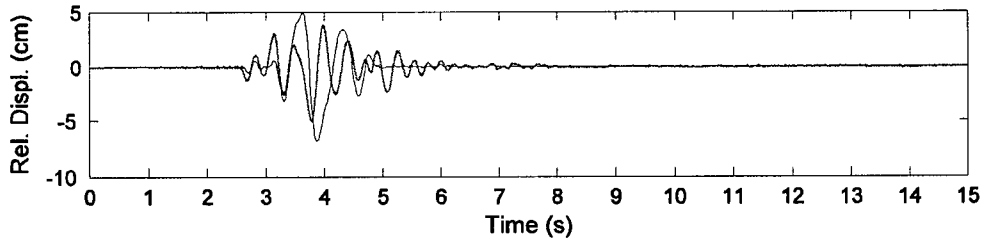


**Relative Displacement Time History at Crack**

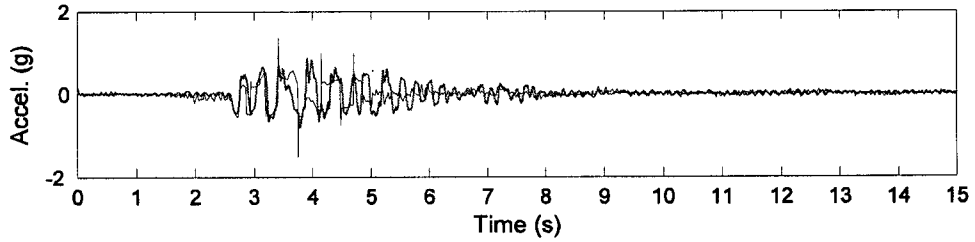


**Acceleration Time History at Crack**

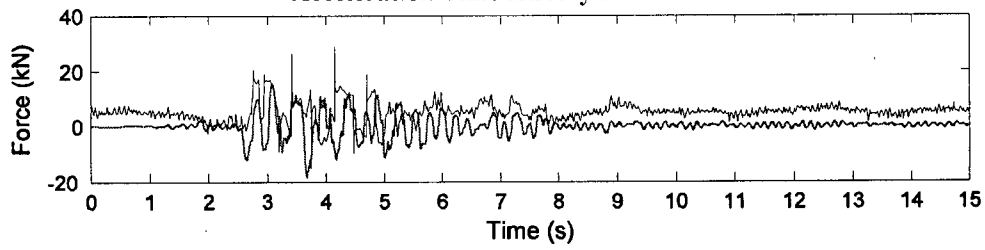


**Force Time History**

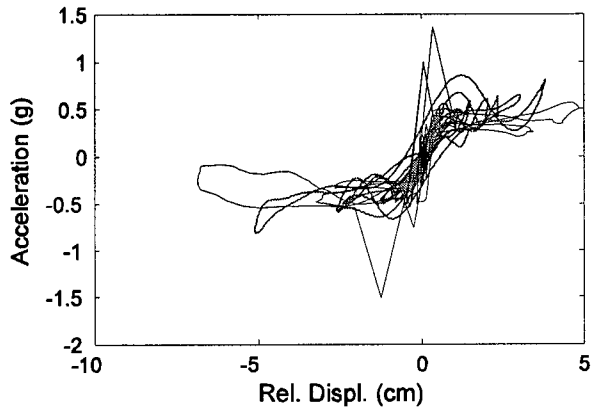


**Crack Acceleration vs. Relative Crack Displacement**

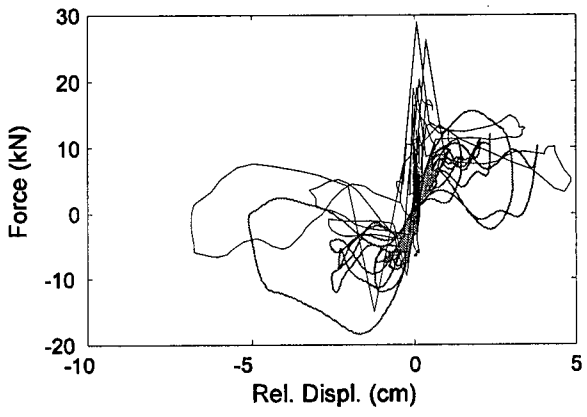


**Total Force vs. Relative Crack Displacement**

**( — Full Scale Test, — Working Model)**

## H.1.4 Test PC4-1.40

| | | | | | | | | | |
|---|---|---|---|---|---|---|---|---|---|
| **Wall:** | Poor Quality Collar Joint | | **Test Sequence:** | 4 | | **Test Number:** | PC4-1.40 | | |
| **Earthquake Record:** | Gilroy | | **Scale:** | 1.40 | **Site Class:** | C | **PGA:** | 1.3g | **PGD:** 9.25cm |
| **Wall Condition:** | Crack at Header 6 | | | | | | | | |
| **Height:** | 4153mm | **Thickness:** | 355mm | **h/t:** | 11.7 | **Width:** | 1498mm | **Density:** | 1764.5kg/m$^3$ |
| **Header Location:** | | **H3:** | 1317mm | **H6:** | 2682mm | **H8:** | 3586mm | | |

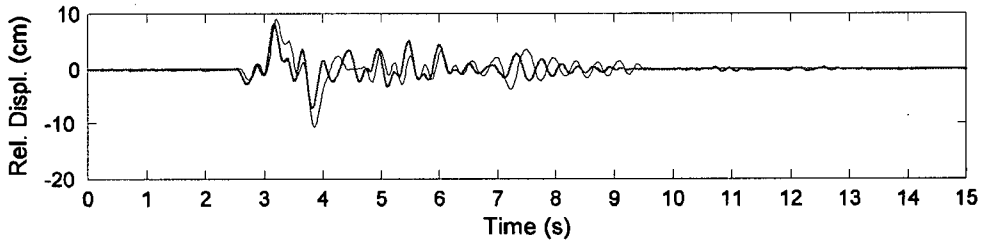


**Relative Displacement Time History at Crack**

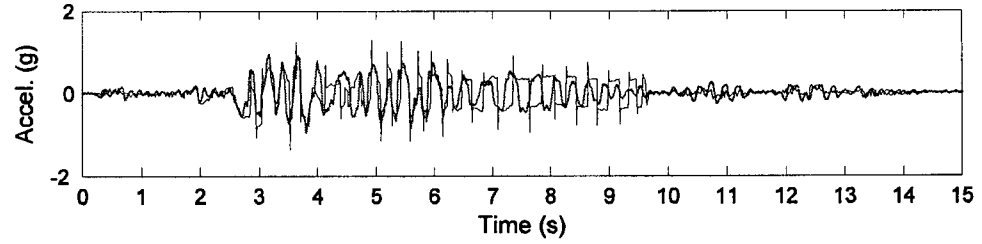


**Acceleration Time History at Crack**

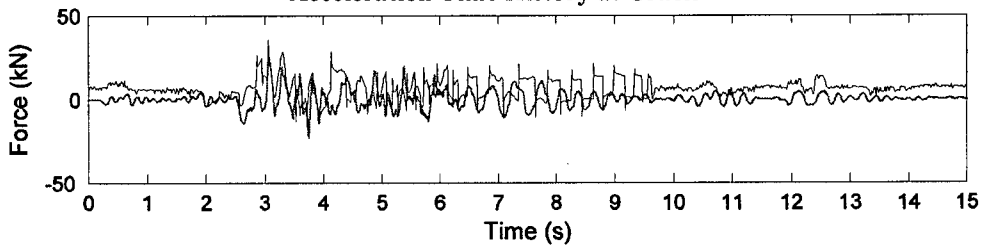


**Force Time History**

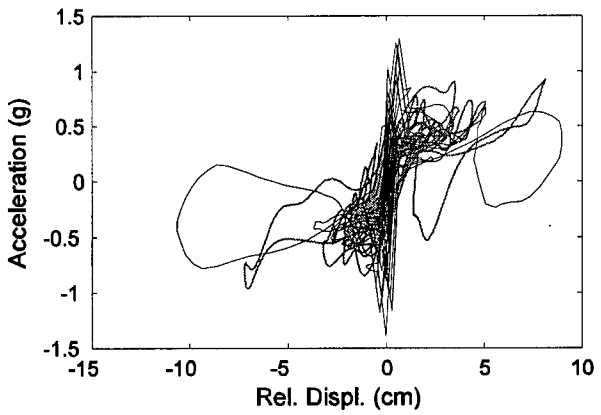


**Crack Acceleration vs. Relative Crack Displacement**

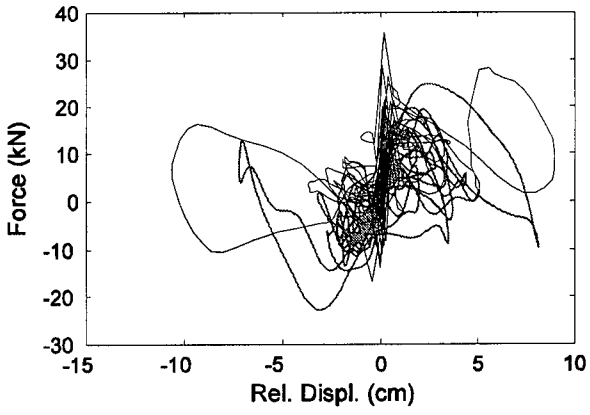


**Total Force vs. Relative Crack Displacement**

**( — Full Scale Test, — Working Model)**

## H.1.5 Test PC5-1.55

| | | | | | | | | | |
|---|---|---|---|---|---|---|---|---|---|
| **Wall:** | Poor Quality Collar Joint | | **Test Sequence:** | 5 | | **Test Number:** | PC5-1.55 | | |
| **Earthquake Record:** | Gilroy | | **Scale:** | 1.55 | **Site Class:** | C | **PGA:** | 1.4g | **PGD:** 11.4cm |
| **Wall Condition:** | Crack at Header 6, Crack formed at Header 1 | | | | | | | | |
| **Height:** | 4153mm | **Thickness:** | 355mm | **h/t:** | 11.7 | **Width:** | 1498mm | **Density:** | 1764.5kg/m$^3$ |
| **Header Location:** | | **H3:** | 1317mm | **H6:** | 2682mm | **H8:** | 3586mm | | |

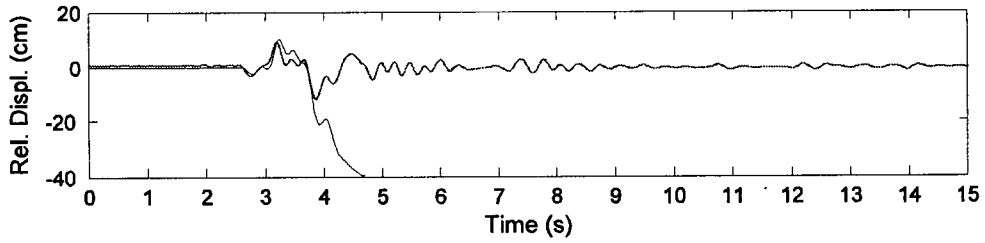


**Relative Displacement Time History at Crack**

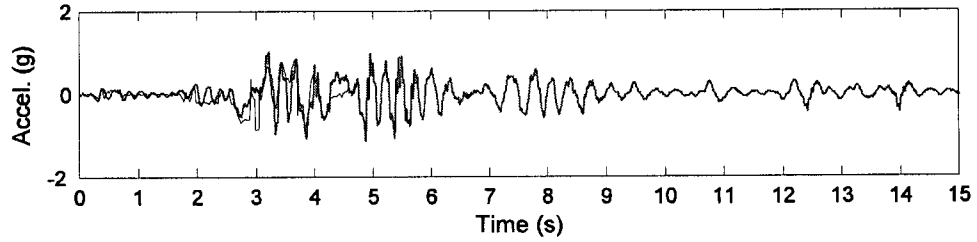


**Acceleration Time History at Crack**

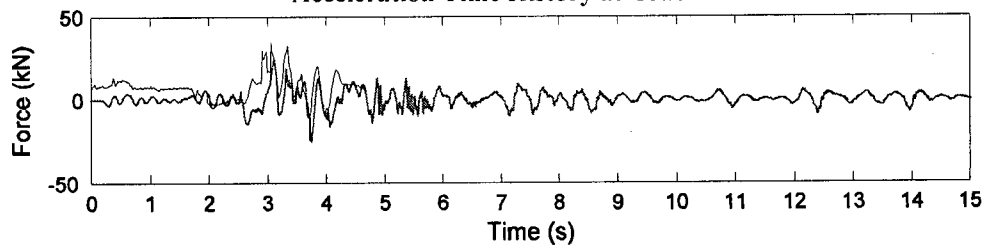


**Force Time History**

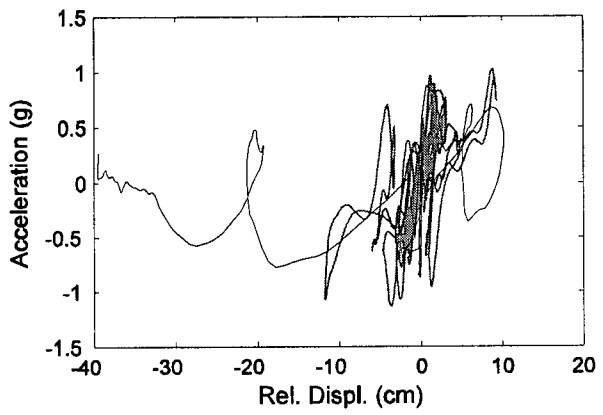


**Crack Acceleration vs. Relative Crack Displacement**

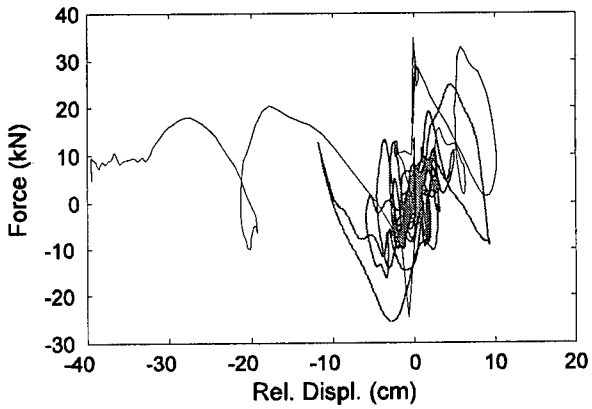


**Total Force vs. Relative Crack Displacement**

**( — Full Scale Test, — Working Model)**

## H.2 Wall PD

### H.2.1 Test PD3-0.97

| | | | | | | | | | |
|---|---|---|---|---|---|---|---|---|---|
| **Wall:** | Poor Quality Collar Joint | | **Test Sequence:** | 3 | | **Test Number:** | PD3-0.97 | | |
| **Earthquake Record:** | Hayward | | **Scale:** | 0.97 | **Site Class:** | D | **PGA:** | 0.77g | **PGD** 5.19cm |
| **Wall Condition:** | Crack at Header 7 and 1 | | | | | | | | |
| **Height:** | 4072mm | **Thickness:** | 353mm | **h/t:** | 11.5 | **Width:** | 1499mm | **Density:** | 1803kg/m$^3$ |
| **Header Location:** | | **H4:** | 1741mm | **H7:** | 3131mm | **H8:** | 3589mm | | |

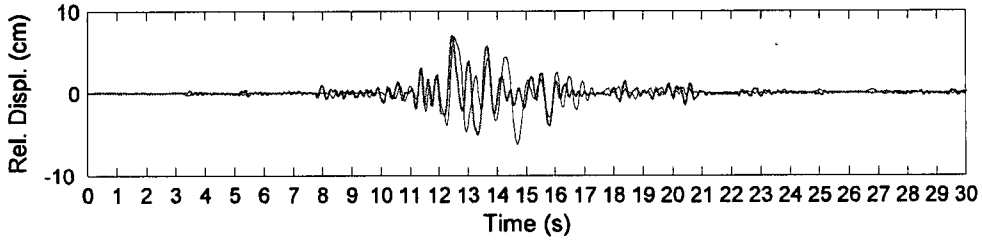


**Relative Displacement Time History at Crack**

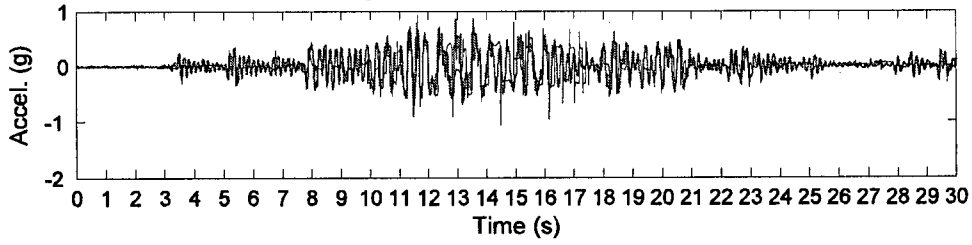


**Acceleration Time History at Crack**

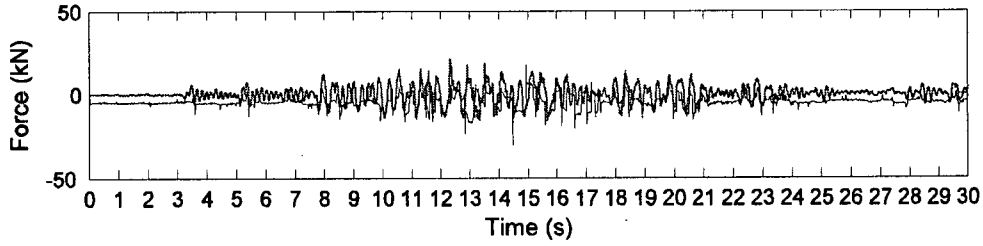


**Force Time History**

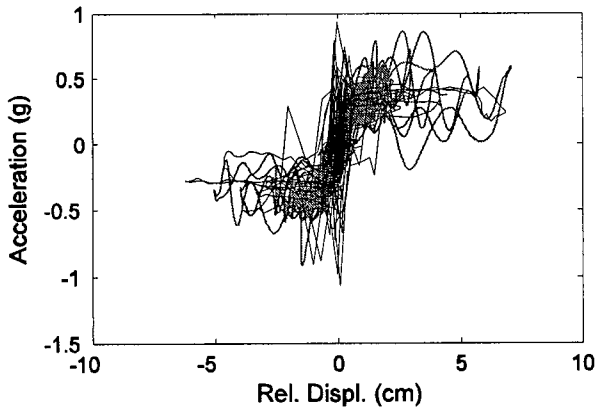


**Crack Acceleration vs. Relative Crack Displacement**

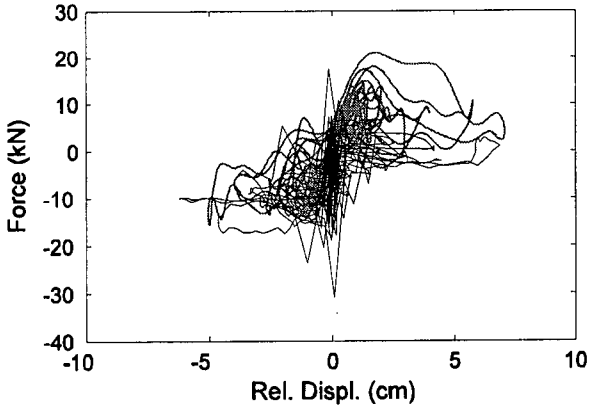


**Total Force vs. Relative Crack Displacement**

( —— Full Scale Test, — Working Model)

## H.2.2 Test PD4-1.20

| | | | | | | | | | |
|---|---|---|---|---|---|---|---|---|---|
| **Wall:** | Poor Quality Collar Joint | | **Test Sequence:** | 4 | | **Test Number:** | PD4-1.20 | | |
| **Earthquake Record:** | Hayward | | **Scale:** | 1.20 | **Site Class:** | D | **PGA:** | 1.1g | **PGD:** 6.25cm |
| **Wall Condition:** | Crack at Header 7 and 1 | | | | | | | | |
| **Height:** | 4072mm | **Thickness:** | 353mm | **h/t:** | 11.5 | **Width:** | 1499mm | **Density:** | 1803kg/m$^3$ |
| **Header Location:** | | **H4:** | 1741mm | **H7:** | 3131mm | **H8:** | 3589mm | | |

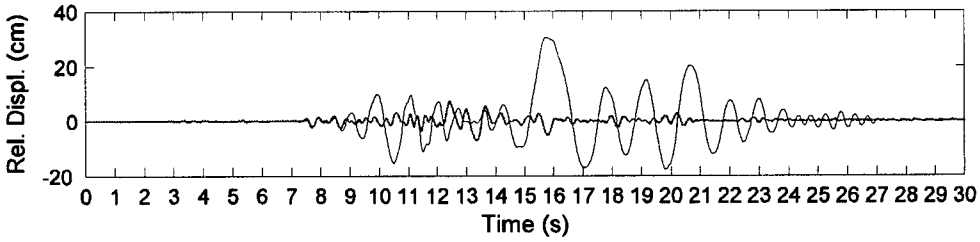


**Relative Displacement Time History at Crack**

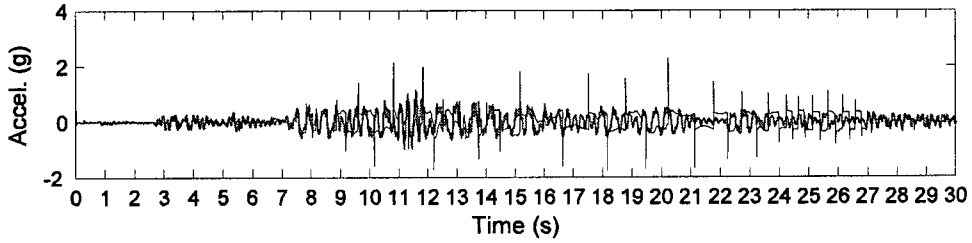


**Acceleration Time History at Crack**

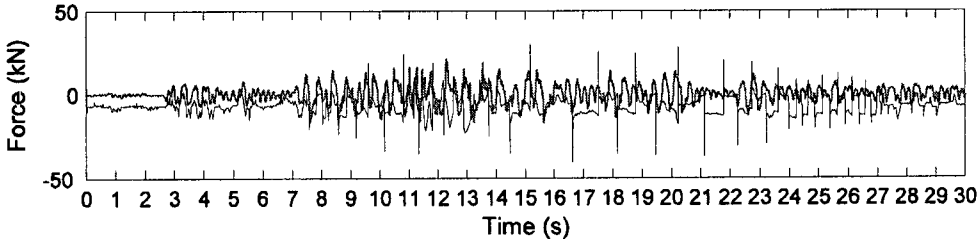


**Force Time History**

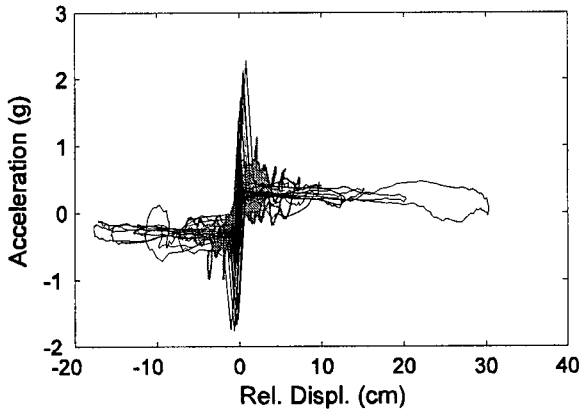


**Crack Acceleration vs. Relative Crack Displacement**

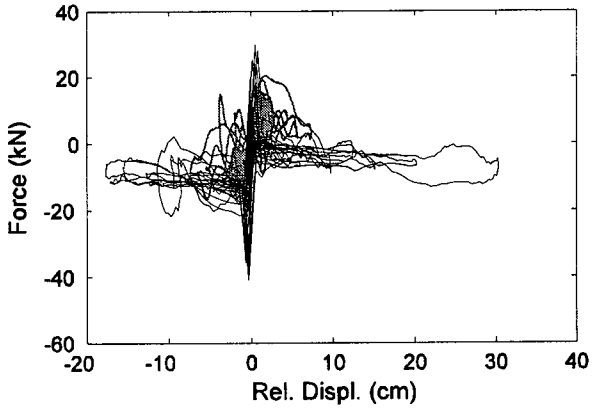


**Total Force vs. Relative Crack Displacement**

**( —— Full Scale Test, — Working Model)**

## H.2.3 Test PD5-1.66

| | | | | | | | | | |
|---|---|---|---|---|---|---|---|---|---|
| **Wall:** | Poor Quality Collar Joint | | **Test Sequence:** | 8 | | **Test Number:** | PD5-1.66 | | |
| **Earthquake Record:** | Hayward | | **Scale:** | 1.66 | **Site Class:** | D | **PGA:** | 1.25g | **PGD** 9.1cm |
| **Wall Condition:** | Crack at Header 7 and 1 | | | | | | | | |
| **Height:** | 4072mm | **Thickness:** | 353mm | **h/t:** | 11.5 | **Width:** | 1499mm | **Density:** | 1803kg/m$^3$ |
| **Header Location:** | | **H4:** | 1741mm | **H7:** | 3131mm | **H8:** | 3589mm | | |

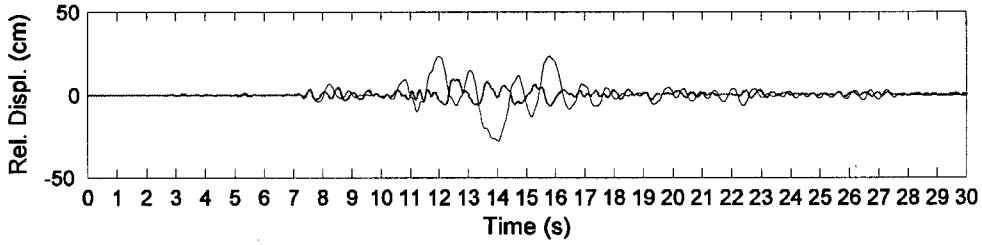


**Relative Displacement Time History at Crack**

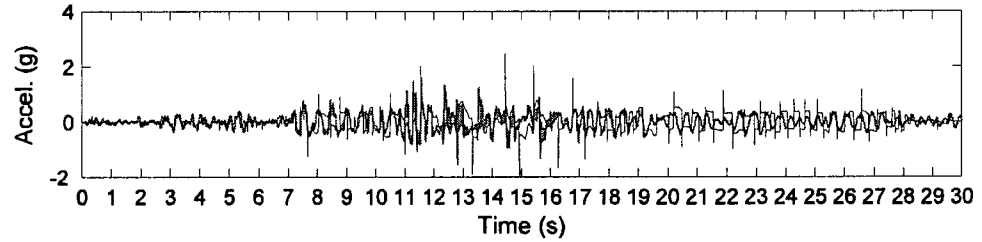


**Acceleration Time History at Crack**

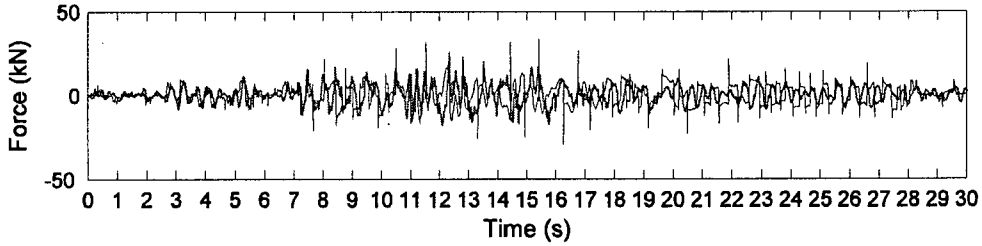


**Force Time History**

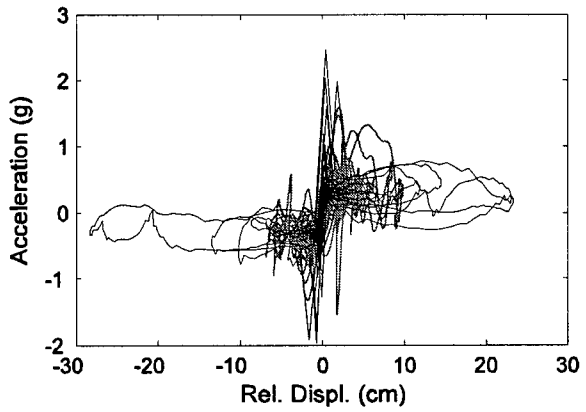


**Crack Acceleration vs. Relative Crack Displacement**

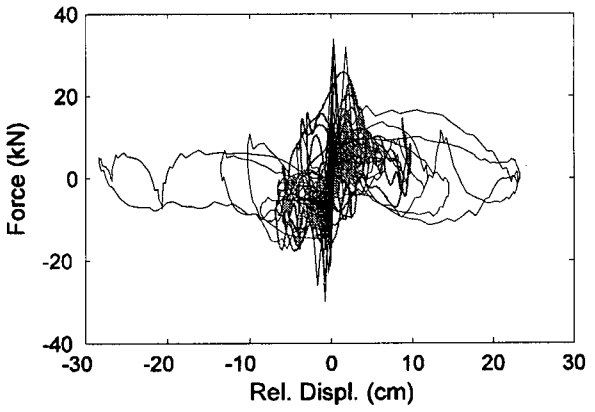


**Total Force vs. Relative Crack Displacement**

**( — Full Scale Test, — Working Model)**

# APPENDIX I. HIGH SPEED DIGITAL VIDEO ANALYSIS

## I.1 Introduction

High speed digital video data can be used as an important technique in measuring displacements, velocity and accelerations during shake table tests. It has the ability to give insight into the behaviour of a test sample/system that would not otherwise be obtainable through traditional video and measurement techniques (e.g. linear potentiometers, string pots, and accelerometers). The use of high speed digital video data is particularly useful in destructive testing which could otherwise cause potential damage to expensive instrumentation. Presented here is a brief introduction on how to carry out a high speed digital analysis using the URM wall shake table tests as an example, and a comparison to results obtained from data acquired through traditional techniques.

## I.2 High Speed Camera and Video Data Analysis Procedure

Many high speed cameras are available and can commonly record at a rate up to 2,100 frames per second with 512x512 resolution; the Civil Engineering Department at UBC has a Phantom v4.2 monochrome digital camera system [Vision Research, 2006]. Commercial software is now available that utilizes high-speed camera data to perform kinematic analysis; the software TEMA [Image Systems, 2005] was used for this purpose. Two dimensional studies are relatively simple to perform, but the results are adversely affected by image distortion due to out-of-plane image movements of the sample. Three dimensional analysis overcomes these problems, but is a more complex procedure, particularly with regard to calibration of the movement space. As the shake table tests of the URM walls only considered out-of-plane (lateral) response only the two dimensional analysis technique will be discussed. The stages for video analysis involve target application and calibration, video recording, and video data analysis.

### I.2.1 Targets and Calibration

The TEMA software provides automated digitization and tracking of a specimen if appropriate markers are placed in locations of interest. The markers should provide sufficient contrast from

the test set-up. Lighting is also an important factor in providing sufficient contrast between the edges of the targets and the surroundings, as shadows and bright reflections may make it difficult for the software to track the targets. For the URM wall shake table tests black and white quadrant markers were used. The markers were approximately 75mm in diameter. The size of the targets is dependent on the camera resolution, with larger markers giving better accuracy when the resolution of the system is poor and the targets are located far from the camera. Figure I.1 shows the test set-up with the quadrant targets placed at each header course, on either side of the crack, and on the testing frame. In order to transform the distances measured in pixels to real world measurements (e.g. meters) calibration/scaling is required. Scaling is specified by defining the real distance between two points or targets. For the URM wall tests the distance between two targets was used.

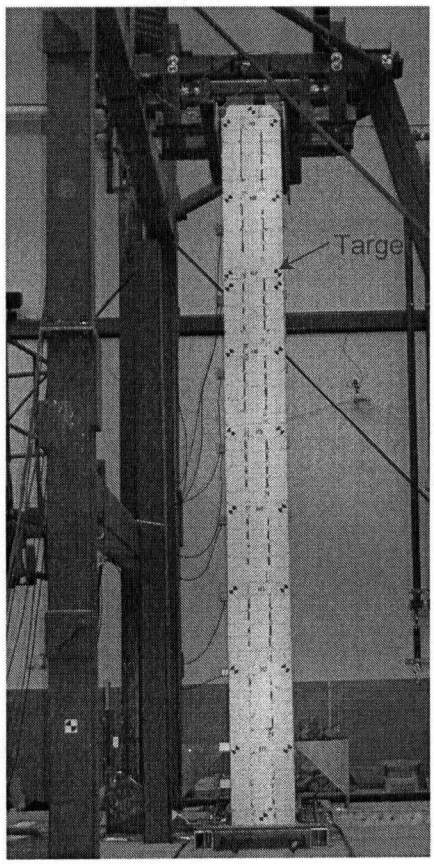


**Figure I.1 Test Set-Up with Quadrant Targets**

### I.2.2 Video Recording

For two dimensional studies, the camera is oriented such that its axis is perpendicular to the plane of interest, the further the camera is positioned away from the targets the less precise the camera orientation needs to be as the error will have minimal effect on the viewing the plane motion. The camera field of view and adjustments are displayed and controlled on the interface computer (Figure I.2) The field of view should always be somewhat larger than the movement space to avoid errors due to distortion at the edge of the lens. Focusing should insure that the targets are clear, and by digitally zooming in onto the targets can help to ensure this. The lens F-stop, exposure and EDR exposure should be adjusted to suit the lighting conditions.

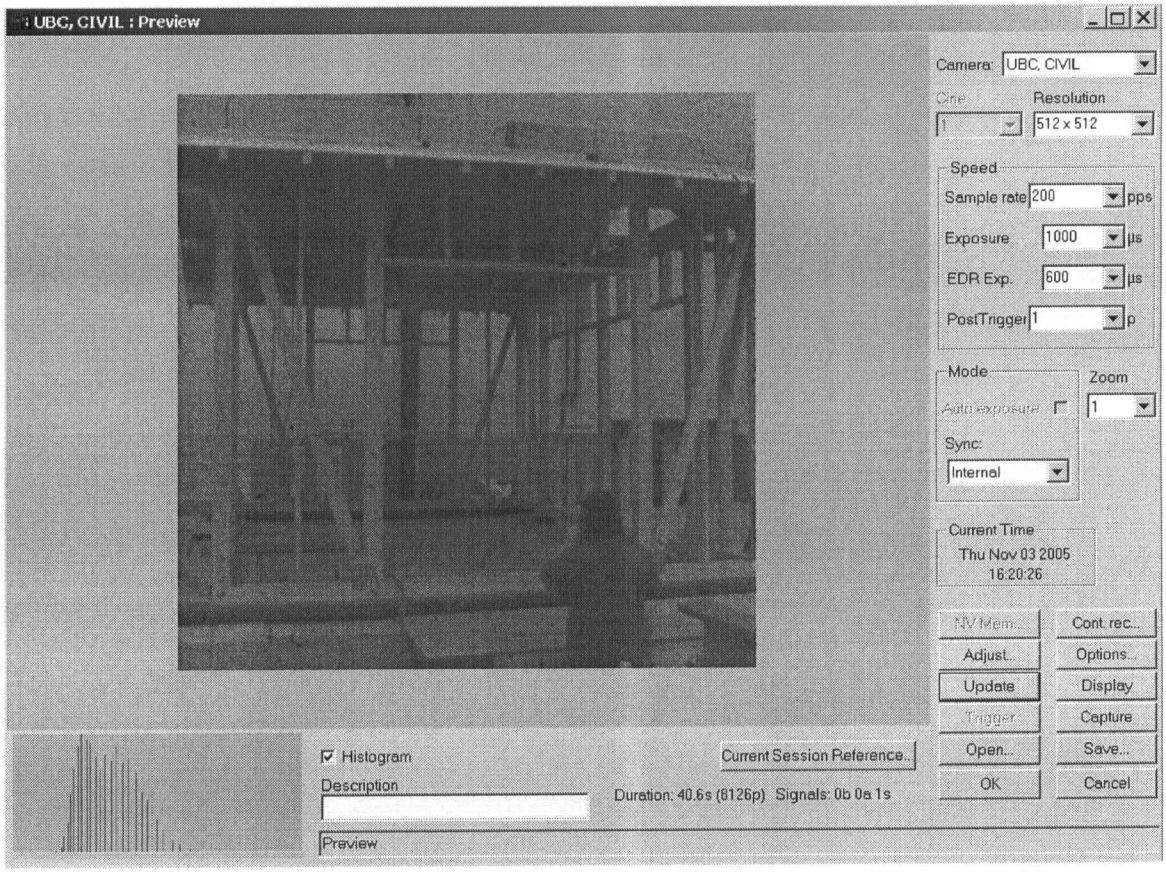


**Figure I.2 Screen View of Camera Settings**

The Phantom v4.2 camera system can record up to 2,100 pictures per second using the full 512x512 pixel SR-CMOS imaging sensor array [Vision Research, 2006]. The operator may also specify other aspect ratios to increase recording speeds or extend recording times. Recording times are limited by the capacity of the built in 2.2 Gb camera memory. Table I.1 shows a

sample of resolution, frame rate, and recording time. For the URM shake table tests a resolution of 384x512 at 200 frames per second, 200 Hz, was chosen to allow 54.2s of recording (most of the earthquake records used in the testing program lasted for approximately 50s).

**Table I.1 High Speed Camera Resolution, Frame Rate, and Approximate Recording Time**

| Resolution (pixels) | Rate (frames/sec) | Recording Time* |
|---|---|---|
| 512x512 | 2,100 | 4s |
| 512x384 | 2,840 | 3.8s |
| 384x512 | 200 | 54.2s |

* Recording time is approximate, and limited by the camera's 2.2 Gb memory.

The camera also will start recording based on the triggering mechanism selected. If 'Pre-Trigger' is selected only images before the trigger is engaged will be saved. To save only images after the trigger has been engaged the user must select 'Post-Trigger'. The trigger can be controlled by either a user at the interface computer or via an electronic signal transferred through the Power/Capture cable. At the time of the URM test the electronic trigger was not available, so the camera was user controlled with a Post-Trigger. The use of an electronic trigger could be used to connect to the data acquisition system such that the data recorded from the camera would be timed to correspond to that of the other test instrumentation (e.g. accelerometers, strain gauges, etc).

### I.2.3 Video Data Analysis

Video data analysis was carried out using the commercially available software TEMA (Figure I.3). Described below is a brief introduction to some of the features available in TEMA and background to how the software operates. This discussion is not intended to be a tutorial on how to use the application, as this information is available in the TEMA User's Guide [Image Systems, 2005], but rather a brief summary of the software's methodology and provide more background information that is not available in the User Guide.

#### I.2.3.1 Scaling

TEMA uses sophisticated algorithms to track the locations of selected targets (i.e. pixels) and determine pixel displacements from video frame to frame. As was previously mentioned in order to transform pixel displacements to real world displacements scaling is required by defining the

real distance between two points. TEMA allows three different means of scaling: static, manual or dynamic. In the static case the user defines a reference time in which the real distance between two points is specified, and the transformation parameters are calculated only once. For example, if the user specified the scaling distance as 1m, it would mean that the two points are 1m apart at the reference time, but may not be 1m apart before or after the reference time. In the manual case the user defines a scaling factor, (e.g. 10 times), it is similar to a static transformation in that the transform parameters are calculated only once, based on the specified scaling factor. In dynamic scaling the transformation is recalculated for each successive image. For example if two points are measured as being 1m apart in the first frame they will be 1m apart in successive frames. Dynamic scaling is useful in situations when there is a need to remove the effects of unwanted motion from the data (e.g. a rotating object).

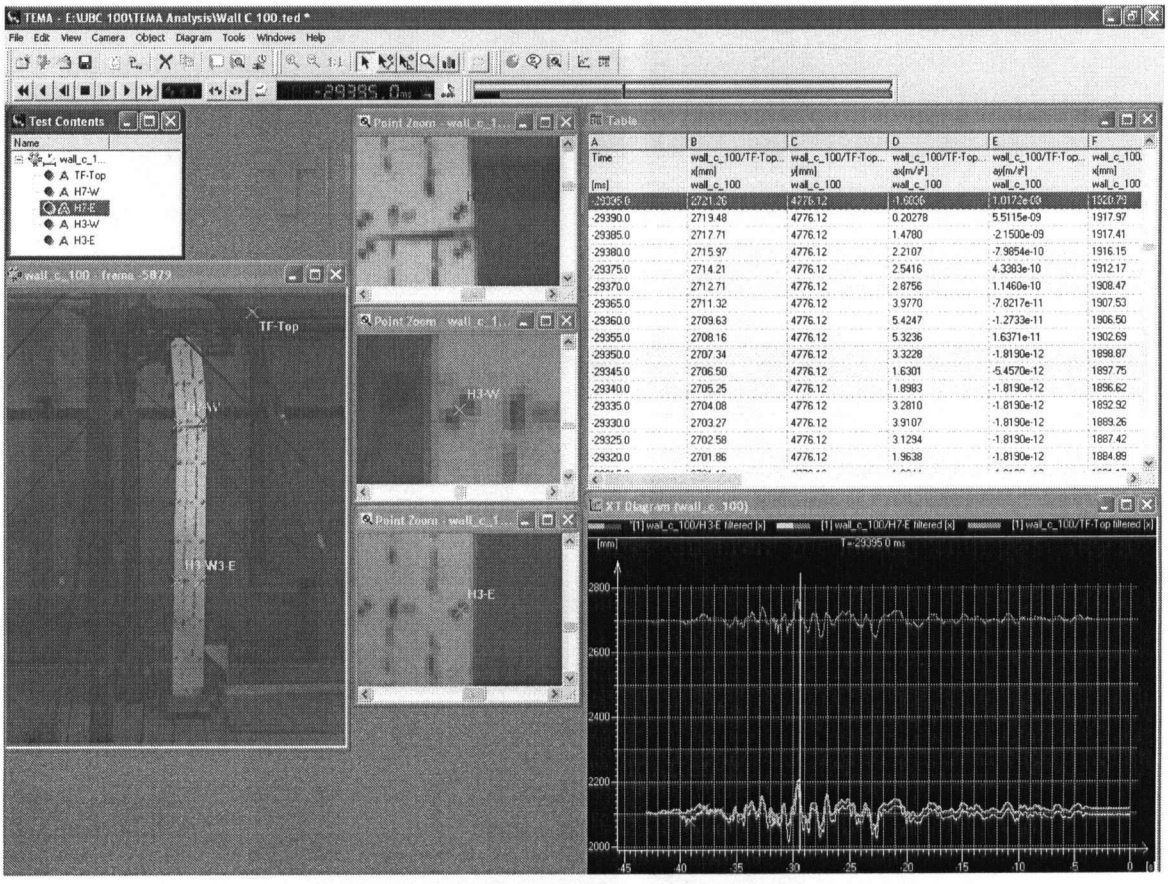


**Figure I.3 Screen View of TEMA Program**

### I.2.3.2 Speed and Acceleration

TEMA uses FIR (Finite Impulse Response) filter algorithms to compute speed and acceleration from tracking data. These filter properties for speed and acceleration can be adjusted in the "Tool – Preferences" tab of the application (Figure I.4). The FIR is a type of digital signal filter, in which every sample of output is the weighted sum of past and current sample of input, using only some finite number of past samples (filter life). This algorithm requires that the input is equidistantly sampled, otherwise the data must be resample by interpolating its values at equidistantly spaced times.

The FIR filter algorithm can be described by the following formula:

$$y_i = \sum_{j=-n}^{n} c_j x_{i+j} \tag{I.1}$$

where $x_i$ are the samples of the input sequence. When the data has more than one component, i.e. a velocity or acceleration vector, this formula applies to each component. The numbers $c_j$ are called the filter coefficients, and the integer $n$ is the filter's half length. There are $2n + 1$ filter coefficients. The filter is analogous to a transfer function, were the coefficients change the input, (displacements), to velocity and acceleration.

Generally, the greater the half length, the less sensitive the filter is to noise in the input data. However, a longer filter, (i.e. longer half life), will leave longer gaps at the ends of the output. This is because the filter can only be applied if there are $n$ input samples before or after the samples being calculated. In order to reduce these gaps TEMA has an option to reduce the filter length at the ends of the input sequence.

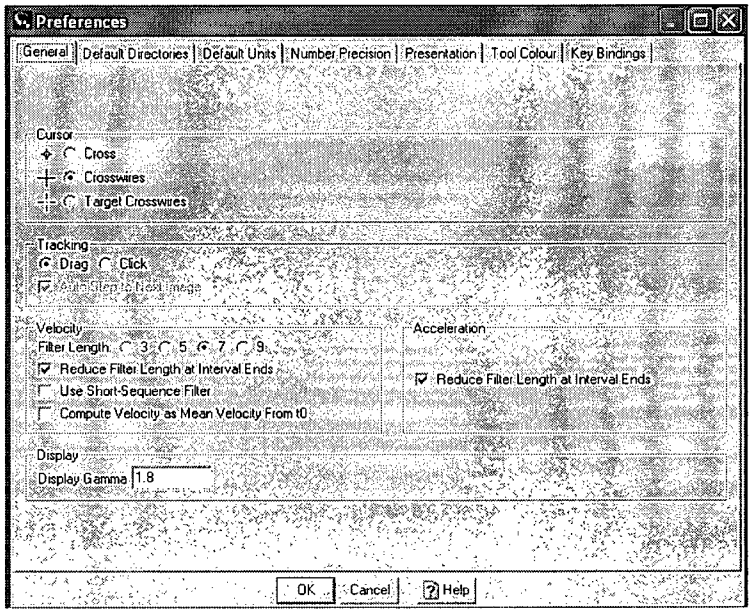


**Figure I.4 Screen View of Velocity and Acceleration Filter Properties**

### I.2.3.3 Velocity and Acceleration Filter Coefficients

***Velocity Filter Coefficients***

The filters used to compute velocities can be derived by least-square fitting a quadratic equation to the 2n+1 input points and then taking the derivative of the fitted function. This yields the following filter coefficient:

$$c_j = \frac{1}{T}\frac{3j}{n(n+1)(2n+1)}, \quad -n \le j \le n \tag{I.2}$$

where $T$ is the sampling interval of the input sequence (i.e. the data rate). The velocity filter coefficients make the FIR filter anti-symmetric, i.e. they extend $n$ samples both before and after the current sample and $c_{-j} = -c_j$. This also makes the filter casual, where its output does not depend on any ``future'' inputs.

***Short-Sequence Velocity Filter***

TEMA also has the option to reduce the filter length at the ends of the sequence. This two-point, short sequence filter has the following form depending on which end of the input sequence is being calculated:

$$y_i = \frac{x_{i+1} - x_i}{T} \quad \text{or} \quad y_i = \frac{x_i - x_{i-1}}{T} \tag{I.3}$$

This filter allows there to be an output sample for every input sample, which may be important for some applications. However, since only two input points are used, these filters are very noise sensitive as a small error in the input will yield a large error in the output velocity. These filters are also not anti-symmetric, and there for the filter will not be causal (i.e. the calculated speed is really the speed at the time halfway between the input samples). Because of these drawbacks this option is recommended only if it is very important that there be no gaps at the ends of the speed data.

***Mean Velocity from $t_o$***

The user can also select the option to calculate velocities as the mean velocity from time zero rather than as the instantaneous velocity. When this option is selected the above mentioned filters are not used, rather the velocity at time $t$ is calculated as the displacement from time zero to time $t$, divided by $t$. This option is only suitable for instances where the tracking targets are moving at a constant velocity.

***Acceleration Filters***

In TEMA the accelerations a computed with similar filters used to calculate velocity. The only difference is that these filters are symmetric as a result of double differentiation. The program allows two filters of different half-length:

$$n = 2,\ c_j = \frac{1}{7T}(2,-1,-2,-1,2) \tag{I.4}$$

$$n = 4,\ c_j = \frac{1}{100T}(4,4,1,-4,-10,-4,1,4,4) \tag{I.5}$$

These filter coefficients can be derived by applying the 3 and 5-point velocity filters twice in succession.

In most cases, the 9-point ($n$ = 4) filter is used. If the user notices the velocity being clipped at the beginning or end of the data, it is due to there not being enough frames to determine the velocity, (for a 9-point filter, at least 5 frames of data are needed). In this situation the length of the velocity/acceleration filter needs to be shortened. This can be done by selecting the "reduce filter length at ends" option, which will automatically change the filter length if there is a gap in

the tracked data. This will force TEMA into reporting a velocity up to the gap in data; otherwise there would be a 9 point gap for a 1 point lost in the tracked data.

For the URM test a 7-point velocity filter was used with reduced filter lengths at the interval ends. For acceleration, the reduced filter length at interval ends option was also selected.

### I.2.3.4 Tracking Points

For each target that is to be tracked there are several options and properties that can be adjusted (Figure I.5). Some options such as: "pull to straight path," "tracker tolerance," "update factor," and "core size" effects how TEMA tracks a target. These options need to be adjusted depending on the application, and target image quality. A good way to ensure that TEMA is tracking the target correctly is start tracking during some frames that experience very little movement. If the tracking drifts too much from the target then the previous mentioned options should be adjusted. More information can be found in TEMA's User Guide [2005].

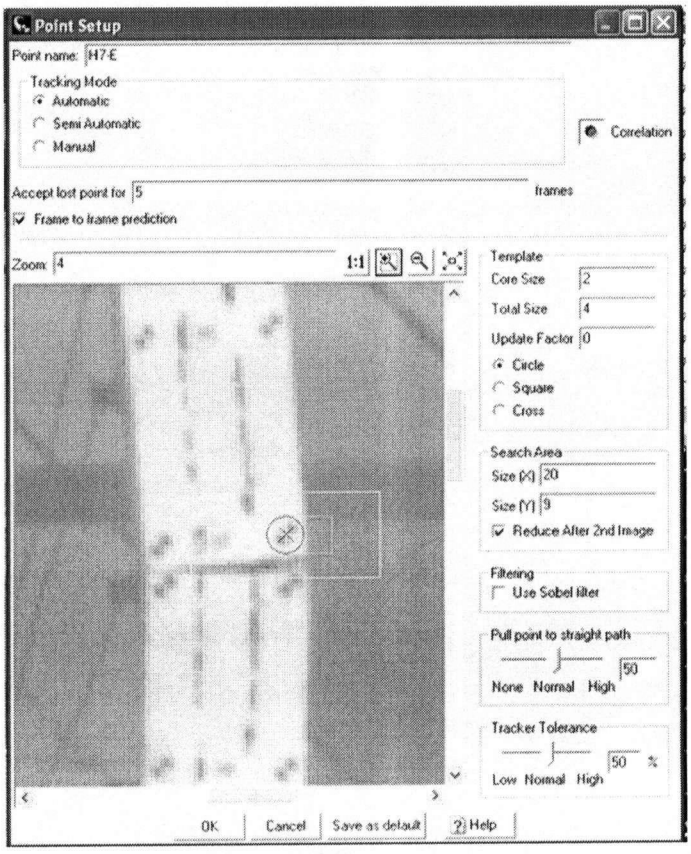


**Figure I.5 Screen View of Tracking Point Set-Up**

There are three tracking modes available: "automatic," "semi-automatic," and "manual." In the "Automatic" mode the TEMA automatically tracks the object from frame to frame, and will only ask the user to confirm the tracking position if the target is lost for more than the number of frames specified by the user. The "Semi-Automatic" function is similar to "Automatic," however the user must confirm the tracking position for each frame. This option is useful when TEMA has difficulty tracking a target for a short period of time. During the "Manual" mode the user must define the tracking point in each image frame. A detailed description of the modes can be found in the user manual.

TEMA also allows the user to use a Sobel filter. This is an image filter that enhances edge detection of the target by creating an embossing effect. An example of an image that has had a Sobel filter applied to it is shown in Figure I.6.

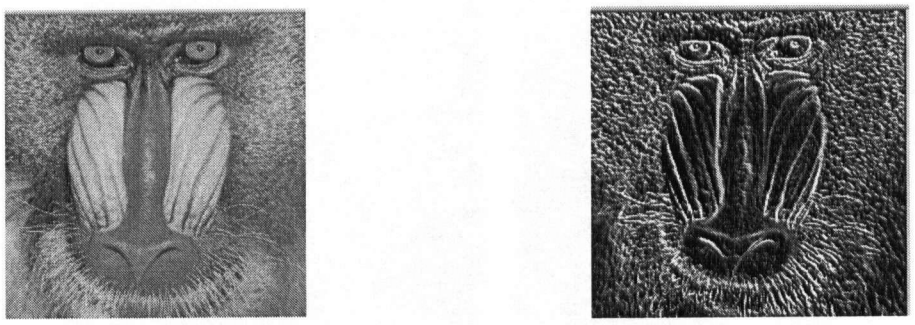

(a) Raw Image (b) Filtered Image

**Figure I.6 Effect of Sobel Filter**

[Hades, 2005]

While carrying out the analysis the TEMA program had difficulty tracking the targets and would often prompt the user to confirm the location of the tracked target. In order to speed up the analysis the tracking setting were adjusted such that the tracking criteria was less stringent (i.e. less precise). However, for Test PD5-2.22, in which the wall collapsed, the tracking criteria was set more stringent; calling for the user to confirm the tracking points more frequently.

### I.2.3.5 Filtering/Smoothing Results

During digitization of the data small errors are introduced that creates noise in the output data. The effect of noise is not too great in the displacement data, but it becomes increasingly apparent in the velocity and acceleration data. This added noise can be removed by using appropriate

digital filters. Two types of filters are available in TEMA, a Finite Impulse Response (FIR), and Channel Frequency Class (CFC), type filter. The FIR filter is a variable low pass filter, which removes higher frequencies with no phase distortion. In TEMA the frequency cut-off is based on the 'Filter Factor' and frame rate:

$$Cutoff\ Frequency = (Frame\ Rate)\cdot(101 - Filter\ Factor)/202 \tag{I.6}$$

The Filter Factor is defined as a percentage, with '0' specifying no filtering, while '100' specifies maximum filtering. Figure I.7 shows the relationship between the cut-off frequency and filter factor for some sample frame rates.

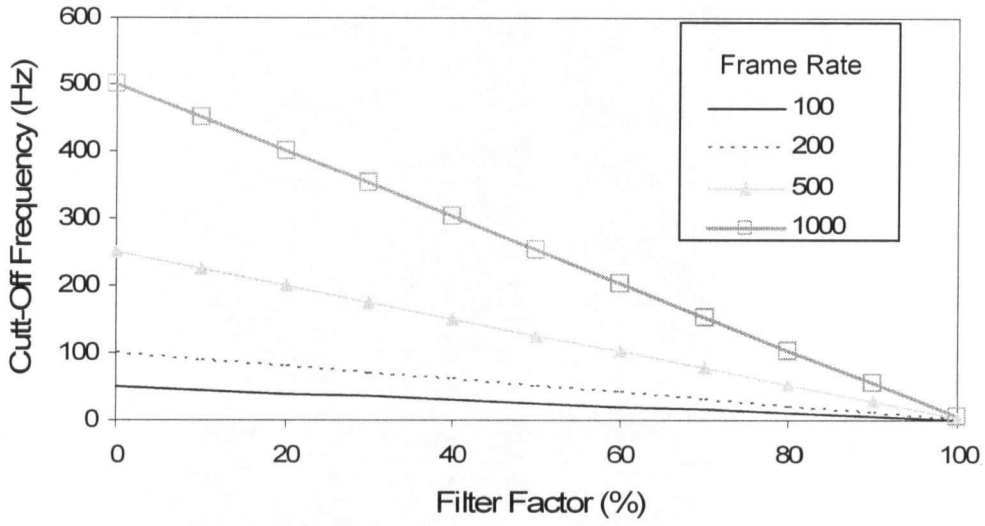


**Figure I.7 Cut-Off Frequency vs. Filter Factor**

If the CFC filter is chosen TEMA applies a fourth order Butterworth filter. The specified CFC value determines the cut-off frequency which is the highest frequency of the input signal that will pass through the filter. It should be set well above the highest signal frequency of interest; otherwise part of the signal will be filtered out along with the noise (due to filter roll-off).

For the URM tests a CFC filter was chosen with a cut-off frequency of 25Hz to filter the displacement data. The acceleration data was filter with a cut-off frequency of 25Hz in a similar manner as the data obtained from the string pots and accelerometers (Chapter 3).

## I.3 TEMA Results

### I.3.1 TEMA Verification and Results

Results generated by TEMA for a couple tests were compared to those obtained using standard instrumentation (string pots and accelerometers) from the URM shake table tests. Both time histories of absolute displacement and accelerations from various header locations were used for comparison. To compare the TEMA generated time histories to those obtained using string pots a reference time was required. It was assumed that the peak displacement occurred at the same time for both methods and was chosen to be the reference point. Sample time histories are shown in Figure I.8 through Figure I.15.

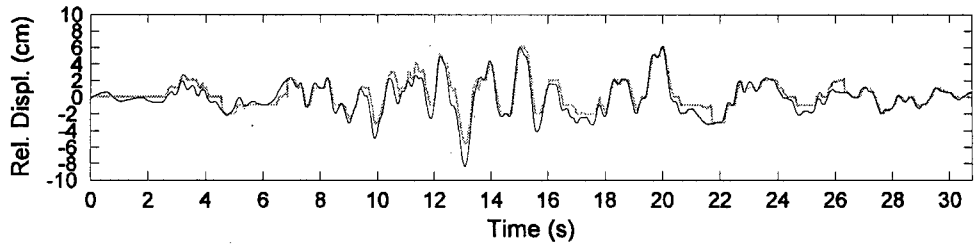


(..... TEMA, — String Pot)

**Figure I.8 Header 2 Absolute Displacement Time History, Test PD4-1.20**

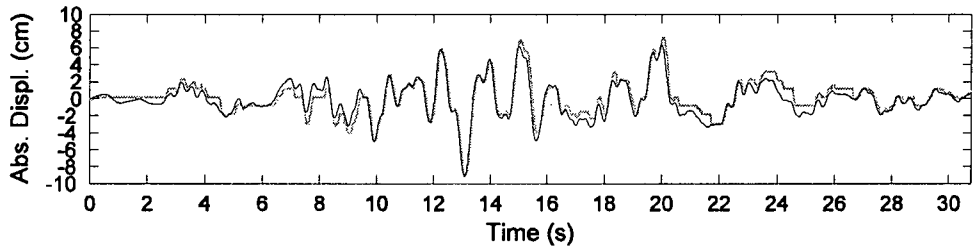


(..... TEMA, — String Pot)

**Figure I.9 Header 4 Absolute Displacement Time History, Test PD4-1.20**

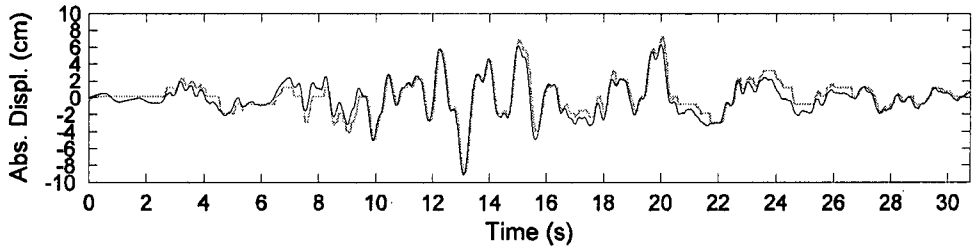


(..... TEMA, — String Pot)

**Figure I.10 Header 7 Absolute Displacement Time History, Test PD4-1.20**

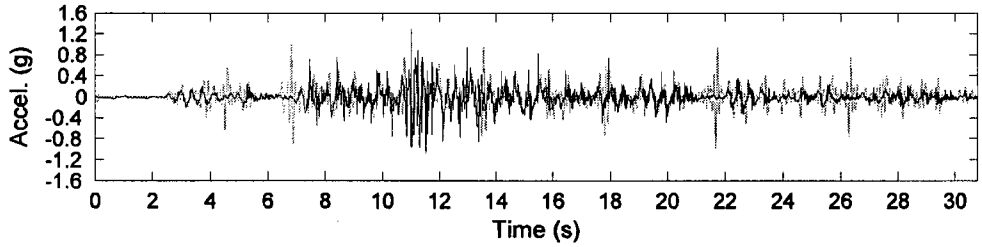


(..... TEMA, — String Pot)

**Figure I.11 Header 2 Acceleration Time History, Test PD4-1.20**

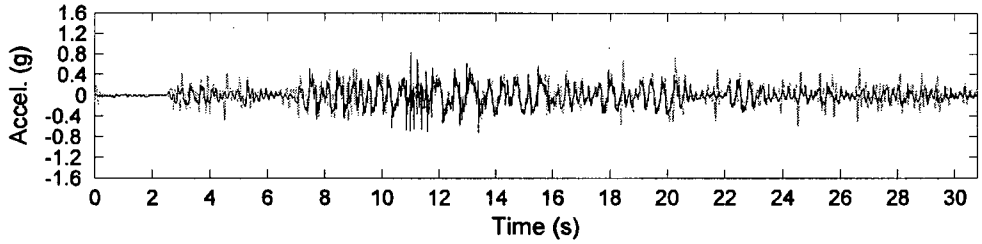


(..... TEMA, — Accelerometer)

**Figure I.12 Header 4 Acceleration Time History, Test PD4-1.20**

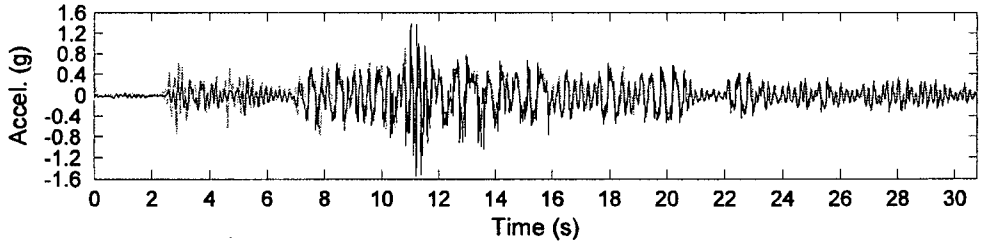


(..... TEMA, — Accelerometer)

**Figure I.13 Header 7 Acceleration Time History, Test PD4-1.20**

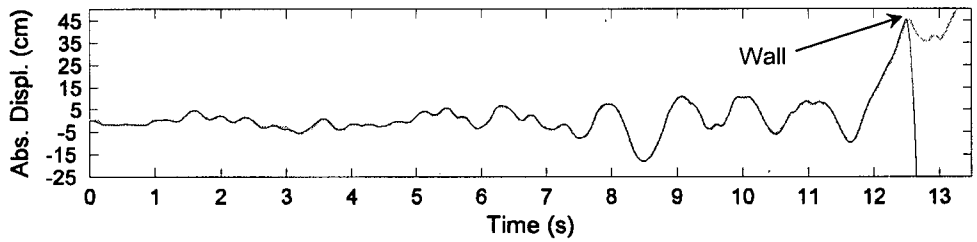


(..... TEMA, — String Pot)

**Figure I.14 Header 7 Absolute Displacement Time History, Test PD6-2.22, Collapse Level**

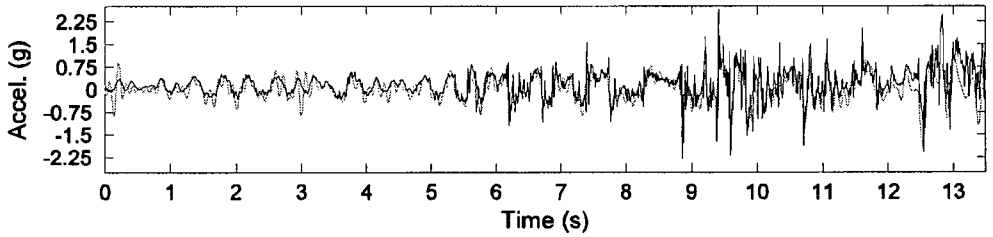


(..... TEMA, — Accelerometer)

**Figure I.15 Header 7 Acceleration Time History, Test PD6-2.22, Collapse Level**

In Test PD4-1.20, the results generated by TEMA gave fairly similar absolute displacement results to those obtained using conventional string pots. Looking closely at the displacements we can see that there are areas in the TEMA time history response that show constant displacement over a small period of time, while the displacements recorded from the string pots show a change in displacement. This is due TEMA having difficulty tracking the target. If the program is unable to track the point of interest it will record the previous results for that instant in time, resulting in a constant displacement. As the accelerations are derived from the displacements, any inaccuracy determining the displacements will result in inaccurate accelerations.

As previously mentioned, when carrying out the analysis for Test PD6-2.22, the tracking options were set more stringent and called for the user to confirm the correct location of the target more often. This lead to better results as seen in Figure I.14 and Figure I.15 between the TEMA generated results and those obtained by the string pots and accelerometers.

In order to compare the results from the two methods the peak displacement was used as a reference point. This may introduce some errors in the comparison. Using an electronic triggering system as previously mentioned would help to minimize possible discrepancies.

## I.4 Conclusions and Recommendations

The use of high speed digital video analysis is a very powerful tool, particularly in destructive tests were instrumentation would be very difficult or costly to install or replace. It can allow researchers to use less instrumentation such as string pots and accelerometers, and provide data that would be otherwise difficult to obtain, e.g. crack openings. The high speed video can be used to see the detailed behaviour of test samples with more insight than regular video recordings due to high frame rates, e.g. when wall first cracks.

However, it is sometimes difficult to track targets, as the tracking point may drift away from the target, requiring the user verify location of the tracked target. This can make the process time consuming, for example, assuming a typical earthquake record, tracking 5 targets toke approximately 2.5 hours to process on a P4 computer. The accuracy of the accelerations and velocities may also be inaccurate as they are derived from differentiation of the displacements, however these errors can be greatly reduced by setting more stringent tracking criteria and having the user verify the tracking position.

It is recommended that only displacements be used from the high speed video analysis if the user sets the TEMA tracking properties correctly and ensures that the software adequately tracks the targets from frame to frame. As the accelerations are derived from the displacements they may track the general acceleration trend, but should be used cautiously as they may be inaccurate. The use of appropriate targets, camera resolution and lighting conditions can make the tracking of targets easier and more accurate.

## References

Image Systems, 2005, "TEMA User Manual", Images Systems, Denmark.

Hades, 2005, http://tams-www.informatik.uni-hamburg.de/applets/hades/webdemos/00-intro/02-imageprocessing/sobel.html, *Hamburg Design System,* October.

Vision Research, 2006, http://www.visiblesolutions.com. April.